# Design of self-oscillating biomimetic vocal folds : materials, mechanics and vibrations

Hamid Yousefimashouf

THÈSE

Pour obtenir le grade de

**DOCTEUR DE L'UNIVERSITÉ GRENOBLE ALPES**

École doctorale : I-MEP2 - Ingénierie - Matériaux, Mécanique, Environnement, Energétique, Procédés, Production
Spécialité : 2MGE : Matériaux, Mécanique, Génie civil, Electrochimie
Unité de recherche : Laboratoire Sols, Solides, Structures et Risques

# Conception de plis vocaux biomimétiques auto-oscillants : matériaux, mécanique et vibration

# Design of self-oscillating biomimetic vocal folds : materials, mechanics and vibrations

Présentée par :

**Hamid YOUSEFI-MASHOUF**

Direction de thèse :

| | |
|---|---|
| **Lucie BAILLY**<br>Chargée de Recherche, Université Grenoble Alpes | Directrice de thèse |
| **Nathalie HENRICH BERNARDONI**<br>Université Grenoble Alpes | Co-encadrante de thèse |
| **Laurent ORGEAS**<br>Directeur de recherches, CNRS | Co-encadrant de thèse |

Rapporteurs :

**Laurent CORTE**
PROFESSEUR DES UNIVERSITES, École des Mines ParisTech
**Christiane WAGNER-KOCHER**
MAITRE DE CONFERENCE, Université de Montpellier

Thèse soutenue publiquement le **15 décembre 2022**, devant le jury composé de :

| | |
|---|---|
| **Lucie BAILLY**<br>CHARGE DE RECHERCHE, CNRS | Directrice de thèse |
| **Laurent CORTE**<br>PROFESSEUR DES UNIVERSITES, École des Mines ParisTech | Rapporteur |
| **Christiane WAGNER-KOCHER**<br>MAITRE DE CONFERENCE, Université de Montpellier | Rapporteure |
| **Frédéric BOSSARD**<br>PROFESSEUR DES UNIVERSITES, UGA | Président |
| **Florian MARTOïA**<br>MAITRE DE CONFERENCE, INSA de LYON | Examinateur |
| **Michael DöLLINGER**<br>PROFESSEUR DES UNIVERSITES, Friedrich-Alexander-Universität Erlangen-Nürnberg | Examinateur |

Invités :

**Nathalie HENRICH BERNARDONI**
DIRECTEUR DE RECHERCHE, CNRS
**Laurent ORGéAS**
DIRECTEUR DE RECHERCHE, cnrs

# Contents

# Preface and thesis outline

Speech is the oldest and most widely used means of communication by humans. As the main component of speech, the human voice plays a central role in this communication, and its quality therefore affects the personal, social, and professional life of the speaker. Thus, voice disorders significantly disrupt the normal life of individuals. The lifetime prevalence of voice disorders has been reported to be about 29% in the general population [20, 186], and about 50 % in France for professionals with a high vocal load such as artists and teachers. Disorders can be due to dysfunctional pathologies with the formation of benign vocal-fold lesions (*e.g.* nodules, polyps, etc.), to surgery sequelae for laryngeal cancer (3500 cases/year in France, 15% of total cancers), or to a laryngeal paralysis. In the extreme case of laryngectomy (8000 cases in France), many traumatic complications appear, among them the loss of voice and very high psychological distress. Nowadays, two therapeutic options are considered in function of the patient's case :

- *Speech therapy*, to correct an ill-adapted vocal gesture thanks to manual laryngeal manipulation, body work, glottal source, resonance and breathing coordination together with a relearning of communicative behaviour. These techniques are built on a strong empirical know-how of the practitioners, continuously expecting an increase in fundamental knowledge in phonatory biomechanics to improve their clinical plans.
- *Microlaryngeal surgery*, consisting in the excision of the vocal-fold lesion or in the resection of the damaged tissue, from superficial to complete cordectomy. However, it is observed that dysfunctional scarring lesions are very frequent in cases of invasive procedure and can yield to inconsistent results including loss of phonatory abilities. Over the past decades, many encouraging attempts have emerged to create appropriate biomimetic materials to overcome these post-operative lesions : injectable hydrogels, implanted synthetic polymers, stem cell and growth factor administration. To date however, no artificial biomaterial is able to replace the damaged native mucosa for durable voice restoration. This failure can be explained by a field of fundamental research which is still barely developed on the substitutes of biological oscillators.

Therefore, to tackle the current clinical limitations and provide the most efficient treatments, it is necessary to keep improving the scientific knowledge acquired on the fundamental processes driving human phonation.

Phonation is a complex phenomenon involving many coupled physical interactions, including aerodynamics through the larynx, biomechanics of the vocal folds, and acoustics generated by their vibrations [154, 217]. The study of these combined phenomena requires a thorough identification and characterization of the key factors impacting the voice. According to many studies, such an accurate measurement is almost impossible *in vivo* due to several access and technical limitations [66, 147]. On the other hand, the reproduction of realistic phonation circumstances under *ex vivo* condition is also very restrictive (access to biological sample, loss of active factors, etc). Therefore, the experimental study of the voice using artificial larynx models has been proposed as an alternative solution to overcome these obstacles and progress in voice research. In this field, many different configurations have been developed, and have contributed to a better understanding of the coupled fluid/structure/acoustics interactions driving phonation. However, to date, compared to the knowledge acquired on the aero-acoustic characterization of the human voice, the

histo-mechanical specificities of the vocal tissues are still barely explored, and their impact on the outstanding vibratory properties of the vocal fold remains poorly understood. *In vitro* simulators of the phonatory system have been developed, made of artificial deformable replicas of the vocal folds. However, most of them are made up of homogeneous elastomers, with structural and mechanical properties which are still far from those of the original tissues.

Therefore, **the general objective of this thesis is to design new *in vitro* self-oscillating biomimetic vocal folds with tailored structural and mechanical properties, allowing to gain a better understanding of the link between the microstructure of vocal-fold tissues, their mechanical behavior and macroscale vibratory behaviour.** To this end, the chosen strategy is based on step-by-step experimental developments and analyses, from the synthesis of soft materials and architectured structures, to the optimisation of their macroscale mechanical properties with respect to that of native tissues, and the assessment of their vibratory behaviour under realistic morphological conditions and fluid-structure interactions.

The thesis is structured in four major parts, describing the step-by-step developments carried out for this purpose :

- **Part I describes the general context and objectives of the study**, and is divided in two chapters :
  – Chapter 1 presents a state-of-the-art on human vocal folds and biomimetic oscillators. It first surveys the current knowledge acquired on the histo-mechanical properties of human vocal folds. Then, it presents the different materials developed to mimic them within *in vitro* simulators of the phonatory system for voice research, as well as in clinical routine for tissue repair. Finally, it presents the current limitations for the biomimetic design of vocal folds, and the guidelines for optimal candidates.
  – Chapter 2 summarizes the specific objectives of the thesis, and the experimental strategy to address the issues detailed in Chapter 1. In particular, it introduces the three major types of materials handled and compared during the thesis : gelatin-based hydrogels, polyethylene glycol (PEG)-based hydrogels and silicone elastomers.

- As a first step towards biomimetic design of vocal tissues, **Part II describes the experimental works conducted to process homogeneous and isotropic materials with tailored mechanical properties, and to identify relevant matrix candidates for future vocal-fold composite replicas**. This part is divided in two chapters :
  – Chapter 3 presents the processing route, mechanical characterisation and selection of gelatin-based hydrogels to best fit the average mechanical response of native vocal folds under various physiological loadings.
  – As a brief complement, Chapter 4 compares the mechanics of gelatin-based hydrogels to alternative isotropic candidates already used in a clinical context (PEG-based hydrogels), or in current *in vitro* testbeds of phonation (silicone elastomers).

- **Part III extends the biomimetic approach initiated in Part II towards the optimisation of anisotropic and architectured materials.** This part is divided in two chapters,

based on two different solutions to introduce a suitable structuration in the hydrogels presented in Part II :
– Chapter 5 firstly presents the experimental works performed to embed a fibrous reinforcement in PEG-based hydrogels, allowing to produce versatile composite hydrogels and mimic both the microscale collagen structure of native vocal tissues, as well as their macroscale multiaxial mechanics.
– As a brief complement, Chapter 6 summarizes a preliminary work aiming to induce a structuration in hydrogels and controlling their anisotropy by another means through freeze-drying techniques. These exploratory tests have been conducted on gelatin-based samples.

- Finally, **Part IV presents the elaboration of 3D vocal-fold replica based on the materials elaborated in previous parts, and the evaluation of their flow-induced oscillations using a customised *in vitro* testbed of phonation**. This part is divided in two chapters :
  – Chapter 7 firstly presents the design of an original larynx replica, and the vibratory behaviour of artificial vocal folds made of several homogeneous and isotropic materials studied in Part II. A large experimental database is analysed, in order to better understand the impact of the material properties of the vibratory patterns of the vocal folds and the aero-acoustical correlates of the produced sounds.
  – As a brief complement, Chapter 8 presents some preliminary experimental results obtained on first composite replicas using the fibrous reinforcements selected in Part III.

This thesis has been realized within the framework of the ANR MicroVoice project (ANR 17 CE19 0015 01, 2018-22), which brought together four partners with complementary expertises : the **3SR laboratory** (Univ. Grenoble Alpes/CNRS/Grenoble INP) expert in multi-scale mechanics of materials and structures, the **GIPSA-lab** (Univ. Grenoble Alpes/CNRS/Grenoble INP) expert in characterization and modeling of the human voice and speech, the **LBTI** (CNRS/Univ. Claude Bernard Lyon 1) expert in physico-chemistry of materials and tissue engineering, and the **LADAF** (CHU Grenoble/Université Grenoble Alpes) expert in anatomy and medical sciences. My work benefited from the numerous exchanges and collaborations with the whole consortium. More specifically, Chapter 5 results from a close collaboration with Daniel Ferri-Angulo (Post-doc) and Jérôme Sohier (CR) from LBTI (Lyon), and Chapter 7 results from a close collaboration with Raphaël Giraud (IR) and Paul Luizard (Post-doc) from GIPSA-lab (Grenoble).

# Part I : Context of the study and objectives

# 1

# Human vocal folds and biomimetic oscillators : a state of the art

# Contents

## 1.1 Vocal folds : structure and mechanics

The voice organ is composed of three anatomical units [204, 220] : the breathing apparatus (lungs and trachea), the vocal folds (VF) located in the larynx, and the vocal tract (*i.e.* the cavities between the vocal folds and the lips and nostrils). In human voice production, the role of the breathing system is to compress the air in the lungs and to generate an airflow through the larynx. During phonation, vocal folds vibrate as the airstream passes them, which generate a primary sound called the voice source. This section gives an overview of the specific structural properties and vibro-mechanical properties of human vocal folds.

### 1.1.1 Morpho-histological properties

#### At the larynx scale

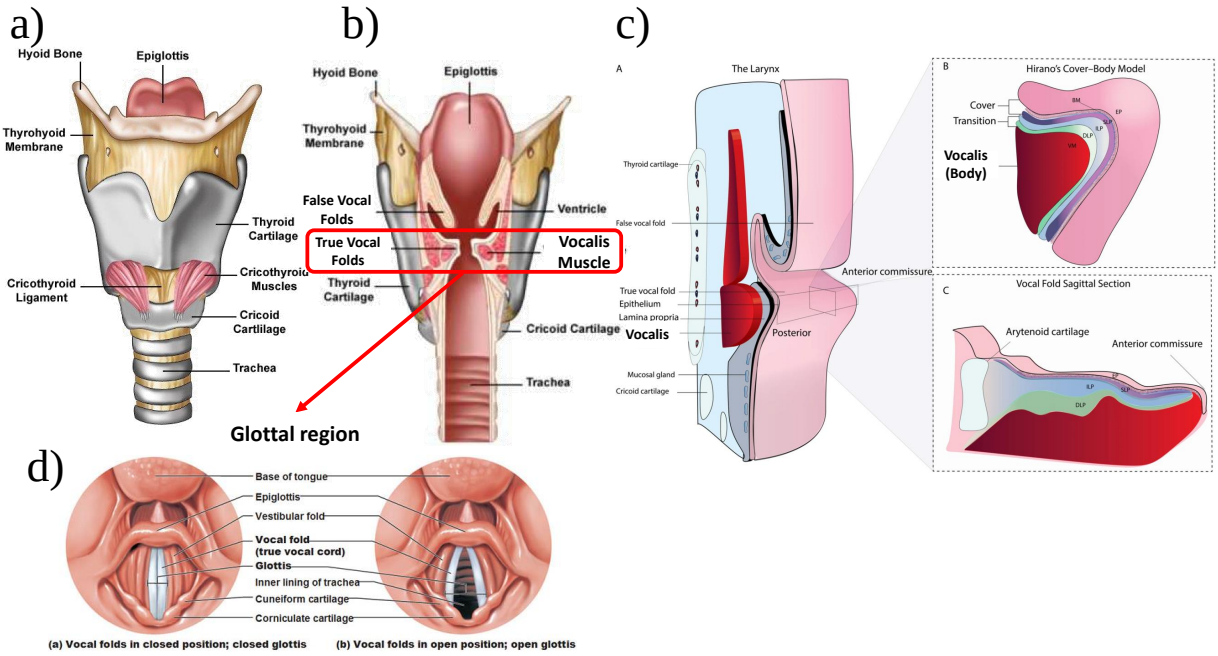


**Figure 1.1:** Schematic presentation of the human larynx and its components : a) anterior views; b) mid-coronal plane [200]; c) mid-sagittal plane : zoom on the different sublayers of the vocal folds; [15] d) adduction and abduction states of the vocal folds in transverse plane [161]

The human larynx is an organ located in the neck, above the trachea connecting it to the lungs, and below the pharynx representing the aero-digestive junction. This organ plays a fundamental role in phonation by driving the vocal-fold stretching, adduction and abduction, but also in breathing and swallowing functions, by protecting the lower airways against foreign objects. Typical dimensions of an adult human larynx is comprised from 4 to 6 cm in length, and 3 to 6 cm in width. It is composed of a series of hard and soft tissues (see Fig .1.1), which are actively collaborating to ensure these physiological

functions, and briefly reported below (more details on the anatomy of the larynx can be found in Cochereau **??** and Terzolo **??** for instance) :

- The **hard tissues** form a rigid holding framework for the actuation of the laryngeal mobility and the alteration of the airway resistance. They include nine cartilages (thyroid, cricoid, epiglottis, arytenoids, corniculates and cuneiforms) and a single bone (hyoid). Part of them are illustrated in Fig 1.1a. and b.

- The **soft tissues** comprise numerous ligaments and muscles connecting the laryngeal cartilages to each other and ensuring their mobility, the ("true") vocal folds at the heart of the laryngeal structure, and the false vocal folds (or ventricular folds), which do not have any direct contribution to voice production (except in pathological or specitic singing cases).

More specifically, the **vocal folds** are two soft structures shaped as folds, anteriorly connected to the thyroid cartilage (near the thyroid angle). The folds run posteriorly, and each fold inserts in an arytenoid cartilage. They are about 9 to 13 mm and 15 to 20 mm in adult females and males, respectively. The *glottis* refer to the space area between the vocal folds, as shown in Fig .1.1d. During breathing, the *glottis* is wide open with a typical Λ-shape, allowing air to flow from the lungs to the oral and nasal cavities. Before phonation, vocal folds are brought together by the laryngeal muscles, closing the *glottis* in a quasi-elliptic shape, which produces a pressure drop essential to trigger the vocal-fold vibration (see details of the flow-induced phonation process in section Section 1.1.4).

**At the scale of the vocal tissue's layers**

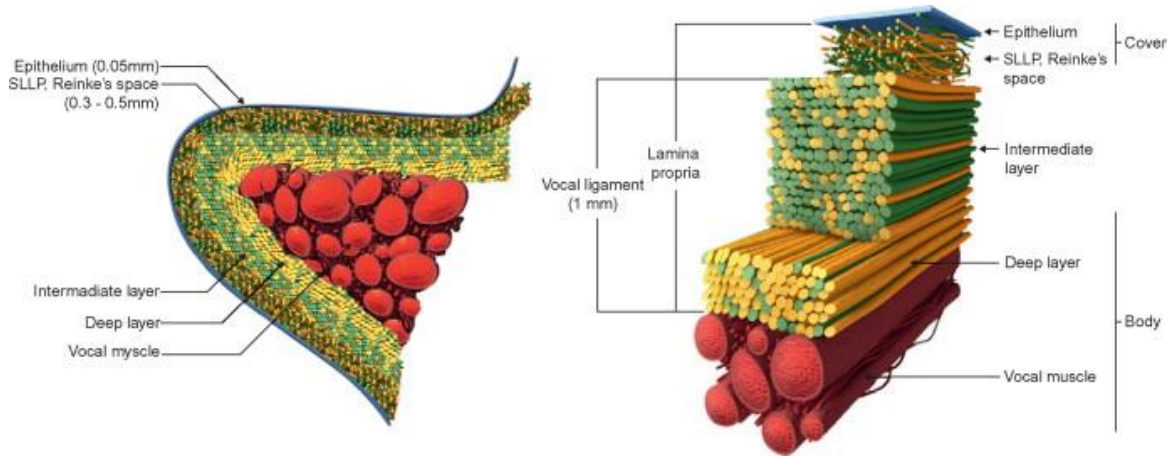


**Figure 1.2:** Schematic organization of the lamellar heterogeneous structure of human vocal fold tissue : (*left*) coronal cross-section of a vocal fold, (*right*) 3D representation of the layers. *In blue* : *epithelium*; *yellow* : collagen fibers; *green* : elastic fibers; *red* : muscular fibers. Adapted from [58].

The inner mesostructure of adult vocal folds is divided into five main layers owning different composition and function [93], as illustrated in Fig .1.1.c and Fig. 1.2 :

- The ***epithelium*** (EP, thickness $\approx$ 50-100 $\mu$m) is the outermost layer covering the vocal tissue. It is mainly composed of stratified squamous cells, making a protective membrane over the tissue surface against the multiaxial loadings to which the folds are subjected. Covered by mucus, the EP layer also plays a role in maintaining the required humidification of the tissue.

- The ***lamina propria*** (LP, thickness $\approx$ 1-3 mm) is the second layer through the depth of the tissue. It is a loose connective tissue, made of cells and an extracellular matrix (ECM) comprising amorphous ground substances (*e.g.* hyaluronic acid) and entangled fibrous networks of collagen and elastin. The LP layer is further divided into three sublayers with distinct fibre types, densities and arrangements as illustrated in (Fig. 1.2) :
  - ▷ the superficial one (SL, thickness $\approx$ 0.5 mm), also known as **"Reinke's space"**, is composed of loose fibrous components comparable to soft gelatin. Together with the *epithelium*, the superficial layer makes the so-called *mucosa* as a covering texture, similar to the other internal cavities of the body [69].
  - ▷ the intermediate one (IL, thickness $\approx$ 1 mm), has almost the same components as the superficial layer but with a higher density.
  - ▷ the deep sublayer (DL, thickness $\approx$ 1 mm) is mainly composed of collagen fibers, and constitute the so-called "vocal ligament" together with the intermediate layer.

  The structure of the *lamina propria* evolves by age and the intermediate layer has been found to become thinner as the person gets older [94]. As a whole, the LP is known to contribute to the tissue's "passive" biomechanical properties and to the regulation of its water content.

- The inferior thyroarytenoid muscle or ***vocalis*** also called "vocal muscle" (V, thickness $\approx$ 7-8 mm) is the deepest layer of the vocal folds. It is the "active" part of the tissue by contraction of its muscular fibers. This part occupies the most of the tissue's volume. Fine-tuning of the tension in the LP fibers and rapid shortening of folds are also attributed to the *vocalis* muscle [221].

Vocal folds are often simplified as a **bi-layered "body/cover" system** [91], as displayed in Fig. 1.2 : the "body" includes the *vocalis* muscle and the deep layer of the *lamina propria*; the "cover" includes the *epithelium*, the superficial and intermediate layers of the *lamina propria*. This concept, introduced to model the vocal-fold vibrations, suggests that the vocal fold can be grouped into two tissue layers with different histological and, thus, mechanical properties [210].

**At the scale of the tissue components**

Both *lamina propria* and *vocalis* layers can be seen as composites made of a soft gel-like matrix (comprising cells and ground substance of the ECM), reinforced by a network of

fibres.

*Cells and ground substances*

- Cells are mostly concentrated inside the deep layer of the *lamina propria* and the *vocalis*, while the superficial and intermediate layers of the LP have extracellular texture. The three types of cells found within these major layers are the fibroblasts, the myofibroblasts and the macrophages.

- The ground substance of the ECM contains biological macromolecules such as proteoglycans, glycoproteins and glycosaminoglycans (GAGs). GAGs are long polymeric chains of repeated disaccharide units. The largest and most uniquitous GAG is **hyaluronic acid (HA)**. By forming a hydrogel network structure, HA regulates the water content of the ECM. This component is no more regarded only as a filler, but also known to deliver multifunctional roles in the repair, regulation and protection of the interstitial content of tissue. Like all the hydrogels, HA also gives damping features to the tissue by dissipation of impact energy received during the periodic collision of the folds [127]. The distribution of HA in the tissue was found to be gender-dependant [79, 81], but it was not considerably varied with respect to age. Quantitative analysis of HA distribution in the LP of normal human tissue revealed a relatively less amount of HA in the more superficial depth of females, while higher content found in the deeper layers [25].

*Fibrous networks* – The fibrous proteins found within the ECM matrix of the human lamina propria are collagen and elastin. Collagen is, by weight, the most abundant fibrous protein in the LP, representing at least 50% of the total proteins (less than 10% for elastin) [77, 78, 146, 207]. Regarding the *vocalis*, it is primarily made of muscle fibers (also called "muscle cells" or "rhabdomyocytes"), wrapped together by connective tissue sheaths dominated by collagen in mass. As shown in Fig. 1.3, recent micro-imaging techniques have allowed to observe these different fibrous networks in 3D, and to progress in the quantification of their major micro-structural descriptors at rest (waviness, diameter, density and orientation of fibers).

- **Collagen** fiber is known as the most abundant and also strongest protein in the human body. It is composed of triple helix of molecular polypeptide chains. Beside its role for strength of tissue in tension, it is also responsible in remodelling during growth and wound healing. Among the multitude of different types of collagens, six of them can be found in the vocal tissue[50]. Type I and III are however the most abundant species. Each collagen fiber can be seen as a bundle of quasi-aligned collagen fibrils with wavy shapes and preferred orientations at rest.
  Quantitatively, in the LP layer, the volume fraction of collagen is reported to vary between 0.15 and 0.55 depending on the tissue depth [23, 153, 207]. While collagen fibril's diameter is known to range between 10 nm (collagen Type III) and 500 nm (Type I), collagen fibres are often grouped into larger bundles of average diameter lying from 1 to 20 $\mu$m (Fig.1.3 b,c). The spatial period and amplitude of wavy collagen fibrils at rest is found within the corridors (10–70 $\mu$m; 1–10 $\mu$m) respectively [7, 15, 148,

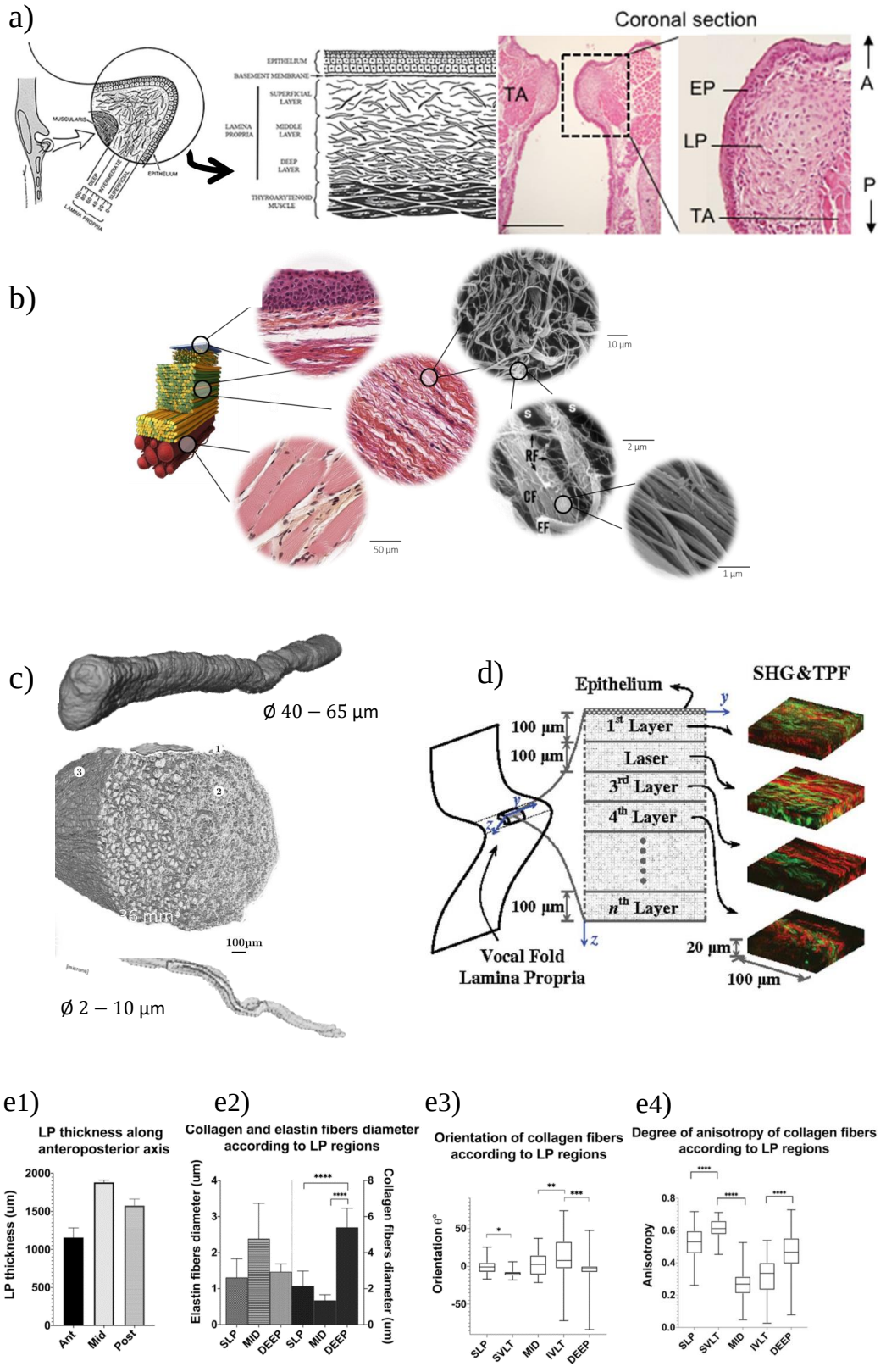


**Figure 1.3:** a) Schematic distribution of fibrous content in typical images of elastic and collagen fibrils networks [70]; b) Multiscale microscopy of the tissue histological features; c) 3D reconstruction of a *vocalis* sample imaged by synchrotron high-resolution X-ray micro-tomography reported by Bailly et al. [9]; d) Three-dimensional reconstruction of the SHG and TPF sectioning images [148]; e) Quantitative analysis of the SHG imaging techniques (SLP: superficial *lamina propria*; MID: intermediate *lamina propria*; DEEP: deep *lamina propria*; SVLT: superior vocal ligament transition) [15]

153]. At rest, the 3D angular distribution of collagen fibrils in the *lamina propria* shows a pronounced preferred orientation along the antero-posterior direction and a slight orthotropy in the perpendicular plane [7, 153]. The alignment with the vocal-fold edge seems predominant in the superficial and deep sublayers (Fig1.3 e3).
In the *vocalis*, the volume fraction of collagen is found around 0.05 to 0.15 [210]. Mean tortuosity and diameter of collagen fibrils can be considered similar as in the LP layer.

- **Elastin** fiber is believed to contribute more to the elasticity/flexibility/resilience of the tissue. With respect to the other elastic tissues of the human body ($\approx$ 3% of total protein in skin), it constitutes a high portion of the vocal fold tissue [76, 80]. Elastic fibers (mean diameter 1-3$\mu$m) are thinner than collagen fibers, as shown in Figure 1.3 e2. They are made of fibrillin, forming a network of microfibrils (10 nm in diameter) embedded in a cross-linked elastin larger mass.

- In the *vocalis*, the skeletal **muscle fibers** can be seen as a bundle of quasi-aligned myofibrils with wavy shapes and preferred orientations at rest. Myofibrils volume fraction are found within the range 0.60 to 0.80 [210]. While the equivalent myofibrils diameter is around 1 $\mu$m, muscular fibre have a cylindrical shape with much thicker diameter (10-100 $\mu$m) as shown in Fig.1.3 b,c. Spatial period and amplitude of wavy myofibrils can be found around (1300–1700 $\mu$m; 70-140 $\mu$m) respectively, being much straighter than collagen fibers at unloaded state. Regarding their 3D fibre orientation distributions, muscle fibres are mainly aligned along the anteroposterior axis, with a transverse isotropy texture [7].

Quantitative values of each microstructural descriptor fluctuate with the gender or age. Additionally, the composition and homeostasis of fiber/matrix components can be impacted when the tissue is subjected to the pathology, surgery or treatment, which in turn disrupts the normal phonatory performance. Hence, diagnosis of the healthy or malignant tissue is highly dependent on our knowledge of the organization of the tissue fibrous network. In the end, all these specific histological properties are responsible for specific mechanical properties of the vocal folds, which are presented in the next section.

### 1.1.2 Mechanical behaviour

The mechanical characterization of human vocal folds has remained a challenge for several decades, due to inter/intra-subject variability, their specific anatomical localization that is not easily accessible by any 3D imaging technique, and their very small dimensions. In the following section, the physiological loadings of the vocal folds encountered during phonation are summarised, as well their mechanical response *in vivo* and *ex vivo*.

### Physiological loadings

During phonation, vocal folds are deformed due to pulmonary airflow and laryngeal motions, enduring vibrations of various amplitudes, frequencies, and degrees of collision. These multiple configurations imply complex and coupled multi-axial mechanical loadings experienced by the tissue upon finite strains and at various strain rates. More particularly, three major loading modes can be found in physiological conditions, as described below and illustrated in Fig 1.4 [146, 216] :

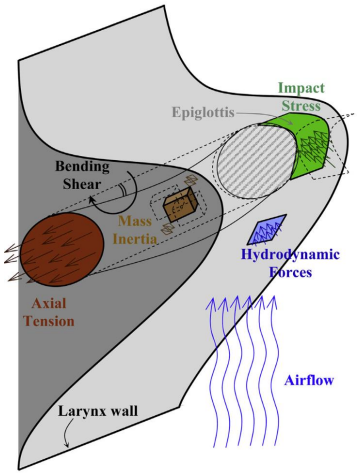


**Figure 1.4:** Scheme of physiological loadings on human vocal folds during phonation. Extracted from [146].

These loadings include combined longitudinal tension and compression which are mainly due to laryngeal muscular contractions along the antero-posterior (or longitudinal) direction; but also transverse compression due to aerodynamic forces and vocal-fold collision along the medio-lateral direction; and longitudinal and transverse shears due to oscillatory motion along the infero-superior direction and friction stresses between both vocal folds.

- **Longitudinal tension** – phonation starts with the act of adduction which applies a quasi-static tensile stress on the tissue in longitudinal direction and the tissue will remain stretched as long as the phonation continues. The magnitude of the tensile stress at this state is reported in the order of few to several hundreds of kPa.
- **Hydrodynamic forces** – The pressure of the compressed air on the surface of the tissue exerts a combination of small shear and compressive force in the range of less than 5 kPa.
- **Compression** – by start of the oscillation the mucosal wave provokes a shearing stress inside the tissue in superior-inferior direction (coronal plane?)
- **Shear** – by start of the oscillation the mucosal wave provokes a shearing stress inside the tissue in superior-inferior direction (coronal plane?)
- **Impact loads** – In the normal phonation, each cycle of vibration is accompanied by a full collision of the both folds upon the closure phase of the glottis to create the pulsed air wave. Therefore it varies depending on the frequency of vibration and can impose compressive forces in the mediolateral axis at the order of 0.1 to 5 kPa.

- **Inertial stresses** – The act of acceleration and deceleration of the tissue which contain high fluid content, causes an inertial force inside the tissue.

### *In vivo* mechanical response

In order to measure the response of the such complex loading, different experimental methods has been developed in the recent decades.

Reproduction of the same physiological condition is the main challenge in the mechanical characterization of the tissue. Therefore, *in vivo* techniques provides the closest measurement condition to the realistic environment of the VF response to the applied loads. In this regard, several *in vivo* methods were developed during the last decades. From the employed instrumental point of view, we can classify them into direct contact measurement or the models based on acquired data through imaging techniques:

One of the first attempt to measure the vocal fold mechanical properties was an aspiration tool proposed by Tanaka and Hirano [206] based on a fiberscope, capable of sucking the tissue inside a tube as an indicator of the tissue stiffness. The stiffness values was estimated about 3 to 4 g/cm for healthy folds, while it was obtained significantly greater in case of cancerous tissue(>20 g/cm). However, intrinsic heterogeneity of the tissue prevents obtaining accurate results in such measurement approach. Berke[16], later used an intra-operative tension meter to extract transverse (horizontal) elastic modulus from the applied force-displacement data of a canine model. The outcome of the study confirmed a decrease of elastic modulus in acute laryngeal paralysis as an index of mucosal wave biorheology, nevertheless, neglecting the stress relaxation and strain creep arising from the viscoelastic nature of the tissue interrogates the validity of results. The same device was further improved [223] and known as modified "Jako laryngoscope" (Fig. 1.5 a–top) in order to take a more objective approach for the inspection of abnormal stiffening of the human vocal folds. The obtained response of the tissue at rest was reported in terms of the mean shear modulus of 12.6 kPa. Exposing the tissue to the low and high transcutaneous nerve stimulation also resulted in 12.1 and 21.5 kPa respectively. Anyhow, the young's modulus increased linearly with displacement, for all stimulation conditions as shown in Fig. 1.5 a–bottom). The discrepancies of these results with the previously reported values of longitudinal Young's moduli, [5] was justified by the sensitivity of the devise and the *in vivo* nature of the measurement.

Additionally, the above-mentioned measurements were done under general anaesthesia which in turn provokes further deviation of results from the values of realistic (in motion) condition.

Later advances in medical imaging techniques allowed the use of mucosal wave propagation to explore the biomechanical characterization of vocal tissue[165, 197] without invasive impacts. Quantification of elastic properties was also performed by color Doppler imaging combined with the ultrasonic scanner [100] as a non-invasive method which was no more under anaesthesia (Fig. 1.5 b–top). Results revealed a range of Young's moduli values of 30

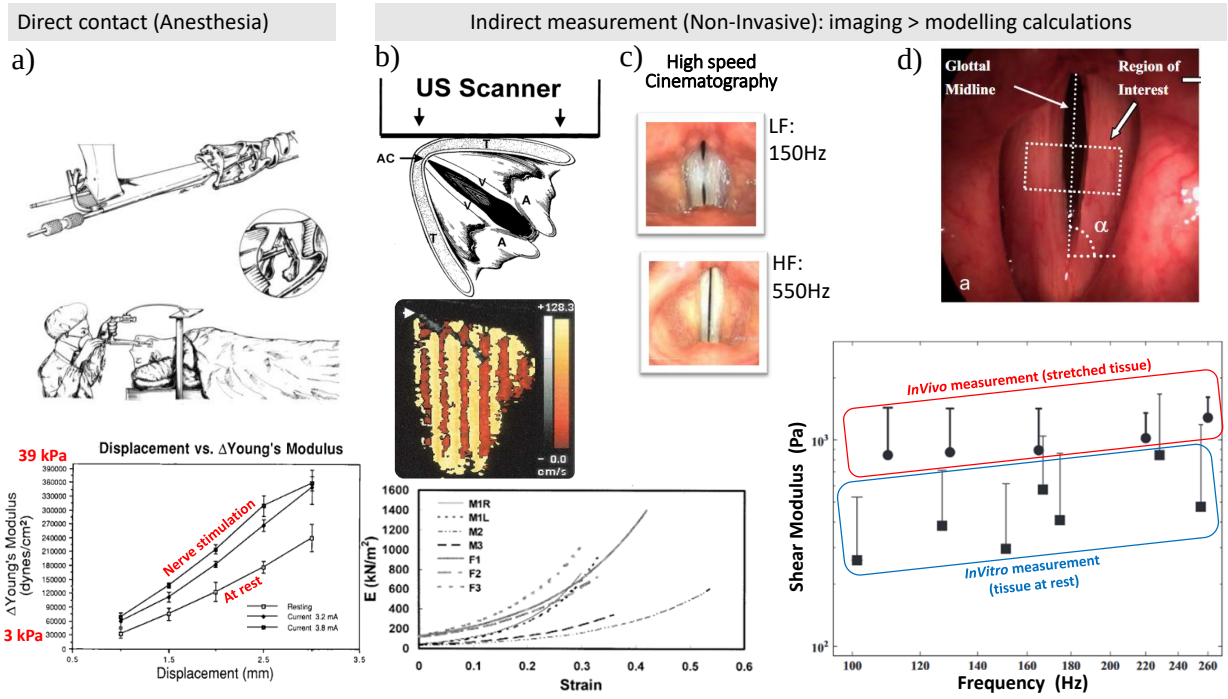


**Figure 1.5:** *in vivo* characterization of the vocal folds acquired through: a) Direct contact method: Jako Laryngoscope (top), and obtained evolution of elastic moduli [223]; b-d) indirect image processing techniques: b) Nonlinear response of the VF computed based on mucosal wave (color strip) propagation speed obtained by US and CDI techniques [100] c) Extension of vocal folds at low and high frequency ranges in Video-LaryngoStroboscopy to d) Estimation of the shear modulus based on HSDI and MRI methods and viscoelastic model [110].

to 120 kPa for male and 120 to 300 kPa for female individuals. They have also measured the effective vibrating lengths of the vocal fold in low pitch about 1.4 to 1.6 cm and 1.3 to 1.5 cm for men and women, respectively. This lengths extended to about 1.7 to 1.8 cm in pitch over an octave higher and the stress-strain relation was nonlinear (Fig. 1.5 b–bottom and 1.5 c). However, in the range of lower pitch, the stress-strain response of the VF was reported relatively linear. Later, HSDI (High speed digital imaging) and MRI as non-invasive imaging techniques [110] were used to calculate the *in vivo* transverse shear modulus. This was achieved based on Voigt viscoelastic model and the principles of Rayleigh wave propagation for the mucosal wave at various phonation pitches from 110 to 440 Hz. The results of this study revealed that due to the inherent viscoelasticity of the tissue and increased applied tension on it at higher pitches, the shear modulus is generally rising with the increase of voice pitch(Fig. 1.5 d–bottom). Also an enhancing effect of large deformation in the VFs during phonation can be seen on the shear modulus compared to the same results obtained by *in vitro* shear rheometry without extension[39].

Generally, *in vivo* techniques provides rapid and **non-invasive** tool to measure the response of the vocal folds to the multiple loading configuration. Qualitatively, mechanical indicators leads to the detection of tissue disorders through the variation of stiffness values. These techniques were also capable to record the **large deformation** of the tissue at the range of **10 to 50** % of strain over an increasing range of the voice **pitch** ( **50 to 500**

**Hz**). Reported values of the tissue **stiffness** are relatively dispersed (**10-1000 kPa**) but they validated the **nonlinear** trend of the tissue response to the applied stresses. *in vivo* results revealed a strong dependence of the elastic and shear moduli on the frequency of vibration and applied strain, nevertheless, reliability of results are highly sensitive to the employed methodology and patient subjects.

***Ex vivo* mechanical response : quasi-static and dynamic loadings**

As discussed in the previous section, *in vivo* techniques for characterization of the tissue mechanical properties are limited to the image processing data. Hence, there is restrictive challenges to measure the realistic loadings applied to the tissue. In order to overcome the shortcomings of the *in vivo* techniques, *ex vivo* approaches were employed to quantify some of the mechanical characteristics . The objective here was mainly to provide easier access to the tissue sublayers and also distinguish/determine the different response of the tissue to the different axial and phonatory *in situ* loading condition. (...even though all the performing condition of the vibrating tissue was not possible to be conserved compared to the natural anchorage of the tissue environment *in vivo*).

The primary mechanical factor for the tuning of the voice pitch is believed to be the **stiffening** of the vocal folds through the contraction and stretch of the tissue in longitudinal axis. Thus, **quasi-static** uniaxial tensile setup (fig 1.6 a) were designed and measured the longitudinal Young's modulus of body and cover as about 20.7 and 41.9 kPa respectively for the excised vocal folds at the frequency range of 0.1 to 10 Hz [5]. Results of such studies [5, 38, 172] at first sight display the **nonlinear** response of the tissue to cyclic stretch-release loading as a main identity of the vocal fold tissue. This evidence can also explain the broad variety of the values of the elastic modulus reported in the last section (*in vivo*). Moreover, inter-layer **heterogeneity** in the mechanical response of the tissue was observed which indicates different stretchability of the sublayers that in turn arises from the variation in the distribution of density and morphology of fibrous content of the tissue discussed earlier in section **??**.

On the other hand, investigation of the **dynamic** response of the tissue, the shear rheometry is the most frequently employed technique to obtain the frequency dependence of elastic shear moduli of the excised vocal folds [36, 37, 66]. Despite the limited range of the surveyed frequencies (usually <50 Hz), results were highly dispersed in wide range of values from 0.01 to 3.3 kPa (fig 1.6 b).

Such large discrepancies in the acquired moduli values, highlights the necessity of the compatible characterization method for delivering actual description of the mechanical behaviour compatible with tissue circumstances. To this end, a test-specific preparation method was developed by Miri et al [147, 149] in order to provide a consistent measurement of the elastic properties in traction and shear modes on the excised porcine tissues (due to their high similarity to human VFs in composition and phonatory properties) as shown in Figure 1.6 c (left). The stiffness ratio turned out to be within the range of 5.19 to 7.11 over the frequency range of 0 and 8 Hz (Fig 1.6 c (right)). Due to the substantial presence

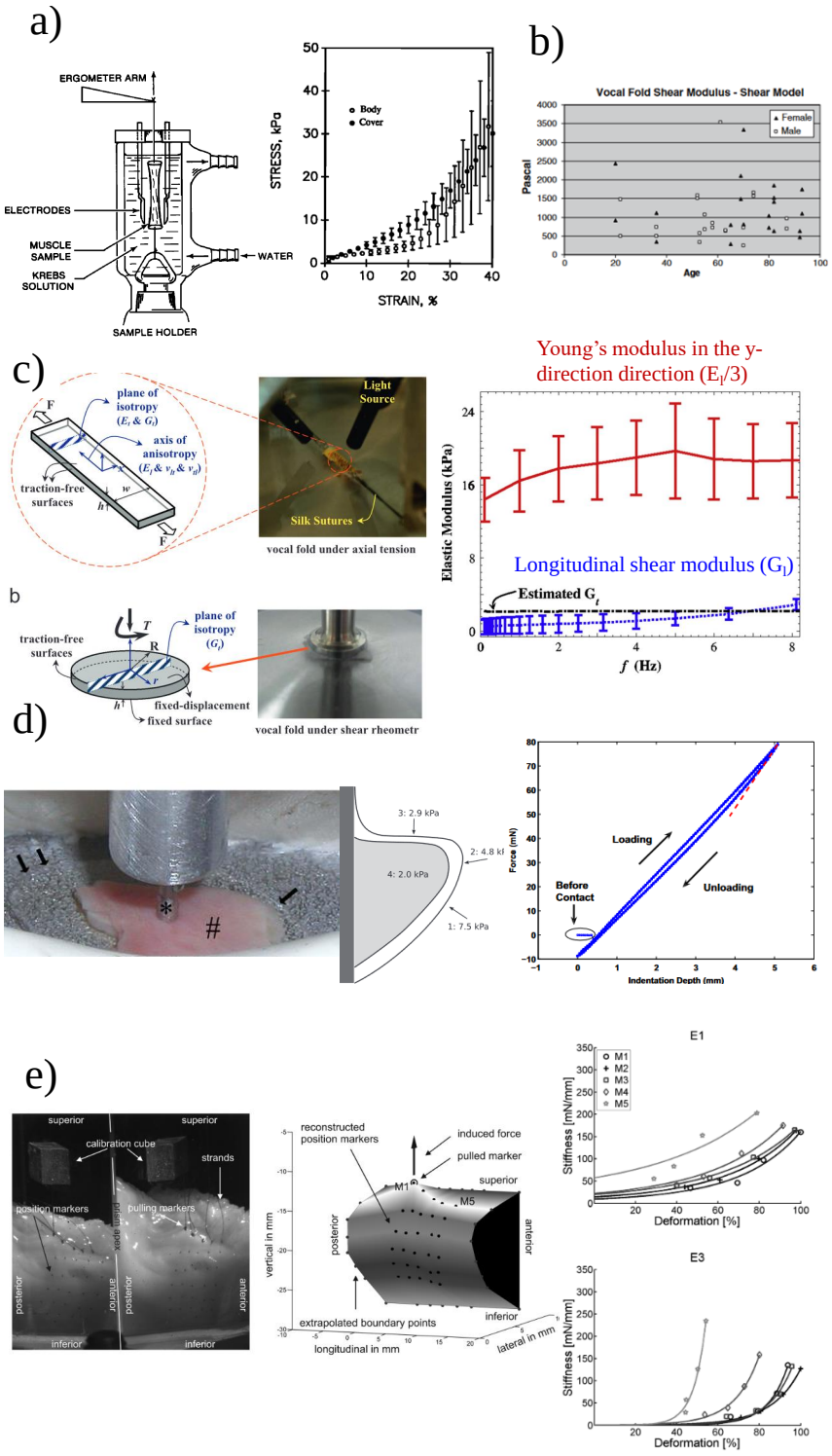


**Figure 1.6:** *ex vivo* characterization of the vocal folds: a) schematic of the axial tensile setup and corresponding obtained response; b) Distribution of shear moduli with age; c) Porcine vocal fold sample under traction-test and shear-rheometry(left), Transversely isotropic moduli (right); d) Indentation setup, Coronal section of ex vivo vocal fold illustrating the order of the estimated Young's modulus from stiffest (1) to softest (4) : 1 = medial inferior cover; 2 = medial cover; 3 = superior cover; 4 = TA muscle (body), and the typical loading response for the calculation of Young's modulus (slope (dF/dh) at the initial portion of the unloading cycle (red line)); e) The prism of a vocal fold with sewn position markers and 3D reconstruction of the vocal fold surface (left), Stiffness *vs* normalized deformation for a male (E1) and female sample (E3)

of the collagen fibres in longitudinal direction (anterior-posterior axis), tissue shows its greatest stiffness in this direction. This in turn provokes large variation in the achieved tensile elastic properties. Moreover, an analytical quantification on a simple Timoshenko beam model [228] of the vocal folds estimated a 20 % **anisotropy** effect on the fundamental frequency using achieved moduli.

The Validity of the *ex vivo* loading configuration aws also investigated by Chhetri [41] using the cylindrical probe indentation method on the intact and dissected vocal fold tissue. obtained a range of 4 of 13 kPa values for the stiffness as shown in Figure 1.5 d. The stiffness of the vocal folds was the highest in a hemilarynx setting when the vocal fold structure was still attached to the laryngeal framework. When the vocal fold was separated from the laryngeal framework and each part was isolated, the stiffness changed from the highest to the lowest as depicted in Figure 1.6 d.

In order to provide a 3D distribution of local deformation field along the whole superior surface of the vocal fold tissue, Döllinger *et al.* [51] used static tensile loading on a grid of suture points in a hemilarynx configuration. Results of this study offered an nonlinear rising trend of stiffness ratio from the posterior to the anterior region. The deformation trend can be divided into two parts: A range with a small slope for small deformations (range I) fading over to a range with a high slope (range II). The boundary between the two ranges is approximately at 25% to 30% normalized deformation. Another advantage of the setup is the ability to be combined with the dynamic experimental model. However, the anterior-posterior tension of the tissue was still missing in the setup and the applied deformation was limited to 30 %.

In a recent study, Cochereau *et al.* [43] performed a multiaxial characterization of the excised human tissue under quasi-static ($10^{-3}\ s^{-1}$) configuration (Fig.1.7). This work provides for the first time, the cyclic response of the same tissue sample to the applied finite strain in tensile, compressive and shear loading modes. The significance of the last the last two loading condition in the entire performance of the tissue has been previously highlighted through many simulation studies [146, 226] as illustrated in the schematic distribution of stress field in Figure 1.7 a, despite its negligence in many experimental records. These experiments were also carried out on the tissue sublayers: *vocalis* muscle and *lamina propria*.

Generally, the typical nonlinear strain-stiffening response of the tissue was markedly obtained in tension and compression. In order to prevent damages to the tissue structure before the subsequent loadings, the applied strain was limited to 10 - 25 % in these loading modes. In both loading modes *lamina propria* appeared to be much stronger than *vocalis*, which clearly demonstrates the enhanced contribution of the fibrous content in LP. Concerning the effect of loading mode, the anisotropic nature of the tissue results in higher stress values in longitudinal tension, while the compressive and shearing response of the tissue stay in the same lower order of magnitude. This can be ascribed to the preferential orientation of the collagen and elastin fibers in the longitudinal axis discussed earlier in this chapter.

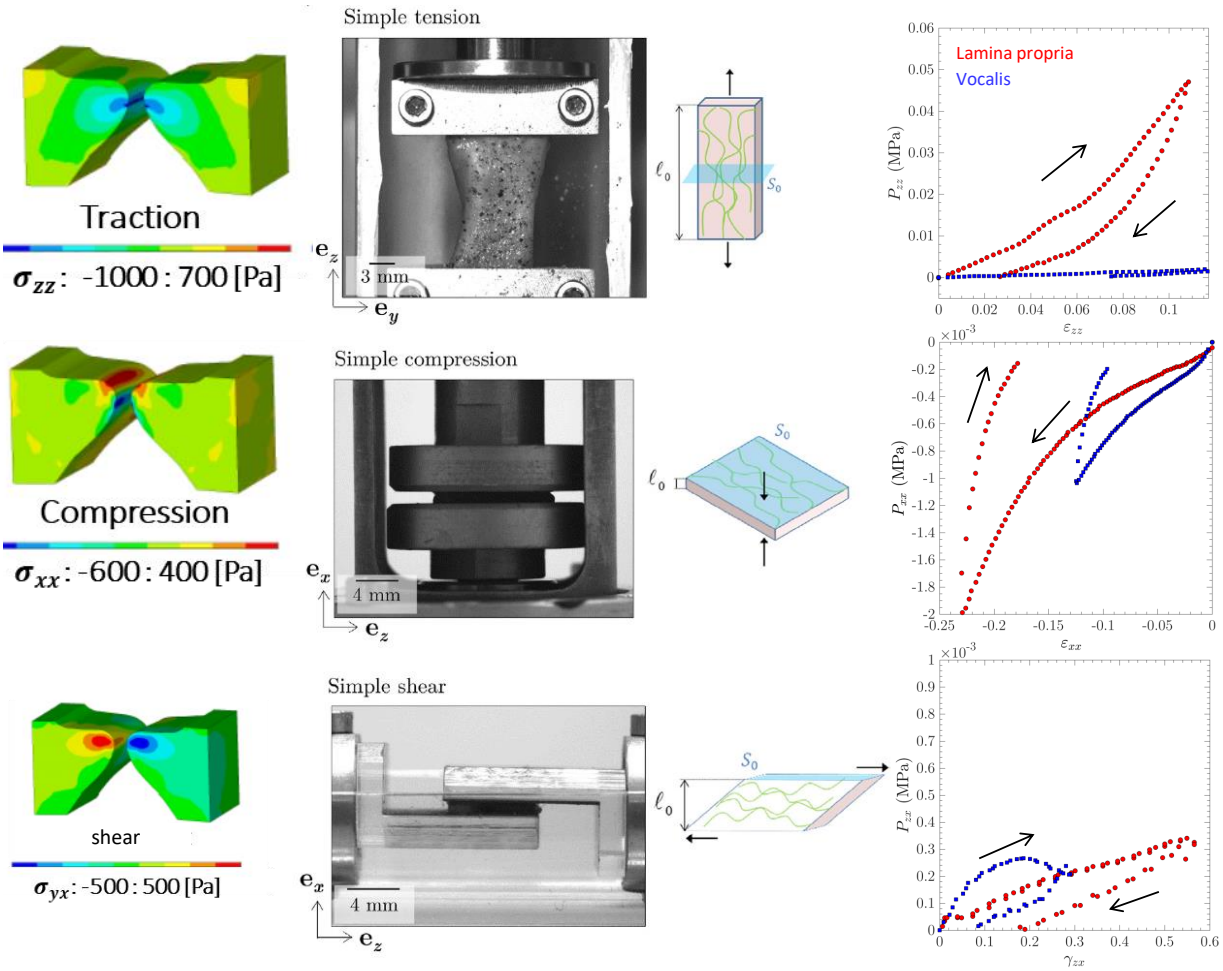


**Figure 1.7:** Stress distribution field within the vocal fold [226] (left) and cyclic multiaxial response of the vocal folds sublayers[43](right)

By including the multiaxial solicitation of all the tissue sublayers, these results constitutes a comprehensive database for the design of bio-mimetic materials and development of the more realistic *in vitro* models of the vocal folds to clarify the link between their mechanical characteristics and corresponding vibratory performance.

### 1.1.3 Effects of the hydration level of the tissue on mechanical properties

Another important factor that should be taken into account for a reliable mechanical characterization is the hygrometric dynamics of the tissue environment.

Several studies have shown that vocal fold hydration level is a decisive physiological variable in regulation of the vibration pattern, voice quality, and vocal health in general. As the major volume of the ECM is occupied by water, the loss or uptake of humidity will highly contribute to the definition of viscoelastic properties of the tissue and consequently the required phonatory effort (PTP= phonation threshold pressure), particularly at high pitches[60].

The hydration contributes at three different levels, including body hydration (at the systemic level), vocal fold hydration (at the local tissue level), and vocal fold surface hydration (involving mucous and luminal fluid in the airway). The biomechanical hypothesis on the involvement of such hydration levels on the dynamics of vocal folds oscillation was investigated in many studies.

The hypothesis of the inverse dependence of phonatory effort on the Hydration level has been validated for high-pitched phonation tasks [229]. This fact is mostly attributed to the variation in speed of mucosal wave propagation, damping coefficient and decrease in the viscosity of the tissue.

The effects of hydration on the mucosa was validated and quantified by torsional rheometry (Fig.1.8 a) at 0.01 to 15 Hz frequency range [34]. Their study result demonstrates the Elastic shear modulus (G′) and dynamic viscosity ($\eta'$) of the samples were increased significantly (order of 4-7 fold) by osmotically induced dehydration and decreased by 22-38% when subjected to rehydration. The same trend for damping ratio ($\zeta$) were also observed but in smaller order.

Other studies showed that even while the tissue is systematically getting rehydrated from the ligaments, exposure of the mucosa to the dry air (0%RH) also causes significanly faster rise of the viscosity and stiffness as shown in Figure 1.8 b (red arrow), compared to samples oscillated under humid (100%RH) air[84].

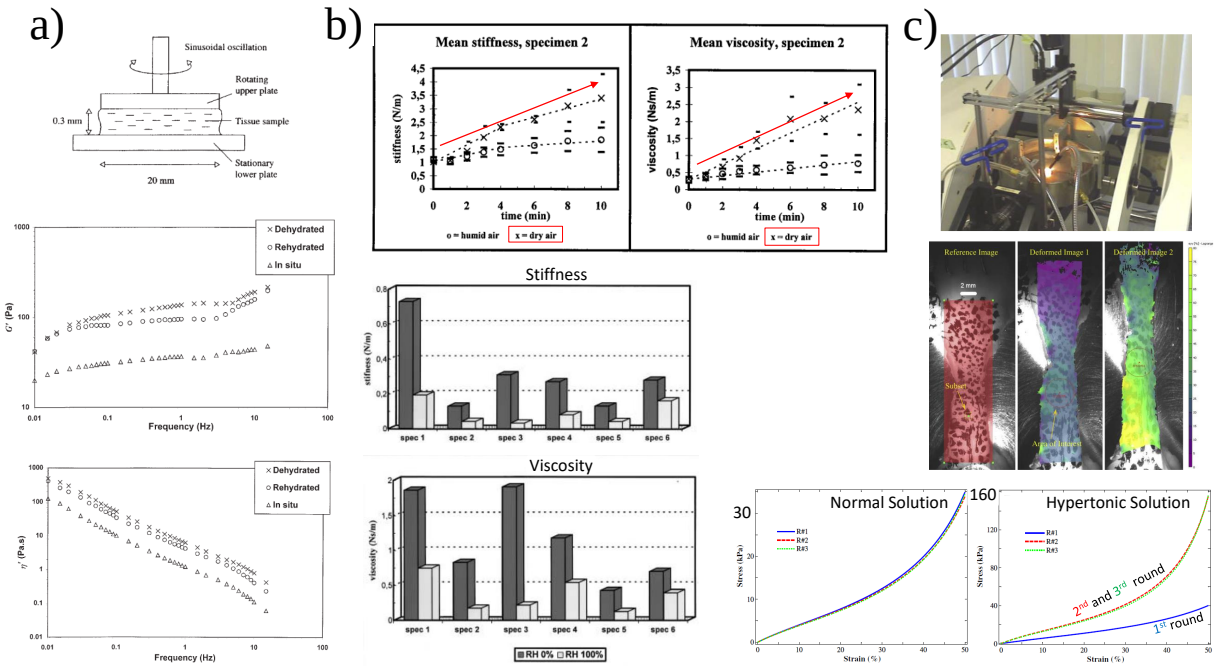


**Figure 1.8:** Effect of hydration level on the viscoelastic properties of the vocal tissue: a) Rheology of the dehydrated and rehydrated tissue[34], b) Increase of the mean stiffness and viscosity of the tissue exposed to dry air as function of time [84], c) Tensile response of the porcine VF tissue immersed in normal (left), and hypertonic (right) solutions under quasi-static longitudinal loading[147]

The vocal folds are also subjected to quasi-static large-amplitude oscillation in transverse plane. Therefore, the impact of tissue dehydration on the stiffness evolution under such

loading condition must be well understood. Miri *et al.* [147] performed quasi-static and dynamic (1 Hz) ramp loading up to 50% strain on the dehydrated *lamina propria* of porcine tissues (Fig.1.8 c). The dehydration was carried out by submerging tissue in hypertonic solution (30% NaCL). Results of this study revealed:

- an increase of mechanical energy loss ($\zeta$) by factor of 5 to 7 caused by an estimated 20 % of water loss (tissue porosity=80%). Note that the phonation occurs when there is a small energy loss in LP (usually ($\zeta$) <10%).
- Shear modulus ($\mu_0$) (which is known as an index of the viscoelastic behaviour of the tissue) was also 4-fold increased for dehydrated samples.
- a poor dependence of dynamic stiffness (tangent modulus) on the water content than in quasi-static loading. This result also sheds light to the fact that rehydration is much more important for long and continuous high-pitch phonation where the VFs are extended for long periods of time.

The significant influence of ambient humidity on the vibratory performance of VF is inevitable. However, such an influential fact was poorly taken into consideration in the choice of vibrating materials for the design of larynx in vitro models (and also its mechanical characterization). Thus, it seems there is an evident need to conduct the strategy towards the development of (bio)materials that can actively interact with the environmental condition, including humidity.

In broad terms, the response of the vocal folds tissue to the collection of physiological loading at wide range of oscillation frequency can be summarized as follow: Vocal folds tissue are capable to maintain their oscillation at a wide range of **fundamental frequencies of 50 to 1500 Hz** while undergone **large reversible deformations** from **10 to 50** %.

Under tensile loading, the fibrous composition of the tissue results in a **nonlinear** behaviour upon the applied finite strain. Shear rheomtry of the tissue also suggests a **viscoelastic** response due to the highly fluid-rich nature of the ECM. Particular orientation of the fibrous content of the tissue causes an **anisotropic** nature of the mechanical properties. Considerable adaptability of the mechanical response with the degree of relative **hydration** in the phonatory state of the VFs is also a remarkable feature.

It worth mentioning that many basic presumptions has been adopted to establish the description of mechanical response (including the incompressibility, low frequency, linear-based modulus) which lead to understated hypotheses in descriptive models. Although all these simplifications in the models helps to identify the proper role of each factor, the realistic investigation of the mechanical behaviour within a comprehensive **multiaxial loading** under proper **environmental** condition and also considering the inter-individual parameters is essential to suggest a reliable characterization of the VF behaviour.

### 1.1.4 Vibratory properties

From the phonatory point of view, larynx can be divided into the superior and inferior regions in the direction of airflow with respect to the position of glottis. Each part has specific role in the aerodynamic performance of the larynx [212].

**Subglottal area** is the region below the glottis where the airflow coming from the lungs is accumulated upon the closure of the glottis. In the production of speech sound, the subglottal system provides the energy in the airflow. This transfer of aerodynamic energy is created by the sufficient air pressure which excites the folds to vibrate and makes the basic tone of the speech. **supraglottal structure** is responsible for the modulation of the airflow to produce audible sound. During the normal speech supraglottal structures do not directly contribute to the formation of acoustic signal, and they have rather aerodynamic role by regulation of pressure and maintaining a constant flow rate through the transglottal constriction. Also, for the professional singers, supraglottic constriction function is of great importance at pitch extremes [173, 213].

In this section the typical Vibratory characteristics of the vocal tissue during the (normal?) human phonation is briefly introduced. The phonation process is a result of periodic compromise between subglottal air pressure which tends to keep the glottis open and the elasticity of tissue to bring them back together. This repeating mechanism, coupled with the pressure drop caused by Bernoulli effect, triggers the oscillation of vocal folds (Fig.1.9 a) with a few millimeters amplitude [215] and consequently a pulsatile air flow and the acoustic wave which is known as the voice basic tone.

The fundamental frequency of this vibration can vary from 50 to 1500 Hz in human; however, in the normal speech this range is limited to 100-150 Hz in males, 140 to 240 Hz for females and up to 300 Hz in children[203].

The required subglottal pressure for the start of the vibration- known as the “on-set” pressure- is a measure of voice intensity. This voice characteristic also spans from 300 to 3600 Pa. [103]

#### Resonance and damping properties

In order to characterize the dynamic characteristics of the vocal folds’ oscillation, the resonance approach is usually adopted. Modal analysis is a basic technique traditionally used to evaluate the performance of many vibrating structures. It consists of the process of defining the normal modes of a linear system. It is largely adopted due to the fact that it allows a decomposition of the system into a set of observable independent oscillation patterns with corresponding characteristic frequencies, facilitating the interpretation of complex three-dimensional patterns of vocal folds.

#### Eigenanalysis

Such analysis allowed to detect a limited predominant mode which can predict the essential dynamics of up to 98% of the nodal trajectories of normal phonation and 70% of irregular one. Titze and strong[218] defined for the first time an infinite number of the eigenmodes and their corresponding displacement patterns of the vocal folds(Fig. 1.9 c).

The empirical eigenfunctions was extracted later from the biomechanical simulations of normal and chaotic vocal folds vibration with an acceptable accordance to the low-order theoretical normal modes[17].

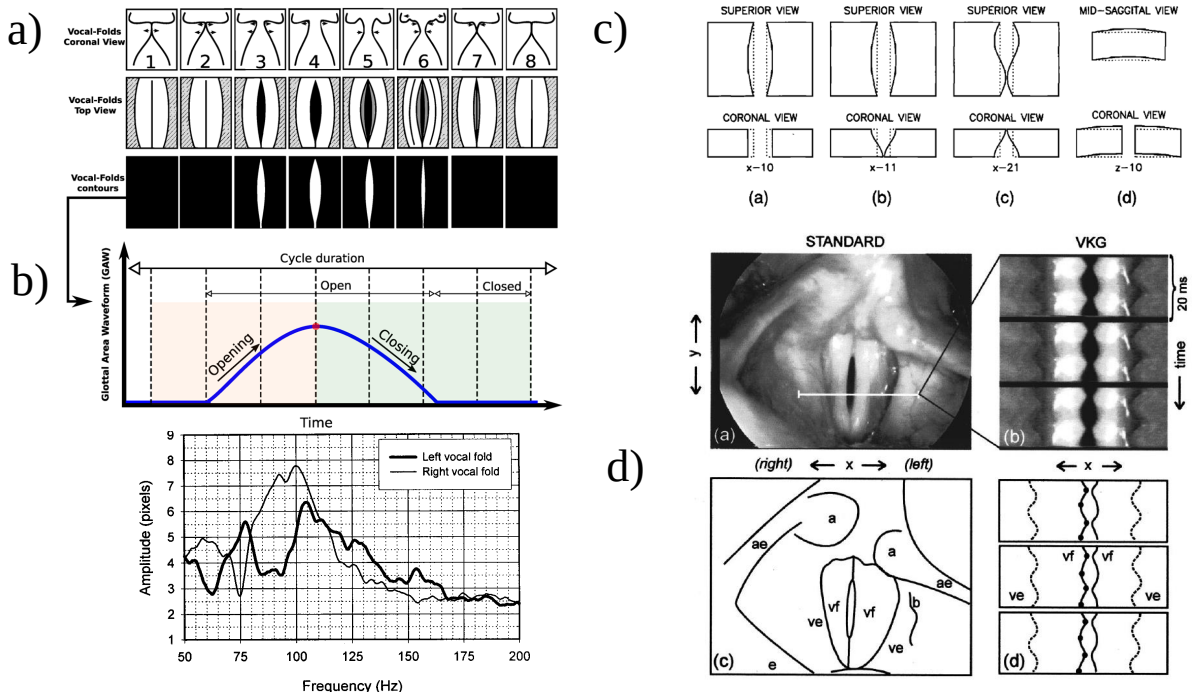


**Figure 1.9:** a) Illustration of the vocal folds motion during a phonation cycle[6], b) Frequency response functions of the vocal folds at low frequency ranges[205], c) Superior and coronal views of a few low-order, theoretical, normal modes[17], d) Standard and videokymographic (VKG) images of the larynx. Standard, laryngostroboscopic image of the vocal folds in neutral phonatory position and their sketches below[205]

Resonance frequencies and corresponding eigenmodes were observed by external excitation using a shaker and the resulting vibratory pattern was captured by means of Videokymography and Videostroboscopy (Fig. 1.9 b)within two distinct high and low frequency sweeps of 100 to 400 Hz and 50 to 200 Hz[205]. The results revealed three distinct resonance peaks at frequencies of 110, 170 and 240 Hz were detected which are associated with the x-1, x-2, and x-3 modes respectively (1, 2, 3 being the number of the half-wavelengths along the longitudinal axis of the vocal folds) (Fig. 1.9 c).

Psg, etc...

### Influence of environmental changes (RH, T, surfactant)

As discussed earlier, exposure of the tissue to humid or dry ambient, highly contribute to the definition of viscoelastic properties of the tissue. Consequently, vibratory behaviour of

the tissue will be influenced, including the required phonatory effort (PTP) is , particularly at high pitches. *blabla...*

Finally, complex aerodynamics of the vocal folds vibrations are fully coupled with the mechanical and geometrical parameters. Thus the due to the highly limited *in vivo* access to the tissue, *in vitro* testbeds provides the opportunity to dissociate these parameters for an in-depth insight to the vocal folds perfomance.

## 1.2 Biomimetic materials

Main biomechanical characteristics of the tissue was discussed in the past section. Nevertheless, studying the influence of the variations in these properties on the resulting voice quality is further complicated due to the limited availability of the excised larynges and also difficulty of the *in vivo* measurements in the restricted/confined larynx environment. Therefore, *in vitro* models have been developed to provide a vast accessibility for the manipulation of all the involved parameters in the phonation process. This section deals mainly with the development of such *in vitro* models and particularly the materials used for the fabrication of vocal fold replica in these platforms. First part is dedicated to the group of works aiming to study the interaction of (aero) phonatory parameters and structural characteristics within the developed setup reproducing the laryngeal circumstances. In the second part the type of biomaterials used in clinical applications for the healing purposes are also discussed.

### 1.2.1 *In vitro* vocal-fold replicas for voice research

*In vitro* study of the human voice production based on the physical models has been subject of research since long-ago. Such physical models allow a geometrical simplification of the larynx complex architecture, which paves the way to measure and discover the interconnection of the involving parameters and mechanisms in the phonation.

The outcome of such physical models also make the input data for the design and validation of the theoretical and computational models and thus plays a complementary role towards a more precise quantification of phonation physiology and biomechanics.

#### Classification : Rigid static/ Externally-driven/ Deformable self-sustained

*In vitro* models can be divided into three groups based on their experimental strategy *i.e.* choice of vocal folds replica and its oscillatory motion as illustrated in Fig.1.10. These three classes include the **Static vocal folds models** (Fig. 1.10 a), **Externally-driven replicas** (Fig. 1.10 b), and the **Airflow-induced self-oscillating setups** (Fig. 1.10 c-g). First two groups are based on the models containing **rigid** pieces replicating the vocal folds. These models are intended mainly for the experimental investigations of **aerodynamic** performance in the

vocal apparatus, which are out of the scopes of current thesis. However, the last category involves a full contribution of the **structural dynamics** of the flexible vocal folds' replica, coupled with the flow-induced oscillatory response. Thus, in this part we focus on the evolution of the third group.

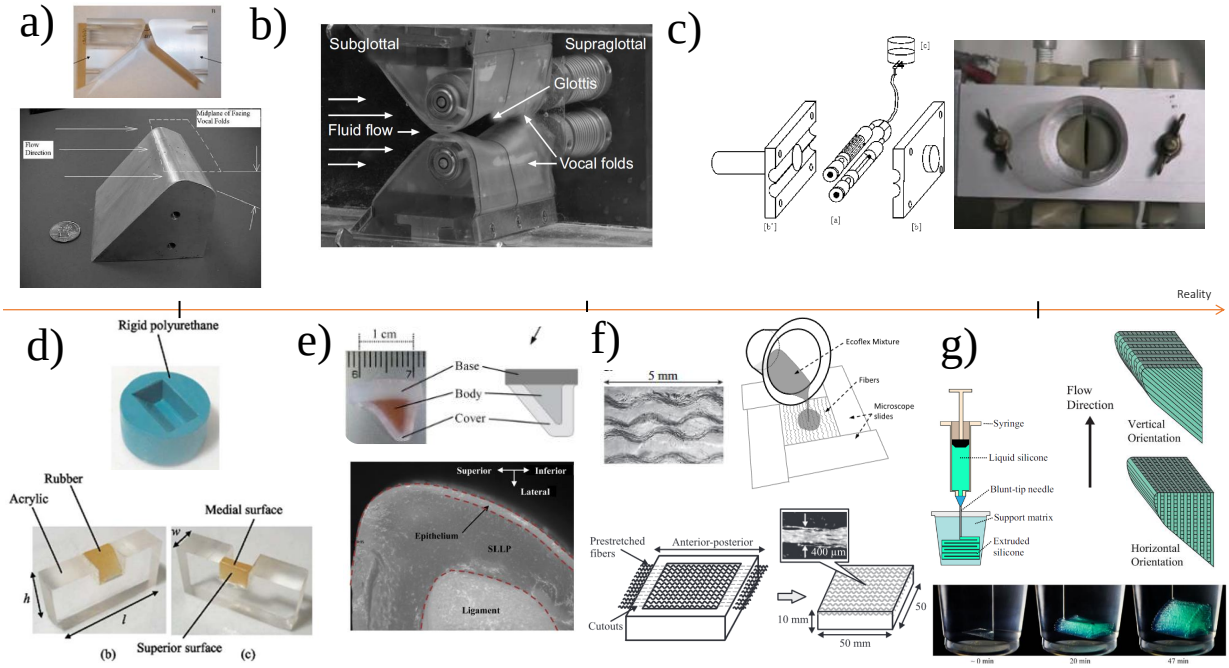


**Figure 1.10:** Evolution of different generations of the *invitro* synthetic models of vocal folds : a) Rigid, b) Externally driven [224], c) Soft membranous [7, 189], d) soft monolayer cast e) soft multi-layer, f) materially nonlinear, and g)3D printed models

The concept of **self-oscillating** vocal folds models is based on the elastic materials which are mainly simplified in geometry and the heterogeneity of the structure. The level of elasticity in such structures should be carefully regulated as it should deliver reversibility of periodic deformation (compressive and tensile) in the the structure induced by the aerodynamic force (Bernoulli effect) and hence, allows continuity of the oscillatory motion.

### Evolution of the synthetic *in vitro* models and corresponding mechanical characteristics

The evolution of the self-oscillating synthetic folds is presented here in five subcategory with a particular regard into the composition of the utilised material and the impact of their mechanical properties on the produced vibration.

The mimicry approach of using flexible vocal folds models was initially studied using **silicone membrane tubes** filled with liquid to act as the mucosa. This model allowed the measurement of the phonation threshold pressure for the obtained flow-induced self-oscillation at varying control parameters including the glottal width and the viscosity of the encapsulated liquid.

Apart from the viscosity of the fluid, the impact of the stiffness of the rubber tube was evaluated on the variations of fundamental frequency per transglottal pressure (dF/dP).

The stiffness was controled by varying the amount of injected air inside rubber tube and manual elongation of vibrating parts[167]. The negative correlation between $f_o$ and (dF/dP) in the results of this study was in agreement with the fact that the raising of human voices pitch is achieved by the contraction (and consequently stiffening) of the *vocalis* muscle. similarly, control of the water pressure in a pair of silicone tubes [189] has also lead to promising human-like phonation in terms of $P_{th}$, $f_o$ in the subglottal region.

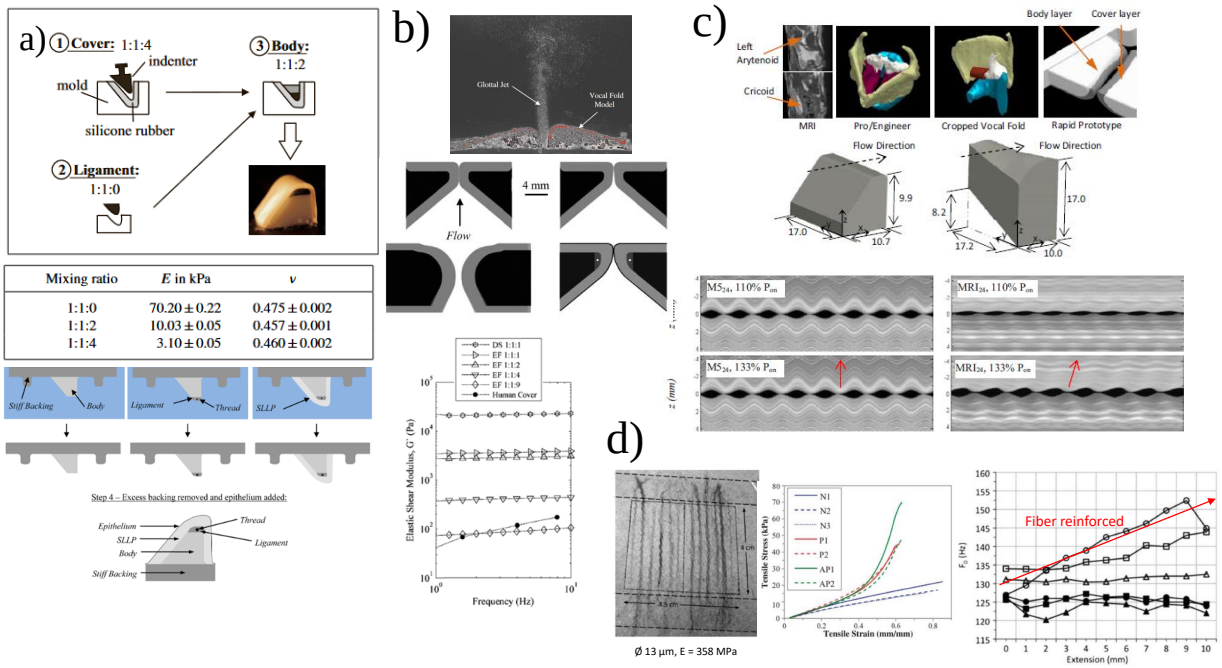


**Figure 1.11:** Examples of the synthetic vocal folds replica made of silicone rubber and corresponding mechanical and vibratory response : a) Design and fabrication procedure of the multilayer model and its stiffness values; b) comparative study of the geometry; c) Rheological characterization of the EF silicone under frequency sweep; d) MRI model and resulting vibratory pattern; e) Fiber reinforced anisotropic model, tensile behaviour and frequency response under elongation

With the membranous models however, it was difficult to vary and investigate the impact of models geometry on the aerodynamic and vibratory performance. In order to enhance the control over the geometrical characteristics of the replicas toward a more realistic modelling condition, they were fabricated using **castable elastic materials** inside the properly designed molds.

A first example of such replicas was investigated by Thomson *et al.* [213] using **homogeneous** polyurethane rubber based on the well-known M5 geometry proposed by Scherer *et al.* [190] in life-size scale. The elastic modulus of the material was reported as 13.7 kPa over the strain range of -20 to 30 %. The model was designed in a hemilarynx configuration which gave rise to a regular oscillation with the frequency of 120 Hz and an onset subglottal pressure of about 1.2 kPa.

A full larynx model was prepared by Becker *et al.* [13] using different polyurethane rubber compounds as synthetic folds to adjust the stiffness. The homogeneous fold model which was composed of equal quantity of Evergreen $^{TM}$ mixed$^{TM}$ with$^{TM}$3.33 part Everflex$^{TM}$ resulted in a structure with the Young's modulus of 6.5 kPa that was considered in the

range of human vocal folds case. Initially the result of such structure was an absence of recognizable oscillation and tonal acoustic signal. The glottal width was remained in the range of 0-2 mm depending on the rate of airflow. The reason was ascribed to the lower pressure difference over the glottal duct due to the extended vocal tract.

In order to solve the limited amplitude of vibration, a spherical metallic body of 0.4 g was added to the synthetic folds tip during the casting phase inspired by the increased inertia of the mucous membrane due to its higher fluid portion.

Increased inertia caused the glottal width to reach its maximum of 2mm where the pressure and the shear forces of fluid made a balance with the elastic forces of the fold material. The oscillation frequency however was about 33-35 Hz which is quite less that real human phonation case. Another significant phenomenon observed in this model was a stochastic deviation of the jet from one fold and separated from the other one which forms a sort of asymmetric distribution in the airflow attributed to the textbfCoanda effect [86].

**Multi layer configuration:** Drechsel and Thomson [53] proposed a double-layer silicone model composed of a 2mm-thick cover of 4.1 kPa over a Body with 22.5 kPa stiffness. This was achieved by altering the thinner component added to the mixture of addition-cure Ecoflex 0030 silicone components. Nonetheless, it was shown that the two-layer model exhibited the same coupling of the vibration with the acoustics of subglottal tract as the single-layer model of Zhang *et al.* [246]; and there was no more evidences reported concerning the impact of inhomogeneity and variation of transverse moduli on the vibratory behaviour of the synthetic folds(??to be certainly verified??).

In order to compare the vibratory response of the real and synthetic vocal folds Weiss *et al.* materials characterization[235] developed multilayer models with a film sensor to measure the collision forces during phonation. different layers of the model was fabricated by varying the mixing ratio of Ecoflex 0030 to obtain the desired stiffness as shown in Figure 1.11 a. Also the influence of age and environmental effects on the static parameters was evaluated. Results showed that a higher temperature leads to an increase in static elasticity modulus of up to 15 % for very soft materials (1:1:4 mixture), whereas the relative humidity has only marginal influence (less than 1%) on the material properties.

Riede *et al.* 2008 [183] also used the same strategy to make a bi-layered replica and study the asymmetry in the motion of nonhuman mammalian vocal folds. But it lacks a comparison of the response as function of model stiffness.

A bi-layer model with was developed by Pickup and Thomson [174] to investigate asymmetry of materials stiffness and resulting motion of the folds. This study revealed that a close matching of the left-right stiffness is essential for a normal phonatory response, as the asymmetry results in the rise of onset pressure, phase difference between the folds and a reduction of the glottal area.

In an attempt to achieve a more realistic geometry they designed a synthetic soft model based on the MRI data[175]. Compared to the similar models based on M5 geometry, this new design resulted in an improved mucosal wave motion, less vertical movements and more typical alternating convergent-divergent glottal profile pattern (Fig.**??** d).

In order to introduce nonhomogeneous, transversely isotropic materials in the model, Weiss *et al.* [234] used polyester fiber bundles of about 332 $\mu$m diameter to fabricate fiber reinforced silicone models. a static tensile Young's modulus estimate of about 358.4 MPa was measure for the fibers. The results showed deviations in profile axisymmetry in comparison to isotropic materials. The results showed deviations in profile axisymmetry in comparison to isotropic materials when subjected to vibration of 120 Hz.

The impact of different geometrical configurations and stiffness of the sublayer and their repeatability was studied on four synthetic folds [162] (Fig 1.11 b). geometries varied based on M5 (UNI and convergent) and MRI design and the structure was composed of body and cover, except in one case where 5 different layers were considered (EPI). The rheological properties (1-10 Hz) of different composition of used silicone materials in the layers are shown in Fig 1.11 c. The MRI and EPI models showed better vibratory features of the human phonation than the M5 models including vertically travelling mucosal wave and alternating convergent-divergeant motion. However, beside its complicated fabrication and integration issues among the layers, it was still materially isotropic.

Therefore, Shaw *et al.* use acrylic fibers to fabricate materially nonlinear models of synthetic vocal folds to investigate their effect on the variations of fundamental frequency ($F_0$) during the longitudinal stretching. The tensile stress-strain response of the materials confirmed the non-linearity of the composites compared to linear response of isotropic silicone models(Fig. 1.11 d). A significant difference were detected for the ($F_0$) and ($F_o nset$) of the fibrous models, which appeared closer to the variations of ($F_0$) in human phonation.

The application of synthetic models in the study of vocal folds behaviour is associated with many advantages: they provide highly durable testing platforms that are capable to sustain several hours of uninterrupted vibration. They have removed the difficulties of preservation and freezing that was indispensable in the case of excised larynges. It in turn improves the repeatability of the experimental study and thus the results are more reliable. Using soft deformable folds in them, apart from the low cost and facility of access, allows the exploration of the effects of variations in materials property and geometry of the models. The outcome of such models has been proved to be highly reliable in terms of fundamental frequency, phonation threshold pressure and the mucosal wave.

Nevertheless, there are still limitations in their performance including the challenges to purely to reproduce/mimic the in vivo condition (including the hygrometric and temperature dependence of the model response) in order to achieve the desired physiological response. There are also difficulties in the fabrication process of such models namely the choice of appropriate material, time-consuming and intricate mold design, casting defects, control of curing mechanism, and demolding, which has been recently much improved thanks to the advanced techniques *e.g.* 3D printing [184], although every newly emerging technology and processes are accompanied with their own challenges.

### 1.2.2 Hydrogel-based biomaterials : tissue mimetic capacities and its application for clinical voice rehabilitation

#### Hydrogel Intro: structure and properties

A simple definition of the Hydrogel could be suggested by a combination of three main keywords: 3D-Network, polymer chains, and hydrophilicity. In this regard, this new bio-inspired generation of engineered soft materials has been emerged to basically provide high water-content structures with tuneable characteristics in order to realize the required function in a wide variety of applications. As mentioned above, hydrogels form generally by crosslinking of the macromolecular compounds in the aqueous media. The hydrophilicity of the polymer chains allows the water absorption of many times their dry mass.

Their remarkable properties including low toxicity, great capacity of water absorption and highly tuneable physical properties make them much preferable candidate to replace the existing synthetic polymers and biomaterials. Variety of constituting monomers and possibility to adjust the structure and consequently the properties, has endowed them a wide range of applications, which are still extending every day from research to industry. Tissue engineering scaffolds [**empty citation**], drug delivery vectors[**empty citation**], soft electronic devices[**empty citation**] and actuators[**empty citation**] are some of the most frequent fields of applications for hydrogels.

#### Classification, Chemical formulations and forming processes

Basically, hydrogels are developed based on the demanded physical, chemical, biological or mechanical properties. These features depend highly on their polymer source and arrangement of the bonding type that crosslink the chains together. The hydrogels can be classified thus based on many parameters including the source of their polymer chain, gelation (crosslinking) mechanism, their ultimate form and applications, etc.

Polymer source of a hydrogel can be **naturally-derived** macromolecules such as proteins from animal origins or plant-based polysaccharides. **Synthetic** polymers such as PVA (poly(vinyl alcohol)), PAA, PEG (poly-(ethylene glycol)), etc have also gained a large amount of attention due to their versatility in structure and properties.

Gelation methods of the molecular chain also comprises many different mechanisms, including physical entanglement, electrostatic interactions, chemical bonding, or even a combination of them (formation of interpenetrating networks: IPN, Double-Network Hydrogels (DN), and Hybrid structures).

**Physical gelation:** thermos-responsive gels form upon the alteration of their solubility temperature. It can be classified as Upper critical solution temperature (**UCST**) such as gelatin where the gel forms below the Upper Critical Solution Temperature [63, 233] or as lower critical solution temperature (**LCST**) like the case of synthetic PNIPAAM polymer (poly(N-isopropylacrylamide)), which forms the gel above this temperature. This

temperature can be tuned by the modification of their basic properties such as molecular weight and side chain manipulations[139].

Apart from the thermal responsivity of the polymers, the **electrostatic** arrangement of their functional sidechains can also be employed to form physical gels. 3D structure of the hydrogel can be perfectly built through the noncovalent bonding mechanisms including the van der waals forces and hydrogen bonds particularly in the protein based hydrogels (Fig.1.12b). A familiar example of such hydrogels is the hierarchical assembly of triple helix of amino acids in the structure of collagen subunits (fibrils and fibers) [241]. Despite most of the natural polymers having carboxyl groups on their backbone (such as hyaluronic acid and alginate) which are negatively charged at neutral pH, some of the macromolecules *e.g.* gelatin and chitosan present positive charges when dominated by amine groups, facilitating their gelation mechanisms. However, it is evident that control of the electrostatic properties in the synthetic polymers is more possible and consequently offers further varieties of the structures.

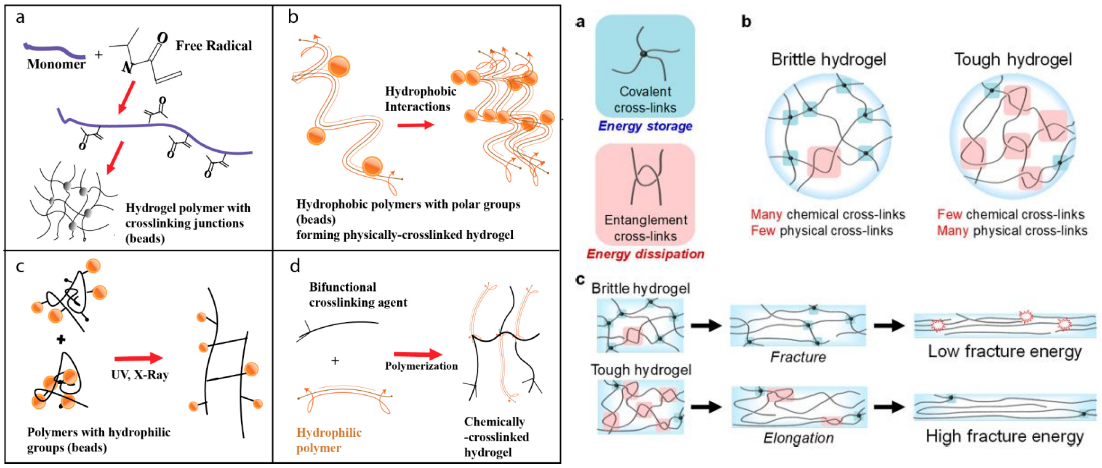


**Figure 1.12:** Schematic presentation of the crosslinking mechanisms in hydrogels (left) and the associated mechanical configuration of the chemical and physical gels.

**Covalent bonding:** Formation of the covalent bonds provides a higher degree of stability in the gelation procedure and a precise control over their properties. Thus, it makes the chemical crosslinking methods much more attractive for the design and fabrication of advanced hydrogel structures with the desired properties. Most well-known mechanisms of chemical crosslinking include high-energy radiation, enzymatic reactions, condensation and radical polymerization(Fig.1.12a,c,d) [85]. Even though there has been enormous progress in the chemical processing of hydrogel during the past decades, they have always been confronted with their own challenges including the high cost of raw materials, environmental concerns, and biocompatibility of the products. In order to overcome the

associated challenges and exploiting the advantages of both methods, **hybrid crosslinking** methods has emerged which are usually contains the physical entanglement of the polymer chains combined with the covalent bonds that results in the hydrogels with superior properties [examples of Li and Annabi-improved toughness and stiffness]. Furthermore, the ultimate mechanical properties of the hydrogel can be easily tuned by adjusting the involvement level of each mechanism **??**.

**Use of hydrogel for voice therapy and phonation research:**

The unique mechanical and structural features of the vocal folds combined with the complex process of phonation has faced the voice restoration with many challenges. Therefor an optimal solution for the recovery of the human voice is still in progress. During the decades, employing many different biomaterials such as silicon, Teflon, and bovine collagen for the augmentation of vocal folds did not result in significant improvement in voice recovery[62, 185].

Among the numerous advantages of the hydrogels, there are certain aspects that motivates the choice of hydrogel for the (biomimetic replicas// in vitro study of the phonatory performance) of the vocal folds: The same as all the other soft tissues, the water-rich property of the hydrogels is a key factor for the choice of appropriate biomimetic design. Furthermore, the fact that the normal performance of the vocal folds is significantly tied with the hydration level of the tissue [147] has emphasized this aspect. It also plays a pivotal role to reproduce the viscoelastic and damping properties of the tissue [35]. Additionally, porous structure of the most hydrogels promotes the transfer of the necessary gas and nutrients for the cell activity through such aqueous media. Structural modification has allowed an outstanding progress in the mechanical properties of hydrogels. Improved recoverable stretchability of the tuned hydrogels up to 400 % of applied strain [108, 239] is hence another appealing property as the vocal tissue are usually subjected to the reversible large deformations during the phonation process.

In case of healing or regenerative treatment of the tissue, hydrogels can be an interesting choice due to its nontoxicity and biocompatible nature and providing suitable environment for the adhesion, growth and differentiation of the fibroblast cells [**empty citation**].

The idea of using hydrogels for voice therapy has been proposed primarily by Chan and Titze [35] as bioimplants (often by injection) for the repair of vocal folds mucosal injuries. However, clinical applications of hydrogels confronted many practical issues including the short duration of action, tissue adhesion, lack of stretchability, long curing time, and the functional feasibility in phonatory application [**empty citation**] .

**Examples: (composition + associated mech properties)**

Chan and Titze [35] investigated the viscoelastic shear properties of hyaluronic acid (0.5-1 %) hydrogels reinforced with/without fibronectin over a frequency range of 0.01 to 15 Hz as bioimplant candidate and found close similarities to the native tissue characteristics. They also compared the elastic and viscous properties of Male and female mucosal tissue with

some of the biomaterials commonly used in the treatment of vocal folds defects (Fig.1.13) . This comparison concluded that beside many similarities of the studied biomaterials with the human tissue in terms of their shape and slope, the "mucosal group biomaterials" including HA and fat behave relatively closer to the tissue response. Particularly HA with the concentration of 1% highly resembles the average male and at 0.5 % behaves like the female VF mucosa.

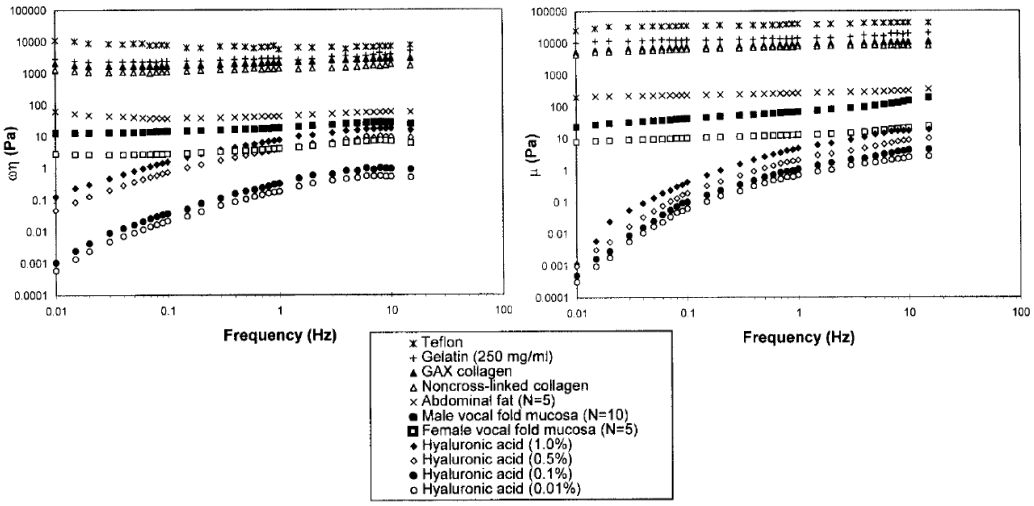


**Figure 1.13:** Elastic and viscous shear moduli of the human VF tissue compared with their implantable biomaterial candidates

Injection of chemically modified HA improved the scar healing of the vocal tissue in a study by Hansen *et al.* [82]. The viscous and elastic shear moduli of the hydrogel treated tissue was found significantly lower than scarred tissue. Nevertheless, the long-term performance of such treatment remained under question. Therefore, they optimized the HA hydrogel with the 5 % thiolated derivatives of gelatin in order to improve the in vivo efficacy of injectable VF wound healing in terms of biocompatibility, inflammatory response, mechanical properties at longer functioning periods (6 months post-treatment) [211]. Many further investigations were performed to develop the hydrogel structures as injectable biomaterials and tissue engineering of vocal folds. The objective was particularly improving the biological compatibility of the gels including cell adhesion, viability and migration, enzymatic degradation and viscoelastic characterization [88, 111]. These studies were mainly focused on HA and collagen derivatives. But Heris *et al.* explored the Glycol Chitosan-based hydrogels as a the second most abundant natural polymer derived from chitin[87]. Although, the discussion on the influence of the mechanical characteristics of the hydrogels on the vibratory performance were remained unclear. Later Latifi *et al.* [125] developed the same hydrogel through an interpenetrated network with hybrid heterotypic collagen fibrils (Fig. 1.14 a) and b), mainly with the purpose to improve HVFF cell adhesion.

Compressive toughness of gel was measured through monotone test up to 50 % strain at the rate of 10 micrometre per seconds on cylindrical samples. Maximum strength was found about of 5 kPa for Col-III/G1 far above the rest of gels (at the range of 0.5 to 2kPa) as shown in Fig. 1.14 c. Greater elastic moduli was also obtained for the Col/GCS samples with higher GCS level. Oscillatory Shear rheometry was also performed under time (1h) and frequency (0.01 to 20 Hz) sweep modes at 37 °C and oscillatory starin of 10 % (Fig. 1.14 d). Addition of collagen to the GCS hydrogel did not cause any adverse effects on the dynamic performance of the gel, contrary to the case PEG-crosslinked HA gels which were reported fragmented under continuous dynamic loadings. This is of great importance for the mechanically solicitated soft issues like heart valves and vocal folds.

The advent of bioreactors provided a powerful tool for fully coupled *in vitro* investigation of phonation process in an integrated platform combining the mechanobiological evolution of cell-laden hydrogel under axial loading and prescribed aerodynamic vibration. It is particularly useful to examine the mechanical durability of the employed biomaterials under realistic solicitations.

One of the first examples of such bioreactors which employed the hydrogels for the study of human phonation was developed by Kutty and Webb[121]. ECM gene expression and fibroblast synthesis of the encapsulated cells was evaluated in a HA hydrogel matrix exposed to vibratory stimulations. Rheological characterization of the hydrogel at the frequency range of 0.01 to 15 Hz resulted in almost the same response for the acellular and cell-loaded samples. The rate of cell viability and corresponding collagen synthesis was relatively lower than the static control. Vibration was applied to the cell culture through controlled actuator bars, and thus far from the realistic case of human phonation.

An airflow-induced self-oscillatory bioreactor was developed by [121] in which the cell-loaded hydrogel was embedded within a pair of silicone synthetic replicas of the vocal folds. The hydrogel was composed of Hyaluronic acid and gelatin crosslinked with polyethylene glycol to host the human vocal fold fibroblasts (HVFF). Gelatin was added to HA in order to improve its short *in vivo* half-life. It also highly enhances the adhesion and migration of HVFF cells, meanwhile make it prone to the enzymatic degradation. This hydrogel scaffold compound was inserted inside the cylindrical cavity of the synthetic replica in M5 geometry and made of Ecoflex ® 0010 covered by a thin layer of DragonSkin® as shown in Fig. 1.14 e. Finally the folds were integrated within a silicone body made of Ecoflex 0030, representing the anatomy of human vocal apparatus.

The measured mechanical and viscoelastic properties of the hydrogel and silicone components of the bioreactor are presented in the table of Fig. 1.14 f, although further details about the characterization method is missing. Phonatory characteristics of the resulting oscillation was found to be within the human range phonation (FF 94 Hz and Psg 1.1 kPa). Cellular activity and collagen synthesis was promising within the designed hydrogel structure while the stiffness of it was reported insufficient as was faced with cases of fragmentation under continuous vibratory forces. This issue was later controlled by the modification the hydrogel components having higher shear elastic moduli[125].

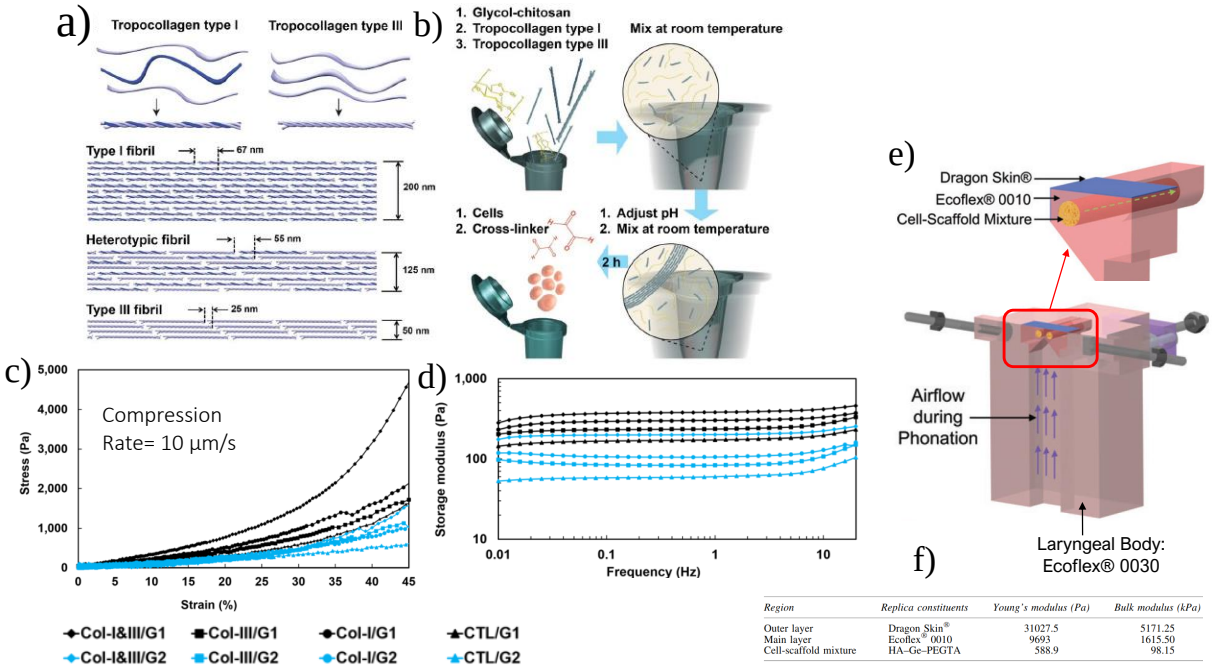


| *Region* | *Replica constituents* | *Young's modulus (Pa)* | *Bulk modulus (kPa)* |
|---|---|---|---|
| Outer layer | Dragon Skin® | 31027.5 | 5171.25 |
| Main layer | Ecoflex® 0010 | 9693 | 1615.50 |
| Cell-scaffold mixture | HA–Ge–PEGTA | 588.9 | 98.15 |

**Figure 1.14:** a) Schematic of tropocollagen types I and III followed by their arrangements to form type I fibrils, heterotypic fibrils of types I and III (I&III), and type III fibrils. b) Schematic fabrication procedure of glycol-chitosan (GCS) solution c) Stress-strain curves of the hydrogels obtained through compression test. d) Average storage moduli of the hydrogels for the frequencies between 0.01 and 20 Hz. e) Material composition and f) corresponding mechanical characteristics of the self-oscillating vocal fold embedded in the bioreactor [124]

Conclusion of the hydrogels: To sum up, development of the bioreactors provided many facilities for the integrated *in situ*tudy of fluid-structure-acoustics interactions, particularly with the recent involvement of hydrogel scaffolds. Even though, bioreactors are also confronting with certain limitations:

- Undesirable physical perturbation for the cell culture caused by mechanical stimulation, such as turbulent media flow
- Non-uniform strain distribution throughout the porous substrate
- Deviation of the transmitted amplitude and resonation frequencies transferred to the vibrating part due to the complicated architecture of platform frame, connectors, and bars
- Maintenance of the long-term cell viability

In this regard, evaluation of the compatibility of the hydrogels with the biochemical requirements of the vocal folds has been largely developed in the past years. On the other hand, the self-oscillation of the vocal folds is directly influenced by a complex configuration of multiaxial mechanical loadings. Such loadings include the tensile stretching in the thyroarytenoid axis, compressive and impact forces arising from the collision of folds, shearing stresses associated with the propagation of mucosal waves and the aerodynamic loadings involved with the glottal area air pressure.

Nevertheless, tuning the constituting materials used for the fabrication of synthetic vocal

fold models combined with a comprehensive mechanical characterization of them is still seems to be missing in order to provide a realistic vision of such complex system.

## 1.3 Conclusion

To sum up, the advances in anatomical and histological characterization of the multi-scale hierarchical structure of the vocal tissue has provided a powerful tool to better understand its remarkable features in detail. Particularly, the basic roles of the elastic and collagen fibers in the stiffness and elasticity of the tissue, is believed to be the core basis of its mechanical response to the complex loading condition in the larynx. This is more precisely reflected in: (i) the nonlinear strain-hardening response of the tissue to large deformations ascribed to the reorientation of collagen fibers, (ii) the rapid rebounding feature at high frequency of vibration through the pliability and recoiling of the elastic fibers, and (iii) the viscoelastic and damping capacity under collision arising from the gel-like nature of the ECM.

However, discerning the individual role of each principal characteristic descriptors of the fiber/matrix, including the fibers diameter, preferential orientations, degree of waviness and gradient of fibrous network density in profile, requires further in depth investigation specifically their evolution under multi-axial loading condition. Therefore, simplified parametric *in vitro* studies in this field will be strongly valuable towards a sharper and more realistic understanding of the VF vibratory behaviour.

This first chapter was devoted to present the framework of the study by summarizing the background knowledge on the human voice anatomical and functional features in the first part and the recent developments on the in vitro modelling and biomaterials therapeutical methods in the second part.

As it was discussed in detail, (i) There is still a growing clinical demand for an improved understanding of relationship between the complex laminated architecture of the tissue and its unique vibratory performance.

(ii) in vitro experimental models of the vocal folds have provided a powerful tool for an enhanced understanding of the aforementioned characteristic interactions in the simplified platforms. However, there are still some challenges towards a more realistic simulation of the phonatory circumstances, including the contribution of hygrometric condition and also the use of appropriate (characterised) bio-mimetic flexible materials.

(iii) biomaterials/Hydrogels: the science and application of optimized hydrogels has largely developed during last few decades. The optimization of their chemical composition and hierarchical structure in the therapeutic and tissue engineering applications allowed them to be successfully employed in many clinical therapies. However, their comprehensive mechanical characterization and tailoring them to the appropriate functional application is still far from the ideally desired condition; particularly for replicating purposes of

mechanically agile tissues such as the case of vibrating vocal folds supposed to sustain high-frequency multiaxial loadings.

The current thesis is hence particularly aims in the design, synthesis and multiaxial characterization of a hydrogel model and evaluating its response inside the aero-acoustic testbed.

In order to obtain these objectives, the strategy of the study was organised as follow:

- First a gelatin-based hydrogel was prepared to represent the aimed matrix for the vibrating tissue replica. Then, after the adjustment of chemical composition, its mechanical behaviour was evaluated under a series of multiaxial loading modes to which the excised tissue was subjected prior to the current study.
- In order to explore the contribution of fibrous network in the mechanical performance of the hydrogel-based composite structure, a PEG hydrogel was reinforced with the PCL fiber mats and the resulting composite was investigated in terms of its structural and mechanical properties.
- Finally an aero-acoustic platform with the motorized stretching capacity was designed and install to host the artificial soft vocal folds and evaluate their self-sustained vibratory behaviour under variable flow of air and prescribed longitudinal strain levels.

# 2

# Objectives of the thesis

# Contents

## 2.1 Scientific hypotheses and global objective

under revision

The human vocal folds are known to function with a unique oscillating pattern compared to the other mechanically involved tissues of the body. This feature is usually ascribed to the complex microstructure of its tissue.

Normal phonation is a result of the interaction between the different internal constituents of the tissue and the external environment of the vocal apparatus. This interaction is in turn complicated and need to be clarified. There are both scientific and clinical evidence that affirms the interdependence of the vibratory performance of the vocal folds on this hierarchical microstructure. On the other hand, this link is highly dependent on several contributing parameters, including the surrounding environment, mechanical (quasi-static) and rheological (dynamic) characteristics of the tissue and the distribution of aerodynamic forces in glottal tract.

Therefore, the global objective of the thesis is to develop a composite-based replica in which the associated mechanical properties in finite deformation can be modulated through the manipulation of the composition, arrangement, morphology, and geometry of the fiber/matrix combination.

## 2.2 Experimental strategy

In order to evaluate the pertinence of the aforementioned hypothesis and achieve the objectives of the study, an experimental approach was adopted. This experimental strategy can be summarized in following points:

- Choice of candidate materials: soft matrices with sufficient potential versatility of the properties.
- Biomimetic design and fabrication of the materials: adjustment of their basic structural properties through the manipulation of chemical composition of matrix or structural geometry and morphology of the reinforcements.
- Characterization of the mechanical properties in finite deformation and multiaxial loading modes under controlled environmental condition.
- Design and fabrication of soft vocal fold replicas out of the mechanically characterised materials and investigation of their basic vibratory features.

### 2.2.1 Choice of candidate materials

In order to properly conduct the strategy toward the desired objectives, the choice of an appropriate material is of great importance. These choices should satisfy at least certain features:

1- **Processing criteria:** due to the experimental nature of the study, facility of the fabrication and structural modification plays an important role in the flow of the work. Material should be easy to cast into the 3D molds and rapidly cures and prepare for long and repetitive mechanical and vibratory measurements.

2- **Mechanical properties:** as stated above, conforming with the suggested hypothesis, mechanical properties of the candidate material should fit to the measured target tissue behaviour, *i.e.* soft and flexible enough to endure large reversible deformation up to 50 %, sufficient damping properties (mechanical energy loss factors of less than 10%) to reproduce the required viscoelasticity and maintain the oscillation at desired frequencies.

3- **Functional stability:** selected material should be capable of sustaining their properties for relatively long experiments under prescribed hygrometric conditions (*i.e.* almost saturated humidity and physiological temperature) to assure a reliable characterization of both mechanical and oscillatory behavior.

4- **Versatily in structural orientation:** Following the different mechanical response of the vocal tissue at the preferential orientation, candidate material should present the capacity to be designed in a different anisotropic ratios. This capacity can be obtained either by addition of reinforcement to the matrix or through the petterning the structure during the fabrication process.

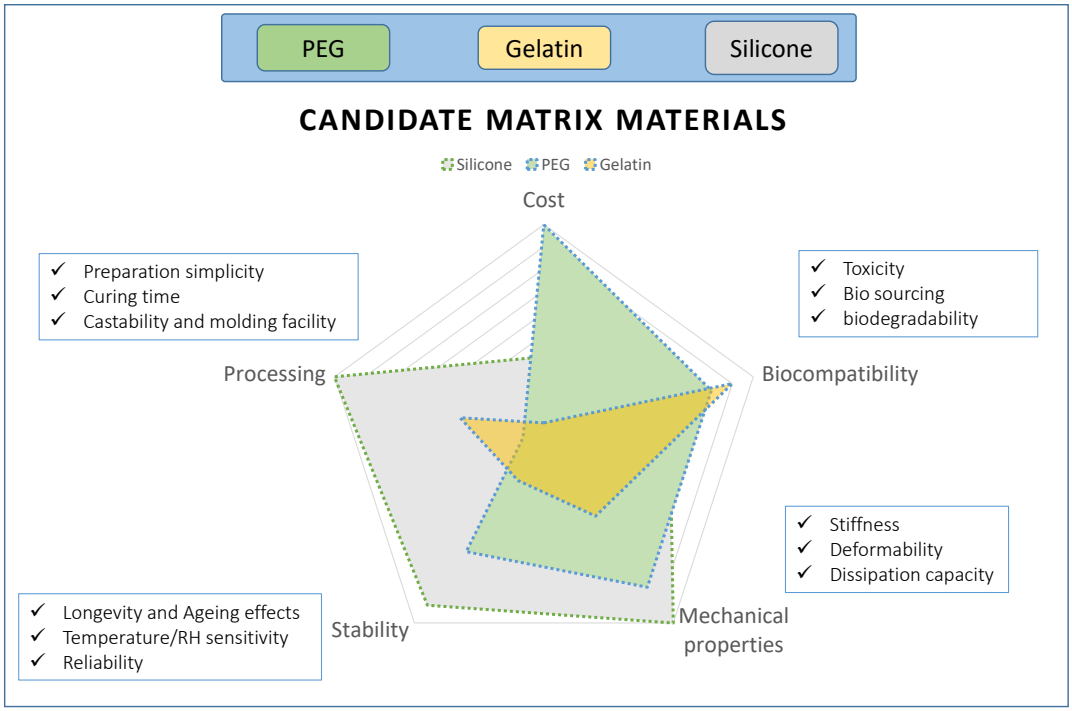


**Figure 2.1:** Qualitative evaluation of the proposed candidate materials

After evaluation of the possibilities and requirements of the project, following candidate materials were proposed:

1-**Gelatin-based hydrogels:** this grade of hydrogels are abundant bio-based materials that can be easily produced and tested for several experimental campaign. The mechanical

properties of the hydrogel are tunable through the adjustment of the crosslinking reaction. finally due to the high water-content of the structure, not only the damping ration can be regulated for the visco-elastic aspect, but also the possibility of the structural anisotropic design is available.

2-**PEG-based hydrogels, reinforced by PCL fibers:** this famous grade of biomaterial has been successfully employed in biomedical applications including the tissue regeneration and wound healing. Recent studies has also confirmed its promising mechanical performance as an efficient skin replacement when reinforced with micro-structured fibrous network. Such fruitful compatibility of fiber/matrix interface is motivating for the fabrication of tailored composite structures. Varying the hydrogel molecular weight and concentration allows modulation of the mechanical properties. Moreover, morphology, orientation and distribution of fibrous network can be satisfactorily controlled though the feeding parameters of the fabrication process.

3- **Ecoflex Silicone rubber:** Highly durable mechanical properties (significantly large reversible deformation high-strengh) together with facility of fabrication in intricate geometries made them among the best candidates for the mimicry of the soft tissue as physical models. According to the discussed literature in the previous chapter, this grade of elastomers have been extensively used in the *in vitro* study of the vocal fold vibratory behaviour and constitute a reliable database in this field. Thus, Ecoflex in varying stiffness was selected as a reference material to be characterized under the same multiaxial solicitations and make available the comparison of the hydrogel oscillation pattern on the aeroacoustic platform.

Figure 2.1 depicts a rough qualitative analysis of the three group of candidate materials in terms of the aforementioned criteria.

### 2.2.2 A step-by-step approach in 3 phases

As depicted in Figure 2.1, in an approximate evaluation, selected candidate materials for matrix were compared in terms of their inherent characteristics and operational capacities. The idea is to define the path in which, each material should undergo optimisation process towards the tailored properties that fits the target tissue behaviour.

In this regard, gelatin hydrogel as our first choice need to be improved in mechanical properties. This task is tackled in a first step through the multiaxial mechanical characterization of the chemically modified materials to obtain large reversible deformation capacity. This step was then completed by performing the same experimental campaign on the two other matrix candidate.

In the next step, in order to introduce the anisotropy in the structure as an important feature of the tissue architecture, fiber reinforcement was evaluated in mechanics as a tailoring strategy on the PEG hydrogel. Additionally, the ice-templating technique was explored on gelatin hydrogel precursors to form the matrix structure in a preferred orientation.

Finally, the optimised formulation of the materials were fabricated in the form of 3D replicas of the vocal folds to be tested under airflow-induced oscillation within the appropriately designed platform. In a first attempt, gelatin and Ecoflex matrices were assessed in terms of their vibratory characteristics including the required subglottal pressure and fundamental frequency. Then an exploratory evaluation of the primary composite structure was carried out to assess their impact on the vibration pattern.

# Part II : Isotropic materials with tailored mechanical properties : target matrix candidates for future vocal-fold composite replicas

# 3

# Mechanics of gelatin-based hydrogels during finite strain tension, compression and shear

This chapter is based on an article submitted to the *Journal of the Mechanical Behavior of Biomedical Materials* in October 2022 , by H. Yousefi-Mashouf, L. Bailly, L. Orgéas and N. Henrich Bernardoni.

# Contents

## 3.1 Introduction

Hydrogels are 3D networks of hydrophilic polymers able to absorb and hold a large amount of water without dissolving (*e.g.* up to several hundred times their dry weight) [24, 158, 244]. Their softness and structural similarities with the extra-cellular matrix of human soft tissues make them materials of choice for biomedical applications [2, 129, 193]. Among the polymers used to form hydrogels, gelatin is very attractive due to its *in vivo* biocompatibility, biodegradability, versatile physico-chemical properties, and its abundance in renewable natural resources which allows for low-cost and eco-friendly implementations [2, 166]. Therefore, during the last decade, gelatin-based formulations have been proposed for electrospun fibres [116, 169, 181] and 3D scaffolds for tissue regeneration [65, 96, 112, 178], microcarriers in drug delivery [54, 57, 90, 104, 201] and foams for wound dressing [105, 179]. More particularly, active research is underway to develop gelatin-based hydrogels to be injected into the vocal folds for surgical voice restoration [89, 90, 95, 104, 112, 126, 182].

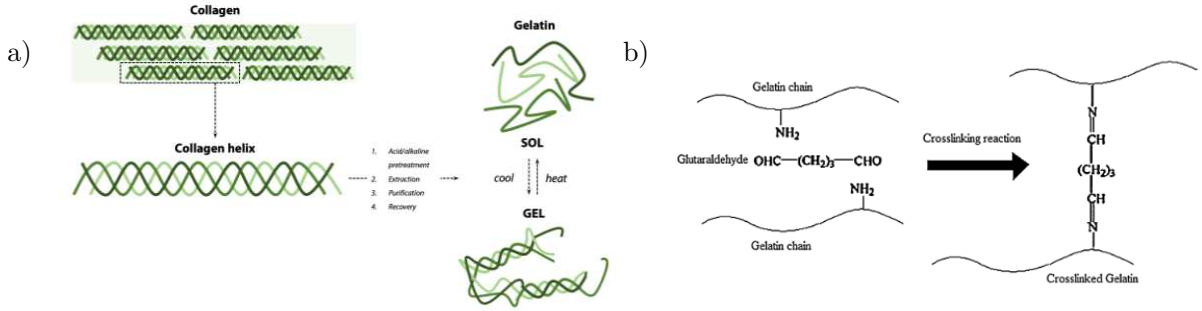


**Figure 3.1:** (a) Scheme of the gelatin extraction from the processing of collagen, and of its reversible sol-gel transition when dissolved in water by heat-cool process; (b) Cross-linking reaction of Ge with GA. Sources : Extracted from [27, 105]

Gelatin is a hydrophilic protein fragment derived from collagen (Type I), that is the major fibrous structural protein in skin, bone and connective tissues of animals. Gelatin comes from the hydrolysis of the triple-helix structure of collagen, yielding to a randomly coiled structure (Fig. 3.1(a)). When cooling an aqueous solution of gelatin below $\approx$ 30–35 °C, provided that the concentration is high enough (above $\approx$ 2 % w/v), a thermo-reversible gel is formed by physical cross-linking, in particular due to partial recovery of the collagen helical structure [19, 27, 45, 68, 237]. Gelation features of gelatin (*e.g.* molecular weight, gel-forming temperature, chemical composition) depend on the collagen animal source [144] or their processing route [68]. Despite excellent physical and biochemical compatibilities, standard hydrogels based on neat gelatin present three main barriers to their potential applications : poor mechanical performances (*e.g.* low elastic modulus and toughness, brittle failure), poor thermal stability in temperatures close to human body (*e.g.* dissolution of the gel around 40 °C), undesirable swelling under excessive hydratability, up to full disintegration into the solvent [18, 45, 55, 97]. Such limitations can be overcome by promoting intermolecular associations along the gelatin amino acid sequences, and bonding gelatin polymer chains by covalent bonds. Among the possible candidates, glutaraldehyde (GA) allows to link together proteins via a high chemical reactivity towards $NH_2$ groups, forming

stable covalent bonds (see Fig. 3.1(b)). GA is by far the most frequently used due to its low cost and efficiency in increasing the gel tensile strength, ductility as well as its denaturation temperature by a shift of $\approx 30°C$ [18, 30, 179]. Although GA treatment is also known to leave cytotoxic residues, adverse effects can be minimized by using it in low concentrations : 0.05% v/v is reportedly enough to cross-link about 60% of gelatin amino groups [18].

Faced with the growing need for such gelatin-based hydrogels and the proliferation of proposed formulations, characterization of their mechanical behavior becomes essential to understand the process/function relationships, to classify the added value of one formulation over another, and to evaluate its relevance for a targeted biomechanical application. Therefore, during the last decade, a few studies have investigated the mechanics of gelatin gels, (non)cross-linked with various reagents and shaped into various structures (films, foams or filled volumes) :

- Some of these works have focused on single (shear or tensile) response of the gels using standard Dynamic Mechanical Analysis (DMA), *i.e.* within the linear regime [45, 56, 237]. These works allowed to quantify the shear (or tensile) dynamic moduli of the various formulations subjected to a frequency/temperature sweep. Typically, for neat gels, shear storage modulus (range of values 9 – 13 kPa) was reported one order of magnitude higher than the loss modulus, highlighting a predominant elastic response [45]. Whatever the considered chemical cross-linkers (*e.g.* functionalized cellulose nanowhiskers, 1-ethyl-3-(3-dimethylaminopropyl) carbodiimide or GA-glycerol), their reaction induced an increase of the dynamic moduli by a ratio of 1 up to 100, depending on the degree of cross-linking.

- Other pioneer works have extended the field of study to large deformations in tension [18, 56, 179] or in compression [123, 179]. These first results are sensitive to the gel processing route, yielding to reversed trends in some cases : considering air-dried films cross-linked with GA at several concentrations and immersed in a mixture of water and ethanol [18], a significant stiffening was obtained even at low GA concentrations. However, the extensibility was here found to decrease while increasing GA concentration, and to reduce by about one order of magnitude with respect to that measured for uncross-linked films. Conversely, addition of GA in gelatin-pectin-glycerol films allowed to increase the tensile strength but also the elongation at break (by about 40%) [56]. Finally, to our knowledge, a single study has characterized the mechanics of gelatin-based hydrogels in tension and compression so far, in the case of very specific porous scaffolds shaped by gas foaming [178].

In the end, the current experimental study of gelatin-based hydrogels is often limited to either a specific loading mode, with a single monotonic path to failure, or to standard infinitesimal strain analyses. These configurations are still far from those endured *in vivo* by living tissues, which are often subjected to many complex and coupled mechanical loadings upon finite strains and various strain rates. Therefore, this work aims to further investigate the mechanics of gelatin hydrogels under different loading modes (tension, compression, shear) and kinematics (finite strains, cyclic paths and various strain rates).

Neat gelatin and gelatin cross-linked with GA of various concentrations were manufactured and characterized purposely. As an illustration and opening towards a current biomimetic challenge, we also confronted the mechanical performances of the gels to those of a native soft tissue particularly complicated to restore, namely the human vocal folds.

## 3.2 Materials and methods

### 3.2.1 Sample preparation

Pigskin gelatin powder (Type A, gel strength ≈ 300 g Bloom, Sigma-Aldrich®) and a glutaraldehyde mother solution (Grade I, 50% w/w in water, Sigma-Aldrich®) were used to produce the hydrogels. Two different processing routes were employed to elaborate samples made of neat gelatin (Ge) or gelatin cross-linked with glutaraldehyde (Ge-GA).

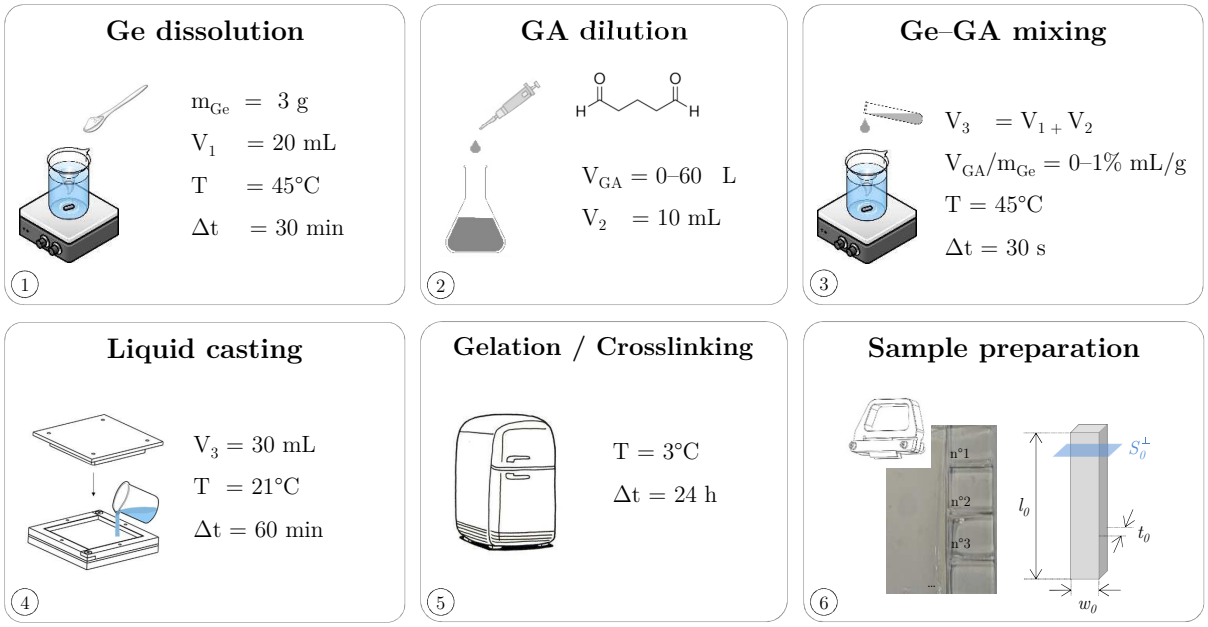


**Figure 3.2:** Processing route of gelatin hydrogels cross-linked with glutaraldehyde (Ge-GA samples).

**Neat Ge hydrogels –** 30 mL of a gelatin aqueous solution (10% w/v) was obtained by dissolving 3 g of Ge powder in water for 30 min at 45 °C [177]. Ultrapure water (18.2 MΩ) was used to minimize the non-uniform physical bonding network caused by unbalanced ionic charge distribution [237]. The prepared solution was firstly homogenized using magnetic stirring (350 rpm). Then, it was poured into a customized Teflon® mold at room temperature (T ≈ 21 °C) and relative humidity (RH ≈ 45 %) for 1 h, and kept at 3 °C for 24 h to form a rectangular gel plate (100 × 100 × 2 $mm^3$). Finally, rectangular samples were cut from the plate at desired dimensions using two parallel razor blades, and marked with a random pattern made of small speckles for optical tracking during the mechanical tests.

**Ge hydrogels cross-linked with GA –** The preparation of cross-linked hydrogels comprised several steps (Fig. 3.2). A gelatin aqueous solution was first prepared as described above, albeit for a smaller final volume (20 mL) and a higher gelatin concentration (15% w/v). In parallel, a given micro-volume $V_{GA}$ of the GA mother solution was collected, and diluted in ultrapure water to prepare 10 mL of daughter solution. $V_{GA}$ was parametrically varied (15; 30; 45; 60 $\mu$L) in order to manufacture samples with various degree of cross-linking. Ge and GA solutions were mixed together during 30 s at 45 °C. The Ge-GA mixture (30 mL) was then casted into a rectangular mold to form a gel with a fixed concentration in gelatin (10% w/v), and a parametrical concentration of cross-linker so that $V_{GA}/m_{Ge} \in$ [0.25 %; 0.5 %; 0.75 %; 1 %] mL/g. The steps of gelation in a cool atmosphere and shaping of samples were similar as for the neat Ge hydrogels. Note that for $V_{GA}/m_{Ge} > 1$ % mL/g, the cross-linking kinetics was so fast that it prevented the castability of the Ge-GA mixture (see Supplementary Fig. 3.8 in Appendix A).

### 3.2.2 Mechanical characterization

An experimental protocol was designed to characterise the finite-strain mechanics of Ge and Ge-GA samples under tension, compression and shear, as previously done on vocal-fold tissues [43].

**Hygro-mechanical set-up –** Hydrogel samples were tested using an electromechanical tension-compression testing machine (Instron® 5944) equipped with a load cell of $\pm$ 10 N. All tests were conducted in a thermo-regulated atmosphere (T $\approx$ 25 °C) and at proper hygrometric conditions to prevent samples from air drying : the samples were placed in a chamber (Fig. 3.3(a)) in which a saturated air flow ($\approx$ 98–100 % RH, quasi-null flow rate $\Phi_{air}$) was regulated with a heated humidifier (Fisher and Paykel® HC150). The time to reach the prescribed hygrometry was about 30 min, and the capacity of the set-up to maintain it for $\approx$ 1 week while preserving the mass and hygro-thermal stability of the samples was also verified (see Supplementary Fig. 3.9 a in Appendix A).

During mechanical testing, pictures of the deformed sample were recorded using a high-resolution CCD camera (JAI® BM-500GE, 15 Hz), to quantify its dimensional changes and track cases of sample slippage (Fig. 3.3(b)). For tensile tests, clamps were coated with sandpaper to facilitate the sample positioning and to minimize its slippage. For compression tests, rectangular compression platens (25 mm length and width) were lubricated by a film of liquid silicone oil, avoiding friction and undesired barrelling effect. For shear tests, plates (16 mm length and 13 mm width) were coated with double-sided adhesive to restrain sample slippage.

**Testing procotol –** Whatever the sample, its mechanical characterization was performed within 24 h to 48 h after its manufacturing, following the sequential steps reported below. Each test was repeated at least 5 times to ensure its reproducibility (Supplementary Fig. 3.10 in Appendix A showing the typical level of scatter in the measurements). For all cases,

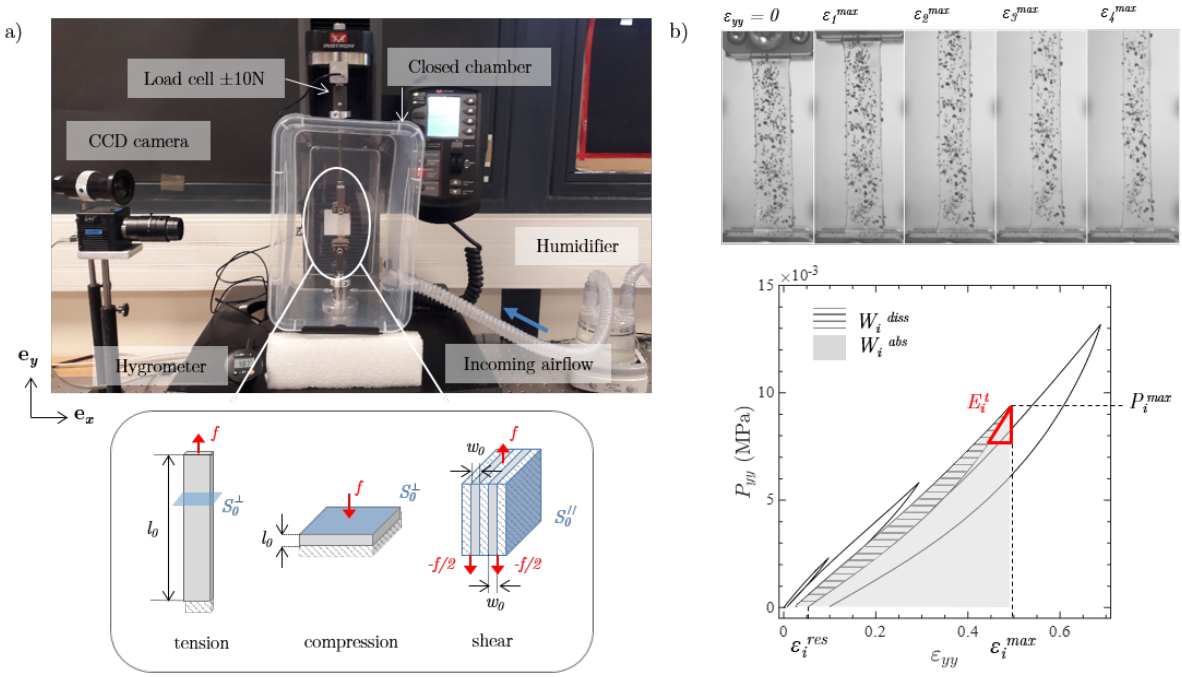


**Figure 3.3:** (a) Overview of the experimental set-up *(top)*, and schemes illustrating the three loading conditions (tension, compression, shear) applied on the samples (*in gray*) as well as their dimensions in the reference undeformed configuration *(bottom)*. $\boldsymbol{f}$ represents the average load measured by the load cell. (b) Pictures showing a Ge-GA hydrogel stretched during cyclic tension at increasing peak strain levels, and typical stress-strain response, where the mechanical descriptors introduced to quantify the recorded data for each cycle $i$ ($\varepsilon_i^{max}$, $\varepsilon_i^{res}$, $P_i^{max}$, $E_i^t$, $W_i^{diss}$, $W_i^{abs}$) have been reported.

the loading direction was defined by the vector $\mathbf{e}_y$ shown in Fig. 3.3(a). In the following, dimensions of undeformed samples along $\mathbf{e}_y$ (*resp.* $\mathbf{e}_x$, $\mathbf{e}_z$) are noted $\ell_0$ (*resp.* $w_0$, $t_0$).

- Simple tensile tests were first performed on samples cut for an effective length-to-width ratio $\ell_0 : w_0 = 5{:}1$, with a gauge length $\ell_0 = 50$ mm and a cross-section $S_0^{\perp} = 20$ mm$^2$ (see Fig. 3.3(a)). The cell force $f$ signal and the displacement of the machine crosshead $\delta$ were used to estimate the first Piola-Kirchoff stress $P_{yy} = f/S_0^{\perp}$, as well as the Hencky tensile strain $\varepsilon_{yy} = \ln(1 + \delta/\ell_0)$. The load cell was tared while the sample was subjected to its own weight only. Once mounted between the jaws, the sample was very slightly pre-loaded ($f \approx 5.10^{-5}$ N), and its initial gauge length recalculated accordingly. Then, samples were subjected to N = 4 load-unload cycles with an increasing peak strain amplitude ($\varepsilon_i^{max}$ = 0.1, 0.3, 0.5, 0.7, $i = [1..N]$ – see Fig. 3.3(b)), and a very low force at each unload phase for the inversion condition ($f > 5.10^{-3}$ N). The applied strain rate $|\dot{\varepsilon}_{yy}| \approx |\dot{\delta}/\ell_0|$ was parametrically varied from $\approx 10^{-3}\ s^{-1}$ up to $\approx 10^{-1}\ s^{-1}$. In addition to this first campaign, kinematic conditions were further adjusted to reproduce the tension tests recently conducted on human vocal folds by Cochereau *et al.* [43] (*i.e.* with N = 10, $\varepsilon_1^{max} \approx 0.1$ and $|\dot{\varepsilon}_{yy}| = 10^{-3}\ s^{-1}$).

- Simple compression tests were then performed on samples at length-to-width ratio $\ell_0 : w_0 = 1{:}5$, with a gauge length $\ell_0 = 2$ mm and a cross-section $S_0^{\perp} = 100$ mm$^2$ (Fig. 3.3(a)). Compression stress $P_{yy} = f/S_0^{\perp}$ and compression strain $\varepsilon_{yy} = \ln(1 + \delta/\ell_0)$ were recorded during the test. The initial contact between the

sample and the top platen was determined once $f \approx 5.10^{-5}$ N (*i.e.* initial compressive stress $\approx \mathcal{O}(10^{-7}$ MPa)). Then, samples were subjected to N = 4 load-unload cycles down to $\varepsilon_i^{min}$ (-0.1, -0.3, -0.5, -0.7) at a strain rate $|\dot{\varepsilon}_{yy}|$, it being parametrically varied from $\approx 10^{-3}\ s^{-1}$ to $10^{-1}\ s^{-1}$. As for tension, the kinematic conditions were also adjusted to reproduce those previously chosen to characterize the compressive response of vocal folds [43] (*i.e.* with N = 10, $\varepsilon_1^{min} \approx$ -0.2 and $|\dot{\varepsilon}_{yy}| = 10^{-3}\ s^{-1}$).

- Finally, two samples ($\ell_0 = 10$ mm, $w_0 = 2$ mm, $t_0 = 10$ mm) were tested together in a symmetrical double-lap configuration ensuring simple shear of the samples along the ($\mathbf{e}_y$, $\mathbf{e}_x$) plane, as illustrated in Fig. 3.3(a) [176]. Before testing, a slight pre-compression of the samples was imposed (*i.e.* pre-strain of ≈0.05 N in the transverse direction). During the tests, shear stress $P_{yx} = f/2S_0^{//}$ was measured as a function of shear strain $\gamma_{yx} = \delta/w_0$. Samples were subjected to N = 10 load-unload cycles up to $\gamma_{yx}^{max} = 0.5$ at a shear rate $|\dot{\gamma}| = |\dot{\delta}/w_0| \approx 10^{-3}s^{-1}$ for comparison with the living tissue database [43].

Whatever the case, the obtained stress-strain data were quantified by a series of 6 mechanical descriptors displayed in Fig. 3.3(b) : the peak stress achieved during cycle $i$, $P_i^{max}$; the corresponding peak strain, $\varepsilon_i^{max}$; the tangent modulus assessed at the early stage of the $i^{th}$ unloading phase, $E_i^t$, so as to capture instantaneous stiffness of the material; the residual strain occurring at the end of cycle $i$, $\varepsilon_i^{res}$; the energy density of the gel stored during the $i^{th}$ load, $W_i^{abs}$; and the one dissipated after the $i^{th}$ unloading phase, $W_i^{diss}$ [133].

## 3.3 Results and discussion

### 3.3.1 Effect of cross-linking concentration on the tensile properties of hydrogels

The tensile responses of Ge and Ge-GA hydrogels recorded during the last loading at $|\dot{\varepsilon}_{yy}| \approx 10^{-2}\ s^{-1}$ up to $\varepsilon_i^{max} = 0.7$ are displayed in Fig. 3.4, together with the evolution of the tangent moduli $E_{load}^t = dP_{yy}/d\varepsilon_{yy}$ with $\varepsilon_{yy}$. Ge samples demonstrate a quasi-linear tensile response with a nearly constant tangent modulus $E_{load}^t \approx 27$ kPa, up to failure which occurs when $\varepsilon_{yy} \approx 0.32$ (see Fig. 3.4(a)). By contrast, the addition of chemical cross-linking during the manufacture of the gels results in : (i) improved ductility, in that Ge-GA samples do not break at $\varepsilon_{yy} = 0.7$, even at the lowest GA concentrations ; (ii) improved tensile strength, with higher stress levels registered from moderate GA concentrations (*i.e.* $V_{GA}/m_{Ge} \geq 0.5$ % mL/g). By comparing such Ge-GA mixtures to neat gelatin at $\varepsilon_{yy} \approx 0.3$ for instance, the ratio of peak stresses $P_i^{max}$ ranges from 1.1 to 1.6. By further comparing the most and the least concentrated GA hydrogels at higher strains ($\varepsilon_{yy} \approx 0.7$), this ratio rises up to about 2.1. (iii) induced non-linearity of the stress-strain response and strain hardening of tangent moduli once $V_{GA}/m_{Ge} \geq 0.5$ % mL/g, as clearly evidenced in Fig. 3.4(b). This critical threshold of GA concentration needed to enhance the mechanical properties of Ge

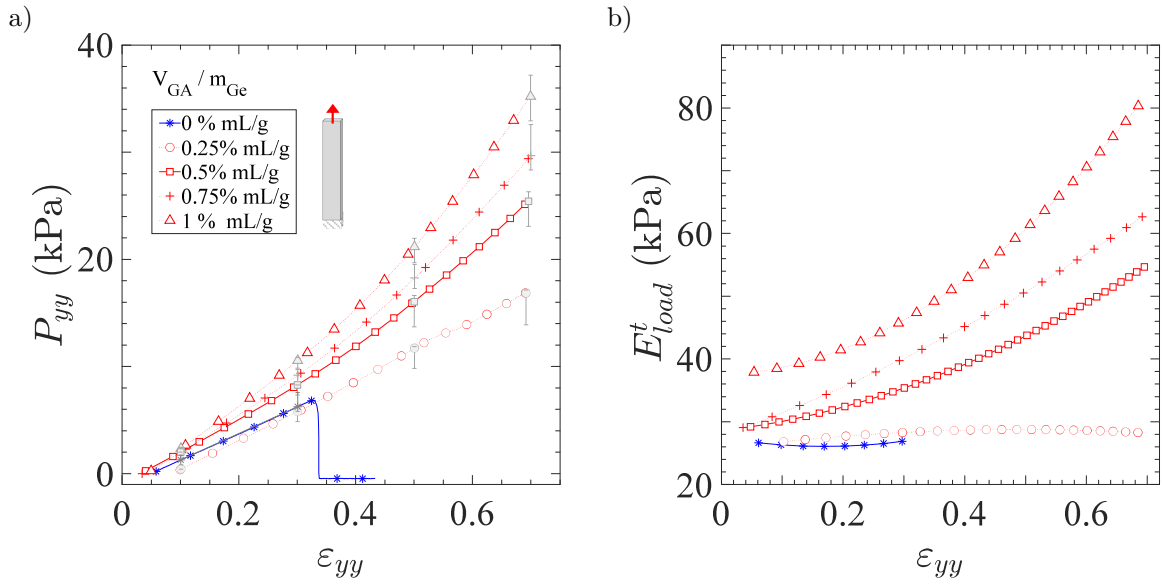


**Figure 3.4:** Tensile behavior of Ge (*in blue*) and Ge-GA hydrogels (*in red*) with various concentrations of cross-linker : (a) Stress-strain curves (during the only loading part of last cycle) and (b) corresponding tangent modulus $E^t_{load}$ as a function of $\varepsilon_{yy}$. $|\dot{\varepsilon}_{yy}| \approx 10^{-2}\ s^{-1}$.

hydrogels is also highlighted in Supplementary Fig. 3.11 (Appendix A) for all cycles applied from $\varepsilon_i^{max} = 0.1$ to 0.7. In the following, due to casting difficulties and undesired cytotoxic effects likely to occur at higher GA concentrations [18], focus is made on the cross-linked hydrogels with this critical degree of cross-linking ($V_{GA}/m_{Ge} = 0.5$ % mL/g). Finally, although contrary qualitative trends were observed by Bigi *et al.* [18] with, in particular, the extensibility of Ge films not favored by increasing GA concentration, our results are consistent with those obtained by Farris *et al.* in gelatin-pectin-glycerol films cross-linked with GA [56].

### 3.3.2 Mechanics of hydrogels in tension and compression

In this section, the mechanics of the previously selected cross-linked hydrogel ($V_{GA}/m_{Ge}$ = 0.5 % mL/g) is compared to that of neat gelatin in tension and compression at various strain rates $|\dot{\varepsilon}_{yy}|$ (from $10^{-3}\ s^{-1}$ to $10^{-1}\ s^{-1}$). Fig. 3.5 shows typical stress-strain curves obtained with Ge and Ge-GA samples subjected to progressive cycles from $\varepsilon_i^{max}$ = 0.1 to 0.7 in tension and compression at $|\dot{\varepsilon}_{yy}| \approx 10^{-2}\ s^{-1}$. The strain evolution of the mechanical descriptors for each cycle is detailed in Fig. 3.6 (*diamond symbols*). Note that the descriptors of neat Ge (*in blue*) were only calculated in compression mode, as it was not able to sustain tensile strains beyond 0.35 over the whole database.

*General trends* – Compared to tension, neat gelatin is able to withstand much larger strains and stress levels in compression without breaking (Fig. 3.5). Typically, the ultimate tensile strength of Ge samples was measured around 6 kPa, whereas the compressed samples were able to endure $\approx$ 5 times higher stress levels at $\varepsilon_i^{min} = -0.7$. Looking in more detail at

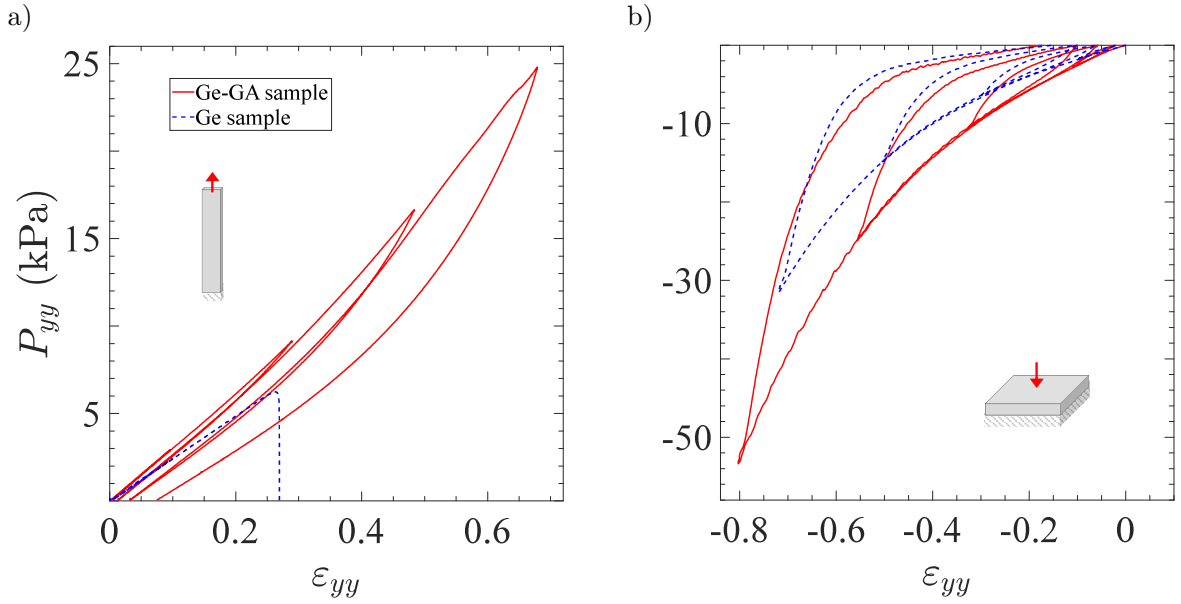


**Figure 3.5:** Stress-strain response of Ge samples and Ge-GA samples ($V_{GA}/m_{Ge} = 0.5$ % mL/g) measured in cyclic tension (*left*) and compression (*right*) at $|\dot{\varepsilon}_{yy}| \approx 10^{-2}\ s^{-1}$.

the compressive response of gelatin while cycling, the progressive load-unload sequences yield here to a non-linear mechanical response with a strain hardening, and a stress hysteresis with non-negligible residual strain $\varepsilon_i^{res}$ after unloading (up to 0.15 at the last cycle). Fig. 3.6 (b) clearly highlights the non-linear increase of $E_i^t$, $\varepsilon_i^{res}$, and $\eta = W_i^{diss}/W_i^{abs}$ with $\varepsilon_{yy}$.

Regarding the Ge-GA samples, let us first note that the orders of magnitude of the nominal stresses we obtained in compression are in line with measurements recently performed by Michelini *et al.* [144] on a similar gelatin (from porcine skin, 300 g Bloom, Type A), cross-linked by GA and tested at a comparable strain rate down to $\varepsilon_i^{min} = -0.3$, although at 37 °C under hydrated conditions. Then, while the addition of GA in gelatin has a strong impact in tension in terms of ductility (see previous section and Fig. 3.5 (a)), the comparison between the properties of Ge and Ge-GA hydrogels in compression gives much closer qualitative and quantitative trends (see Fig. 3.5 (b)). This is particularly demonstrated in Fig. 3.6 (b), where rather similar (*blue vs. red*) values are obtained for all (un)cross-linked samples, in terms of tangent moduli $E_i^t$, residual strains $\varepsilon_i^{res}$ or damping ratio $\eta = W_i^{diss}/W_i^{abs}$ per cycle. Finally, note that the nonlinear increase of $E_i^t$, $\varepsilon_i^{res}$ and $\eta$ with the strain is also observed for Ge-GA samples stretched in tension (Fig. 3.6 (a)). However, it remains much less pronounced than in compression, thereby implying a lower degree of non-linearity, weaker hysteretic cyclic response and more reversible deformations in tensile mode.

*Effect of strain rate* – Fig. 3.6 shows the evolution of $E_i^t$, $\varepsilon_i^{res}$, $\eta = W_i^{diss}/W_i^{abs}$ obtained for Ge(-GA) hydrogels with $|\dot{\varepsilon}_{yy}|$ in both tension and compression. The corresponding stress-strain curves measured for all cases are reported in Supplementary Fig. 3.12 (Appendix A). First of all, the overall stress-strain response of the hydrogels, and thus its mechanical descriptors

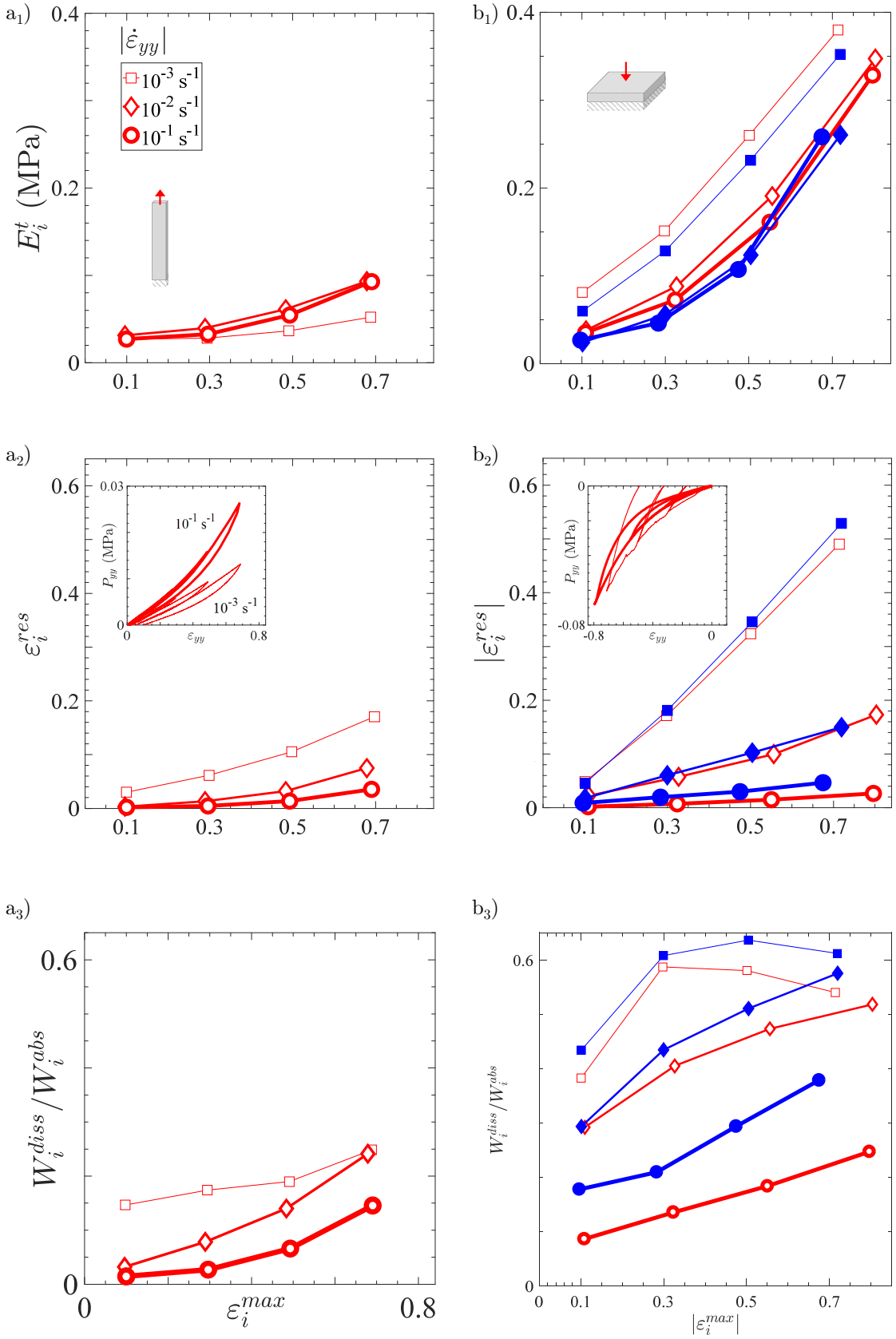


**Figure 3.6:** Mechanical descriptors of Ge (*in blue, filled symbols*) and Ge-GA hydrogels (*in red, blank symbols*) according to the loading type and the applied strain rate : ($a_1$) tangent modulus, ($a_2$) residual strain per cycle, and ($a_3$) dissipated energy per cycle in function of the cycle strain amplitude in tension. ($b_1$, $b_2$, $b_3$) Same as ($a_1$, $a_2$, $a_3$) but in compression.

($E_i^t$, $\varepsilon_i^{res}$, $\eta$) remain rather close when deformed at $|\dot{\varepsilon}_{yy}| \approx 10^{-2}s^{-1}$ or $10^{-1}s^{-1}$ (see Fig S2 and Fig. 3.6). In any case, for both loading modes, the measured changes are consistent with the expected responses of standard viscoelastic materials : the higher the loading rate, the higher the stress level and stiffness, and the lower the residual strain and dissipated energy (*e.g.* see quasi-null $\varepsilon_i^{res}$ in Fig. 3.6 ($b_2$) and lowest ratio $\eta$ in Fig. 3.6 ($b_3$)). These standard trends have been previously observed in many living soft tissues [43], elastomers, gellan gum gels [164, 194, 209], or hydrogels with reversible hydrophobic associations during uniaxial extension [232]. Such macroscale properties of polymers are often ascribed to time-dependent nanostructural rearrangements (*e.g.* unfolding of entangled molecular chains overcoming friction from other chains, (un)binding, deformation or rupture of cross-links) and/or fluid motion [21, 26, 101, 194, 232], which are not instantaneous processes, but instead require some time to occur.

Astonishingly, these common trends are not all fulfilled for the lowest strain rate $|\dot{\varepsilon}_{yy}| \approx 10^{-3}s^{-1}$, regardless of the type of loading and material :

- Among the expected trends, residual strains are strongly increased, shifting from 0.15 (for $|\dot{\varepsilon}_{yy}| \approx 10^{-2}s^{-1}$) to 0.53 for example for compressed gelatin after unloading at $\varepsilon_i^{min} = -0.7$. This inelastic effect is accentuated cycle by cycle with the amplitude of the applied strain whatever the loading mode, and all the more marked in compression (see Fig. 3.6 ($a_2$) *vs.* ($b_2$)). Likewise, the damping properties of the gels are particularly enhanced at this slowest speed, for both tensile and compressive modes : whatever the case, the ratio of dissipated to absorbed elastic energy after deformation of hydrogels, $\eta = W_i^{diss}/W_i^{abs}$, remains higher than that obtained at higher strain rates (see inlets in Fig. 3.6 ($a_3$) and ($b_3$)). Typically, with respect to the highest (resp. intermediate) strain rate $|\dot{\varepsilon}_{yy}|$, the relative increase of $W_i^{diss}/W_i^{abs}$ measured during compression ranges from 118 % up to 341 % (resp. 4 % up to 45 %) depending on the applied strain.

- However, in a strange and still unexplained way, the instantaneous stiffness of the hydrogels after unloading is altered in reverse trends in tension and compression : in tension, the gel viscoelasticity yields well to a moderate decrease of stress levels (Fig. S2 ($a_{1,2}$)) and tangent moduli $E_i^t$ (Fig. 3.6 ($a_1$)) compared to the highest rates, especially for $\varepsilon_i^{max} > 0.3$. However, a very singular behavior is evidenced in compression, showing both higher stress levels (Fig. S2 ($b_{1,2}$)) and tangent moduli $E_i^t$ (Fig. 3.6 ($b_1$)) from the early deformation stages ($\varepsilon_i^{min} \leq -0.1$).

To our knowledge, we have not seen this type of behavior before in the literature. Focusing more specifically on gelatin gels, a few studies have already reported the strain rate sensitivity of gels in compression [61, 123]. In particular, or the three strain rates studied in our database, Forte *et al.* [61] observed that gelatin gels (beef origin) exhibit a strong rate dependent failure response (with both ultimate stress and strain rising with the applied rate). This rate effect was reproduced by modelling the gel as a poroelastic material with water flow through the porous solid polymer network. By simulating monotonic compression tests on a neat gelatin sample assumed to be fully saturated, their predictions

show that solid matrix stresses increase while pore pressure decreases as the strain rate decreases. At low strain rates (typically $10^{-3}\ s^{-1}$), the liquid is expected to easily flow into the solid matrix network (or even leave the sample), thus contributing very little to the gel's load resistance and failure. Thus, in the critical case of gel cracking and liquid migration, we would expect an increase in stress levels and gel stiffness at low strain rates. However, this consolidation scenario is not viable in our case for no cracks or water flow out of the sample were observed during the experiments. The origin of the singular behavior evidenced in our results remains an open question.

### 3.3.3 Comparison with human vocal folds

To finally quantify the relevance of gelatin-based hydrogels as biomimetic candidates, the cyclic and finite strains mechanics of the Ge-GA hydrogels processed above is compared with that of human vocal folds. The target mechanical behavior of native tissues was chosen as characterized *ex vivo* by Cochereau *et al.* [43] under multiple loadings relevant in phonation, *i.e.* longitudinal tension, transverse compression and longitudinal shear. Over the whole database, we determined the Ge-GA candidate whose mechanical properties best reproduced the reference data on average for these three loading modes. The best candidate was obtained for the concentration of cross-linker $V_{GA}/m_{Ge} = 0.5$ % mL/g.

Fig. 3.7 shows typical stress-strain curves obtained after subjecting the selected hydrogel to 10 load-unload cycles in tension, compression and shear (*in red*), using the same geometrical and kinematical conditions chosen for the native tissue [43]. Reference data obtained on vocal folds and their major layers (the *lamina propria*, *i.e.* the upper loose connective tissue, and the *vocalis* muscle below) dissected from two healthy human larynges are reported in Fig. 3.7 : graphs ($a_1$, $a_2$, $a_3$) give data from a 79-year-old male donor (height 1.70 m, weight 65 kg), whereas graphs ($b_1$, $b_2$, $b_3$) refer to a 79-year-old female donor (height 1.60 m, weight 45 kg). Regarding these biological targets, note that only the $1^{st}$ and $10^{th}$ cycle are displayed for the sake of clarity. In addition, gray corridors represent stress-data uncertainty ($1^{st}$ cycle only) induced by the estimation of the sample cross section.

Firstly, it is important to remind that both *lamina propria* and *vocalis* can be seen as 3D incompressible composite structures made of a gel-like matrix reinforced by a network of collagen fibers, with wavy shapes and preferred orientations at rest [9, 114, 153, 210]. Knowing that, our results show that the average properties of the Ge-GA hydrogel (stiffness and strength) are quite comparable (albeit higher) to those of the two vocal-fold layers in transverse compression and longitudinal shear, *i.e.* under loading conditions where fibers unfolding, tension and rotation are limited, while the mechanical contribution of the isotropic matrix is much more critical [210]. Higher quantitative discrepancies are also found with the tensile response of the entire fold and its upper layer, due to the progressive recruitement and reorientation of the collagen fibers towards the load direction in this case [64, 145, 210]. For instance, at a strain of 0.1 (absolute value), the stress level in the Ge-GA sample is about 17 times lower than that achieved in the *lamina propria* in tension (mean value on both donors), while it is about 5 times higher in compression and 4 times

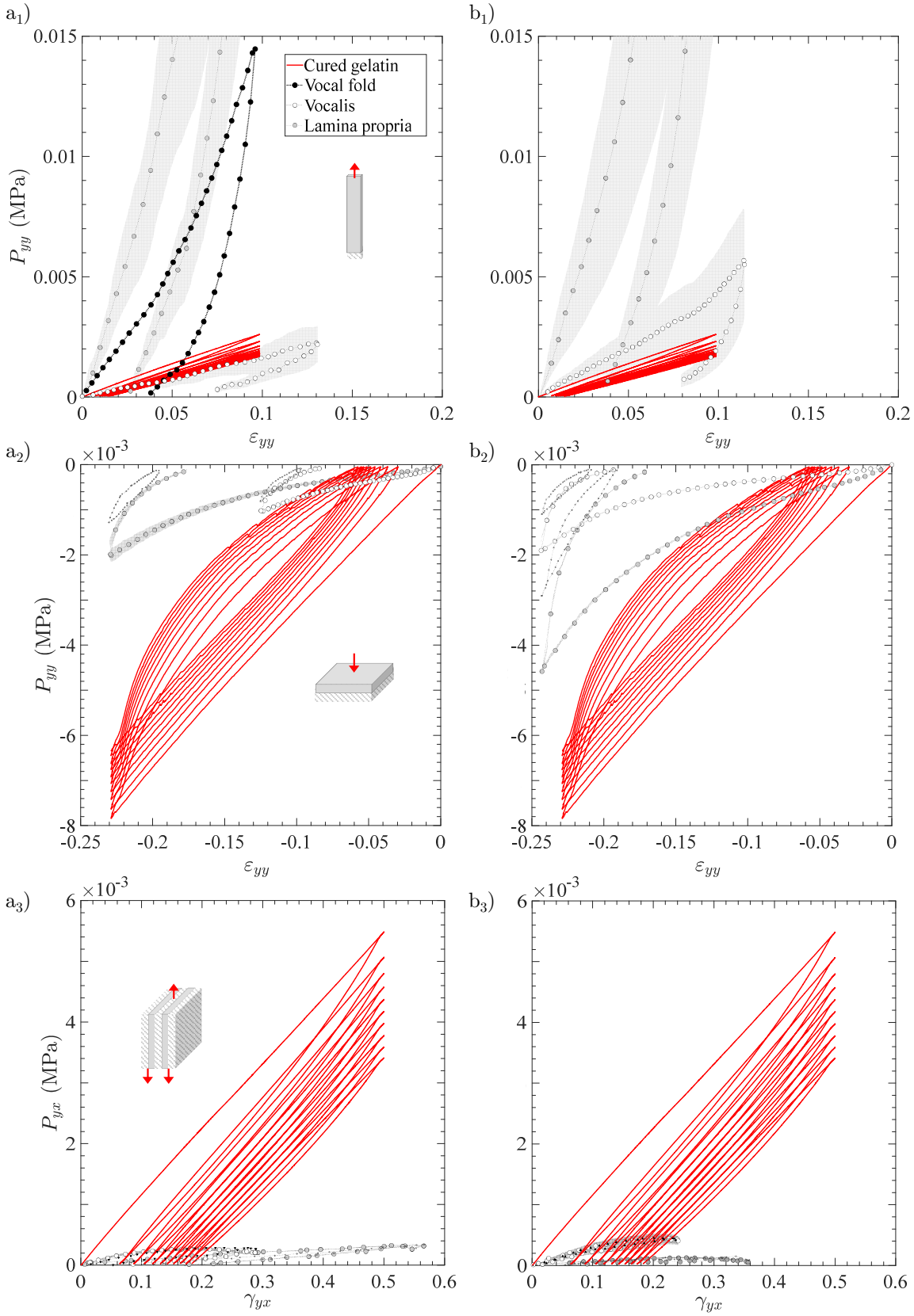


**Figure 3.7:** Typical stress-strain curves of the Ge-GA hydrogel with $V_{GA}/m_{Ge} = 0.5$ % mL/g (*in red*), and those measured on one human vocal fold and its main sublayers (*lamina propria*, *vocalis*) when subjected successively to 10 load-unload cycles in ($a_1$) longitudinal tension, ($a_2$) transverse compression, ($a_3$) longitudinal shear. ($b_1$, $b_2$, $b_3$) Same as ($a_1$, $a_2$, $a_3$) but for another donor. *Source :* Adapted from Cochereau *et al.* [43].

higher in shear. Note that in tension, deviations from the *vocalis* muscle become far less pronounced, because the muscle fibers are straighter and softer than the collagen fibers of the *lamina propria* at rest [9, 210].

In the end, despite its isotropy, the chosen Ge-GA hydrogel proves to be a first and rather basic solution to approximate the average behavior of the *vocalis* and the *lamina propria* for the three loading modes. While it is thus able to mimic the tensile behavior of the *vocalis* fairly well, it fails to mimic quantitatively that of the *lamina propria* due to the strong tissue anisotropy. Embedding a fibrous reinforcement in the hydrogel or inducing a suitable nanostructuration using freeze-drying techniques [71, 75, 142] should allow to approach the J-shaped anisotropic target response in tension, without further stiffening the current properties in compression and shear.

## 3.4 Conclusion

The mechanics of homogeneous hydrogels made of neat or cross-linked gelatin with parametric concentrations of glutaraldehyde were characterized under tension, compression and shear upon finite strains and over three decades of strain rates. In summary, the collected database has highlighted several original outcomes : (i) a critical concentration of cross-linker is needed to enhance the mechanical strength, stiffness and ductility of neat gelatin in tension ($V_{GA}/m_{Ge} \geq 0.5$ % mL/g) ; (ii) by contrast, the mechanical properties of neat and cross-linked hydrogels in compression are rather close; (iii) In both tension and compression, the non-linear stress hardening, stress hysteresis and residual strains observed during cyclic paths are enhanced when the gels are subjected to increasingly large strains; (iv) whatever the type of loading and material, a drastic change in mechanical behavior is observed for the lowest strain rate around $10^{-3}\ s^{-1}$ compared to the upper two decades. In particular, a very singular behavior is evidenced in compression from the early deformation stages, showing both higher stress levels and tangent moduli than those recorded at higher strain rates; (v) finally, in order to mimic the tension, compression and shear responses of the vocal-fold fibrous tissues, the cross-linked hydrogels elaborated in this work prove to be rather relevant candidates despite their isotropy.

Developments are still needed to better understand the mechanical behavior of gelatin-based hydrogels we evidenced at the macroscale, such as their specific strain-rate sensitivity. In particular, information about the internal network structure of the various gels such as their pore topology should be explored, using *ante-/post-mortem* micro-imaging techniques [141]. Regarding the target application, the response of the gels at higher strain rates should also be scrutinized using Large Amplitude Oscillatory shear (LAOS) for instance, so as to approach typical fundamental frequencies encountered during human phonation ($\approx 10^2\ s^{-1}$). Finally, the introduction of a suitable structuration in the proposed hydrogels should now be conducted to mimic the J-shaped anisotropic tensile response of the vocal folds.

# APPENDIX A

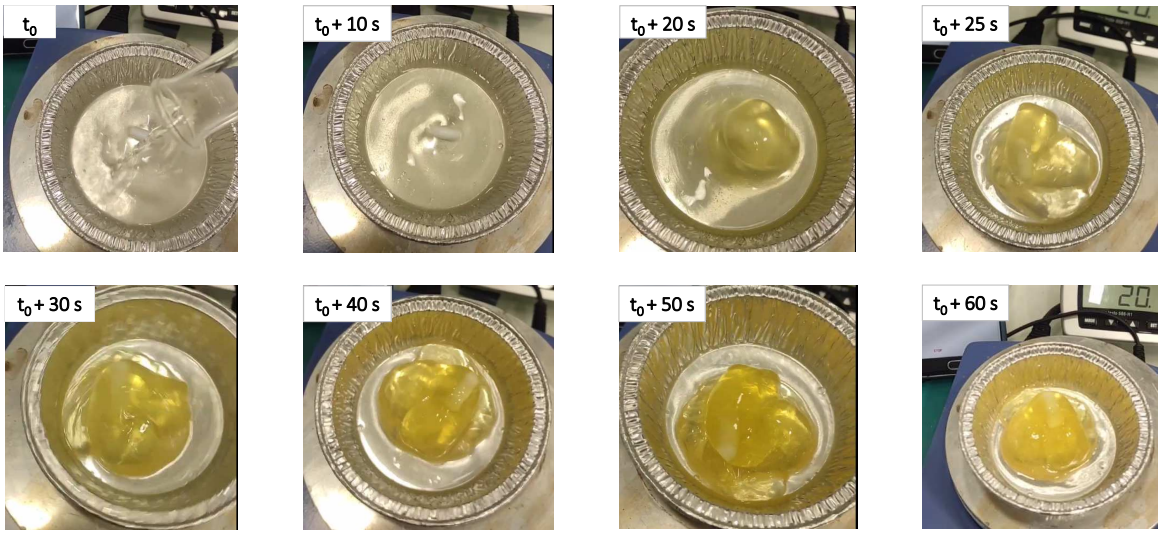


**Supplementary figure 3.8:** Kinematics of the cross-linking reaction during the elaboration of Ge-GA hydrogels in case $V_{GA}/m_{Ge} > 1\,\%$ mL/g.

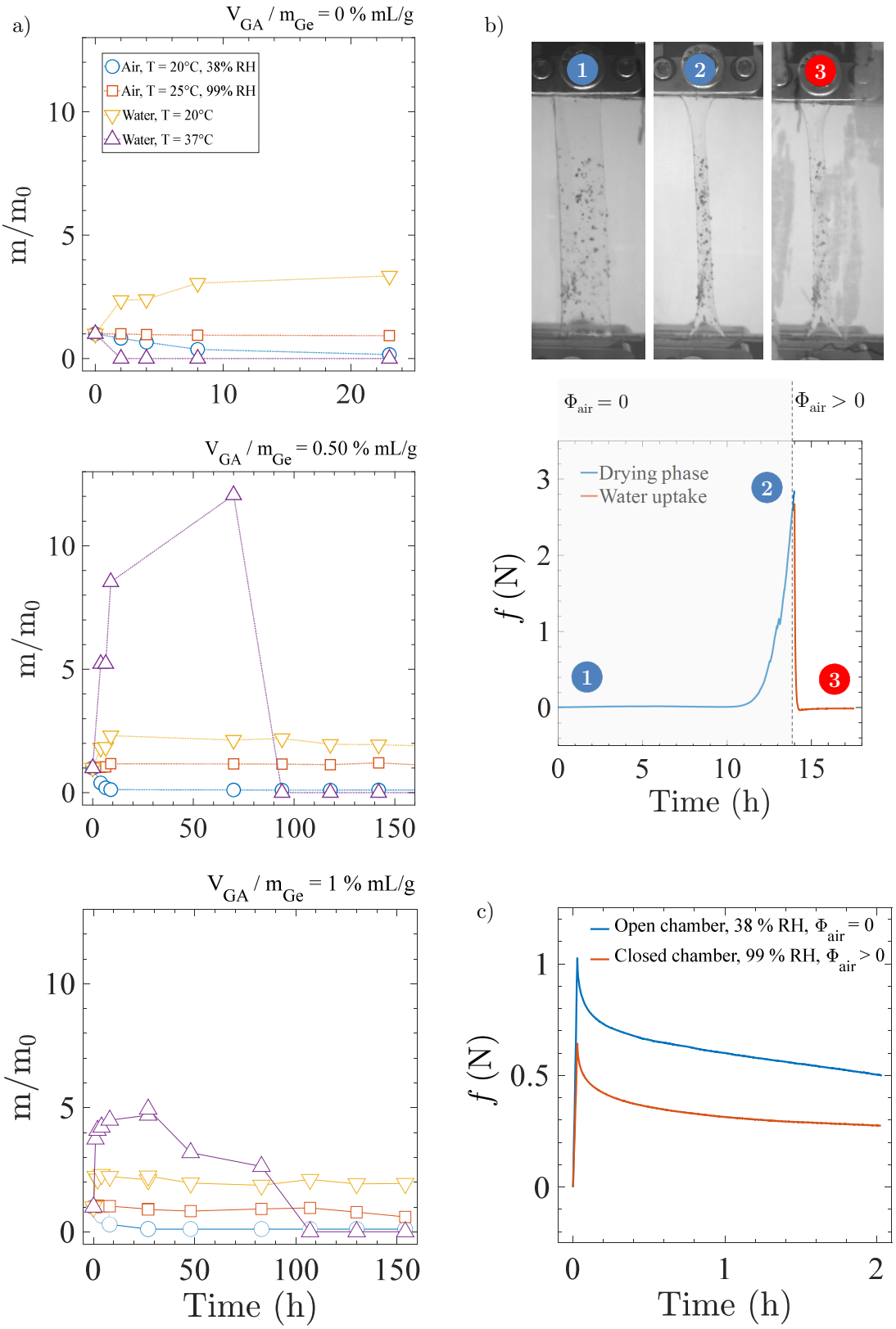


**Supplementary figure 3.9:** Stability of Ge-GA hydrogels assessed in various hygro-thermal environments. a) Mass evolution of a typical Ge-GA sample in function of time for three different $V_{GA}/m_{Ge}$ ratios (*from top to bottom*) : 0.00%, 0.50% and 1.00% mL/g. b) Typical time-evolution of the axial load measured while maintaining a humidified Ge-GA sample (99 % RH) between the tensile jaws, once $\Phi_{air} = 0$ (*drying phase in gray zone from time ① to time ②*) and $\Phi_{air} > 0$ (*water uptake from time ② to time ③*). c) Typical stress relaxation behavior of Ge-GA hydrogels after a pre-strain of 70% with $|\dot{\varepsilon}_{yy}| \approx 10^{-2}\ s^{-1}$, placed in two distinct hygro-thermal conditions : (*in blue*) T = 20 °C, 38 % RH, $\Phi_{air} = 0$; (*in red*) T = 25 °C, 99 % RH, $\Phi_{air} > 0$.

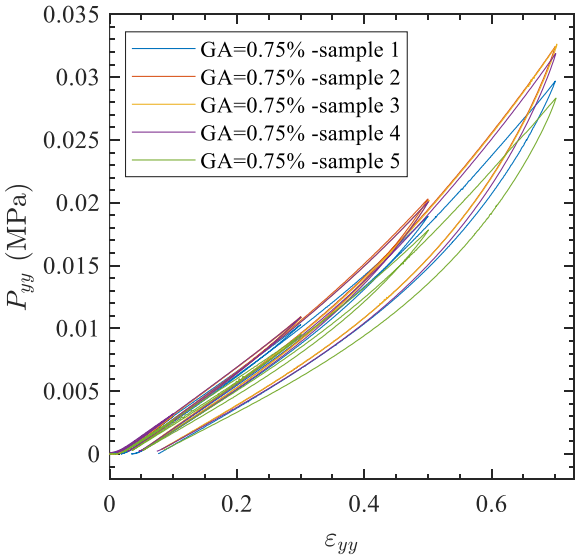


**Supplementary figure 3.10:** Typical stress-strain repeatability obtained for the cyclic tensile test performed on Ge-GA hydrogels over 5 measurements. Illustrative case of the Ge-GA hydrogel with $V_{GA}/m_{Ge} = 0.75$ % mL/g.

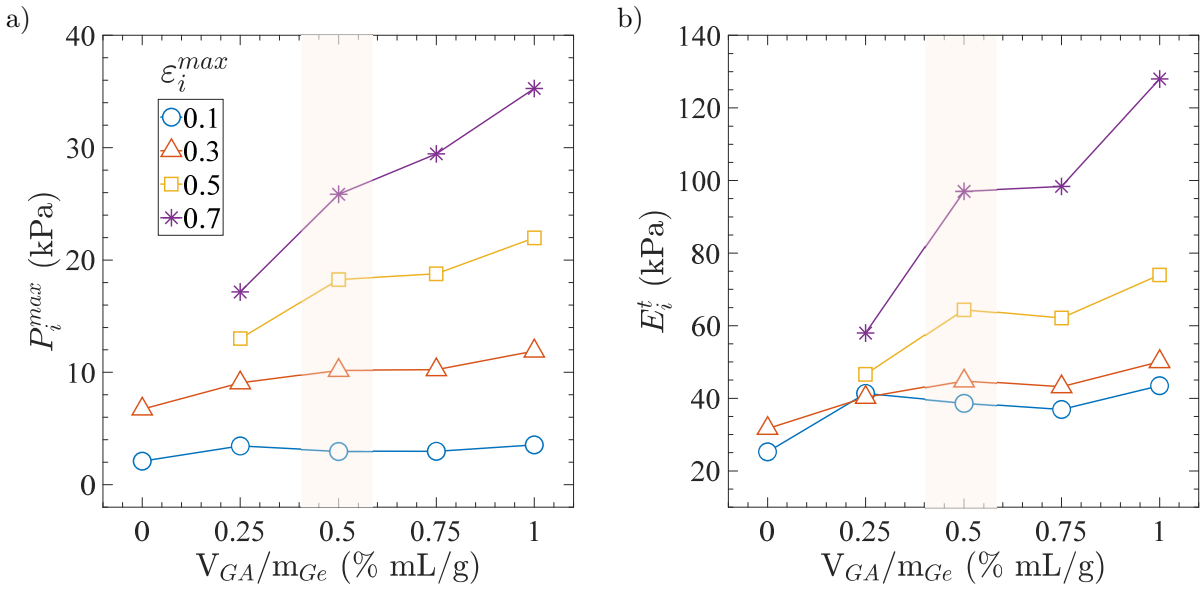


**Supplementary figure 3.11:** Influence of the cross-linker concentration ($V_{GA}/m_{Ge}$) on two mechanical descriptors of Ge-GA samples during tensile cyclic loading, as a function of maximum strain amplitude $\varepsilon_i^{max}$: a) peak stress achieved during cycle $i$, $P_i^{max}$; b) tangent modulus at the early unloading phase of each cycle, $E_i^t$. $|\dot{\varepsilon}_{yy}| \approx 10^{-2}\ s^{-1}$. Red-colored area corresponds to the critical degree of cross-linking.

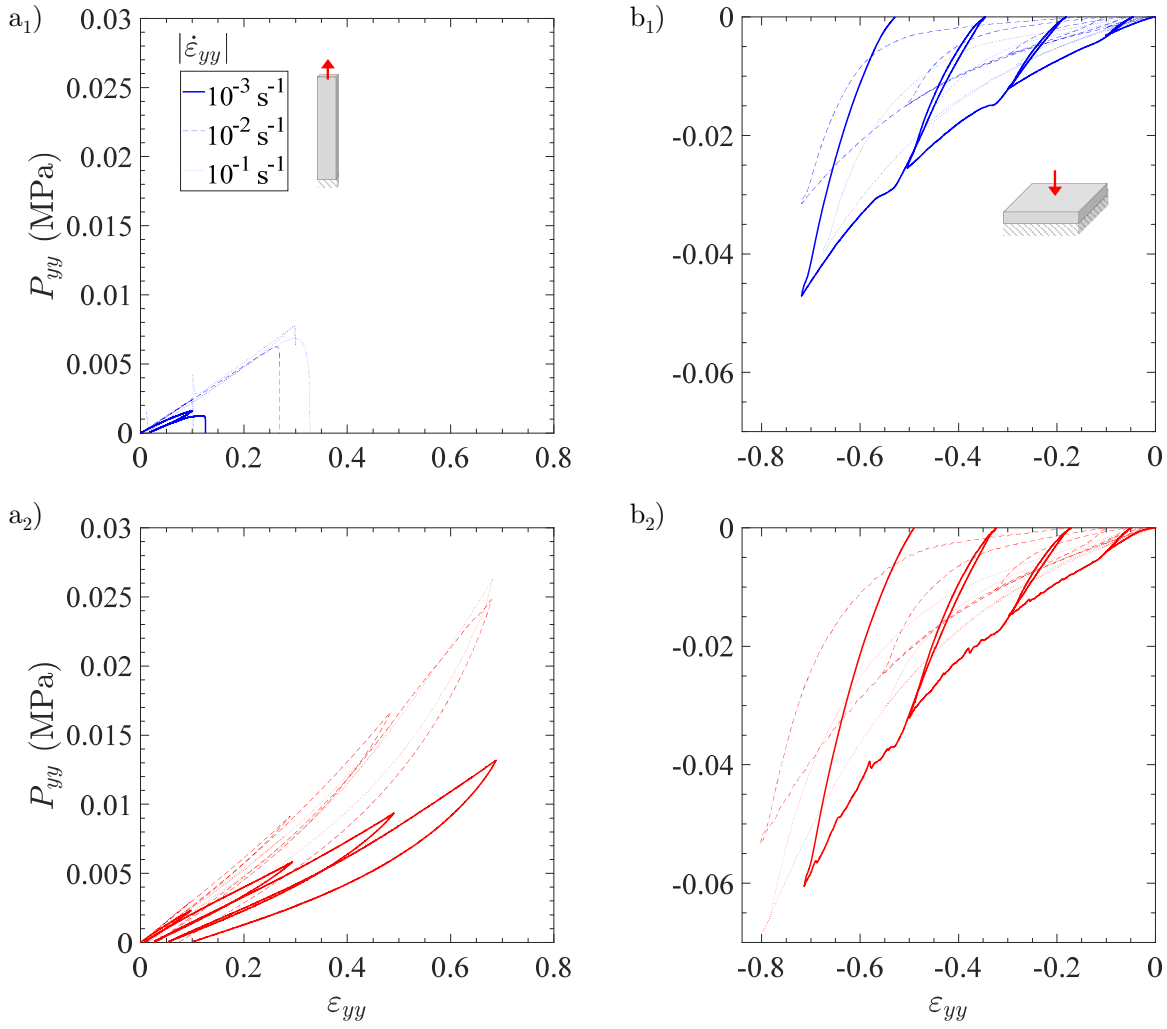


**Supplementary figure 3.12:** ($a_1$, $a_2$) Tensile stress-strain response of Ge samples (*in blue*; $V_{GA} = 0$ mL) and Ge-GA samples (*in red*; $V_{GA}/m_{Ge} = 0.5$ % mL/g) for three orders of magnitude of strain rate $|\dot{\varepsilon}_{yy}|$. ($b_1$, $b_2$) same as ($a_1$, $a_2$) but in compression.

# 4

# Complement to Chapter 3 – Comparison with alternative isotropic candidates : PEG-based hydrogels and silicone elastomers

# Contents

## 4.1 Introduction

As discussed in the previous chapter, gelatin based hydrogels are known with plenty of advantages such as low toxicity and immunogenicity, high water content and facility of fabrication at relatively low cost. Even though, their long-term durability and integration with the cell-culture media requires further investigations which are not the subject of current study.

Beside the developed hydrogels in the previous chapter, also other candidate materials have interesting capacities to be employed as model materials for the *in vitro* study of the structural properties of the vocal fold tissue and their consequent impacts on the vibratory response.

Thus, we have decided to benefit the opportunity of the developed experimental set-up for performing the same methodology of mechanical characterization designed for this particular application, on some of the other promising candidates with different basic features.

In this regard, two different class of alternative materials were investigated: **Silicone-based rubbers** as a synthetic elastomer due to the wide use of them in the recent phonatory testbed studies and *in vitro* models [124, 143, 195]. Use of silicone will also help to establish an elucidating analogic basis of our obtained result (both in terms of mechanics and self-oscillation) with the achievements of numerous similar works using silicone rubbers.

Second group is **Polyethylene glycol (PEG) based hydrogels** as a widely used biomaterials in variety of fields from pharmaceutical and biomedical applications to the commercial and industrial products. Use of such biomaterials is interesting as they have already successfully passed through approval process of the Food and Drug Administration and also obtained many clinical progress in tissue regenerative medicine. Thus in the perspective of the injectable materials for the vocal fold tissue repair, involvement of such biomaterials in the mechanical and aero-acoustic investigations can be of great interest.

#### PEG-based hydrogels

Polyethylene glycol (PEG) is a polyether compound derived from petrochemical products. The versatility of the PEG polymer chemistry, together with its excellent biocompatibility, has provoked many development in the study and fabrication of different functional compounds derived from or based on this macromolecular structure. Among them, the non-ionic, hydrophilic PEG gel systems are increasingly used . PEG is considered biologically inert and safe by the FDA, thus, PEG-based hydrogel is one of the main component in the design and fabrication of biomedical scaffolds for regenerative medicine and controlled release of biomolecules due to its excellent biocompatibility. The design, fabrication, and characterization of PEG hydrogels rely on the understanding of fundamental gelation kinetics as well as the purpose of the application.

While various methods of gelation (i.e., physical, ionic, or covalent interactions) can be used to form PEG gels[42], chemically or covalently-crosslinking leads to relatively stable hydrogel structures with tunable physicochemical properties such as permeability, molecular diffusivity, equilibrium water content, elasticity, modulus, and degradation rate[171].

Same a most of the other Hydrogels, the base of using PEG hydrogels biomedical therapeutics and regenerative medicine applications stems from its hydrophilicity. A loosely crosslinked PEG hydrogel can easily absorb more than 95 % of water in its total mass[42].

Tayloring the mechanical properties of the resulting hydrogel has been extensively studied through the control of the chemistry of synthesis reactions and particularly degree of crosslinking. Even though, interference of the structural modification with the other functional capacities of the gel should be carefully considered. Recently developed photopolymerization methods has allowed tuning the mechanics of PEGDA hydrogels in a concentration dependent manner from <1 to 17 kPa, a more physiologically relevant range than previously possible with PEG-based hydrogels, without altering the hydrogel's degradation and permeability[192].

**Ecoflex® silicone elastomers**

Silicone elastomers are one of the most extensively used polymer products in a vast range of applications from the domestic utensils and sealants to the advanced technologies such as flexible electronics and implants[156]. Silicone rubbers are known for several advantages particularly in the field of biomaterials. Their long durability is considerably interesting for for long experimental campaigns. Compared to many of the similar elastomers, they have rapid and easy curing procedure. Due to their strong molecular structure, they maintain their wide functioning capacity in many extreme temperatures and humidity levels[157]. High degree of stretchability has made them an excellent candidate for the mimicking the soft and flexible structures. The facility of the formation and casting is also an interesting point in manufacturing the intricate shapes. Finally, their chemical and electrical inertness make them relatively biocompatible, and assures the skin safe manipulations for the experimental utilities[170].

A silicone elastomer formulation usually consists of a polymer and a crosslinker, where the stiffness of the final product is controled by mixing ratio of the two components. Crosslinking process of the silicone elastomers are typically carried out through hydrosilylation (usually Pt-catalysed addition), condensation (usually Sn-catalysed) and radical reaction[28].

Silicone elastomers are generally characterized with their viscoelastic behaviour, *i.e.* they possess both elasticity and viscous dissipation, with the main contribution being elasticity. In terms of mechanical properties, their elastic moduli are usually very low (in the order of few MPa) and they are very extensible, with ultimate strains usually more than 300 % [202]. Some additive materials are commonly used to improve the mechanical performance of such elastomers(such as fumed silica to enhance failure strength), but they may affect

other properties (significant rise of the elastic modulus). Nevertheless, correct choice of formulation of silicone elastomers suggests a wide range of mechanical properties while maintaining mechanical integrity.

**Note: Ecoflex™ 00-10 cures with a "tacky" surface.**

**TECHNICAL OVERVIEW**

| | Mixed Viscosity (ASTM D-2393) | Specific Gravity (g/cc) (ASTM D-1475) | Specific Volume (cu. in./lb.) (ASTM D-1475) | Pot Life (ASTM D-2471) | Cure Time | Shore Hardness (ASTM D-2240) | Tensile Strength (ASTM D-412) | 100% Modulus (ASTM D-412) | Elongation at Break % (ASTM D-412) | Die B Tear Strength (ASTM D-624) | Shrinkage (in./in.) (ASTM D-2566) |
|---|---|---|---|---|---|---|---|---|---|---|---|
| Ecoflex™ 5 | 13,000 cps | 1.07 | 25.8 | 1 min. | 5 min. | 5A | 350 psi | 15 psi | 1000% | 75 pli | < .001 in./in. |
| Ecoflex™ 00-50 | 8,000 cps | 1.07 | 25.9 | 18 min. | 3 hours | 00-50 | 315 psi | 12 psi | 980% | 50 pli | < .001 in./in. |
| Ecoflex™ 00-30 | 3,000 cps | 1.07 | 26.0 | 45 min. | 4 hours | 00-30 | 200 psi | 10 psi | 900% | 38 pli | < .001 in./in. |
| Ecoflex™ 00-33 AF | 3,000 cps | 1.07 | 26.0 | 45 min. | 4 hours | 00-33 | 200 psi | 10 psi | 900% | 38 pli | < .001 in./in. |
| Ecoflex™ 00-20 | 3,000 cps | 1.07 | 26.0 | 30 min. | 4 hours | 00-20 | 160 psi | 8 psi | 845% | 30 pli | < .001 in./in. |
| Ecoflex™ 00-20 FAST | 3,000 cps | 1.07 | 26.0 | 20 min. | 1 hour | 00-20 | 160 psi | 8 psi | 845% | 30 pli | < .001 in./in. |
| Ecoflex™ 00-10 | 14,000 cps | 1.04 | 26.6 | 30 min. | 4 hours | 00-10 | 120 psi | 8 psi | 800% | 22 pli | < .001 in./in. |

*All values measured after 7 days at 73°F/23°C

***Mix Ratio:*** 1A:1B by volume or weight
***Color:*** Translucent
***Useful Temperature Range:*** -65°F to 450°F (-53°C to 232°C)
***Dielectric Strength*** (ASTM D-147-97a)**:** >350 volts/mil

**Figure 4.1:** Technical specifications of the silicone Ecoflex® series. *Source :* https://www.smooth-on.com/.

## 4.2 Materials and methods

### 4.2.1 Sample preparation

#### Ecoflex® silicone elastomers

For the choice of silicone rubber, three grades of Ecoflex®was bought from Smooth-On® . For the sake of variety in the stiffness of ultimate sample, three grades of 00-10, 00-30 and 00-50 was selected as representatives of two extremes and an intermediate Shore Hardness. These grade will be referred in this chapter as EF10, EF30 and EF50 respectively.

The final composition of this product is obtained through a so-called "addition-cure" process *i.e.* mixing of the equal portion (by weight) of the two provided A and B parts. Upon the addition of the two part, a platinum complex catalyst triggers the crosslinking reaction through an ethyl bridge creation between the two parts.

After mixing the components, the mixture was held inside degassing vacuum condition in order to remove the air bubbles appeared during the mixing agitations. Then the mixture was then cast into the flat molds (the same as the rectangular molds of gelatin hydrogel in the previous chapter) and left for the curing to be accomplished. [same compositions of the Ecoflex®mixtures were also cast into the designed 3D-printed molds of the vocal fold replicas for the vibroacoustic evaluations (see chapter **??**)]. The curing was carried

out in the open air and room temperature. Duration of crosslinking varies depending on the grade between 2 to 4 hours. Rectangular samples of the tensile, compressive and shearing was also cut in the same geometries as the gelatin samples for the mechanical characterization.

### PEG-based hydrogel

revision req The fabrication process of the PEG hydrogels is explained in chapter5 (see **??**). Briefly, poly(L-lysine) dendrigrafts (DGL) was mixed with poly-ethylene glycol (PEG–crosslinked by NHS) in aqueous solutions with various DGL/PEG ratios (1/1, 1/2, 1/2.5 or 1/3 w/w) and PEG molecular weight, noted $\text{PEG}_{MW}$ (2 or 10 kDa).

In a typical experiment, PEG–NHS in anhydrous dimethyformamide (DMF) solution at different concentrations $C_{PEG}$ (5, 10 or 12 w/v %) was added to DGL in phosphate buffer saline (PBS) in eppendorf tubes at 4 °C. This mixture was swiftly vortexed and transferred to 3D-printed molds, where it cross-linked between 15 to 30 minutes at room temperature. After cross-linking, the hydrogels were removed from the mold and stocked in PBS solution at 4 °C until use. The resulting samples were typically from 1 to 5 mm in thickness. For the tensile tests the length of the rectangular samples was about 22 mm (10 mm effective length and 12 mm in the jaws), and 5 mm in width as shown in figure 4.2 a. In shear and compression modes, the samples were used in sqaure geometry having 10 mm length and width

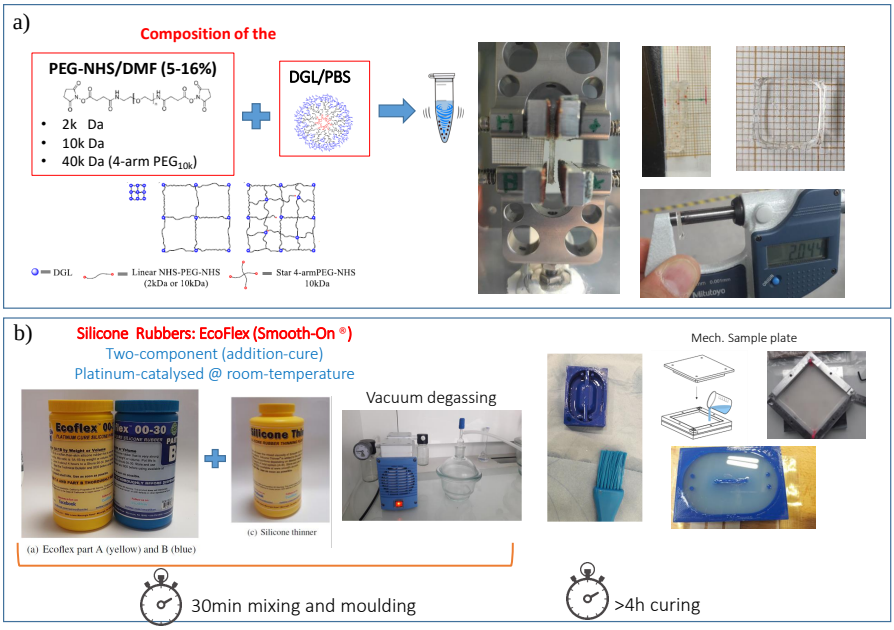


**Figure 4.2:** Sample preparation of the alternative candidates for the isotropic matrix

### 4.2.2 Adjusments in the mechanical procedure

The mechanical characterization was carried out generally on the same setup described in chapter 3. The loading rate was limited to a single rate of $10^{-3}$ $s^{-1}$ for both materials and in all the loading modes, except for the silicone under traction which was done at $10^{-2}$ $s^{-1}$. Loading regime was progressive cycles in tensile mode and repetitive cycles at the same strain level for shear and compression. There are also exceptions for certain cases of PEG hydrogels due their highly sensitive and fragile structure and associated difficulties of manipulations, which are explained below:

First, a series of the **tensile** tests on various compositions of PEG hydrogels was conducted in another platform with different loading regime. These hydrogels were subjected to the repetitive cyclic loading with the strain rate of $2\times10^{-3}$ $s^{-1}$. Then they were stretched until the full rupture point of the sample. Then in another experimental campaign, the PEG hydrogel with a 2k Da- 5 % composition was selected as an optimised candidate for characterization in other loading modes and also subsequent fabrication of fiber-reinforced composite. In compression the cyclic loading was carried out in the form of progressive loading until the $P_{max}$ of about 50 %. Finally, the shearing response of the gel was also measured under repetitive loading cycles up to the maximum strain of about 65 %.

## 4.3 Results

This section is dedicated to describing the obtained results of the experimental characterization campaign on the PEG hydrogels and silicone rubbers as matrix candidates for the vocal folds replicas.

### 4.3.1 General trends

Compared to the previously characterized gelatin-based hydrogels, the PEG hydrogels appeared to be more fragile, behaving with a relatively limited capacity of elongation. The compressive response of the gel was also weaker than the gelatin counterpart, but under shear loading, they behaved almost in similar manner.

Synthetic alternative materials were found to be either softer or stiffer than gelatin samples in traction, depending on their grades. The mechanical response of all the three tested grades of Ecoflex®seems to be generally more robust and reversible than the hydrogels and there is a negligible cyclic deterioration of the properties at the interested strain ranges of current work.

### 4.3.2 Mechanics in tension

**Ecoflex® :** Figure 4.3.a illustrates the tensile response of the Ecoflex®samples undergone four loading cycles with progressive strain levels from 10 to 70%. The response of the gelatin hydrogel to the same loading condition is superimposed for the sake of comparison. In a first glimpse, it is perceived that the stiffness of the materials is correlated with their commercial Shore-Hardness degree, even though this correlation is not linear and EF50 and EF30 present closer behaviour with respect to the EF10 which is much softer. Small hysteresis and low residual strains at the end of the cycles proves the predominance of the highly elastic nature of such materials against their viscous dissipating capacity. On the other hand, the stiffness of the Ecoflex®passes through a slight transition from low strain to higher strain, which is more pronounced in EF30 and EF50.

**PEG:** cyclic tensile characterization of the PEG hydrogels are presented in Fig. 4.3.b.

Almost all the hydrogel samples behaved more linearly during the cyclic phase and beyond that up to the rupture point, which confirms their brittle structure. Depending on their composition, the stiffness of these gels can be widely tuned. Hydrogels with molecular weight of 10k Da and 40k are placed at the two extremities of the stiffness, while the 2K Da gels can be placed in between. The cyclic loading has a minor effect on the response of the gels and their elastic properties are highly recoverable. However, compared to the gelatin hydrogels and silicone rubbers, their capacity to bear large strains is clearly limited; as can be seen for most of the samples where the elongation ends up in rupture at strains of less the 40%.

### 4.3.3 Mechanics in compression and shear

**Ecoflex® :** the compressive behaviour of the Ecoflex® materials are presented in figure4.3c. the same as tensile response gradual increase of the stiffness is still visible here as function of shore hardness. However, the residual strain and hysteretic behaviour at this loading mode is more significant (small compressibility). Again, the closest response to the gelatin hydrogel is the case of EF10. In shearing mode as there appears a softening effect for the strains of above 30% which is more pronounced in EF50 and EF30.

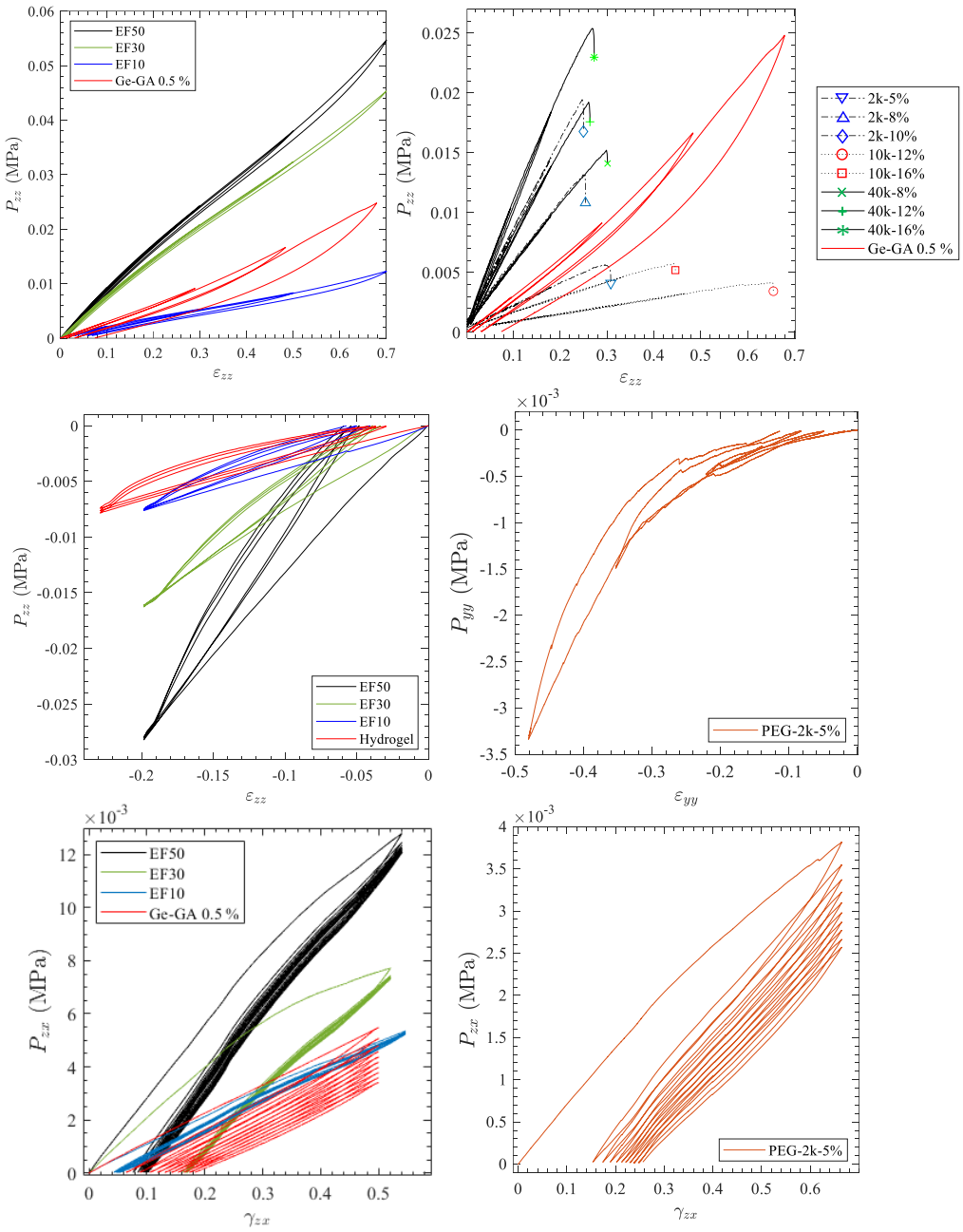


**Figure 4.3:** Multiaxial behaviour of EF and Ge (left) and PEG(right)

## 4.4 Discussion and concluding remarks

*Silicone Rubbers*– The tensile response of the Ecoflex®silicone as an unfilled rubber is very close to the similar rubbers such as Polyurethane[132, 242]. Our results in tensile mode are also in good agreement with the recent thermo-mechanical characterization of the Ecoflex®rubbers [134]. As the chemical composition of the product provided by the manufacturer offers, the stiffness is rising with the increase of shore hardness. Concerning the stretchability of them, in the elongation range of our interest (*i.e.* less than 100%) they behave almost the same, since the ultimate tensile strength is far beyond of our desired target (up to 700-900 % [134]) due to the presence of strong covalent bonds. These studies report a significant presence of the stress softening phenomena in the loading path known as Mullins effect[159, 160]. Although this effect is mainly visible for the larger deformations (beyond 100%), it can be detected on the peak points of our results as well in the form of an envelope over the progressive multi-cycle path.

*PEG Hydrogels*– The tensile response of hydrogel can be explained according to the molecular weight of the gels: in the 2k Da gels, shorter molecular length results in a higher resistance against applied loading and thus the gel fails at limited deformation and relatively higher stiffness. Nevertheless, 10k Da gels have larger chain units and thus, there is fewer bonding nodes for a given length of molecular chain compared to the 2k Da equivalent. This will allow the structure to be stretched easier and breaks at higher strain levels and a weaker strength. In the hydrogels with the molecular weight of 40k Da, increased molecular weight is not necessarily associated with longer chain, rather it is achieved by a 3D arrangement of the chains together. Therefore, the number of nodes in a same volume of the gel will be multiplied. Such enhanced number of entanglements gives rise to an improved strength of the gel against the applied strain. Nonetheless, such relatively enhanced stiffness is not significantly different from the response of the 2k Da gel. Thus, from this point of view, the 2k Da hydrogel can be identified as a promising candidate for the fabrication of tailored composite. The dissipative capacity of all the gels is very weak as shown by the negligible hysteresis in the cycles. Besides, the quasi-null residual strain reveals that the structure is highly elastic, and the organization of internal network is fully recoverable under applied deformation before the ultimate failure. This is an interesting character which can be combined with a stronger fibrous network to produce desired properties of the target.

**Conclusion**

To sum up, the choice of Ecoflex®silicone can be justified by their simple fabrication compared to the hydrogels. their long-life functional features is of great interest for long duration of experimental campaign. The mechanical response of the studied samples shows that at the strain range of the current work, EF illustrates closer response to the developed gelatin-based hydrogels. PEG hydrogels are relatively fragile and presented more linear response. how ever their biocompatibility and high water content, still keeps them as a good candidate for the matrix of oscillating structures, although their mechanical

properties should be adjusted by the use of fibers to introduce anisotropy and improved stretchability and damping capacity.

# Part III : Towards the optimisation of anisotropic and architectured materials

# 5

# Versatile fibre-reinforced hydrogels to mimic human vocal fold microstructure and mechanics

This part is based on a collaboration with Daniel Ferri-Angulo and Jérôme Sohier (LBTI, Lyon), experts in chemistry and jet-spraying technique for the synthesis of fibre-reinforced hydrogels. The following chapter is based on an article in preparation for a submission to *Acta Biomateriala*, by D. Ferri-Angulo, H. Yousefi-Mashouf, M. Michel, A. McLeer, L. Orgéas, L. Bailly and J. Sohier.

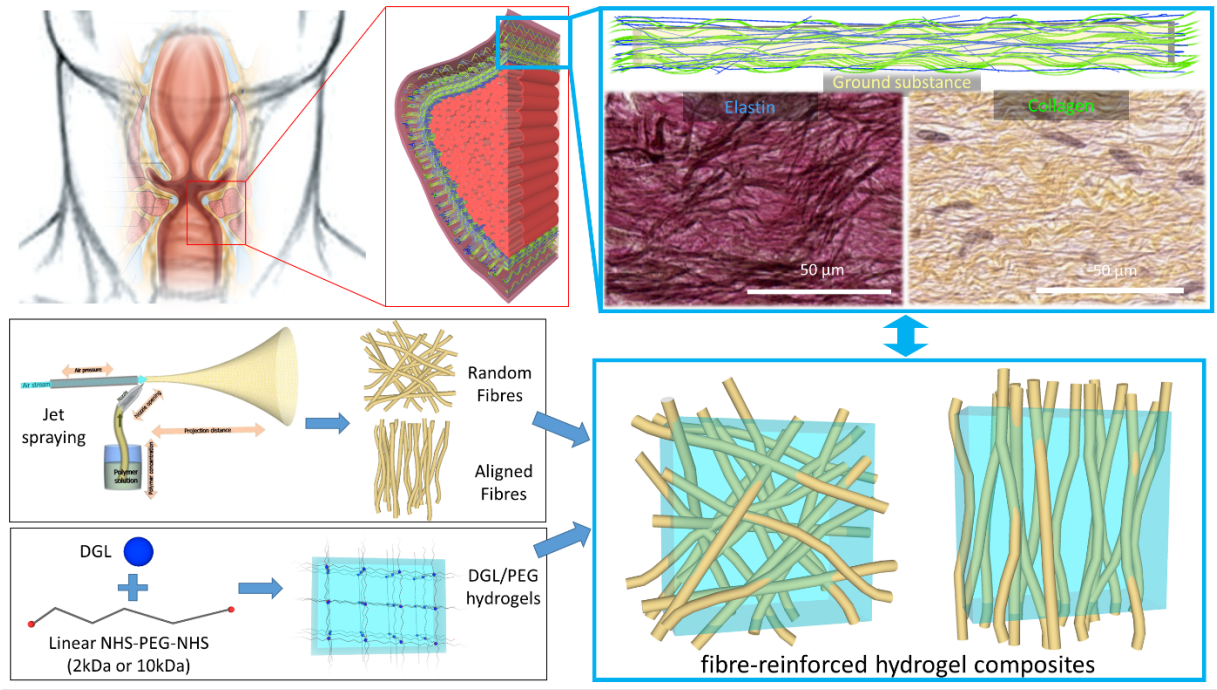


**Figure 5.1:** Synthetic approach followed to mimic the major structural and mechanical specificities of human vocal-fold *lamina propria* through the design of soft DGL/PEG hydrogels reinforced with tunable PCL fibrous microstructures. Top right illustration adapted from Murthy *et al.* and Kumar *et al.* [120, 163].

# Contents

## 5.1 Introduction

As already detailed in Chapter 1, human vocal folds are soft laryngeal structures owning remarkable vibro-mechanical performances, allowing them to generate an outstanding range of sounds [92, 214]. These performances are possible due to major properties of the vocal-fold tissue including : (i) the ability to endure large and reversible strains under various multi-axial loading modes during phonation, *i.e.* combined tension, compression and shear [44, 150, 226], (ii) the ability to adapt their vibro-mechanical behaviour to external loadings and environmental changes [8, 33, 137, 151]. Typically, vocal-fold vibrations occur at 100 % of relative humidity, and gradually stop when the tissue's upper mucosa dries out at ambient *ex vivo* hygrometry. These properties are highly related to the multi-layered structure of the vocal folds (*epithelium*, *lamina propria* and *vocalis* muscle), their fibrous microstructures and their surrounding ground substance. Most particularly, the *lamina propria* (LP, thickness $\approx$ 1-2.5 mm) is a loose connective tissue known to play a major role in vocal-fold vibrations [107, 240, 245]. LP extracellular matrix (ECM) comprises amorphous ground substances (*e.g.* hyaluronic acid) and oriented fibrous networks (*e.g.* collagen Type I, Type III and elastin). As a whole, the LP contributes to the tissue's 'passive' biomechanical properties (non-linear stiffness, elasticity, viscosity, anisotropy) and to the regulation of its water content.

Due to its physiological functions in voicing but also breathing and swallowing, the vocal-fold tissue has to accommodate to many traumas (*e.g.* vocal misuse or chemical aggression) [22, 122]. Though characterized by an enhanced healing capacity of micro-lesions, the vocal-fold tissue can be damaged past a critical threshold of injury, resulting in benign lesions (*e.g.* polyps, nodules [83]), or cancerous lesions (*carcinomas* [191]). Whatever the lesion, the LP layer's microstructure is quasi-systematically altered, which induces dysfunctions in the vocal-fold vibro-mechanical performances. Current surgical procedures consist in the excision of the lesion or in the resection of the damaged tissue. However, in some complex cases, operative interventions can result in scarring lesions with partial disappearance of the LP layer and/or undesired fibrous rearrangement, which may lead to loss of phonatory abilities [131, 236].
To treat such vocal-fold destructive lesions, several options are explored among which growth factor therapies, cell therapies and biomaterials, so as to rebuild the delicate layered structure of the *lamina propria* [11, 31, 73, 104, 122, 131, 135, 136, 231]. Among biomaterial candidates, hydrogels are attractive due to their tunable physical properties [12, 32] and tissue-like water content [49, 98, 128], which provide cells with an environment comparable to the extracellular matrix of native tissues [48]. For instance, the implantation of hyaluronic acid (HA)-based hydrogels in the surgical wound has shown to maintain the superficial sublayer of the *lamina propria* and prevent the *epithelium* from adhering to the deepest sublayers during the healing process [59]. Similarly, injectable PEG30 polymers have also yielded positive vocal outcomes [109], albeit with a limited action in time due to gradual material degradation. However, due to the isotropic and poor mechanical properties of homogeneous hydrogels in general, their relevance to potentially guide tissue remodelling processes towards a native-like microstructure seems compromised. The role of preferred

microstructural orientations and induced mechanics starts to be acknowledged as an important regulatory signal for matrix synthesis, notably of elastin [102].

The mechanical features of native tissues are linked to their complex architecture, where fibrous protein networks support the hydrated ground substance [1]. Mimicking such a composite architecture through the reinforcement of hydrogels with fibrillar structures therefore appears as a promising tool to match target mechanical properties, as it was shown for cartilage for instance [230]. Along this line, injectable hydrogels comprising networks of collagen nanofibrils (Types I and III) in a glycol-chitosan matrix have been proposed very recently for vocal folds applications [126]. However, the resulting fibrous architecture (*e.g.* diameter, orientation, density) was not tailored during the material processing route. Overall, the impact of the fibrous network topology on the mechanical properties of hydrogels in view of matching vocal folds properties has been barely explored so far. Moreover, the quantitative agreement between the composite's mechanical performances and that of native vocal folds has been often limited to a single loading mode (mainly shear) and to the linear regime at very small strains (typically below 1 % strain), as derived from standard small-amplitude oscillatory shear rheometry (*e.g.* storage and loss moduli). In particular, the development and characterization of composite hydrogels able to reproduce vocal-fold tissue mechanics upon realistic cyclic and large strains under multi-axial loadings, as experienced during phonation, still remains an open challenge.

Thereby, the general objective of this work is twofold : (i) developing and characterizing novel soft hydrogels reinforced by tunable fibrous microstructures, inspired by quantitative histological data and owning versatile mechanical properties upon cyclic and finite strains; (ii) proposing candidates able to mimic the major structural and mechanical specificities of the human vocal-fold *lamina propria* in both longitudinal tension and transverse compression, by comparison with a reference mechanical database.
To this end, poly($\varepsilon$-caprolactone) microfibers of adjustable densities and orientations [198, 199] were embedded within an elasto-mimetic hydrogel (mix of poly-lysine dendrimers and polyethylene glycol) of highly modular mechanical properties [29]. The structural and mechanical behaviour of the resulting composites were characterized, and compared with histo-mechanical properties of native tissues.

## 5.2 Materials and method

### 5.2.1 Materials and sample preparation

#### Vocal folds

Histological experiments were carried out with one fresh healthy human larynx (no freezing step), excised from a donated body within 48 h *post-mortem* (male, 76-year-old). Procedures were conducted following the French ethical and safety laws related to Body Donation. Right and left vocal folds were cut along the longitudinal (antero-posterior)

direction, following a dissection procedure detailed by Bailly *et al.* [9], and released from their cartilaginous ends. This yielded 4 tissue samples, approximated as parallelepiped beams with typical dimensions of 10 mm × 3 mm × 3 mm. The samples were characterised by a sandwich lamellar structure, made of all vocal-fold sublayers from the *epithelium* to the *vocalis*. When possible, markers were also sewn on the samples for a better anatomical identification during imaging experiments (anterior end and sublayers located thanks to Samco® surgical nylon monofilaments 10/0 and suture knots).

To enable 3-dimension (3D) imaging of their ECM fibres at micrometre-scale resolution, one part of the vocal-fold samples was then immersed in successive baths of ethanol (EtOH, Sigma-Aldrich) solutions with increasing alcoholic concentration (30 %, 50 % and 70 %) for 24 h each, and conserved in a 70 % EtOH solution at 4 °C until observation with two-photon microscopy. The other part was prepared in order to compare two-photon microscopy observations with conventional histology. The samples were pre-immersed in a 10 %-formaldehyde ($CH_2O$, Sigma-Aldrich, France) solution after body excision, dehydrated and embedded with paraffin as previously reported [9]. Five-$\mu$m sections were then cut using a microtome, collected on glass slides before paraffin removal and rehydration through sequential immersion in xylene (Sigma-Aldrich, France), alcohol and water baths, prior to staining.

**Synthetic samples**

*PCL fibrous mats* – In a first step, several mats of poly($\varepsilon$-caprolactone) (PCL, molecular weight 80 000 g/mol, Solvay Caprolactones, United Kingdom) microfibres with tunable orientation were prepared using a previously reported method, with modifications [198, 199]. Briefly, to provide hydrophilicity to the produced PCL fibres, tween® 80 (245 mg, 187 mmol, Sigma-Aldrich, France) was stirred in chloroform (140 mL, Sigma-Aldrich, France) at room temperature (T ≈ 25 °C) for 10 min, prior to the addition of PCL (9.8 g, 0.122 mmol). The mixture was then stirred for 3 h to obtain complete dissolution. The resulting solution was placed in a reservoir and projected onto different targets through the spraying device (standard class, Revell, Germany). Due to a Venturi effect, an airflow drives the polymer solution from the reservoir to an adjustable nozzle, where it is diffracted on a needle and sprayed. Solid polymer fibres are formed during transit due to chloroform evaporation. Two types of target were chosen to generate optional preferred orientations within the fibrous network, and control their induced mechanical properties : a static grid to create mats of randomly oriented fibres, and a rotating cylinder to create mats with fibres aligned into a preferential direction [199].

The thickness of the fibrous mats was controlled by spraying time, and measured using a Keyence laser sensor. Typical values ranged within ***. To increase fibre density in the fibrous mats, a compaction system was also devised. A given level of compaction was obtained by depositing one or multiple layers of fibrous mats of known thickness between various layers of glass slats (0.14 mm thick), which were then covered by a glass plate. A 500 g weight was placed over the covering glass plate, and the compaction applied for 1 h at room temperature prior release, new thickness measurement and further use. Various

levels of compaction could thus be obtained from ≈ 25 % up to ≈ 80 %.

*DGL/PEG hydrogels* – In a second step, hydrogels were obtained by mixing poly(L-lysine) dendrigrafts (DGL®, Colcom, France) and O,O′-Bis[2-(N-succinimidyl-succinylamino)ethyl] polyethylene glycol (PEG–NHS, Sigma-Aldrich, France) in aqueous solutions with various DGL/PEG ratio (1/1, 1/2, 1/2.5 or 1/3 w/w) and PEG molecular weight, noted $PEG_{MW}$ (2 or 10 kDa). In a typical experiment, PEG–NHS in anhydrous dimethyformamide (DMF, Sigma-Aldrich, France) solution at different concentrations $C_{PEG}$ (5, 10 or 12 w/v %) was added to DGL in phosphate buffer saline (PBS, Euromedex, France) in eppendorf tubes at 4 °C. This mixture was swiftly vortexed and transferred to 3D-printed molds, where it cross-linked between 15 to 30 min at room temperature. After cross-linking, the hydrogels were removed from the mold and stocked in PBS solution at 4 °C until use. The resulting samples were typically 22 mm in length, 5 mm in width, and from 1 to 5 mm in thickness depending on ***. In the following, for the sake of clarity, the DGL/PEG hydrogel characterised by the triplet of manufacturing parameters ($C_{PEG}$ in %, $PEG_{MW}$ in kDa, DGL/PEG ratio) will be denoted as Hyd($C_{PEG}$ %, $\|PEG_{MW}\|$k, DGL/PEG ratio), as reported in Table 5.1.

*Fibre-reinforced hydrogel composites* – The aforementioned PCL fibrous mats (with random or aligned orientations, with or without compaction) and DGL/PEG hydrogels were used to manufacture various fibre-reinforced hydrogel composites (FHC). Each processed PCL mat was placed on a hydrophobic glass slide, while a fresh mix of PEG-NHS and DGL was rapidly poured over it, to allow diffusion through the fibrous mats before the cross-link reaction. After cross-linking, the composite samples were cut in parallelepiped beams (22 mm in length, 5 mm in width, 0.5-2 mm in thickness). The resulting samples, labelled FHC($C_{PEG}$ %, $\|PEG_{MW}\|$k, DGL/PEG ratio, fibrous orientation), were stocked in PBS solution at 4 °C until use.

## 5.2.2 Structural, physical and mechanical characterization

### Histological analyses of biological samples

For conventional 2D histology, Hematoxylin-eosin-saffron (HES, in-house protocol), and Verhoeff Van Gieson (Labo Moderne, France) stains were used on vocal-fold sections to reveal both Type I and Type III collagen, as well as elastin fibres. Stained slices were imaged using an Aperio AT2 scanner (Leica, France).

The 3D structural arrangement of collagen and elastin fibres within the vocal-fold samples was analysed using two-photon excitation microscopy (Zeiss LSM 780) at the Cell Imaging Platform of the Cancer Research Centre of Lyon (CRCL, UMR Inserm 1052 CNRS 5286 – Centre Léon Bérard, France). Samples conserved in a 70 %-ethanol solution were placed on a microscopy glass slide, moistened with PBS and covered by a glass coverslip, which was then sealed with patafix (UHU, Bühl, Germany) to prevent sample drying during observation.

Collagen fibres were then observed using second harmony generation (excitation at 900 nm; emission at 412–464 nm), while auto-fluorescence was used for elastin (excitation at 900 nm; emission at 499-534 nm). Combining optics with CCD sensor features, regions of interest were sequentially scanned at multiple resolutions with effective voxel size of (0.69 $\mu$m $\times$ 0.69 $\mu$m $\times$ 6.17 $\mu$m), (0.35 $\mu$m $\times$ 0.35 $\mu$m $\times$ 0.91 $\mu$m) and (0.17 $\mu$m $\times$ 0.17 $\mu$m $\times$ 0.75 $\mu$m) with respect to the ($\mathbf{e}_{ap}$, $\mathbf{e}_{ml}$, $\mathbf{e}_{is}$) anatomical frame, where $\mathbf{e}_{ap}$ coincides with the anteroposterior direction, $\mathbf{e}_{ml}$, with the mediolateral direction, and $\mathbf{e}_{if}$ with the inferosuperior direction. The whole vocal-fold sample was investigated in the plane ($\mathbf{e}_{ap}$, $\mathbf{e}_{ml}$), over a total maximum depth of 377 $\mu$m (along $\mathbf{e}_{if}$).

Distributions of diameter and orientation of collagen and elastin fibres were calculated using the DiameterJ and OrientationJ plug-ins from Fiji® [99, 180]. For a given acquisition stack, one $\mathbf{e}_{if}$-position was randomly selected, and 6 close-up areas of interest were analysed to determine diameter and orientation populations (more than 6000 values for each image). To further determine the diameter distribution of fibre bundles, a manual quantification was also performed on 3 random $\mathbf{e}_{if}$-positions for a given stack. Along the main axis of each fibre bundle, a minimum of 10 thickness measurements were done (more than 100 values for each image). Finally, to determine the volume ratio of collagen and elastin fibres in the tissue, the BoneJ plug-in (Fiji®) was employed [52]. Three close-up areas of interest from an acquisition stack were thresholded for collagen and elastin signals, and the volume ratio calculated using the area/volume fraction algorithm.

**Structural and physical characterization of synthetic samples**

*PCL fibrous mats* – Jet-sprayed networks were observed by scanning electron microscopy (SEM, FEI XL30 ESEM-FEG, Philips, CLYM-INSA-Lyon, France) using 2 kV accelerating voltage. The fibres were coated with gold prior to observation using a sputter coater (BAL-TEC SCD 005). For each sample, six SEM pictures were taken randomly at different magnifications ($\times$ 250, $\times$ 500 and $\times$ 2000). Quantification of fiber diameters and orientations was performed in the same manner as for native tissue. More than 1 000 values of each microscale descriptor were obtained for a given picture.

*Hydrogels and fibre-reinforced composites* – The morphology and structure of hydrogels and fibre-reinforced composites (FHC) were evaluated using a binocular microscope (Olympus, France).

First, swelling ratio assays were performed to determine water uptake and swelling properties of both materials. For hydrogels, the desired concentrations of DGL/PEG were mixed, swiftly deposited between a hydrophobic glass slide and a hydrophobic round coverslip (10 mm in diameter) to create hydrogel discs after cross-linking. For FHC, the desired mixture of DGL/PEG was directly poured over fibrous mats cut as 10 mm diameter discs. After cross-link reaction, the samples were immersed in PBS solution during 24 h at room temperature. Prior to freezing in liquid nitrogen, samples were washed with deionized water several times (8 $\times$ 1 h) and then freeze-dried, to measure their dry weight

($w_d$). Subsequently, the samples were immersed in PBS solution, and their swollen weight ($w_s$) measured at various time intervals (from 10 min to 48 h), after having removed excess surface water. The swelling ratio (SR) was then simply calculated for each sample as :

$$SR = \frac{w_s - w_d}{w_d} \tag{5.1}$$

Then, the volume fraction of fibres in FHC samples ($\phi_{PCL}$) was determined using a pycnometer [238], and PBS as working liquid. Composites were prepared with aligned or random fibrous mats of controlled volumes ($V_s$ = 0.00317 and 0.00906 $cm^3$ respectively). The volume of the FHC samples, $V_{FHC}$, was derived from the weight of the composites ($m_{FHC}$), that of the pycnometer filled with both PBS and FHC samples ($m_t$), the PBS density ($\rho_{PBS}$ = 1.002938 $g/cm^3$) and the known properties of the empty pycnometer (volume $V_{py}$, mass $m_{py}$) using :

$$\phi_{PCL} = \frac{V_s}{V_{FHC}} = \frac{V_s\,\rho_{PBS}}{V_{py}\,\rho_{PBS} - (m_t - m_{FHC} - m_{py})} \tag{5.2}$$

Finally, hydrogels mesh size ($\zeta$) was assessed using the rubber elastic theory as follows [187] : $\zeta = (G^{'}/k_bT)^{-1/3}$, where $G^{'}$ is the shear storage modulus of the gel, $k_b$ the Boltzmann constant, and $T$ the temperature. Due to the isotropic homogeneous cross-linking of PEG hydrogels and assuming their quasi-incompressibility [4, 140], mesh size $\zeta$ could be further deduced from the tensile elastic modulus $E$ (see details thereafter) as :

$$\zeta = \left(\frac{E}{3\,k_b\,T}\right)^{-1/3}, \tag{5.3}$$

**Mechanical characterization**

The in-plane mechanical response of PCL fibrous mats, DGL/PEG hydrogels and fibre-reinforced composites was investigated using a standard uniaxial testing machine (Instron® 5944) equipped with a ± 10 N load cell, following a protocol similar to that developed in Chapter 3 to characterize gelatine-based hydrogels. In particular, a dedicated hygro-mechanical set-up was used to maintain hydration in a saturated atmosphere (≈ 98–100 % RH) throughout testing. Besides, for all cases, the load direction was defined by the vector $\mathbf{e}_y$ in the machine reference frame (see Fig 3.3). In the following, dimensions of undeformed samples along $\mathbf{e}_y$ (*resp.* $\mathbf{e}_x$, $\mathbf{e}_z$) are noted $\ell_0$ (*resp.* $w_0$, $t_0$). Tests were repeated at least 5 times for each condition (Supplementary Fig. 5.11 in Appendix A showing the typical level of scatter in the measurements).

In a first step, all materials were characterized in tension (along their main fiber orientation when applicable, *i.e.* for aligned PCL mats and corresponding FHC), it being the standard loading mode chosen to characterize the mechanical behavior of native tissues so far [40, 67, 113, 115]. To do so, materials were cut in parallelepiped beams for an effective gauge length $\ell_0$ = 10 mm and width $w_0$ = 5 mm at rest. Note that their initial thickness $t_0$ could

vary from 0.5 to 5 mm depending on the sample's nature and processing route. The cell force $f$ and cross-head displacement $\delta$ signals measured in the stretch direction $\mathbf{e}_y$ were used to estimate the first Piola-Kirschoff stress $P_{yy} = f/w_0 t_0$, as well as the Hencky tensile $\varepsilon_{yy} = \ln(1 + \delta/\ell_0)$. Each sample was subjected to successive load / unload sequences at increasing strain levels $\varepsilon_{yy}^{max}$ up to failure with a strain rate $|\dot{\delta}/\ell_0| \approx 10^{-3}\ s^{-1}$.
To better quantify the influence of cyclic loading on the database, four mechanical descriptors were derived from the stress-strain curves : the maximum stress value $P_{yy}^{max}$ achieved at every peak strain level $\varepsilon_{yy}^{max}$, the residual strain $\varepsilon_r$ recorded at the end of each cycle, the volumetric energy density $W_d$ dissipated in the material per cycle, and the longitudinal tangent modulus $E_t = dP_{yy}/d\varepsilon_{yy}$ assessed at each peak strain $\varepsilon_{yy}^{max}$ during the unloading phase (with $E = E_t$ at small strains in Eq. 5.3).

In a second step, after comparison with the reference mechanical database on native tissues [44], a suitable biomimetic FHC candidate was selected from the previous campaign, and further tested in compression along $\mathbf{e}_y$. It was tested transversely to the fibrous network main orientation, it being representative of vocal-fold loading during *in vivo* periodic collision [10, 74]. Briefly, following the procedure developed in Chapter 3 in such a case, samples were cut for an effective gauge length $\ell_0$ = 2 mm, a width and thickness $w_0 = t_0$ = 10 mm at rest. They were then subjected to successive load / unload cycles at various strain levels $\varepsilon_i^{min}$ down to failure, with a strain rate $|\dot{\varepsilon}_{yy}| \approx 10^{-3}\ s^{-1}$ as applied in the reference database. Compression stress $P_{yy}$ and strain $\varepsilon_{yy}$ were recorded during the test as mentioned above.

## 5.3 Results and discussion

### 5.3.1 Biomimetism of vocal-fold microstructural specificities

#### Microstructural organisation of native tissue

To better apprehend the microstructural architecture of human vocal folds, the specific organisations of collagen and elastin fibres was analysed by two-photon microscopy, as illustrated in Fig. 5.2. The distribution of collagen and elastin networks varied between anatomical layers (Fig. 5.2A and C). The *epithelium* was devoid of either fibre, few were present in the *vocalis* muscle layer, while the *lamina propria* was rich in both. Within the latter, both elastin and collagen wavy fibres were arranged in an entangled network, the major orientation of which was parallel to the antero-posterior direction $\mathbf{e}_{ap}$, and showing density variations from superficial to deep layers along the medio-lateral direction $\mathbf{e}_{ml}$ (see also Supplementary Video 5.10 in Appendix A). These general qualitative trends are in line with standard histological micrographs obtained on the same sample (Fig. 5.2B), and with previous observations reported on human vocal folds architecture [9, 14, 152].

Typical orientations and diameters of ECM fibres measured at several depths of the *lamina propria* are displayed in Fig. 5.3. Both elastin and collagen fibres were arranged in an

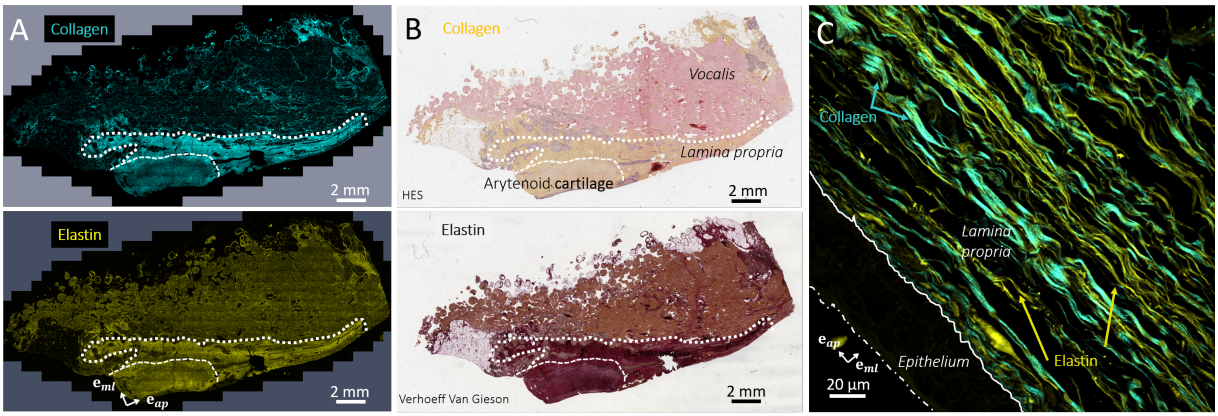


**Figure 5.2:** Structural analysis of human vocal-fold organization. **(A)** Representative 2D micrograph of a human vocal-fold cross-section where collagen (*blue*) and elastin (*yellow*) are visualized through second harmonic generation and auto-fluorescence, respectively (pixel size 0.69 $\mu$m $\times$ 0.69 $\mu$m). **(B)** Correlation with histological staining of collagen (*yellow-orange*, HES) and elastin (*black*, Verhoeff Van Giesen) of the same vocal fold. **(C)** Close up of the *epithelium* and *lamina propria* layers (pixel size 0.17 $\mu$m $\times$ 0.17 $\mu$m).

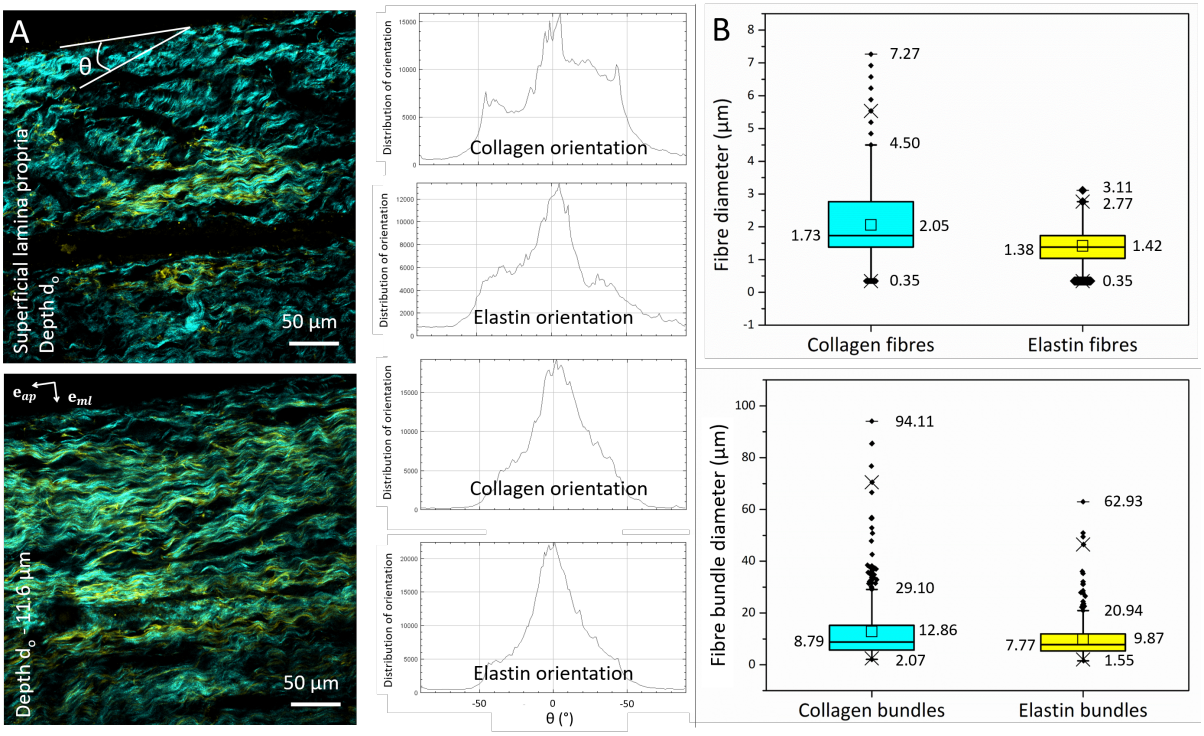


**Figure 5.3:** Quantitative analysis of the fibrous architecture in the human *lamina propria*. **(A)** Representative 2D micrograph at several depths of the lamina propria (voxel size 0.17 $\mu$m $\times$ 0.17 $\mu$m $\times$ 0.75 $\mu$m) and quantification of the angular distribution of the collagen and elastin fibres, defined relative to the *epithelium*. **(B)** Quantification of the diameters of collagen and elastin fibres and fibre bundles.

intertwined network, where they followed a similar preferred orientation (Fig. 5.3A). Close to the vocal fold edge, beneath the *epithelium*, the main orientation of the fibres appeared broad, with a main population parallel to the epithelial layer ($\theta = 0°$). At deeper focal points in the *lamina propria*, both collagen and elastin fibres orientations were narrower and followed mainly the epithelial surface. When quantified by image analysis (Fig. 5.3B), the collagen fibres were found thicker and with broader dispersions (mean $2.1 \pm 1.1$ $\mu$m, values ranging from 0.4 to 7.3 $\mu$m) than the elastin ones (mean $1.4 \pm 0.5$ $\mu$m and values ranging from 0.4 to 3.1 $\mu$m). Both fibre types arranged in bundles, which followed a similar pattern, reaching width up to 94.1 and 62.9 $\mu$m, with mean values of $12.9 \pm 12.1$ and $9.9 \pm 7.7$ $\mu$m for collagen and elastin, respectively. Regarding the volume ratio occupied by collagen and elastin fibres within the *lamina propria*, rather similar values were measured ($9.7 \pm 3.7$% and $10.9 \pm 3.5$% respectively). These descriptors are in rather good agreement and complement the few quantitative microstructural analyses of the human vocal fold reported in the literature so far [9, 14, 152].

**Mimetic synthetic composites**

*PCL fibrous mats* – Therefrom, several fibre-reinforced hydrogel composites (FHC) were developed to mimic the microstructure of native vocal-fold *lamina propria*. The fibrous component of the *lamina propria* can readily be emulated by polymeric materials, such as PCL, since they can be formulated in fibrous mats of controlled diameters, densities and orientations through multiple approaches (jet spraying or electrospinning for instance [155, 198]). However, since vocal-fold collagen and elastin fibres are not unimodal in terms of diameter, jet spraying appeared as a more suitable option to mimic this feature. Furthermore, this fiber production method results in highly porous structures (typical porosity around 97 %), which is a requisite to allow for the absorption, incorporation and dispersion of a hydrogel phase, in view of creating a composite.

Through selection of the jet-spraying parameters, it was possible to emulate some of the target features of collagen and elastin fibres of the *lamina propria*, at the multiple scales of the fibre, the fibre bundle and of the overall fibrous network. As presented in Fig. 5.4A, the orientation of the PCL fibres within the processed fibrous mats could be modulated, to mimic collagen and elastin orientation distribution. The resulting fibres diameters were in the micron range, regardless of fibre orientation (average of $1.6 \pm 1.4$ and $2.9 \pm 2.9$ $\mu$m for respectively random and aligned mats) while the mean width of the fibre bundles produced during spraying was doubled ($3.2 \pm 2.4$ against $6.0 \pm 6.6$ $\mu$m). In comparison to the measured collagen and elastin fibres of the *lamina propria*, mean diameters of both PCL fibre types were similar, but with a wider distribution. PCL fibre bundles diameters were also in the same order of magnitude than bundles of native fibrous proteins, albeit of lower mean and distribution range.

*Fibre-reinforced hydrogel composites* – With the aim of reproducing the ground substance surrounding collagen and elastin fibres in the *lamina propria*, while allowing to modulate overall mechanical properties of the synthetic composites, a hydrogel of modular properties

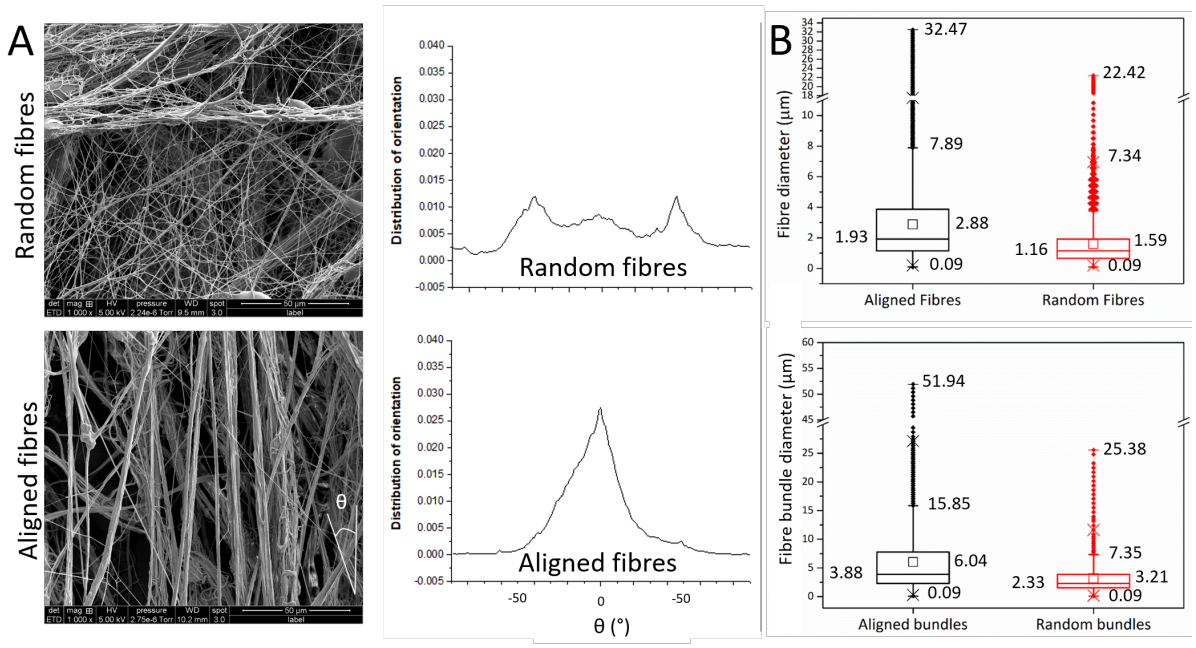


**Figure 5.4:** Mats of random and aligned PCL fibres. **(A)** Representative SEM pictures and quantification of their preferred orientations. **(B)** Quantification of the diameters of random and aligned fibres and fibre bundles.

was evaluated. We have recently reported that poly(L-lysine) dendrigrafts/polyethylene glycol (DGL/PEG) hydrogels have the advantages of being easily prepared by mixing two aqueous solutions, while their elastic mechanical properties can be readily and extensively tailored by component's ratio and concentrations [29, 47, 72]. The reticulation process is based on the reaction between the amine groups on the surface of DGL and the activated polyethylene glycol chain end-bifunctionalized with N-hydroxysuccinimide ester group (PEG-NHS) to generate highly stable amide bonds in physiological conditions. Due to the aqueous nature and low viscosity of PEG/DGL mixes prior to cross-linking, and to the hydrophilicity conferred by the addition of tween® 80 to the PCL fibres, it was possible to infiltrate the hydrogel within the fibrous polymer mats by simple pouring, efficiently resulting in an homogeneous impregnation though the thickness (see Fig. 5.5A). Due to the very high porosity of the mats, neither the orientation of the PCL fibres nor the composition of the DGL/PEG hydrogel hampered the preparation of the composites. Doing so, two series of fibre-reinforced composites (FHC) are presented thereafter :

(i) a first series made of 8 samples, differing by the chemical formulation of their DGL/PEG matrix and by the preferred orientation of their fibrous network (random or aligned), as detailed in Table 5.1. These samples were produced without any pre-compaction of the PCL fibrous mats during the shaping process. In such a case, the average volume fraction of fibres in the unloaded FHC samples ($\phi_{PCL}$) was obtained at $\approx$ 4 % for networks with aligned fibres, and $\approx$ 9 % for networks with random ones.

(ii) a second series made of 8 samples characterised by an identical matrix Hyd(5%, 2k, 1/1) and a single fibrous orientation (aligned), but with a modulated volume fraction $\phi_{PCL}$. Increasing levels of compaction of aligned fibrous mats prior incorporation into

FHC did not hamper the formulation of composites, while it resulted in an increase value of $\phi_{PCL}$, thus tailored from ≈ 4 % up to ≈ 16 % as shown in Fig. 5.5B.

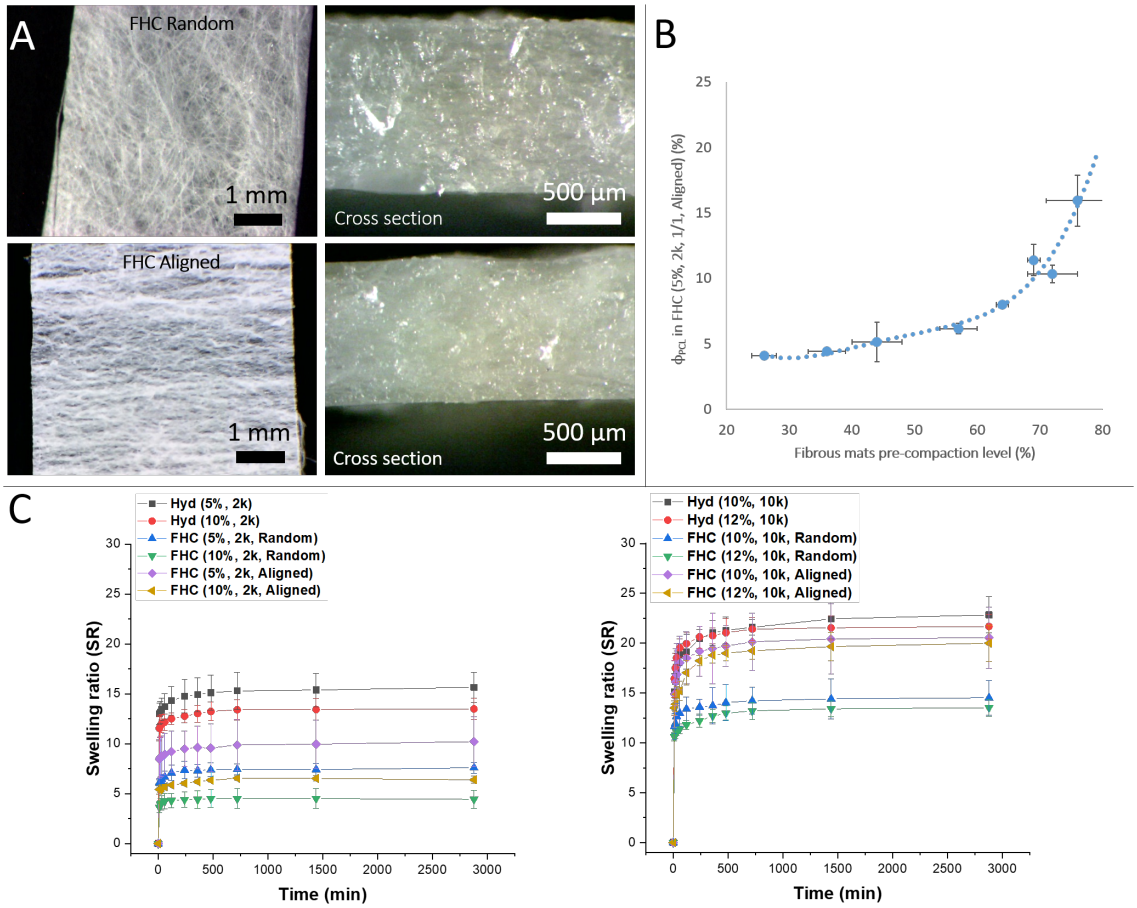


**Figure 5.5:** Characterization of random and aligned fibre-reinforced hydrogel composites (FHC). **(A)** Representative pictures of both composite types. **(B)** Modulation of FHC volume fraction through pre-compaction of aligned fibrous mats. Data are mean ± SD (n = 5). **(C)** Swelling ratio of hydrogels prepared with 2 (*left*) and 10 kDa PEG (*right*) at different concentrations ($C_{PEG}$ = 5 and 10 %) and their homogeneous composites obtained with random and aligned fibrous PCL mats.

| **DGL/PEG hydrogels** | $\zeta \pm$ **SD (nm)** | **FHC composites** | $\phi_{PCL} \pm$ **SD (%)** |
|---|---|---|---|
| Hyd(5%, 2k, 1/1) | 6.09 ± 0.19 | FHC(5%, 2k, 1/1, Random) | 10.34 ± 0.71 |
| | | FHC(5%, 2k, 1/1, Aligned) | 4.55 ± 0.11 |
| Hyd(10%, 2k, 1/2) | 5.56 ± 0.27 | FHC(10%, 2k, 1/2, Random) | 11.27 ± 0.51 |
| | | FHC(10%, 2k, 1/2, Aligned) | 5.21 ± 0.46 |
| Hyd(10%, 10k, 1/2.5) | 10.12 ± 0.44 | FHC(10%, 10k, 1/2.5, Random) | 7.41 ± 0.95 |
| | | FHC(10%, 10k, 1/2.5, Aligned) | 3.37 ± 0.21 |
| Hyd(12%, 10k, 1/3) | 9.46 ± 0.60 | FHC(12%, 10k, 1/3, Random) | 8.08 ± 1.01 |
| | | FHC(12%, 10k, 1/3, Aligned) | 3.73 ± 0.64 |

**Table 5.1:** Average mesh size ($\zeta$) of PEG hydrogels and volume fraction of fibres ($\phi_{PCL}$) in the fibre-reinforced hydrogels.

The efficient association and embedding of fibrous matrices within the hydrogels were

reflected in the modulation of their swelling properties. As presented in Fig. 5.5C, the elevated swelling of DGL/PEG hydrogels in physiological conditions was in line with previously reported behaviours. An increase of PEG molecular weight ($PEG_{MW}$) from 2 to 10 kDa increased the swelling ratio from 15 to 22, conversely to PEG concentration $C_{PEG}$, which reduced hydrogels water uptake. Similarly to other PEG-based hydrogels, these phenomena could logically be ascribed to the closer presence of the amine (DGL) and NHS (PEG) reactive groups with increased reactants concentrations and hence a higher level of cross-linking, which results in smaller mesh sizes and limits the expansion of the network [225]. Conversely, longer PEG chains result in larger mesh sizes and higher swelling, as was suggested by estimating the different hydrogels mesh sizes (Table 5.1). However, for any given DGL/PEG composition and PEG molecular weight, the presence of PCL fibres decreased the resulting FHC water uptake up to 3 times. This constrain can be attributed to the lack of swelling of the PCL fibres, as has been reported for PEG-diglycidylether/polyoxyalkyleneamines hydrogels composites with polyurethanes fibres [3]. Accordingly, the swelling decrease was largely dependent on PCL fibres orientations and volume fractions in the final composite. In particular, the lower volume of hydrogel in the composites with random fibrous mats ($\approx$ 91%, compared to $\approx$ 96% for aligned ones) induced a lower swelling ratio (Table 5.1).

### 5.3.2 Tunable mechanics of fibre-reinforced composites

#### General trends : fibrous mat *vs* composites

Tensile cyclic responses of the elaborated materials (first series reported in Table 5.1) are reported in Fig. 5.6, highlighting the relative contributions of the isolated components (DGL/PEG matrix and fibrous mats) to the overall mechanical behaviour of the composite hydrogels.

DGL/PEG hydrogels showed a quasi-linear reversible behaviour with negligible residual strains and stress-hysteresis (Fig. 5.6A) : all loading and unloading stress-strain curves were almost completely overlapped with each other. As expected [168, 208], increasing the PEG/DGL ratio resulted in an increased stiffness (*e.g.* tangent modulus $E_t$ varying from 10 to 75 kPa for hydrogels with $PEG_{MW} = 2$ kDa at 5% strain), while a rise of $PEG_{MW}$ resulted in higher strains at break (from about 30% to more than 65%). Accordingly, the softer hydrogel produced in the database (*i.e.* Hyd(10%, 10k, 1/2.5)) could hardly be handled, and even less tested according to the present protocol.

Whatever the processed fibrous architecture, incorporating PCL fibers into the hydrogels systematically yielded non-linear stress-strain responses characterized by a J-shape strain hardening (Fig. 5.6C), presumably due to the progressive recruitment and/or reorientation of fibers within the load direction [8]. Compared to homogeneous hydrogels, stress levels could be enhanced by up to two orders of magnitude in finite strains, in line with previous works on fibre-reinforced hydrogels [3, 222]. A typical stress hysteresis was also observed after each unload sequence, generating non-zero residual strains, albeit rather

moderate. This may be ascribed to microstructural rearrangements (*e.g.* fibres rotations and interactions) [210], and to large plastic deformation of PCL fibers working in tension (see Fig. 5.6B). Interestingly, such global trends point out that the overall response of the FHC composites combines the high tensile strength, hysteretic and non-linear behaviour of the fibrous mat under cyclic loading, together with the elastic properties of the pure hydrogels.

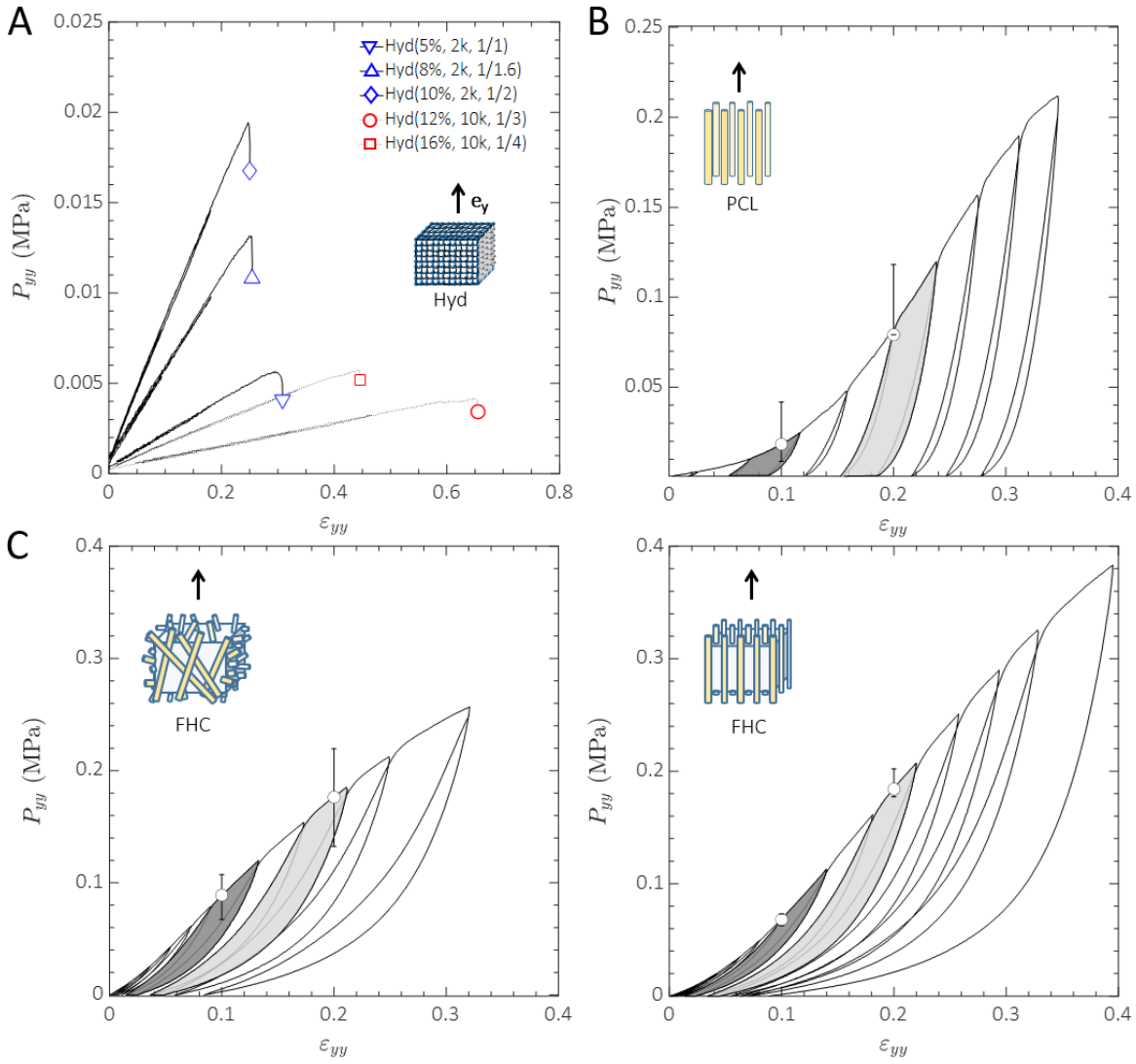


**Figure 5.6:** Mechanical characterization of hydrogels, PCL mats and FHC samples. Typical cyclic tensile stress-strain response of **(A)** various DGL/PEG homogeneous hydrogels as listed in Table 5.1, **(B)** aligned PCL fibrous mat under longitudinal loading, **(C)** and FHC composite hydrogels reinforced by random or aligned fibres : illustrative cases of FHC(10%, 2k, 1/2, Random) (*left*) and FHC(10%, 2k, 1/2, Aligned) (*right*). Error bars represent measurement uncertainty over 5 tests (min-max values). Grey areas illustrate hysteresis loops leading to a dissipation of mechanical energy.

### Influence of the composite's processing route

Fig. 5.7 presents the strain-induced evolution of four mechanical descriptors ($E_t$, $P_{yy}^{max}$, $W_d$, $\varepsilon_r$) derived from the tensile stress-strain curves acquired on the FHC composites listed in

Table 5.1, so as to better understand the relationship between the manufacturing process of the elaborated materials, and their mechanical performance in tension. Whatever the parameter under study, different ranges of values could be achieved depending on the composite's chemical formulation and microstructure.

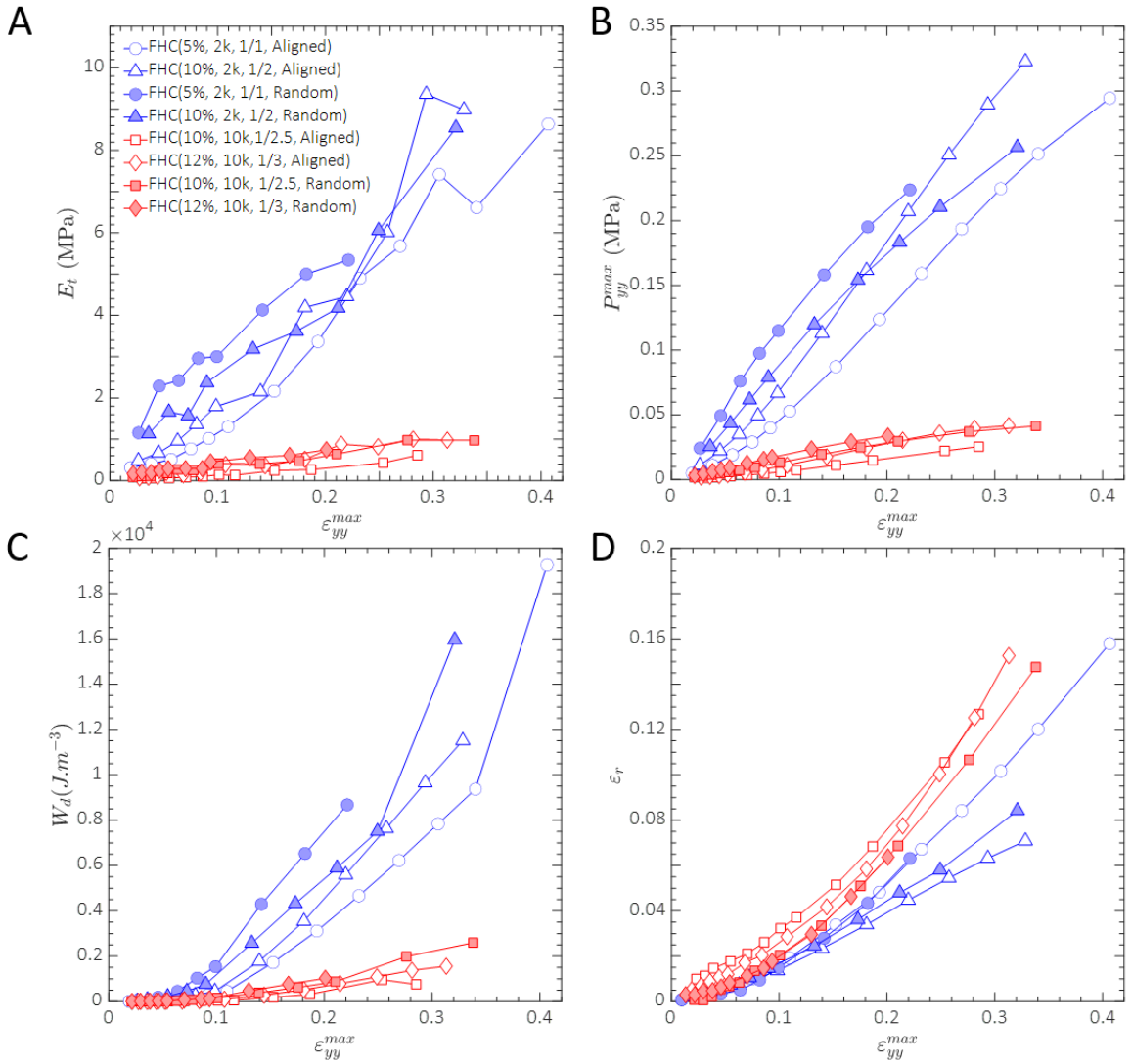


**Figure 5.7:** Cyclic evolution of the mechanical descriptors of the composite hydrogels in function of the applied peak strains $\varepsilon_{yy}^{max}$: **(A)** tangent modulus, $E_t$; **(B)** peak stress level, $P_{yy}^{max}$; **(C)** dissipated energy density per cycle, $W_d$; **(D)** residual strain, $\varepsilon_r$.

A first classification of the composites is clearly highlighted, based on the PEG molecular weight of their matrices. Over the whole strain range under study (up to 40%), composites with the lowest $PEG_{MW}$ = 2 kDa (in *blue*) were found to have much higher levels of tensile stiffness and peak strength (Fig. 5.7 A and B), compared to composites with $PEG_{MW}$ = 10 kDa (in *red*). Such results are in line with expected trends for hydrogels with shorter chains between chemical cross-links (see corresponding shorter mesh sizes in Table 5.1), and thereby, higher cross-linker concentration per unit volume [168]. Besides, past the early stage of deformation (for $\varepsilon_{yy}^{max} > 5\%$), cyclic events with successive strain increment generated higher dissipated energy and lower residual strains in composites with lowest

$PEG_{MW}$ (Fig. 5.7 C and D). No difference was made in this respect when subjecting pure hydrogels with distinct $PEG_{MW}$ to identical kinematical conditions (Fig. 5.6). Therefore, the observed variations of $\varepsilon_r$ and $W_d$ with $PEG_{MW}$ at finite strains may be attributed to a structural rearrangement of the PCL fibres in the composite (*e.g.* rotations, unfolding) and/or mechanical interactions between the constitutive materials (matrix-fibre, fibre-fibre), which are likely to vary according to the matrix stiffness [210].

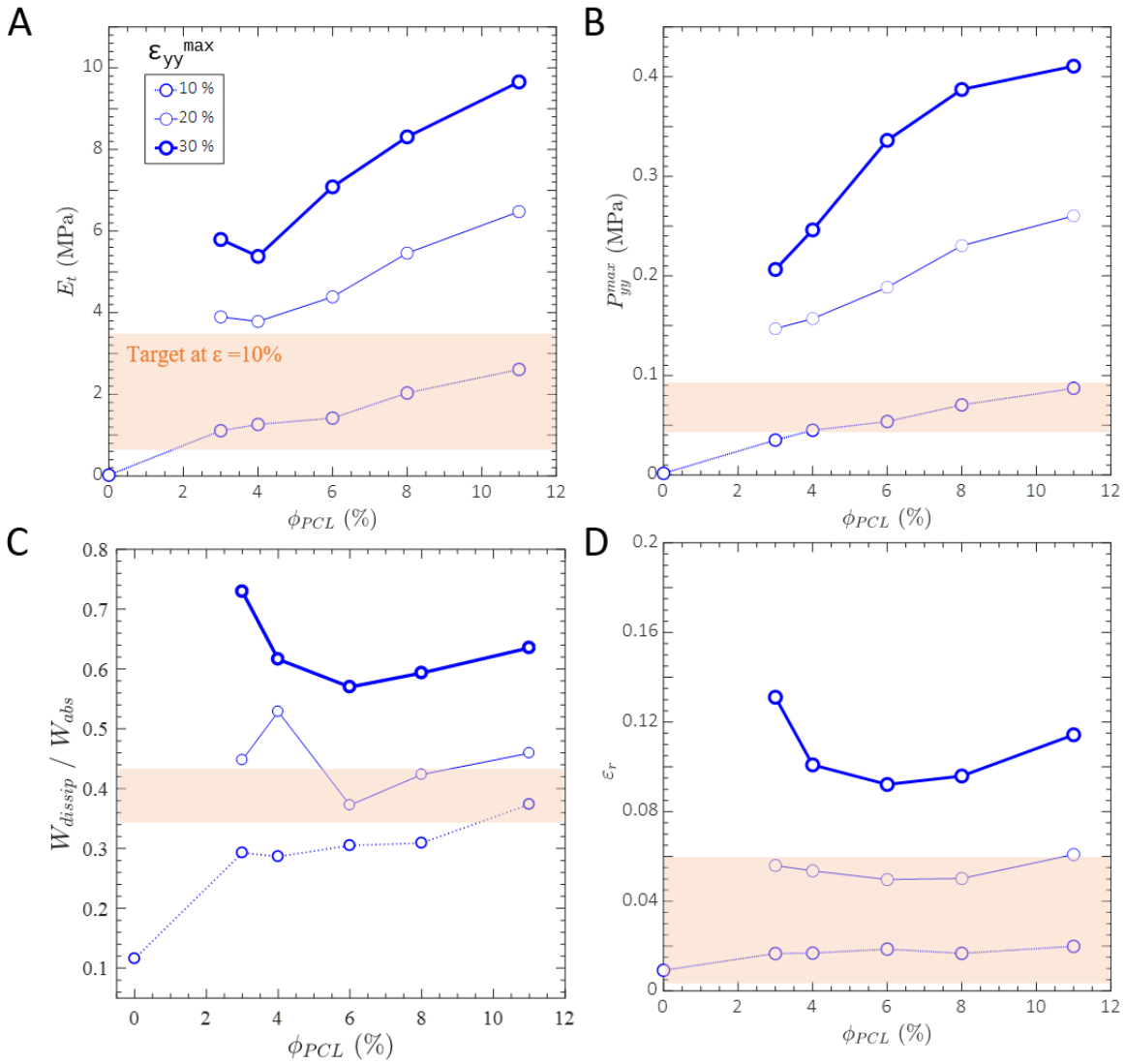


**Figure 5.8:** Same descriptors as in Fig. 5.7 in function of the volume fraction of fibres in FHC samples, $\phi_{PCL}$ and of the applied peak strain $\varepsilon_{yy}^{max}$. Data acquired on composites FHC(5%, 2k, 1/1, Aligned), owning identical matrix and fibrous orientation, but tailored values of $\phi_{PCL}$.

A second-order classification of the elaborated composites is also revealed in Fig. 5.7, based on their fibre content. In fact, for a given matrix family (fixed PEG molecular weight $PEG_{MW}$ and concentration $C_{PEG}$), and for moderate applied strains (up to 20% at least), composites made of randomly-oriented fibres showed *a priori* higher stress levels, tensile stiffness and dissipated energy than composites reinforced with aligned fibres. However, this result cannot be physically explained by discrepancies in the initial fibrous orientation itself [8, 222]. It rather comes from the gap in volume fraction of fibres $\phi_{PCL}$ observed between

both types of composites, which is a key factor of influence in the mechanics of fibrous media [106, 142]. Bearing in mind that no pre-compaction of the fibrous mat was chosen at this stage to elaborate the composites, various fibre contents were obtained for each FHC family, it being more than twice higher in average for hydrogels with randomly-oriented fibres (see Table 5.1). Indeed, when displayed as a function of $\phi_{PCL}$ only, while keeping constant all other parameters of the processing route (using the series of composites made of pre-compacted mats), Fig. 5.8 clearly shows that all mechanical descriptors increase with $\phi_{PCL}$, except for the residual strain $\varepsilon_r$ which remains nearly constant for a given peak strain $\varepsilon_{yy}^{max}$. The versatility of the process is also evidenced on the corresponding stress-strain behaviour, reported in Supplementary Fig. 5.11B for $\varepsilon_{yy}^{max} = 10\%$.

**Biomimetism of vocal-fold mechanical properties**

Given the range of key mechanical descriptors achievable by adjusting the hydrogel composition and fibrous microstructure of the composites (Figs. 5.7 and 5.8), FHC candidates could first be tailored to reproduce the visco-hyperelastic response of human vocal folds in longitudinal tension, *i.e.* along their main fiber orientation. Thus, Fig. 5.9A illustrates the relevance of four composite hydrogels of the database, tuned to mimic *lamina propria* samples tested under comparable large-strains and cyclic uniaxial conditions ($LP_i$, i $\in$ [1..3]). Such reference targets were selected to delineate the range of mechanical responses previously obtained *ex vivo* on 7 *lamina propria* samples [44], and to illustrate the typical scattering related to intra/inter-individual variability ($LP_1$ and $LP_2$ were excised from left and right vocal folds of the same larynx).

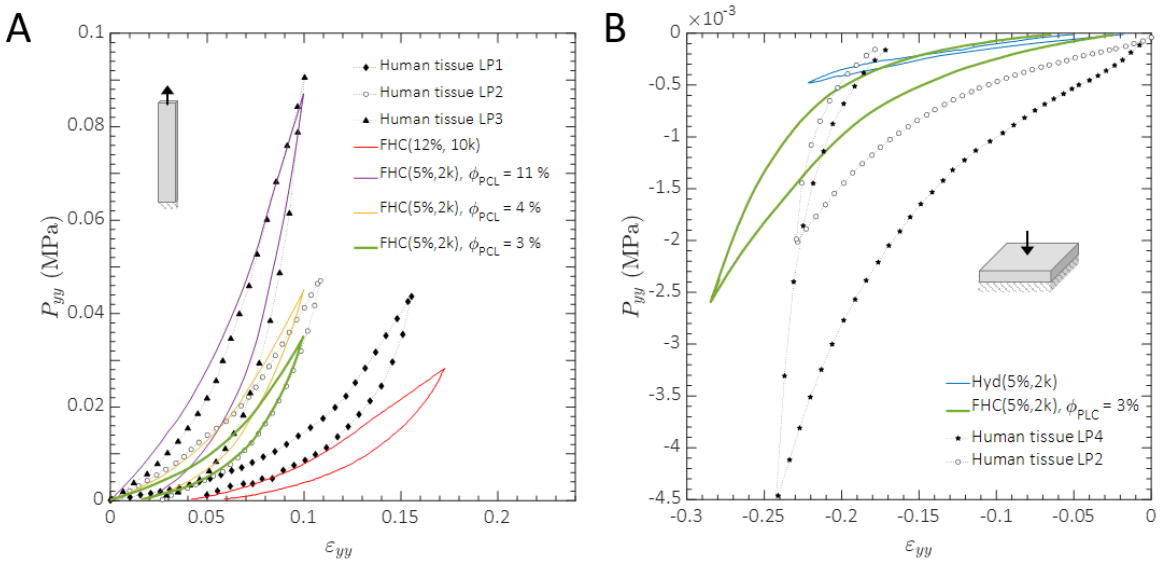


**Figure 5.9:** Comparison with reference data acquired on human vocal folds. **(A)** Stress-strain responses of tailored FHC composite candidates and *lamina propria* samples subjected to cyclic and finite-strains in longitudinal tension [44]. **(B)** Typical stress-strain response of the composite FHC(5%, 2k, 1/2, Aligned) under transverse compression, as preivou selected from the tension curves in **(A)** (curve in *green*), and tested under transverse compression. Comparison with reference data on *lamina propria* samples [44].

The selection was made among FHC composites produced with aligned fibres only, *i.e.* the closest to the vocal-fold fibrous topology. The composites with lowest $PEG_{MW}$ (2 kDa) were favourable choices due to their increased stiffness and dissipative properties from small to finite strains, while showing rather low residual strains after cycling. In particular, the candidate FHC(5%, 2k, 1/1, Aligned) proved to be a very good candidate to cover the desired corridor formed by targets $LP_2$ and $LP_3$, using appropriate values of $\phi_{PCL}$ from 3% to 11%, which are rather close to the volume fraction of collagen and elastin fibres measured in the superficial *lamina propria* (see Section 5.3.1). However, the use of a higher $PEG_{MW}$ was required to match the softest target mechanical response ($LP_1$). Note that a volume fraction $\phi_{PCL}$ less than 3% for the candidate FHC(5%, 2k, 1/1, Aligned) could not be obtained in this study, but this solution may also be suitable to reproduce the behaviour of the target $LP_3$, provided that further adjustments to the manufacturing process are possible.

The suitability of the candidate FHC(5%, 2k, 1/1, Aligned) was also evaluated in transverse compression, *i.e.* applied perpendicularly to the main fiber direction. This loading mode is also very important during phonation, keeping in mind that the quality of contact between vocal folds is a key factor in voice quality, and that high contact pressure are observed in common lesions of the *lamina propria* [83, 196]. In the end, as shown in Figs. 5.9A and B, the choice of $\phi_{PCL} \approx 3$ % (in *green*) allows the macroscale mechanics of the *lamina propria* to be reproduced fairly well both in longitudinal tension and in transverse compression. By contrast with the trends obtained in longitudinal tension (Fig. 5.6 and Supplementary Fig. 5.11B), it is also very interesting to note that the response of the fibrous FHC composite under compression is measured rather close to that of the sole hydrogel matrix at low strains (see Fig. 5.9B), as expected for the native vocal-fold tissue [210]. Besides, it is shown that the mechanical contribution of the matrix in this mode strongly attenuates for $\varepsilon_{yy} <$ -0.05, as also predicted for the biological tissue due to steric interactions likely to occur at the fiber scale [210].

## 5.4 Conclusion

In this study, we propose a set of novel biocompatible fibre-reinforced hydrogels with optimal mechanical properties when subjected to cyclic and large-strains tensile and compressive loadings, such as those experienced by vocal folds during human voice production. These composite hydrogels consist of jet-sprayed PCL fibrous mats embedded in a DGL/PEG matrix. The chemical formulation of their hydrogel matrix (*i.e.* PEG molecular weight and concentration, DGL/PEG ratio), the microstructural architecture of their fibrous networks (*i.e.* diameter, orientation, volume fraction of fibers) and their assembly process were tailored to ensure that the final composites mimic the anisotropic structure of the human *lamina propria* and its non-linear viscoelastic mechanical behaviour. To do so, collagen and elastin fibrous networks of deceased patients were characterized by two-photon excitation microscopy to quantify fibre and bundles diameter, preferential orientation and volume fraction, which, aside from providing concrete targets to match,

completed the rare histological descriptors of the vocal fold. Using a recent mechanical database on native vocal-fold tissues subjected to longitudinal tension and transverse compression, the processed biomimetic composites were validated with respect to their non-linear strain hardening, mechanical strength, residual strain and strain energy density dissipated during cycling. The versatility of the selected architectured materials was also highlighted, showing their ability to capture the dispersion of stress-strain responses related to inter or intra-individual variability.

Further developments are needed to improve the tailored structured hydrogels and their mechanical performances at rising level of mimicry. Regarding material design, the possibility to further reproduce the sandwich structure of the *lamina propria* by superimposing composite hydrogels with various microstructural properties should be studied. Regarding the mechanical validation of the processed candidates, we have planned to extend it to higher strain rates, and to a third loading mode also encountered by the tissue during vocal-fold oscillations (*i.e.* shear - see prior results in Supplementary Fig. 5.11B). Work is also on-going to mold the optimised hydrogels in a more realistic 3D geometry of vocal folds, and assess their ability to vibrate under physiological aero-mechanical and acoustical loadings. Finally, we also plan to cellularize the chosen candidates so as to prospect and better understand the relationships between the cellular activity and the vibrational quality of a reconstructed vocal fold.

# APPENDIX A

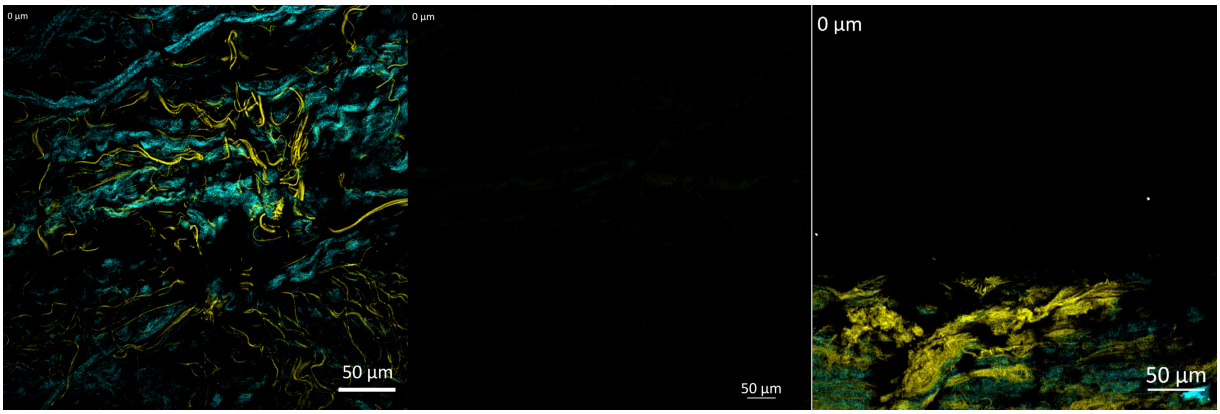


**Supplementary video 5.10:** Representative examples of the organization of collagen (in *green*) and elastin networks (in *yellow*) at various depths of the same human *lamina propria* sample. *From left to right* : **Media1** available at https://cloud.univ-grenoble-alpes.fr/s/AifgGDqYazftme3 (voxel size 0.17 $\mu$m $\times$ 0.17 $\mu$m $\times$ 0.75 $\mu$m, thickness 30.75 $\mu$m); **Media2** available at https://cloud.univ-grenoble-alpes.fr/s/AifgGDqYazftme3 (voxel size 0.69 $\mu$m $\times$ 0.69 $\mu$m $\times$ 6.17 $\mu$m, thickness 58.8 $\mu$m); **Media3** available at https://cloud.univ-grenoble-alpes.fr/s/AifgGDqYazftme3 (voxel size 0.35 $\mu$m $\times$ 0.35 $\mu$m $\times$ 0.91 $\mu$m, thickness 46.2 $\mu$m).

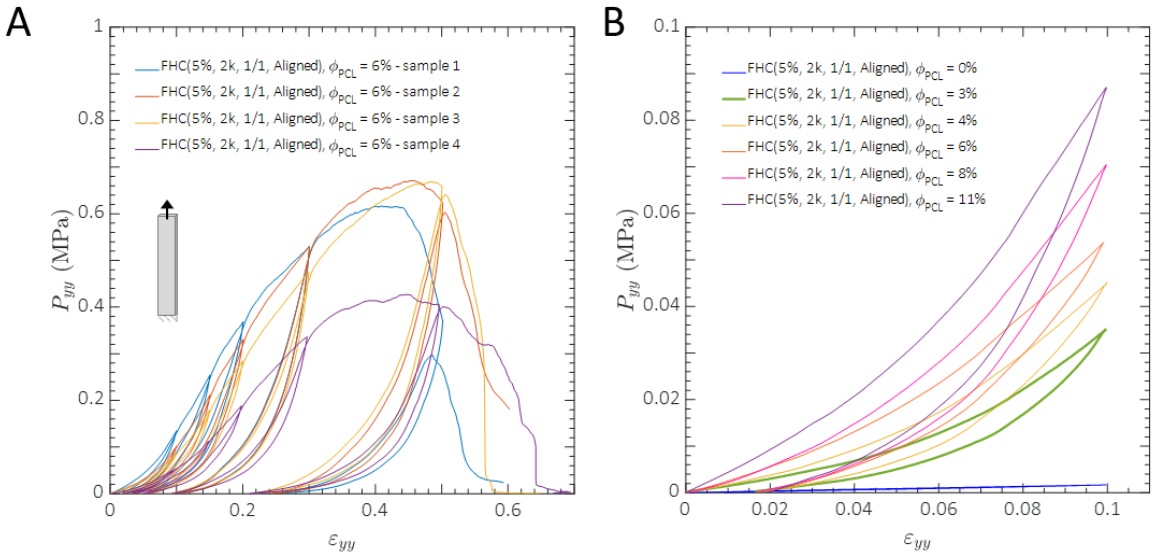


**Supplementary figure 5.11:** Mechanics of FHC composites with aligned fibers, loaded in cyclic tension along the main fiber direction. **(A)** Typical stress-strain repeatability obtained over 4 samples of the same FHC type. Illustrative case of FHC(5%, 2k, 1/1, Aligned) with $\phi_{PCL} = 6$ %. **(B)** Stress-strain behaviours of a series of composites FHC(5%, 2k, 1/1, Aligned) elaborated with different values of $\phi_{PCL}$.

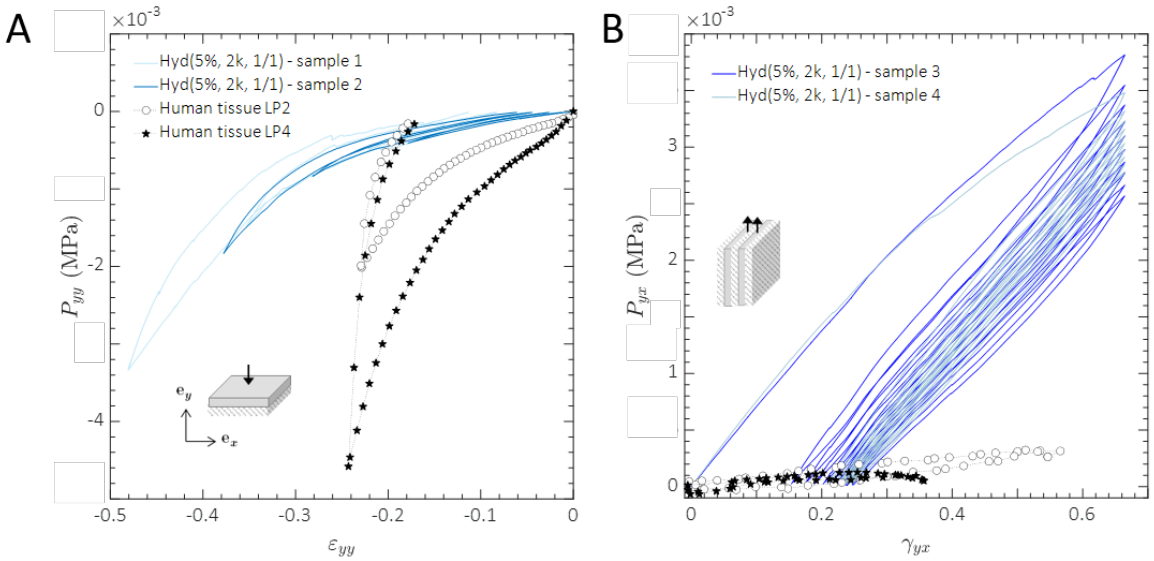


**Supplementary figure 5.12:** Comparison between the mechanical behaviour of homogeneous PEG/DGL hydrogels Hyd(5%, 2k, 1/1) (in *blue*) and that of human *lamina propria* samples (adapted from [44]). **(A)** Typical stress-strain data obtained in transverse compression along ey. **(B)** Same as **(A)** in shear along the 'longitudinal' plane (ey, ex).

# Part IV : Vibratory behaviour of 3D vocal-fold replica

# 6

# Flow-induced oscillations of isotropic vocal-fold *in vitro* replica

This chapter is based on a collaboration with Raphaël Giraud (IR, GIPSA-lab) and Paul Luizard (post-doc, GIPSA-lab), and an article in preparation for a submission to *Scientific Reports*.

# Contents

## 6.1 Introduction

As detailed in Chapter 1, phonation refers to the production of audible air pulse trains emitted by vocal-fold vibrations in the larynx. These aeroacoustic sources resulting from air-wall interactions at the glottis contribute mainly to voiced sounds such as vowels and sonorous consonants. Contrary to the case of heart, glottal oscillations do not result from any periodic muscular activity. Vocal-folds self-sustained oscillations emerge from "passive" fluid/structure interactions between exhaled airflow and vocal-fold tissue, while stretching, adduction and abduction are driven by laryngeal intrinsic muscles [243]. Vocal folds behave as non-linear oscillators, coupled by their collision and able to bifurcate towards complex regimes of vibration, responding to gradual variation of control parameters (ref) : geometrical ones (*e.g.,* vocal length, glottal width and thickness, structure, convergent or divergent profile), mechanical ones (*e.g.,* stiffness) and aerodynamical ones (*e.g.,* transglottal pressure drop and airflow). A minimum threshold value of subglottal air pressure (Phonation Threshold Pressure) is required for initiating the oscillatory behavior [219].

Since the 1960s [227], to overcome the limitations of *in vivo* testing conditions, various artificial larynges were developed to mimic human phonation in a simplified *in vitro* context, but allowing an easy control and quantitative access to the main physical parameters that govern vocal fold vibrations. In recent decades, vocal fold replicas have evolved in complexity from static, driven rigid-walled models to deformable, human-scale models capable of supporting flow-induced vibrations (see Kniesburges *et al.* [118] for a review). Therefore, for years (1990s-2000s), most experimental approaches focused on aerodynamic studies, including the impact of geometrical parameters on the laryngeal flow. With the achievement of the first self-oscillating vocal fold replicas (2005-2010s), interest has progressively shifted to the resulting acoustic production, and the study of the underlying fluid/structure/acoustic interactions. In comparison, the exploration of the specific material properties of artificial vocal folds is rather recent (2010s), and their impact on the fully-coupled process is still poorly understood. To our knowledge :

(i) the number of studies involving experimental models of vocal folds able to control the laryngeal geometry is rather limited. In particular, only one study presents extensible folds in their longitudinal direction [119], even though vocal-fold stretching is a major aspect of phonation biomechanical control;
(ii) A few pioneer works have shown that a change in the mechanical properties of the oscillators (*e.g.* internal pre-tension, non-linear mechanical behaviour) can be critical on the acoustical fundamental frequency [138, 188, 195], but the in-depth investigation of the impact the material properties on the vocal-fold vibratory patterns and aero-acoustical correlates is still barely explored experimentally.

Therefore, this chapter presents the design and experimental characterization of an original larynx replica, allowing to control both the dynamic changes of input aerodynamic parameters (air pressure or air flow) as well as the longitudinal pre-deformation of the vocal folds with adjustable material properties. By combining a large experimental database

with simple analytical models of glottal flow and beam vibrations already used in the voice community [114, 188, 210], this chapter aims to help better understand the influence of the mechanical properties of several isotropic vocal fold replicas on their ability to achieve self-oscillation, and on the variation of associated acoustic and aerodynamic indices.

## 6.2 Materials and method

### 6.2.1 A deformable articulated larynx replica

A new *in vitro* testbed of human phonation was designed (Fig. 6.1), able to reproduce the vocal-fold self-sustained vibrations and the articulatory gestures of the larynx, which are both involved in the production of a voiced sound. It consists of a 1:1 scale vocal-fold replica inserted in a laryngeal envelope, equipped to enable the folds actuation in stretching, abduction/adduction and compression. In the following, the geometry of the artifical larynx is defined in the reference anatomical frame ($\mathbf{e}_{ml}$, $\mathbf{e}_{ap}$, $\mathbf{e}_{is}$), where $\mathbf{e}_{ml}$ coincides with the mediolateral direction, $\mathbf{e}_{ap}$ with the anteroposterior dirction and $\mathbf{e}_{is}$, with the inferosuperior direction.

*Vocal-fold replica* – Several mono-layered and isotropic oscillators were conceived, made up of homogeneous and soft polymers with tailored mechanical properties. Two types of polymers were used, either based on elastomers of reference, or hydrogels chosen for their ability to retain high tissue-like water content :

(i) A first set of folds was fabricated using a two-component addition-cure silicone rubber compound (Smooth-On, Ecoflex® series), as commonly used in previous *in-vitro* testbeds of phonation (ref). In particular, three material candidates were selected with various hardness degrees (Shore 00-10, 00-30 and 00-50), comparable densities (1.04, 1.07, 1.07) and processed with a 1A:1B mixing ratio by weight. They are noted EF10, EF30 and EF50 thereafter. The relative density is equal to 1.04 for EF10, and 1.07 for the others.

(ii) A second set of folds was composed of a gelatin-based hydrogel that we previously optimised in Chapter 3 to get as close as possible to the mechanical response of vocal-fold tissues in tension, compression and shear [43]. Briefly, it is based on 10% w/v porcine gelatin aqueous solution (Bloom number 300 g, Type A), cross-linked with 0.5 % mL of glutaraldehyde per gram of gelatin, to improve the strength, stiffness and ductility of the neat gel. The detailed processing route for dilution and mixing can be found in Chapter 3. The final relative density of the gel is close to 1.

Whichever family of materials was chosen, 20 g of solution was prepared in a becher for homogenization and vacuum degassing. Then, it was cast in 3D-printed molds to form a 3D structure (volume $\approx 16.88$ cm$^3$) reproducing the average morphology of healthy, adult and male vocal folds at rest (Fig. 6.1.A), *i.e.* a vocal length of 20 mm, a glottal of 1 mm in width and 4 mm in thickness. Molds were previously coated with silicone grease to facilitate the demolding step. The elastomers cured at room temperature (T $\approx 45\,^{\circ}$C) and

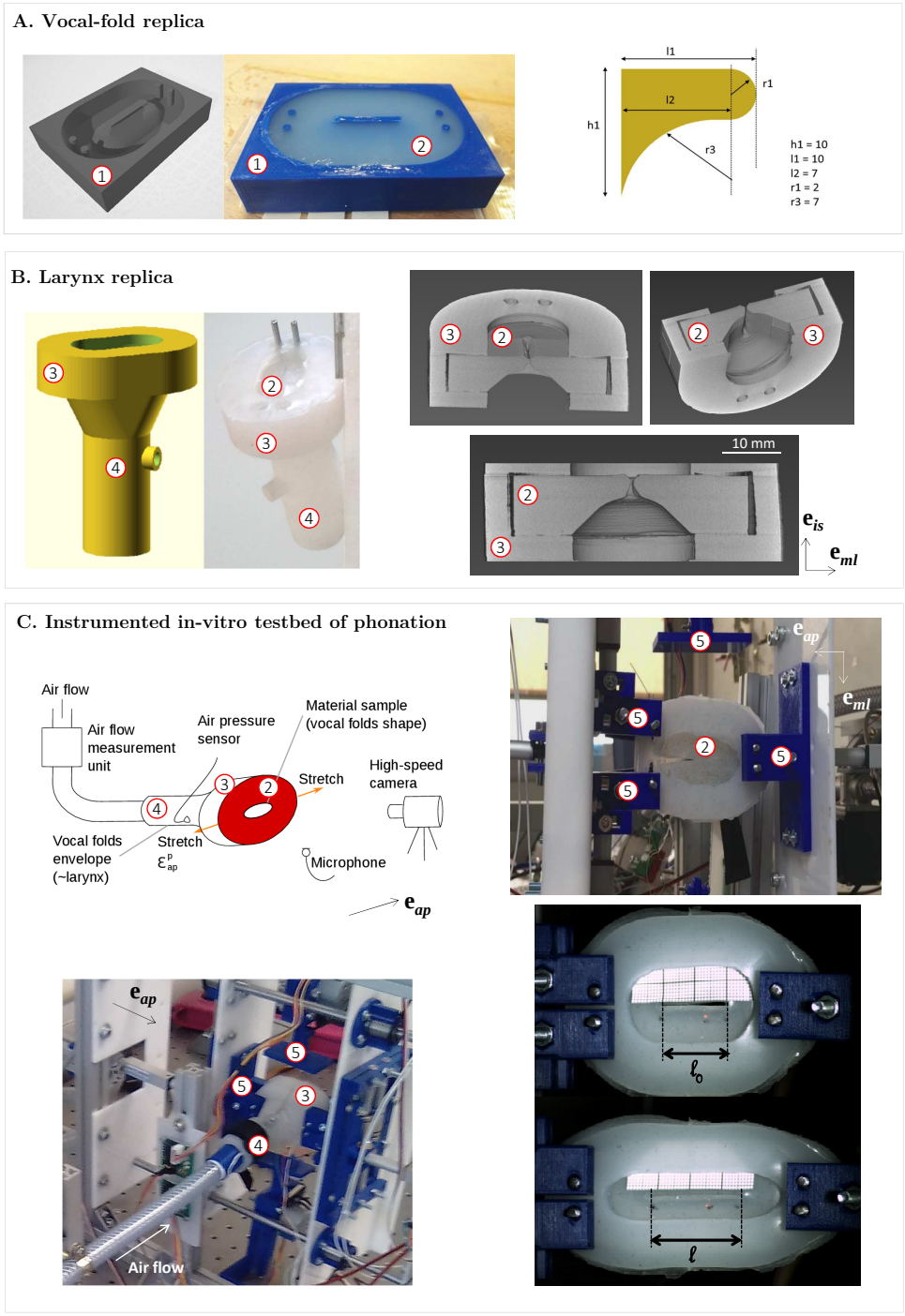


**Figure 6.1:** *In vitro* testbed of phonation. **A) Vocal fold replicas** : (*from left to right*) ① 3D-printed mold, illustration of a molded silicone replica (②) during curing, and scheme of the target geometry in the coronal view of one fold (units in mm). **B) Larynx replica** : (*from left to right*) 3D scheme and picture of the laryngeal envelope after insertion of a silicone vocal-fold replica. Mid-coronal view of the larynx replica (X-ray microtomography, voxel size 50 $\mu$m$^3$). ② vocal-fold replica; ③ glottal stage casing ④ subglottal tract. **C) General view of the instrumented testbed** : (*from left to right, top to bottom*) Scheme of the set-up and metrology; front picture of the folds and their different actuators (⑤); backside picture of the vocal fold replica; illustration of the fold actuation in longitudinal stretching.

relative humidity (RH ≈ 45%) for 2 h for EF30 and EF50 (resp. 4 h for EF10). The hydrogel was kept at 3 °C for 24 h before being demolded. Negligible shrinkage was observed after curing for either material.

*Laryngeal envelope and actuators* – A flexible laryngeal envelope was designed so that the processed vocal fold replicas can be inserted and interchanged, while maintaining a seal. As shown in Fig. 6.1.B, this three-part envelope consists of : (i) a subglottal tract attached to the air inlet tube, representing the trachea upper part (subglottal stage); (ii) an upper casing in which the vocal folds can be positioned (glottal stage); (iii) a divergent tract joining the subglottal and glottal stages.
The envelope was connected to a series of motors aiming at reproducing the action of crico-thyroid tilt, *i.e.* vocal-fold stretching along the antero-posterior (or longitudinal) direction $\mathbf{e}_{ap}$, it being a key mechanism on the pitch control during phonation. The junction with the motors was made thanks to three 3D-printed jaws screwed on the envelope, as illustrated in Fig. 6.1.C. Note that other actions mimicking inter-arytenoid compression (*i.e.* vocal-fold abduction and adduction in the plane ($\mathbf{e}_{ml}$, $\mathbf{e}_{ap}$), and compression of the folds along the mediolateral direction $\mathbf{e}_{ml}$) were also integrated to the bench (albeit not used in the first campaigns presented in this work).
Finally, the laryngeal envelope was molded with EF50 silicone, *i.e.* a soft and extensible material able to deform when the folds are actuated, yet rigid enough to mimic the stiffness of the larynx. Before vibration testing, each vocal-fold replica was manually inserted into the glottal stage whose walls were previously coated with silicone grease, and then attached to the laryngeal envelope and motorized jaws using Teflon®-covered screws to prevent air leakage during fold mobility.

### 6.2.2 In-plane mechanical characterization of the selected materials

In parallel to each vibration campaign on the phonation testbed (see section below), mechanical tests were performed on specimens made of the selected 3D vocal folds materials, elaborated with the same processing route but shaped in a simpler geometry adapted to the tests. Considering the fold actuation presented in this work, focus was given to their tensile in-plane response under cyclic and finite-strain conditions, following the test procedure already detailed in Chapter 3.

Briefly, samples were cut from rectangular material plates elaborated aside from the 3D vocal-folds replicas, at an effective length-to-width ratio 5:1, with a gauge length of 50 mm and a thickness of 2 mm. Mechanical tests were carried out using an electromechanical uniaxial machine (Instron® 5944) equipped with a ± 10 N load cell. The first Piola-Kirchoff stress $P$ and the Hencky strain $\varepsilon$ were calculated from the cell force signal and displacement of the machine crosshead. Samples were subjected to 4 load-unload cycles with increasing strain amplitude up to $\varepsilon = 0.7$, at a strain rate of $10^{-2}$ s$^{-1}$. Finally, in the case of hydrogel samples, tests were conducted in a thermo-regulated atmosphere (T ≈ 25 °C) and at proper hygrometric conditions (≈ 98–100 %RH), to protect the samples from air drying.

Additional measurements were conducted on the same uniaxial machine, to characterize and compare the surface adhesion properties of the different materials selected. In short, two square samples of the same material were glued to opposing compression platen (15 min drying time). Samples were placed in contact against each other, compressed down to a strain level of -0.20 at a rate of $10^{-2}$ $s^{-1}$, and relaxed during 3 min. Then, the upper sample was pulled up to separate both bodies in contact, while measuring the force $f$ resisting the separation. This force was normalized by the force registered during the relaxation step, noted $f_{relax}$.

### 6.2.3 Aero-acoustic characterization of the vocal-fold replica

*Set-up and experiments* – Each 3D vocal-fold replica was assessed as a potential "biomimetic" acoustical source, by quantifying its flow-induced vibratory behavior on the new *in vitro* testbed of phonation (Fig. 6.1). The replica was placed in the artificial laryngeal envelope, which in turn was connected to a uniform "tracheal" tube supplied with a pressurised airflow. Using a dedicated LabView® interface (National instruments) and a motorized control system (actuonix L16), two major parameters could be tailored :

(i) the vocal-folds pre-strain $\epsilon^p_{ap}$ driven by the displacement of a series of jaws along the longitudinal direction $\mathbf{e}_{ap}$ .
$\epsilon^p_{ap} = \ln(\ell/\ell_0)$, where $\ell$ (resp. $\ell_0$) refers to glottal length in the deformed (resp. undeformed) configuration;
(ii) the airflow rate $\phi$, driven by the degree of opening of an electromechanical valve actuator in the tracheal tube replica.

The set-up is equipped with a number of sensors to acquire real-time data for various levels of $\epsilon^p_{ap}$ and $\phi$ (see Fig. 6.1.C) : an airflow measurement unit (TSI 4043); a pressure sensor (Kulite Xcq-093) measuring aerodynamic subglottal pressure $P_s$ relatively to ambient atmospheric pressure; a microphone (DPA 4060) calibrated by means of a sound level meter (Brüel & Kjaer 2250); and a high-speed camera (Mikrotron® MotionBLITZ EoSens® Cube7).

Electrical signals were processed using a preamplifier/conditioning board (PXIe-1073 chassis equiped with NI PXIe-6341 and NI PXIe-4330 modules). The acquired data were processed using the LabView13 software (National Instruments). The sampling frequency for all pressure and flow acquisitions was 22.05 kHz. The high-speed camera images were synchronized by the MotionBlitz software directly called in LabView, so that 100 frames were recorded at each step of valve opening at a frame rate of 1473 frames/s, *i.e.* three frames every 2 ms.

Prior to the experiments, self-oscillation ranges of the model were determined in relation to airflow input values and pre-stretch conditions. Then, a serie of experimental rounds were recorded. An experimental round consisted of setting a given value of fold pre-strain $\epsilon^p_{ap}$. Airflow rate $\phi$ was then increased in steps from its minimum value for self-oscillation (typically $\phi_{min} = 0.3\ L/s$) to a maximum value related to 100% valve opening ($\phi_{max} = 3.5$ L/s. Each quasi-stationary step lasted 4 s, during which the sensor values were recorded

(quasi-static aerodynamic conditions). For each tested vocal-fold replica, the experimental procedure was repeated from rest configuration ($\epsilon_{ap}^{p} = 0$) up to the maximal deformation authorized by the set-up ($\epsilon_{ap}^{p}$ within 30–40 % depending on the chosen material).

*Data processing* – All data recorded in Labview (TDMS format) were converted to Matlab®(MAT format) for being post-processed in this development environment with customized programs. For each run, several aero-acoustic parameters were extracted from the recorded time-varying signals : subglottal airflow $\phi(t)$ and subglottal air pressure $P_s(t)$); fundamental frequency of folds self-oscillation $f_o$ calculated from the audio signal using the YIN-auto-correlation method developed by de Cheveigné and Kawahara [46]; calibrated sound pressure level $SPL$ in dB(C) ; spectral centroid $SC$ determined as the weighted mean of all frequencies present in sound spectrum; glottal impedance $R_g$ estimated as the ratio between subglottal air pressure and flow $R_g = P_s/\phi$.

High-speed images were edited and analyzed using the software Glottis Analysis Tools 2020 [117] which enables glottal area contour detection with a threshold-based region growing approach combined to pretrained deep neural networks. When required, automatic segmentation was manually corrected to account for minor detection errors on one glottal cycle per each quasi-stationary step. Glottal area waveforms $A_g(t)$ were saved in Matlab® format and maximum values of $A_g$ were extracted for each quasi-stationary step. The conversion factor from pixels to $mm^2$ was determined on images recorded for pixel-to-mm conversion purpose (see Fig.6.1) by means of ImageJ software. In the same way, pre-strain $\epsilon_{ap}^{p}$ actually experienced by each vocal-fold replica was measured on these images (one value per experimental round). In order to have a dynamic view of the median oscillatory motion of the replica, kymograms [**SvecandSchutte1996**] were plotted in Matlab®. The kymographic line was selected on a first image in the middle part of the glottis and perpendicular to the antero-posterior glottal axis and then plotted for the whole highspeed sequence as a function of time (see Fig. 6.2). While kymograms do not allow to visualize glottal vibrations along the whole glottal length, they provide a detailed representation of vocal-fold dynamics at the selected position on the glottis.

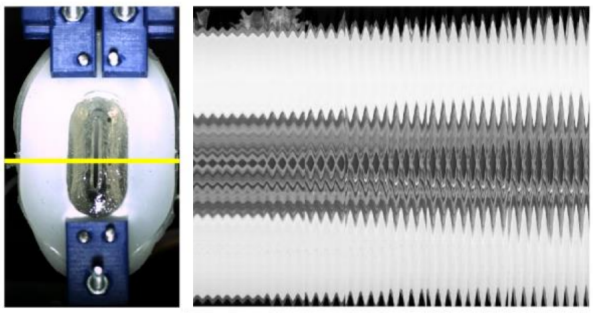

**Figure 6.2:** Illustration of a kymographic visualization of the vibrations for the vocal-fold replica made of gelatin-based hydrogel.

*Analytical aerodynamical modelling* - A simple analytical model based on Bernoulli's principle has been formulated to compare experimental measures with theoretical predictions. This modelling approach has already been applied to understand glottal vibratory behaviour

from an aerodynamical point of view (e.g. [7]). The expected relationship between subglottal air pressure $P_s$, subglottal airflow $\phi$ and glottal area $A_g$ can be expressed by the following equation :

$$P_s + \frac{1}{2}\rho\left(\frac{\phi}{A_s}\right)^2 = P_g + \frac{1}{2}\rho\left(\frac{\phi}{A_g}\right)^2 \tag{6.1}$$

where $\rho = 1.1965$ kg/m$^3$ is the density of air at 22°C, $P_g$ the air pressure within the glottis at the detachment location of glottal jet, and $A_s$ the area of the trachea section upstream of the glottis where subglottal pressure is measured. In the case of our model without vocal tract, $P_g$ is equal to atmospheric air pressure. As the tracheal tube in our model is of 2-cm diameter, $A_s = 3,14$ cm$^2$.

The equation can be reformulated as follows to provide a theoretical estimation of glottal area as a function of subglottal pressure and airflow :

$$A_g = \frac{1}{\sqrt{\left(\frac{2}{\rho}\frac{P_s}{\phi^2} + \frac{1}{A_s^2}\right)}} \tag{6.2}$$

## 6.3 Results and discussion

### 6.3.1 General trends

A similar overall behaviour was found for the aerodynamic and acoustic parameters studied here, regardless of the material and the degree of stretching. Therefore, we will first present and discuss the general trends of the self-oscillating replica.

Fig.6.3 shows the evolution of the main parameters as a function of air flow rate, considered here as the control parameter. A similar figure plotting each parameter as a function of subglottal pressure in provided in the Appendix XX. Each point corresponds to an average of the time-varying x-axis and y-axis parameters over the duration of a quasi-stationary 4-s step. It relates to each case where the model was able to sustain a stable self-oscillating behaviour during the step.

We would have expected an increase of $f_o$ being accompanied by an increase of SPL when airflow rate was increased. This trend was observed at medium to high levels of subglottal airflow and pressure, however in a limited range of a few Hz. At low values of these aerodynamic parameters, $f_o$ slightly decreased with increasing airflow and pressure. Stretching the folds had a minor decreasing impact on $f_o$, contrary to what would be expected based on human physiological behaviour. Obviously, $f_o$ was not related to subglottal tract resonances, which were measured around XX Hz in our experimental configuration.

to complete

### 6.3.2 Impact of the material parameters on the vocal-fold vibration and aero-acoustical correlates

If we now look more closely at the impact of the material chosen to elaborate the artificial vocal folds, both qualitative and quantitative deviations were observed in the general trends described above.

*Impact of the material's mechanical behaviour* – Tensile responses of the four candidates selected to reproduce the quasi-static mechanical behavior of the vocal fold are reported in Figure 6.4, together with the evolution of the tangent moduli $E_t = dP/d\varepsilon$ with $\varepsilon$ (for the last unloading only). Thus, when not interacting with airflow or acoustic waves, such materials can first be distinguished by their tensile stiffness, and classified from the softest to the stiffest (from rest up to $\approx 0.6$ strain) : silicone EF10, hydrogel, silicone EF30 and silicone EF50.

The influence of the "vocal-fold" mechanical properties on their flow-induced vibrations is first highlighted by the symbols reported in Fig. 6.4.b, which illustrate the cases where a stabilized self-oscillation could actually be observed : for each material, below the pre-strain values marked by these symbols, no vibration was observed - the highest value, on the other hand, indicates only the maximum tested during the campaign (oscillations could take place beyond). More specifically, it is interesting to note that none of the replicas could oscillate in their undeformed configuration : they had to be pre-stretched up to $\varepsilon_{ap}^{p} \approx 0.10$ for fluid/structure interactions to give rise to sustained vibrations, except for the replica made of silicone EF10, which started to self-oscillate only for $\varepsilon_{ap}^{p} \approx 0.30$.
The detailed influence of the choice of materials on the aerodynamical, geometrical and audio quantifiers of the vocal-fold vibrations is further evidenced on Fig. 6.3 and Fig. 6.5, reporting all these descriptors in function of the material tangent stiffness, $E_t$. In particular, leaving aside for now the very specific trends observed for the softest material (EF10 silicone, *in blue*), the data show globally that :

- Regarding aerodynamics, material properties of the vocal folds have a large impact on the glottal impedance $R_g$ at the lowest airflow values, *i.e.* up to $\phi \approx 2.5$ L/s (see Fig. 6.3.d). Beyond this critical flow rate, $R_g$ tends towards asymptotic limits around 1500 Pa.s/L which seem to be quite close for all the selected materials, although ranked in increasing order with material stiffness. For the stiffest materials (EF30 and EF50), at largest strains and lowest flow rates, the resistance to the flow can reach up to 3–4 times this asymptotic value.
  The sensitivity to the stiffness of the material is also clearly illustrated by the values of the average subglottal pressure measured during the oscillations, as shown in Fig. 6.5.f : the stiffest the material, the highest the subglottal pressure – the average values $P_s$ for all air flow and strain levels combined being recorded around 1.2 Pa, 2.9 kPa and 3.6 kPa for the hydrogel, EF30 and EF50 respectively. Besides, for a given

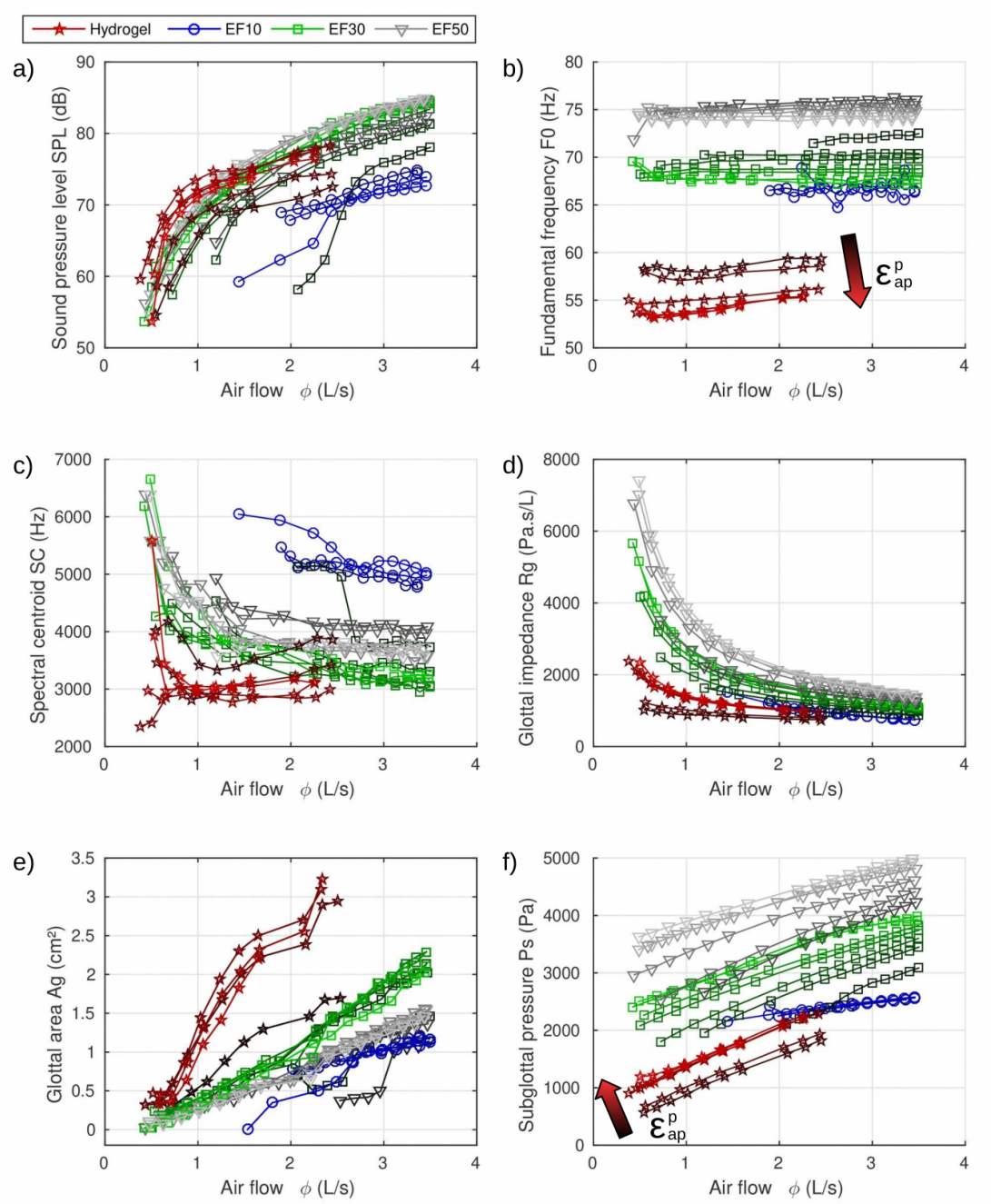


**Figure 6.3:** Audio (sound pressure level, fundamental frequency, spectral centroid), aerodynamic (glottal impedance, subglottal pressure), and geometric (maximal glottal area) descriptors as a function of subglottal airflow, for each material and all stretching conditions. $\varepsilon^p_{ap}$ stands for pre-strain in antero-posterior direction. Dark to light colors stand for increasing $\varepsilon^p_{ap}$ values.

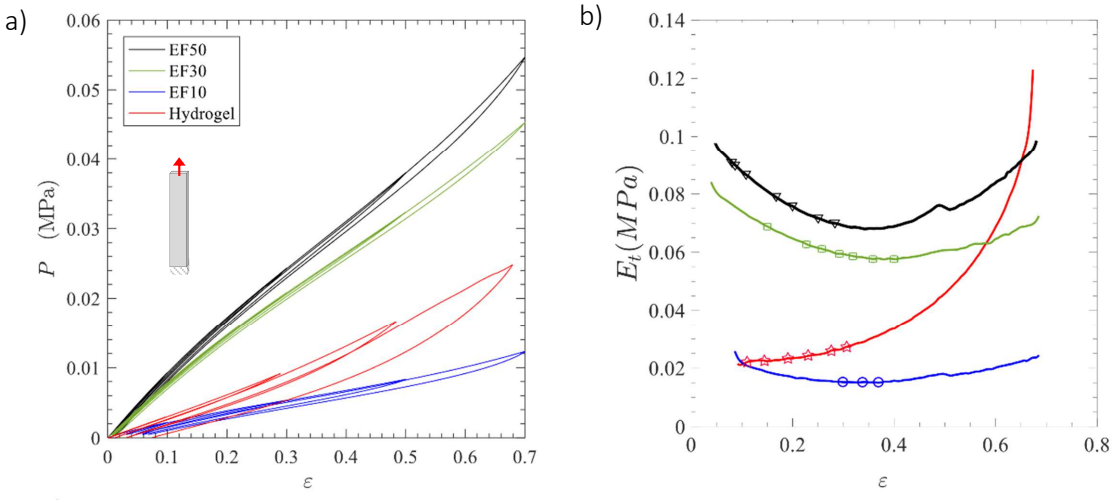


**Figure 6.4:** Tensile behaviour of the four polymers used for the vocal-fold replica during quasi-static and cyclic conditions : a) Piola-Kirschoff stress $P$ *vs.* Hencky strain $\varepsilon$, b) Tangent modulus $E_t$ as function of the applied strain $\varepsilon$. For each material, symbols highlight the pre-strains $\varepsilon_{ap}^p$ which have been applied to the vocal-fold replica, and for which self-sustained oscillations could be observed.

material, the higher the applied pre-strain $\varepsilon_{ap}^p$, the higher the pressure needed to maintain the oscillations, as shown in Fig. 6.3.f. Typically, for a comparable flow rate $\phi \approx 0.7$ L/s and same level of vocal fold pre-strain ($\varepsilon_{ap}^p \approx 0.30$), an increase of about 625 Pa 800 Pa, and 1150 Pa is induced for the hydrogel, EF30 and EF50 silicones respectively, if compared to the value required for the onset of oscillations in the lowest deformed configuration (for which $\varepsilon_{ap}^p \approx 0.1$).

These trends can be explained by looking at the evolution of the geometric parameters of the system, which vary greatly with the material properties of the oscillators. In particular, Fig. 6.3.e and Fig. 6.5.e show that for the same flow rate, the stiffer materials open much less at the glottis, resulting in increased subglottal pressure and greater resistance to airflow. The difference in the maximal glottal opening reached during the oscillations of the hydrogel and the EF30 and EF50 silicones is also illustrated on the high-speed images in Fig. 6.6 (see comparable cases for $\phi \approx 1.5$ L/s and $\varepsilon_{ap}^p \approx 0.30$ for instance). Furthermore, this figure clearly shows that for a given material and a given vocal-fold pre-strain, the glottal opening increases greatly with the flow rate up to the critical value close to $\phi \approx 2.5$ L/s. Beyond that point, the maximal possible aperture between vocal folds seems achieved (it being limited by the material stiffness), thus stabilizing the glottal impedance. Finally, in most general cases, it is shown that the more the material is pre-stretched, the smaller the glottal area during their vibration (see Fig. 6.6 and Fig. 6.3.e). This result also explains the increase in pressure required in the subglottal stage to go from a slightly stretched configuration to a highly stretched configuration for the same flow.

- Regarding acoustics, the impact of the chosen material on the sound intensity remains globally of second order as compared to the impact of the airflow rate, as illustrated in Fig. 6.3.a. Increment of strain in the folds has a (slight) direct effect on the increase

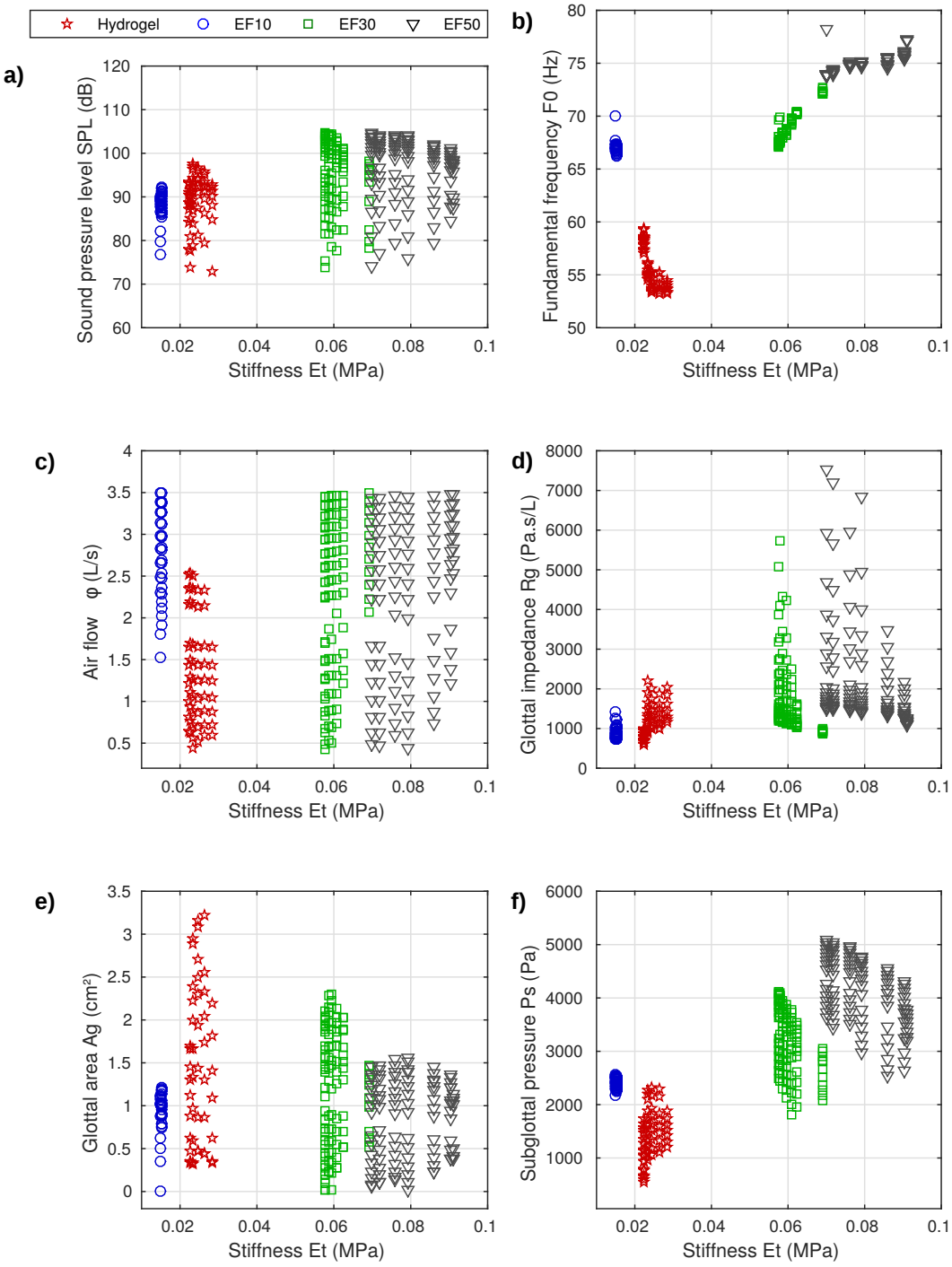


**Figure 6.5:** Geometric and aero-acoustic quantifiers of the vocal fold vibrations against the tensile stiffness of each material, at all recorded airflow values.

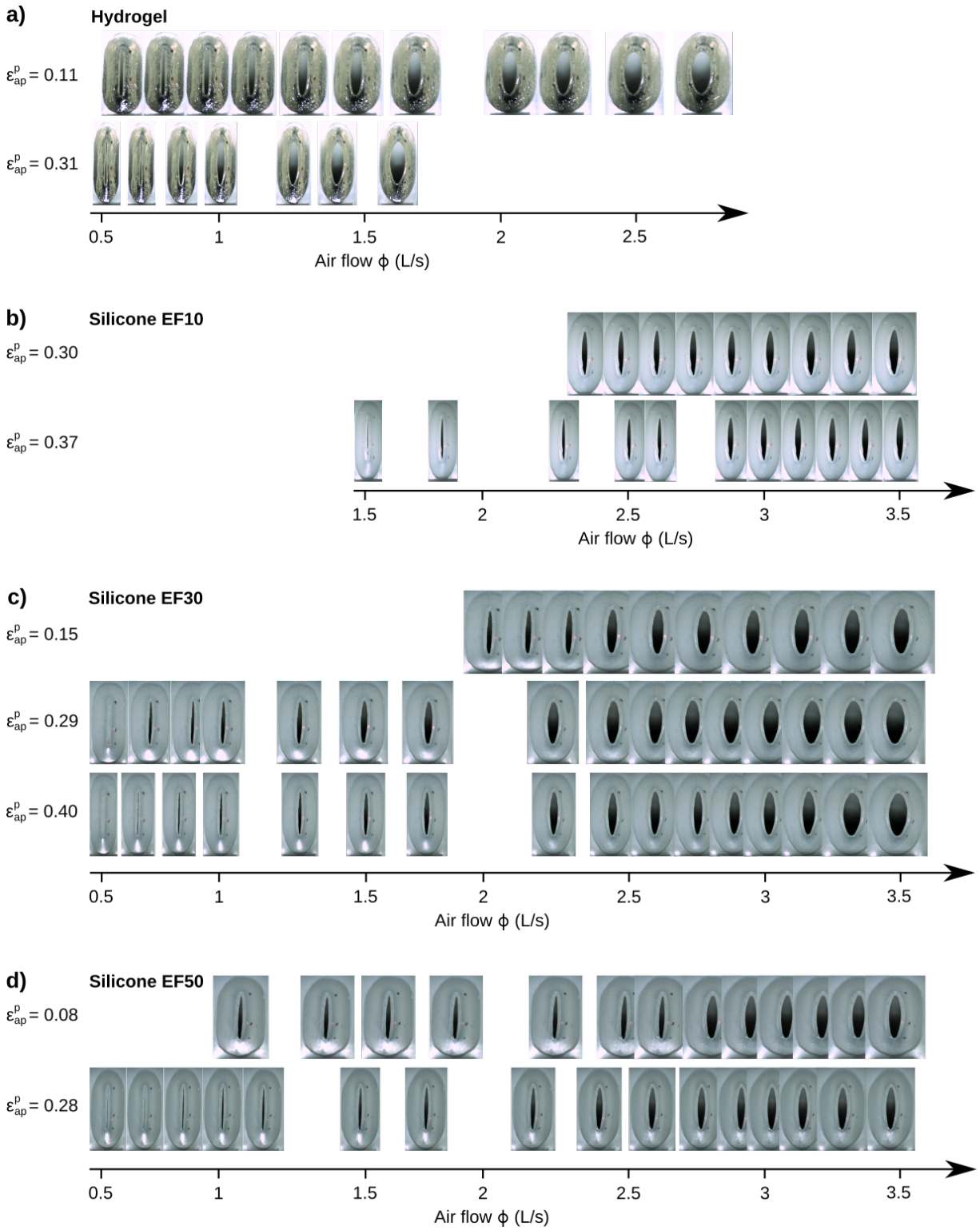


**Figure 6.6:** Pictures of the maximal glottal opening in phonation for various air flow values and stretching values with (a) hydrogel, (b) EF10 silicone, (c) EF30 silicone, and (d) EF50 silicone models. This illustrates specific series shown in Fig 6.3. The blank spaces between pictures correspond to air flow values at which no measurement was performed.

of SPL. On the other hand, the stiffest the material, the highest the fundamental frequency of the produced sound $f_o$, with a discrepancy of about 20 Hz between the hydrogel and the E50 silicone for all combined flow rates (see Fig. 6.5.b). This rise of frequency with the material stiffness is expected [143], even though the measured absolute values of $f_o$ are much lower compared to the average values of 125 Hz/210 Hz in men/women speech. Astonishingly however, stretching the folds has a decreasing impact on the $f_o$ for all tested materials, as shown in Fig. 6.3.b. This decrease remains minor however, in the range of a few Hz for all materials, with a maximal drop of 5 Hz for the hydrogel, vibrating from 60 Hz to 55 Hz when progressively elongated up to $\varepsilon_{ap}^{p} = 0.30$. We will come back to these points in the last section, dedicated to the regulation of the fundamental frequency in our set-up.

*Impact of the interface properties* – The impact of the interface properties of the vocal folds is demonstrated when considering the specific trends observed for the E10 silicone, *i.e.* the only one curing with a "tacky" surface (as notified in the datasheet in Chapter 4). Indeed, Figure 6.7 (*left*) shows that the typical force measured to separate two EF10 silicone samples previously compressed against each other is higher than that obtained to separate two EF30 silicone samples, which cure with a smooth surface. These adhesion tests demonstrate that the separation of samples in EF10 occurs well after the separation of samples in EF30 ($\approx$ 10 s delay). It is interesting to note that the stickiness of E10 silicone after curing is eliminated when lubricated with silicone grease, as demonstrated in Fig. 6.7 (*right*).

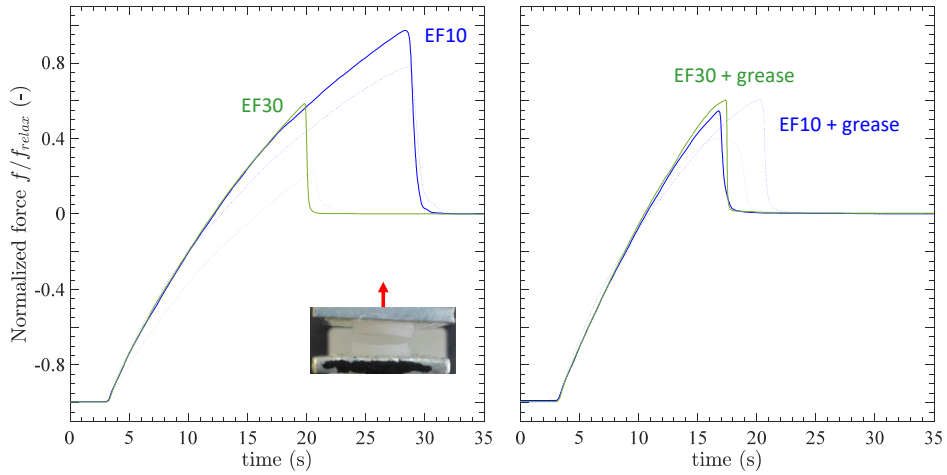


**Figure 6.7:** Results of adhesion testing performed on silicone EF10 (in *blue*) and EF30 (in *green*) : (*left*) samples obtained after curing without any additional coating; (*right*) samples coated with lubricant after curing (silicone grease). Dotted line illustrates the typical repeatability of the test.

Such discrepancies in surface adhesion properties have direct implications for the vibratory patterns allowed by the different vocal fold replicas : while all smooth-surface replicas vibrate with periodic collisions at the perceived pitch frequency, the tacky-surface replica (made of EF10 silicone, no lubricant coating) is not able to generate self-oscillations with periodic contact. Vibrations occur around an equilibrium position, but the opposing vocal folds never touch, as shown in the kymographic visualisation of the high-speed sequences in Fig. 6.8. Thus, although the mechanical properties of EF10 silicone are rather similar

to those of the gelatin-based hydrogel – although even softer and with no J-shape strain hardening of tangent moduli (see Fig. 6.4), the interface differences are such that the EF10 replica shows a very singular vibratory behavior compared to the one molded in hydrogel (and those made of the two other silicones too) :

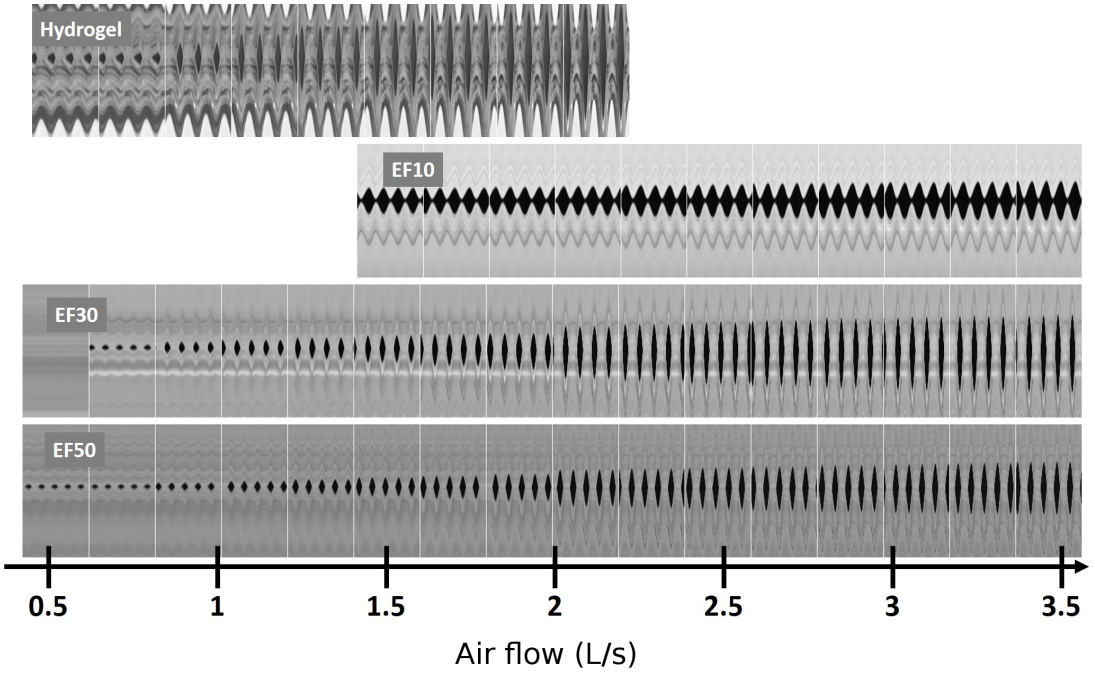


**Figure 6.8:** Kymographic visualization of the vibrations of vocal fold replicas composed of four different materials, in steps of increasing airflow.

- First, the E10 vocal-fold requires much higher flow rates and subglottal pressures to self-oscillate ($\phi$ varying from 1.5 to 3.5 L/s, $P_s$ above 2 kPa), while the hydrogel vibrates in the airflow range from 0.5 L/s to 2.5 L/s and with $P_s$ between 500 Pa and 2 kPa (see Figs. 6.5.c and f for instance). A possible scenario in view of the recorded sequences is that the vocal folds are sucked towards each other at the first air passage by Bernoulli effect, then remain in contact with each other because of their sticky interface. The subglottal pressure then rises, reaching even peaks of 8 kPa to separate them, and generating aerodynamic forces such that the elastic restoring forces are no longer sufficient to bring the folds together until periodic contact.

- Once separated, the maximal glottal area recorded during the EF10 vibrations remains much lower than that observed for the hydrogel (and globally lower than that observed for all smooth-surface replicas, including the stiffest EF50), as shown in Fig. 6.6 and 6.5.e.

- Then, the E10 vocal-fold vibrates only in the higher range of the applied pre-strain ($\varepsilon_{ap}^{p} \approx 0.30$), while the hydrogel vibrates once $\varepsilon_{ap}^{p} > 0.10$.

- Finally, the quality of the sound produced by the EF10 replica without vocal-fold contact is very distinct than that produced by the hydrogel replica. This can be

illustrated by the spectral centroid (SC) reported in Fig. 6.3.c, showing a high-frequency band close to 5 kHz where most of the energy is concentrated. The plateau is closer to 3 Hz for the hydrogel for comparable flow rates. High value of this SC index shows a fundamental frequency $f_o$ rather weak with respect to the level of noise generated in the upper partials.

### 6.3.3 Upon the regulation of the acoustical fundamental frequency

Finally, this section offers a summary on the variation of the acoustical frequency $f_o$ with the parameters of the replica (see Fig. 6.9). Focusing on the material control parameters, as mentioned above, several points were rather unexpected in the collected database :

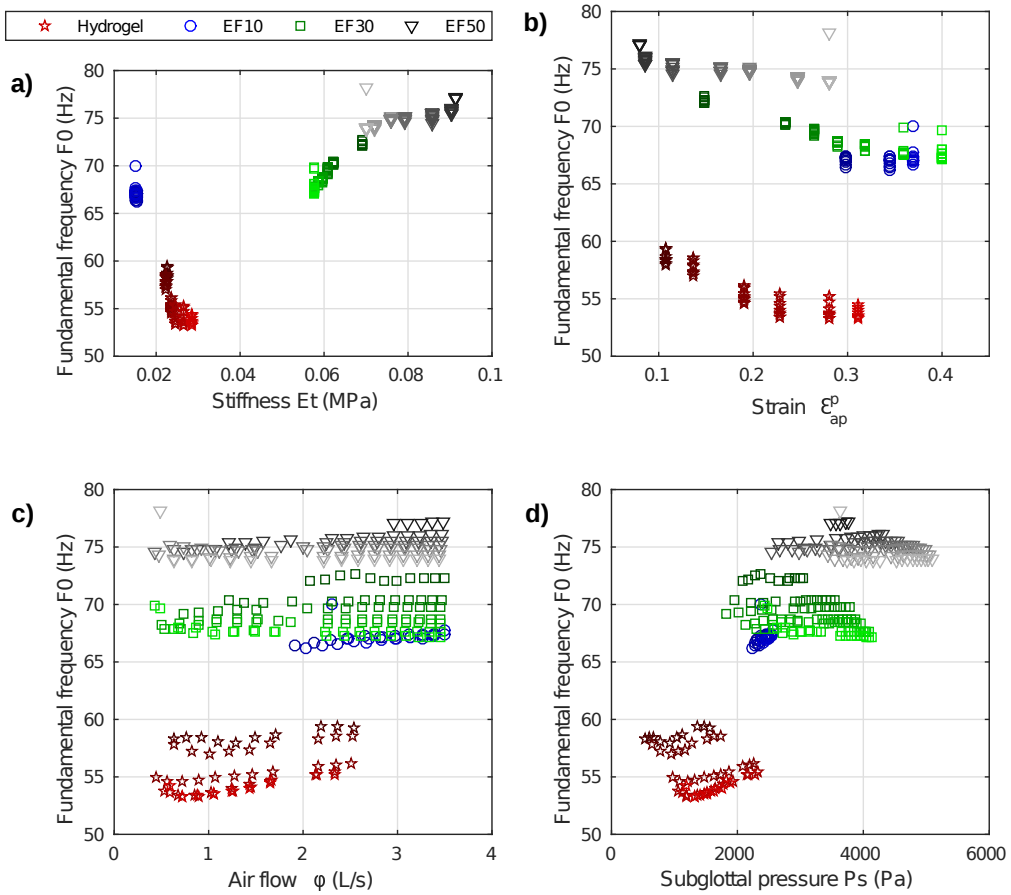


**Figure 6.9:** Fundamental frequency against various parameters that influence phonation characteristics.

(i) in terms of strain-induced evolution – the highest frequencies being measured for the least stretched vocal fold configurations (Fig. 6.9.b), which is the opposite of the *in vivo* observations. Regarding the silicone series, this trend can be explained by the non-linear decrease of their tangent modulus $E_t$ up to about 0.4 strain (see Fig. 6.4.b) – *i.e.* a threshold greater than all the $\varepsilon^p_{ap}$ pre-strain values that were applied to the

vocal-fold replicas. For the hydrogel however, the slight $f_o$-decrease observed at lower stiffness values in Fig. 6.9.a is still an open question.

(ii) in terms of orders of magnitude – for all materials, the measured values being in the low-pitch range of the human voice despite the physiological levels of tensile strains applied.

In order to better understand these trends, we used a simplified analysis to predict the natural frequencies of the replica under transverse vibrations, based on beam theory and an approach previously applied to the living tissue [114, 210]. Therewith, assuming that the acoustical frequency $f_o$ should be rather close to the first natural frequency of the artificial vocal fold $F_1$ (as for the living tissue - see Chapter 1), and that the geometry of the fold can be approximated by a pinned-pinned Timoshenko beam of cylindrical cross-section [114] (initial diameter $d_0$ and length $\ell_0$), Figure 6.10 displays the theoretical predictions expected when deforming the hydrogel vocal-fold replica in tension for various geometrical configurations. Note that the shear properties measured for the hydrogel in Chapter 3 were also used as inputs in this analysis. As a result, assuming that the length of the vibrating beam is limited to the glottal aperture solely (*i.e.* $=$ 20 mm), frequencies are predicted within the range 100-350 Hz depending on the strain level. However, if one considered that all the material held within the fixed boundaries of the replica is effectively free to vibrate (*i.e.* $=$ 45 mm), the expected frequencies range below 100 Hz up to 0.20 strain, reaching a maximum close to 150 Hz at 0.40 strain. Although it can explain some trends, this simplified beam model is too limited to account for the measurements obtained. A next step would be to simulate the dynamical behaviour of the real 3D replica, to better predict its intrinsic vibratory properties.

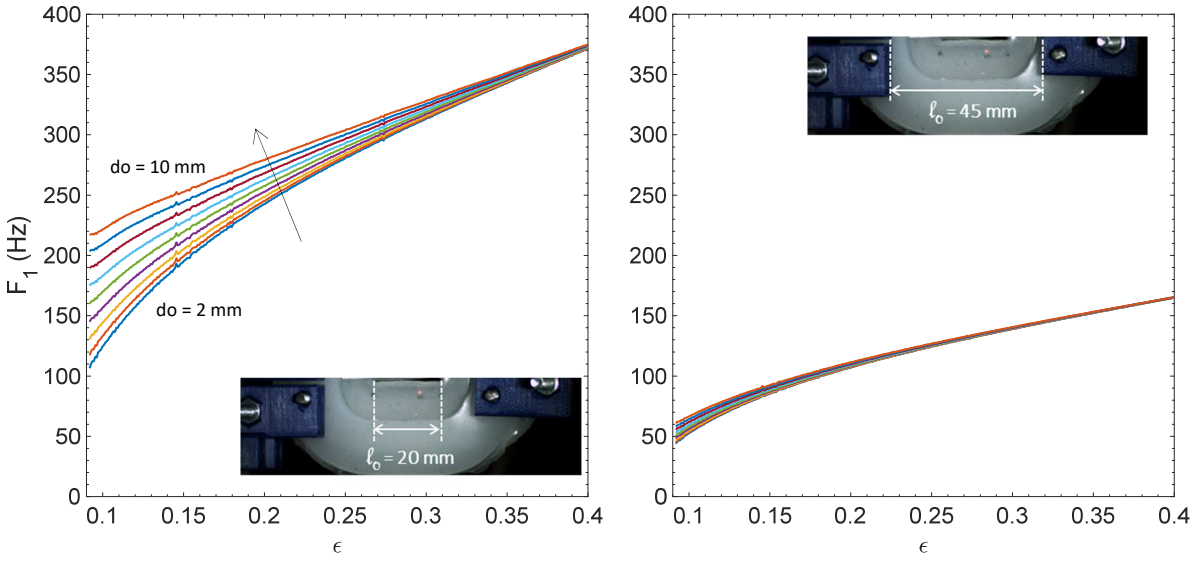


**Figure 6.10:** Theoretical predictions of the replica's vibratory properties as function of the applied tensile strain $\epsilon$ for several geometrical configurations using beam theory. *(left)* $d_O$ varied from 2 to 10 mm, and $=$ 20 mm; *(right)* $d_O$ varied from 2 to 10 mm, and $=$ 45 mm

## 6.4 Conclusion

to revise

A new testbed of artificial vocal folds was constructed, allowing for the first time to change the applied strain and to control the glottis geometry. Several materials were used, enabling to compare their intrinsic mechanical properties in terms of Piola-Kirschoff stress and related tangent modulus to observable aero-acoustic parameters during phonation of the vocal folds, i.e. while the system was self-oscillating.

Results showed aerodynamic and acoustic quantities comparable with previous research based on artificial vocal folds (ref) as well as excised larynges [130], which validated the relevance of this new testbed for static configurations and commonly used elastomer materials.

Furthermore, self-oscillations were also reached in dynamic configurations, *i.e.* by changing the strain applied at each end of the vocal folds. The main effects on the produced sound were partly explained by investigating the mechanical properties of the tested materials in conjunction with the modification of the geometry of the vibrating replicas, especially in terms of glottal area.

The different materials that composed the vocal fold replicas highlighted a major characteristic of the self-oscillation phenomenon, namely the fact that some of the tested replicas did not achieve contact between the folds while vibrating. This specific point affected greatly the patterns of vibration as well as the produced sound and aerodynamic parameters. This is in line with previous research (ref) and the present testbed allowed to illustrate the dependency of the vibration regimes on the material properties while keeping identical all other parameters.

# APPENDIX A

# Conclusions and perspectives

blablabla

Among the biopolymers used to make hydrogels, gelatin is very attractive due to its biocompatibility, biodegradability and versatile physico-chemical properties. A proper and complete characterization of the mechanical behavior of these hydrogels is critical to evaluate the relevance of one formulation over another for a targeted application, and to optimise their processing route accordingly. In this work, we manufactured neat gelatin and gelatin with covalent cross-linking using glutaraldehyde at various concentrations, yielding to hydrogels with tunable mechanical properties that we characterized under finite strain, cyclic tension, compression and shear loadings. The role of both the chemical formulation and the kinematical path on the mechanical performances of the gels is highlighted. As an opening towards biomedical applications, the properties of the gels are confronted to those of native soft tissues particularly complicated to restore, the human vocal folds. A specific cross-linked hydrogel is selected to mimic at best the multi-axial response of the vocal-fold fibrous tissues.

# Bibliography


[1] Abbott, A. "Cell culture: biology's new dimension." In: *Nature* 424.6951 (2003), pp. 870–2 (cit. on p. 87).

[2] Afewerki, S. *et al.* "Gelatin-polysaccharide composite scaffolds for 3D cell culture and tissue engineering: Towards natural therapeutics." In: *Bioengineering & Translational Medicine* 4.1 (2019), pp. 96–115. DOI: 10.1002/btm2.10124 (cit. on p. 53).

[3] Agrawal, A. *et al.* "Strong fiber-reinforced hydrogel." In: *Acta Biomaterialia* 9.2 (2013), pp. 5313–5318. DOI: 10.1016/j.actbio.2012.10.011 (cit. on p. 97).

[4] Alger, M. Polymer Science Dictionary. 2nd. Great Britain: *International Ltd. Padstow Cornwall*, 1997 (cit. on p. 91).

[5] Alipour-Haghighi, F. and Titze, I. R. "Elastic models of vocal fold tissues." In: *The Journal of the Acoustical Society of America* 90.3 (1991), pp. 1326–1331 (cit. on pp. 17, 19).

[6] Andrade-Miranda, G. *et al.* "Laryngeal image processing of vocal folds motion." In: *Applied Sciences* 10.5 (2020), p. 1556 (cit. on p. 26).

[7] Bailly, L. *et al.* "Influence of a constriction in the near field of the vocal folds: Physical modeling and experimental validation." In: *Journal of the Acoustical Society of America* 124.5 (2008), pp. 3296–3308 (cit. on pp. 13, 15, 28, 116).

[8] Bailly, L. *et al.* "In-plane mechanics of soft architectured fibre-reinforced silicone rubber membranes." In: *Journal of the Mechanical Behavior of Biomedical Materials* 40.12 (2014), pp. 339–353. DOI: 10.1016/J.JMBBM.2014.09.012 (cit. on pp. 86, 97, 100).

[9] Bailly, L. *et al.* "3D multiscale imaging of human vocal folds using synchrotron X-ray microtomography in phase retrieval mode." In: *Scientific Reports* 8.1 (2018). DOI: 10.1038/s41598-018-31849-w (cit. on pp. 14, 63, 65, 88, 92, 94).

[10] Bakhshaee, H. *et al.* "Determination of Strain Field on the Superior Surface of Excised Larynx Vocal Folds Using DIC." In: *Journal of Voice* 27.6 (2013), pp. 659–667. DOI: https://doi.org/10.1016/j.jvoice.2013.05.009 (cit. on p. 92).

[11] Bartlett, R. S. and Thibeault, S. L. "Bioengineering the Vocal Fold: A Review of Mesenchymal Stem Cell Applications." In: *Advances in Biomimetics*. Ed. by A. George. Rijeka: IntechOpen, 2011. Chap. 22. DOI: 10.5772/13803 (cit. on p. 86).

[12] Bashir, S. *et al.* "Fundamental Concepts of Hydrogels: Synthesis, Properties, and Their Applications." In: *Polymers* 12.11 (2020), p. 2702 (cit. on p. 86).

[13] Becker, S. *et al.* "Flow-structure-acoustic interaction in a human voice model." In: *The Journal of the Acoustical Society of America* 125.3 (2009), pp. 1351–1361 (cit. on p. 29).

[14] Benboujja, F. and Hartnick, C. "Quantitative evaluation of the human vocal fold extracellular matrix using multiphoton microscopy and optical coherence tomography." In: *Scientific Reports* 11 (2021), p. 2440 (cit. on pp. 92, 94).

[15] Benboujja, F. and Hartnick, C. "Quantitative evaluation of the human vocal fold extracellular ma-trix using multiphoton microscopy and optical coherence tomography." In: *Scientific Reports* 11.1 (2021), pp. 1–16 (cit. on pp. 10, 13, 14).

[16] Berke, G. S. "Intraoperative measurement of the elastic modulus of the vocal fold. Part 1. Device development." In: *The Laryngoscope* 102.7 (1992), pp. 760–769 (cit. on p. 17).

[17] Berry, D. A. *et al.* "Interpretation of biomechanical simulations of normal and chaotic vocal fold oscillations with empirical eigenfunctions." In: *The Journal of the Acoustical Society of America* 95.6 (1994), pp. 3595–3604 (cit. on p. 26).

[18] Bigi, A. *et al.* "Mechanical and thermal properties of gelatin films at different degrees of glutaraldehyde crosslinking." In: *Biomaterials* 22.8 (2001), pp. 763–768. DOI: 10.1016/S0142-9612(00)00236-2 (cit. on pp. 53, 54, 59).

[19] Bode, F. *et al.* "Enzymatically cross-linked tilapia gelatin hydrogels: Physical, chemical, and hybrid networks." In: *Biomacromolecules* 12.10 (2011), pp. 3741–3752. DOI: 10.1021/bm2009894 (cit. on p. 53).

[20] Boltežar, L. and Bahar, M. Š. "Voice disorders in occupations with vocal load in Slovenia." In: *Slovenian Journal of Public Health* 53.4 (2014), p. 304 (cit. on p. 2).

[21] Bot, A. *et al.* "Effect of deformation rate on the stress-strain curves of gelatin gels." In: *J. Chim. Phys.* 93 (1996), pp. 837–849 (cit. on p. 62).

[22] Branski, R. C. *et al.* "Vocal fold wound healing: a review for clinicians." In: *Journal of Voice* 20.3 (2006), pp. 432–442. DOI: 10.1016/j.jvoice.2005.08.005 (cit. on p. 86).

[23] Bühler, R. B. *et al.* "Collagen type I, collagen type III, and versican in vocal fold lamina propria." In: *Archives of Otolaryngology - Head and Neck Surgery* 137.6 (2011), pp. 604–608. DOI: 10.1001/archoto.2011.88 (cit. on p. 13).

[24] Burdick, J. A. and Murphy, W. L. "Moving from static to dynamic complexity in hydrogel design." In: *Nature Communications* 3.1 (2012), p. 1269. DOI: 10.1038/ncomms2271 (cit. on p. 53).

[25] Butler, J. E. *et al.* "Gender-related differences of hyaluronic acid distribution in the human vocal fold." In: *The Laryngoscope* 111.5 (2001), pp. 907–911 (cit. on p. 13).

[26] Cacopardo, L. *et al.* "Engineering hydrogel viscoelasticity." In: *Journal of the Mechanical Behavior of Biomedical Materials* 89 (2019), pp. 162–167. DOI: https://doi.org/10.1016/j.jmbbm.2018.09.031 (cit. on p. 62).

[27] Campiglio, C. E. *et al.* "Cross-Linking Strategies for Electrospun Gelatin Scaffolds." In: *Materials* 12.15 (2019). DOI: 10.3390/ma12152476 (cit. on p. 53).

[28] Carpenter, J. C. *et al.* "Study of the degradation of polydimethylsiloxanes on soil." In: *Environmental science & technology* 29.4 (1995), pp. 864–868 (cit. on p. 74).

[29] Carranca, M. *et al.* "Versatile lysine dendrigrafts and polyethylene glycol hydrogels with inherent biological properties: in vitro cell behavior modulation and in vivo biocompatibility." In: *Journal of Biomedical Materials Research* 109.3 (2021), pp. 926–37 (cit. on pp. 87, 95).

[30] Catalina, M. *et al.* "Influence of crosslinkers and crosslinking method on the properties of gelatin films extracted from leather solid waste." In: *Journal of Applied Polymer Science* 119.4 (2011), pp. 2105–2111. DOI: 10.1002/app.32932 (cit. on p. 54).

[31] Cedervall, J. *et al.* "Injection of embryonic stem cells into scarred rabbit vocal folds enhances healing and improves viscoelasticity: short-term results." In: *Laryngoscope* 117.11 (2007), pp. 2075–81 (cit. on p. 86).

[32] Chai, Q. *et al.* "Hydrogels for Biomedical Applications: Their Characteristics and the Mechanisms behind Them." In: *Gels* 3.1 (2017), p. 6 (cit. on p. 86).

[33] Chan, R. W. and Tayama, N. "Biomechanical effects of hydration in vocal fold tissues." In: *Otolaryngology - Head and Neck Surgery* 126.5 (2002), pp. 528–537. DOI: 10.1067/mhn.2002.124936 (cit. on p. 86).

[34] Chan, R. W. and Tayama, N. "Biomechanical effects of hydration in vocal fold tissues." In: *Otolaryngology-Head and Neck Surgery* 126.5 (2002), pp. 528–537 (cit. on p. 23).

[35] Chan, R. W. and Titze, I. R. "Hyaluronic acid (with fibronectin) as a bioimplant for the vocal fold mucosa." In: *The Laryngoscope* 109.7 (1999), pp. 1142–1149 (cit. on p. 34).

[36] Chan, R. W. and Titze, I. R. "Viscoelastic shear properties of human vocal fold mucosa: Measure-ment methodology and empirical results." In: *The Journal of the Acoustical Society of America* 106.4 (1999), pp. 2008–2021 (cit. on p. 19).

[37] Chan, R. W. and Titze, I. R. "Viscoelastic shear properties of human vocal fold mucosa: theoret-ical characterization based on constitutive modeling." In: *The Journal of the Acoustical Society of America* 107.1 (2000), pp. 565–580 (cit. on p. 19).

[38] Chan, R. W. *et al.* "Relative contributions of collagen and elastin to elasticity of the vocal fold under tension." In: *Annals of biomedical engineering* 35.8 (2007), pp. 1471–1483 (cit. on p. 19).

[39] Chan, R. W. and Rodriguez, M. L. "A simple-shear rheometer for linear viscoelastic characterization of vocal fold tissues at phonatory frequencies." In: *The Journal of the Acoustical Society of America* 124.2 (2008), pp. 1207–1219. DOI: 10.1121/1.2946715 (cit. on p. 18).

[40] Chan, R. W. *et al.* "Relative contributions of collagen and elastin to elasticity of the vocal fold under tension." In: *Annals of Biomedical Engineering* 35.8 (2007), pp. 1471–1483. DOI: 10.1007/s10439-007-9314-x (cit. on p. 91).

[41] Chhetri, D. K. *et al.* "Measurement of Young's modulus of vocal folds by indentation." In: *Journal of Voice* 25.1 (2011), pp. 1–7 (cit. on p. 21).

[42] Chilin, C. and Metters, A. "Hydrogels in controlled release formulations: Network design and mathematical modelling." In: *Adv. Drug Deliv. Rev* 58 (2006), pp. 1379–1408 (cit. on p. 74).

[43] Cochereau, T. *et al.* "Mechanics of human vocal folds layers during finite strains in tension, compression and shear." In: *Journal of Biomechanics* 110 (2020), p. 109956 (cit. on pp. 21, 22, 56–58, 62–64, 111).

[44] Cochereau, T. *et al.* "Mechanics of human vocal folds layers during finite strains in tension, compression and shear." In: *Journal of Biomechanics* 110 (2020). DOI: 10.1016/j.jbiomech.2020.109956 (cit. on pp. 86, 92, 101, 105).

[45] Dash, R. *et al.* "Improving the mechanical and thermal properties of gelatin hydrogels cross-linked by cellulose nanowhiskers." In: *Carbohydrate Polymers* 91.2 (2013), pp. 638–645. DOI: 10.1016/j.carbpol.2012.08.080 (cit. on pp. 53, 54).

[46] De Cheveigné, A. and Kawahara, H. "YIN, a fundamental frequency estimator for speech and music." In: *The Journal of the Acoustical Society of America* 111.4 (2002), pp. 1917–1930 (cit. on p. 115).

[47] Debret, R. *et al.* "Polypeptide derived from tropoelastin and biocompatible material comprising same." In: (2017) (cit. on p. 95).

[48] DeForest, C. and Anseth, K. "Advances in Bioactive Hydrogels to Probe and Direct Cell Fate." In: *Annual Review of Chemical and Biomolecular Engineering* 3.1 (2012), pp. 421–444 (cit. on p. 86).

[49] Deligkaris, K. *et al.* "Hydrogel-based devices for biomedical applications." In: *Sensors and Actuators B: Chemical* 147.2 (2010), pp. 765–774. DOI: 10.1016/j.snb.2010.03.083 (cit. on p. 86).

[50] Dion, G. R. *et al.* "Functional assessment of the ex vivo vocal folds through biomechanical testing: A review." In: *Materials Science and Engineering: C* 64 (2016), pp. 444–453 (cit. on p. 13).

[51] Döllinger, M. *et al.* "Assessment of local vocal fold deformation characteristics in an in vitro static tensile test." In: *The Journal of the Acoustical Society of America* 130.2 (2011), pp. 977–985 (cit. on p. 21).

[52] Doube, M. *et al.* "BoneJ: Free and extensible bone image analysis in ImageJ." In: *Bone* 47.6 (2010), pp. 1076–9 (cit. on p. 90).

[53] Drechsel, J. S. and Thomson, S. L. "Influence of supraglottal structures on the glottal jet exiting a two-layer synthetic, self-oscillating vocal fold model." In: *The Journal of the Acoustical Society of America* 123.6 (2008), pp. 4434–4445 (cit. on p. 30).

[54] Duconseille, A. *et al. Gelatin structure and composition linked to hard capsule dissolution: A review*. 2015. DOI: 10.1016/j.foodhyd.2014.06.006 (cit. on p. 53).

[55] Farris, S. *et al.* "Alternative reaction mechanism for the cross-linking of gelatin with glutaraldehyde." In: *Journal of Agricultural and Food Chemistry* 58.2 (2010), pp. 998–1003. DOI: 10.1021/jf9031603 (cit. on p. 53).

[56] Farris, S. *et al.* "Gelatin-pectin composite films from polyion-complex hydrogels." In: *Food Hydrocolloids* 25.1 (2011), pp. 61–70. DOI: 10.1016/j.foodhyd.2010.05.006 (cit. on pp. 54, 59).

[57] Feyen, D. A. M. *et al.* "Gelatin Microspheres as Vehicle for Cardiac Progenitor Cells Delivery to the Myocardium." In: *Advanced Healthcare Materials* 5.9 (2016), pp. 1071–1079. DOI: 10.1002/adhm.201500861 (cit. on p. 53).

[58] Finck, C. and Lejeune, L. "Structure and oscillatory function of the vocal folds." In: *Handbook of Behavioral Neuroscience*. Vol. 19. Elsevier, 2010, pp. 427–438 (cit. on p. 11).

[59] Finck, C. L. *et al.* "Implantation of esterified hyaluronic acid in microdissected Reinke's space after vocal fold microsurgery: Short- and long-term results." In: *Journal of Voice* 24.5 (2010), pp. 626–635. DOI: 10.1016/j.jvoice.2008.12.015 (cit. on p. 86).

[60] Finkelhor, B. K. *et al.* "The effect of viscosity changes in the vocal folds on the range of oscillation." In: *Journal of Voice* 1.4 (1988), pp. 320–325 (cit. on p. 22).

[61] Forte, A. *et al.* "Modelling and experimental characterisation of the rate dependent fracture properties of gelatine gels." In: *Food Hydrocolloids* 46 (2015), pp. 180–190. DOI: https://doi.org/10.1016/j.foodhyd.2014.12.028 (cit. on p. 62).

[62] Friedrich, G. *et al.* "Vocal fold scars: current concepts and future directions. Consensus report of the Phonosurgery Committee of the European Laryngological So-ciety." In: *European Archives of Oto-Rhino-Laryngology* 270.9 (2013), pp. 2491–2507 (cit. on p. 34).

[63] Gasperini, L. *et al. Natural polymers for the microencapsulation of cells. JR Soc In-terface 11 (100): 20140817.* 2014 (cit. on p. 32).

[64] Gasser, T. C. *et al.* "Hyperelastic modelling of arterial layers with distributed collagen fibre orientations." In: *Journal of the Royal Society, Interface / the Royal Society* 3.6 (2006), pp. 15–35 (cit. on p. 63).

[65] Gomes, S. R. *et al.* "In vitro and in vivo evaluation of electrospun nanofibers of PCL, chitosan and gelatin: A comparative study." In: *Materials Science and Engineering C* 46 (2015), pp. 348–358. DOI: 10.1016/j.msec.2014.10.051 (cit. on p. 53).

[66] Goodyer, E. *et al.* "The shear modulus of the human vocal fold, preliminary results from 20 larynxes." In: *European archives of oto-rhino-laryngology* 264.1 (2007), pp. 45–50 (cit. on pp. 2, 19).

[67] Goodyer, E. *et al.* "Devices and methods on analysis of biomechanical properties of laryngeal tissue and substitute materials." In: *Current Bioinformatics* 6.3 (2011), pp. 344–361. DOI: 10.2174/157489311796904718 (cit. on p. 91).

[68] Gorgieva, S. and Kokol, V. "Collagen- vs. Gelatine-Based Biomaterials and Their Biocompatibility: Review and Perspectives." In: *Biomaterials Applications for Nanomedicine* (2011). DOI: 10.5772/24118 (cit. on p. 53).

[69] Gray, S. D. *et al.* "Vocal fold proteoglycans and their influence on biomechanics." In: *The Laryngoscope* 109.6 (1999), pp. 845–854 (cit. on p. 12).

[70] Gray, S. D. *et al.* "Biomechanical and histologic observations of vocal fold fibrous proteins." In: *Annals of Otology, Rhinology & Laryngology* 109.1 (2000), pp. 77–85 (cit. on p. 14).

[71] Grenier, J. *et al.* "Mechanisms of pore formation in hydrogel scaffolds textured by freeze-drying." In: *Acta Biomaterialia* 94 (2019), pp. 195–203. DOI: https://doi.org/10.1016/j.actbio.2019.05.070 (cit. on p. 65).

[72] Griveau, L. *et al.* "Design and characterization of an in vivo injectable hydrogel with effervescently generated porosity for regenerative medicine applications." In: *Acta Biomaterialia* 140 (2022), pp. 324–337. DOI: 10.1016/j.actbio.2021.11.036 (cit. on p. 95).

[73] Gugatschka, M. *et al.* "Regenerative Medicine of the Larynx. Where are we Today? A Review." In: 26.5 (2012), pp. 7–670. DOI: 10.1016/j.jvoice.2012.03.009 (cit. on p. 86).

[74] Gunter, H. E. "Modeling mechanical stresses as a factor in the etiology of benign vocal fold lesions." In: *Journal of Biomechanics* 37.7 (2004), pp. 1119–1124. DOI: 10.1016/j.jbiomech.2003.11.007 (cit. on p. 92).

[75] Gupta, S. *et al.* "Ice-Templated Porous Nanocellulose-Based Materials: Current Progress and Opportunities for Materials Engineering." In: *Applied Sciences* 8.12 (2018). DOI: 10.3390/app8122463 (cit. on p. 65).

[76] Hahn, M. S. *et al.* "Quantitative and comparative studies of the vocal fold extracellular matrix I: elastic fibers and hyaluronic acid." In: *Annals of Otology, Rhinology & Laryngology* 115.2 (2006), pp. 156–164 (cit. on p. 15).

[77] Hahn, M. S. *et al.* "Quantitative and comparative studies of the vocal fold extracellular matrix I: elastic fibers and hyaluronic acid." In: *Annals of Otology, Rhinology and Laryngology* 115.2 (2006), pp. 156–164. DOI: 10.1177/000348940611500213 (cit. on p. 13).

[78] Hahn, M. S. *et al.* "Quantitative and comparative studies of the vocal fold extracellular matrix II: collagen." In: *Annals of Otology, Rhinology and Laryngology* 115.3 (2006), pp. 225–232. DOI: 10.1177/000348940611500311 (cit. on p. 13).

[79] Hammond, T. H. and Gray, S. D. "A study of age-and gender-related elastin distribution changes in human vocal folds." In: *Otolaryngology–Head and Neck Surgery* 117.2 (1997), P100–P100 (cit. on p. 13).

[80] Hammond, T. H. *et al.* "The intermediate layer: a morphologic study of the elastin and hy-aluronic acid constituents of normal human vocal folds." In: *Journal of Voice* 11.1 (1997), pp. 59–66 (cit. on p. 15).

[81] Hammond, T. H. *et al.* "Age-and gender-related collagen distribution in human vocal folds." In: *Annals of Otology, Rhinology & Laryngology* 109.10 (2000), pp. 913–920 (cit. on p. 13).

[82] Hansen, J. K. *et al.* "In vivo engineering of the vocal fold extracellular matrix with injectable hyaluronic acid hydrogels: early effects on tissue repair and biomechanics in a rabbit model." In: *Annals of Otology, Rhinology & Laryngology* 114.9 (2005), pp. 662–670 (cit. on p. 35).

[83] Hantzakos, A. *et al.* "Exudative lesions of Reinke's space: A terminology proposal." In: *European Archives of Oto-Rhino-Laryngology* 266.6 (2009), pp. 869–878. DOI: 10.1007/s00405-008-0863-x (cit. on pp. 86, 102).

[84] Hemler, R. J. *et al.* "Laryngeal mucosa elasticity and viscosity in high and low relative air humidity." In: *European archives of oto-rhino-laryngology* 258.3 (2001), pp. 125–129 (cit. on p. 23).

[85] Hennink, W. E. and Nostrum, C. F. van. "Novel crosslinking methods to design hydrogels." In: *Advanced drug delivery reviews* 64 (2012), pp. 223–236 (cit. on p. 33).

[86] Henri, C. *Device for deflecting a stream of elastic fluid projected into an elastic fluid*. US Patent 2,052,869. 1936 (cit. on p. 30).

[87] Heris, H. K. *et al.* "Investigation of chitosan-glycol/glyoxal as an injectable biomaterial for vocal fold tissue engineering." In: *Procedia Engineering* 110 (2015), pp. 143–150 (cit. on p. 35).

[88] Heris, H. K. *et al.* "Investigation of the viability, adhesion, and migration of human fibroblasts in a hyaluronic acid/gelatin microgel-reinforced composite hy-drogel for vocal fold tissue regeneration." In: *Advanced healthcare materials* 5.2 (2016), pp. 255–265 (cit. on p. 35).

[89] Heris, H. K. *et al.* "Characterization of a Hierarchical Network of Hyaluronic Acid/Gelatin Composite for use as a Smart Injectable Biomaterial." In: *Macromolecular Bioscience* 12.2 (2012), pp. 202–210. DOI: 10.1002/mabi.201100335 (cit. on p. 53).

[90] Heris, H. K. *et al.* "Investigation of the Viability, Adhesion, and Migration of Human Fibroblasts in a Hyaluronic Acid/Gelatin Microgel-Reinforced Composite Hydrogel for Vocal Fold Tissue Regeneration." In: *Advanced Healthcare Materials* 5.2 (2016), pp. 255–265. DOI: 10.1002/adhm.201500370 (cit. on p. 53).

[91] Hirano, M. "Morphological structure of the vocal cord as a vibrator and its variations." In: *Folia phoniatrica et logopaedica* 26.2 (1974), pp. 89–94 (cit. on p. 12).

[92] Hirano, M. "Morphological structure of the vocal cord as a vibrator and its variations." In: *Folia Phoniatrica et Logopaedica* 26.2 (1974), pp. 89–94. DOI: 10.1159/000263771 (cit. on p. 86).

[93] Hirano, M. "Structure of the vocal fold in normal and disease states: anatomical and physical studies." In: *ASHA Rep* 11 (1981), pp. 11–30 (cit. on p. 11).

[94] Hirano, M. *et al.* "Structure and mechanical properties of the vocal fold." In: *Speech and language*. Vol. 7. Elsevier, 1982, pp. 271–297 (cit. on p. 12).

[95] Hiwatashi, N. *et al.* "The efficacy of a novel collagen-gelatin scaffold with basic fibroblast growth factor for the treatment of vocal fold scar." In: *J Tissue Eng Regen Med*. 11.5 (2017), pp. 1598–1609 (cit. on p. 53).

[96] Hiwatashi, N. *et al.* "Biocompatibility and Efficacy of Collagen/Gelatin Sponge Scaffold With Sustained Release of Basic Fibroblast Growth Factor on Vocal Fold Fibroblasts in 3-Dimensional Culture." In: *Annals of Otology, Rhinology & Laryngology* 124.2 (2015), pp. 116–125. DOI: 10.1177/0003489414546396 (cit. on p. 53).

[97] Hoffman, A. S. "Hydrogels for biomedical applications." In: *Advanced Drug Delivery Reviews* 54.1 (2002), pp. 3–12. DOI: 10.1016/S0169-409X(01)00239-3 (cit. on p. 53).

[98] Hoffman, A. S. "Hydrogels for biomedical applications." In: *Advanced Drug Delivery Reviews* 64 (2012), pp. 18–23. DOI: 10.1016/j.addr.2012.09.010 (cit. on p. 86).

[99] Hotaling, N. A. *et al.* "DiameterJ: A validated open source nanofiber diameter measurement tool." In: *Biomaterials* 61 (2015), pp. 327–38 (cit. on p. 90).

[100] Hsiao, T.-Y. *et al.* "Elasticity of human vocal folds measured in vivo using color Dop-pler imaging." In: *Ultrasound in medicine & biology* 28.9 (2002), pp. 1145–1152 (cit. on pp. 17, 18).

[101] Huang, D. *et al.* "Viscoelasticity in natural tissues and engineered scaffolds for tissue reconstruction." In: *Acta Biomaterialia* 97 (2019), pp. 74–92. DOI: https://doi.org/10.1016/j.actbio.2019.08.013 (cit. on p. 62).

[102] Hughes, L. A. *et al.* "Electrospun fiber constructs for vocal fold tissue engineering: Effects of alignment and elastomeric polypeptide coating." In: *Acta Biomaterialia* 13 (2015), pp. 111–120. DOI: 10.1016/j.actbio.2014.10.039 (cit. on p. 87).

[103] Husson, R. Physiologie de la phonation. *Masson*, 1962 (cit. on p. 25).

[104] Imaizumi, M. *et al.* "Regenerative potential of basic fibroblast growth factor contained in biodegradable gelatin hydrogel microspheres applied following vocal fold injury: Early effect on tissue repair in a rabbit model." In: *Brazilian Journal of Otorhinolaryngology* 87.3 (2021), pp. 274–282. DOI: 10.1016/j.bjorl.2019.09.003 (cit. on pp. 53, 86).

[105] Imani, R. *et al.* "Synthesis and characterization of glutaraldehyde-based crosslinked gelatin as a local hemostat sponge in surgery: an in vitro study." In: *Bio-medical materials and engineering* 23.3 (2013), pp. 211–224. DOI: 10.3233/bme-130745 (cit. on p. 53).

[106] Jang, J. *et al.* "Improving mechanical properties of alginate hydrogel by reinforcement with ethanol treated polycaprolactone nanofibers." In: *Composites Part B: Engineering* 45.1 (2013), pp. 1216–1221 (cit. on p. 101).

[107] Jiang, W. *et al.* "Influence of vocal fold cover layer thickness on its vibratory dynamics during voice production." In: *The Journal of the Acoustical Society of America* 146.1 (2019), pp. 369–380. DOI: 10.1121/1.5116567 (cit. on p. 86).

[108] Jing, X. *et al.* "Stretchable gelatin/silver nanowires composite hydrogels for detecting human motion." In: *Materials Letters* 237 (2019), pp. 53–56 (cit. on p. 34).

[109] Karajanagi, S. S. *et al.* "Assessment of canine vocal fold function after injection of a new biomaterial designed to treat phonatory mucosal scarring." In: *Annals of Otology, Rhinology and Laryngology* 120.3 (2011), pp. 175–184. DOI: 10.1177/000348941112000306 (cit. on p. 86).

[110] Kazemirad, S. *et al.* "Non-invasive in vivo measurement of the shear modulus of human vo-cal fold tissue." In: *Journal of Biomechanics* 47.5 (2014), pp. 1173–1179 (cit. on p. 18).

[111] Kazemirad, S. *et al.* "Viscoelasticity of hyaluronic acid-gelatin hydrogels for vocal fold tissue engineering." In: *Journal of Biomedical Materials Research Part B: Applied Bio-materials* 104.2 (2016), pp. 283–290 (cit. on p. 35).

[112] Kazemirad, S. *et al.* "Viscoelasticity of hyaluronic acid-gelatin hydrogels for vocal fold tissue engineering." In: *Journal of Biomedical Materials Research Part B: Applied Biomaterials* 104.2 (2016), pp. 283–290. DOI: 10.1002/jbm.b.33358 (cit. on p. 53).

[113] Kelleher, J. E. *et al.* "Spatially varying properties of the vocal ligament contribute to its eigenfrequency response." In: *Journal of the Mechanical Behavior of Biomedical Materials* 3.8 (2010), pp. 600–609. DOI: 10.1016/J.JMBBM.2010.07.009 (cit. on p. 91).

[114] Kelleher, J. E. *et al.* "The anisotropic hyperelastic biomechanical response of the vocal ligament and implications for frequency regulation: A case study." In: *The Journal of the Acoustical Society of America* 133.3 (2013), pp. 1625–36 (cit. on pp. 63, 111, 125).

[115] Kelleher, J. E. *et al.* "The anisotropic hyperelastic biomechanical response of the vocal ligament and implications for frequency regulation: a case study." In: *The Journal of the Acoustical Society of America* 133.3 (2013), pp. 1625–1636. DOI: 10.1121/1.4776204 (cit. on p. 91).

[116] Kishan, A. P. *et al.* "In situ crosslinking of electrospun gelatin for improved fiber morphology retention and tunable degradation." In: *Journal of Materials Chemistry B* 3.40 (2015), pp. 7930–7938. DOI: 10.1039/c5tb00937e (cit. on p. 53).

[117] Kist, A. M. *et al.* "A Deep Learning Enhanced Novel Software Tool for Laryngeal Dynamics Analysis." In: *Journal of Speech, Language, and Hearing Research* 64.6 (2021). Publisher: American Speech-Language-Hearing Association, pp. 1889–1903. DOI: 10.1044/2021_JSLHR-20-00498. (Visited on 10/05/2022) (cit. on p. 115).

[118] Kniesburges, S. *et al.* "In Vitro Experimental Investigation of Voice Production." en. In: *Current Bioinformatics* 6.3 (2011), pp. 305–322. DOI: 10.2174/157489311796904637. (Visited on 09/21/2022) (cit. on p. 110).

[119] Kniesburges, S. *et al.* Modeling the pre-phonatory vocal fold posture in the larynx model SynthVOICE. *Universitätsbibliothek der RWTH Aachen*, 2019 (cit. on p. 110).

[120] Kumar, R. and Sagar, P. "Surgical Anatomy and Tumour Spread in the Larynx and Hypopharynx." In: *Carcinoma of the Larynx and Hypopharynx* (2019) (cit. on p. 83).

[121] Kutty, J. K. and Webb, K. "Vibration stimulates vocal mucosa-like matrix expression by hydro-gel-encapsulated fibroblasts." In: *Journal of tissue engineering and regenerative medicine* 4.1 (2010), pp. 62–72 (cit. on p. 36).

[122] Kutty, J. K. and Webb, K. "Tissue Engineering Therapies for the Vocal Fold Lamina Propria." In: *Tissue Engineering - Part B: Reviews* 15.3 (2009), pp. 249–262. DOI: 10.1089/ten.teb.2008.0588 (cit. on p. 86).

[123] Kwon, J. and Subhash, G. "Compressive strain rate sensitivity of ballistic gelatin." In: *Journal of Biomechanics* 43.3 (2010), pp. 420–425. DOI: 10.1016/j.jbiomech.2009.10.008 (cit. on pp. 54, 62).

[124] Latifi, N. *et al.* "A flow perfusion bioreactor system for vocal fold tissue engineer-ing applications." In: *Tissue Engineering Part C: Methods* 22.9 (2016), pp. 823–838 (cit. on pp. 37, 73).

[125] Latifi, N. *et al.* "A tissue-mimetic nano-fibrillar hybrid injectable hydrogel for potential soft tissue engineering applications." In: *Scientific reports* 8.1 (2018), pp. 1–18 (cit. on pp. 35, 36).

[126] Latifi, N. *et al.* "A tissue-mimetic nano-fibrillar hybrid injectable hydrogel for potential soft tissue engineering applications." En. In: *Scientific Reports* 8.1 (2018), p. 1047. DOI: 10.1038/s41598-017-18523-3. (Visited on 01/24/2019) (cit. on pp. 53, 87).

[127] Laurent, T. C. *et al.* "Functions of hyaluronan." In: *Annals of the rheumatic diseases* 54.5 (1995), p. 429 (cit. on p. 13).

[128] Lee, K. and Mooney, D. "Hydrogels for Tissue Engineering." In: *Chemical Reviews* 101.7 (2001), pp. 1869–1880. DOI: 10.1021/cr000108x (cit. on p. 86).

[129] Lee, K. Y. and Mooney, D. J. *Hydrogels for tissue engineering*. 2001. DOI: 10.1021/cr000108x (cit. on p. 53).

[130] Lehoux, H. *et al.* "Subglottal pressure oscillations in anechoic and resonant conditions and their influence on excised larynx phonations." In: *Scientific reports* 11.1 (2021), pp. 1–14 (cit. on p. 126).

[131] Li, L. *et al.* "Tissue engineering-based therapeutic strategies for vocal fold repair and regeneration." In: *Biomaterials* 108 (2016), pp. 91–110 (cit. on p. 86).

[132] Liao, Z. *et al.* "Temperature and strain rate dependent large tensile deformation and tensile failure behavior of transparent polyurethane at intermediate strain rates." In: *International Journal of Impact Engineering* 129 (2019), pp. 152–167 (cit. on p. 80).

[133] Liao, Z. *et al.* "A comprehensive thermo-viscoelastic experimental investigation of Ecoflex polymer." In: *Polymer Testing* 86 (2020), p. 106478. DOI: https://doi.org/10.1016/j.polymertesting.2020.106478 (cit. on p. 58).

[134] Liao, Z. *et al.* "A comprehensive thermo-viscoelastic experimental investigation of Ecoflex polymer." In: *Polymer Testing* 86 (2020), p. 106478 (cit. on p. 80).

[135] Ling, C. *et al.* "Bioengineered vocal fold mucosa for voice restoration." In: *Science Translational Medicine* 7.314 (2015), 314ra187. DOI: 10.1126/scitranslmed.aab4014 (cit. on p. 86).

[136] Long, J. L. and Chhetri, D. K. "Restoring voice: Engineered vocal cords could soon replace damage damaged tissue." In: *Science* 350.6263 (2015), pp. 908–909. DOI: 10.1126/science.aad7695 (cit. on p. 86).

[137] Lucero, J. C. *et al.* "Effect of source-tract acoustical coupling on the oscillation onset of the vocal folds." In: *Journal of the Acoustical Society of America* 132.1 (2012), pp. 403–411. DOI: 10.1121/1.4728170 (cit. on p. 86).

[138] Luizard, P. and Pelorson, X. "Threshold of oscillation of a vocal fold replica with unilateral surface growths." In: *Journal of the Acoustical Society of America* 141.5 (2017), pp. 3050–3058 (cit. on p. 110).

[139] Lutz, J.-F. *et al.* "Point by point comparison of two thermosensitive polymers exhibiting a similar LCST: is the age of poly (NIPAM) over?" In: *Journal of the American Chemical Society* 128.40 (2006), pp. 13046–13047 (cit. on p. 33).

[140] Ma, P. and Elisseeff, J. Scaffolding in tissue engineering. Great Britain: *CRC Press*, 2005 (cit. on p. 91).

[141] Marmorat, C. *et al.* "Cryo-Imaging of Hydrogels Supermolecular Structure." In: *Scientific Reports* 6 (2016), p. 25495 (cit. on p. 65).

[142] Martoia, F. *et al.* "On the origins of the elasticity of cellulose nanofiber nanocomposites and nanopapers: a micromechanical approach." In: *RSC Adv.* 6 (53 2016), pp. 47258–47271 (cit. on pp. 65, 101).

[143] Mendelsohn, A. H. and Zhang, Z. "Phonation threshold pressure and onset frequency in a two-layer physical model of the vocal folds." In: *The Journal of the Acoustical Society of America* 130.5 (2011), pp. 2961–2968 (cit. on pp. 73, 122).

[144] Michelini, L. *et al.* "Characterization of gelatin hydrogels derived from different animal sources." In: *Materials Letters* 272 (2020), p. 127865. DOI: 10.1016/j.matlet.2020.127865 (cit. on pp. 53, 60).

[145] Min, Y. B. *et al.* "Stress-Strain Response of the Human Vocal Ligament." In: *Annals of Otology, Rhinology & Laryngology* 104.7 (1995), pp. 563–569. DOI: 10.1177/000348949510400711 (cit. on p. 63).

[146] Miri, A. K. "Mechanical characterization of vocal fold tissue: a review study." In: *Journal of Voice* 28.6 (2014), pp. 657–667 (cit. on pp. 13, 16, 21).

[147] Miri, A. K. *et al.* "Effects of dehydration on the viscoelastic properties of vocal folds in large deformations." In: *Journal of Voice* 26.6 (2012), pp. 688–697 (cit. on pp. 2, 19, 23, 24, 34).

[148] Miri, A. K. *et al.* "Nonlinear laser scanning microscopy of human vocal folds." In: *The Laryngoscope* 122.2 (2012), pp. 356–363 (cit. on pp. 13, 14).

[149] Miri, A. K. *et al.* "Quantitative assessment of the anisotropy of vocal fold tissue us-ing shear rheometry and traction testing." In: *Journal of biomechanics* 45.16 (2012), pp. 2943–2946 (cit. on p. 19).

[150] Miri, A. K. "Mechanical characterization of vocal fold tissue: a review study." In: *Journal of Voice* 28.6 (2014), pp. 657–667. DOI: 10.1016/j.jvoice.2014.03.001 (cit. on p. 86).

[151] Miri, A. K. *et al.* "Effects of dehydration on the viscoelastic properties of vocal folds in large deformations." In: *Journal of Voice* 26.6 (2012), pp. 688–697. DOI: 10.1016/j.jvoice.2011.09.003 (cit. on p. 86).

[152] Miri, A. K. *et al.* "Nonlinear laser scanning microscopy of human vocal folds." In: *The Laryngoscope* 122.2 (2012), pp. 356–363. DOI: 10.1002/lary.22460 (cit. on pp. 92, 94).

[153] Miri, A. K. *et al.* "Microstructural characterization of vocal folds toward a strain-energy model of collagen remodeling." In: *Acta Biomaterialia* 9.8 (2013), pp. 7957–7967 (cit. on pp. 13, 15, 63).

[154] Mittal, R. *et al.* "Fluid dynamics of human phonation and speech." In: *Annual review of fluid mechanics* (2013), pp. 437–467 (cit. on p. 2).

[155] Mochane, M. *et al.* "Morphology and Properties of Electrospun PCL and Its Composites for Medical Applications: A Mini Review." In: *Applied Sciences* 9.11 (2019). DOI: 10.3390/app9112205 (cit. on p. 94).

[156] Mohammed, M. G. and Kramer, R. "All-printed flexible and stretchable electronics." In: *Advanced Materials* 29.19 (2017), p. 1604965 (cit. on p. 74).

[157] Mojsiewicz-Pieńkowska, K. Review of current pharmaceutical applications of polysiloxanes (Silicones). *Scrivener Publishing LLC Beverly, MA, USA*, 2015 (cit. on p. 74).

[158] Mudiyanselage, T. K. and Neckers, D. C. "Highly absorbing superabsorbent polymer." In: *Journal of Polymer Science Part A: Polymer Chemistry* 46.4 (2008), pp. 1357–1364. DOI: 10.1002/pola.22476 (cit. on p. 53).

[159] Mullins, L. and Tobin, N. "Stress softenings in natural rubber vulcanizates, Part IJ Appl." In: *Polym. Sci* 9 (1965), pp. 2993–3010 (cit. on p. 80).

[160] Mullins, L. "Effect of stretching on the properties of rubber." In: *Rubber chemistry and technology* 21.2 (1948), pp. 281–300 (cit. on p. 80).

[161] Muneer, F. and Manzoor, T. "EFFECTIVENESS OF VOICE THERAPY IN DYSPHONIA: A SPEECH-PATHOLOGIST PERSPECTIVE." In: () (cit. on p. 10).

[162] Murray, P. R. and Thomson, S. L. "Vibratory responses of synthetic, self-oscillating vocal fold mod-els." In: *The Journal of the Acoustical Society of America* 132.5 (2012), pp. 3428–3438 (cit. on p. 31).

[163] Murthy, P. "Phonosurgery: A new subspeciality in otolaryngology." In: *NTR University of Health Sciences* 1.7 (2012) (cit. on p. 83).

[164] Nakamura, K. *et al.* "The influence of compression velocity on strength and structure for gellan gels." In: *Food Hydrocolloids* 15.3 (2001), pp. 247–252. DOI: https://doi.org/10.1016/S0268-005X(01)00021-2 (cit. on p. 62).

[165] Nasri, S. *et al.* "Noninvasive measurement of traveling wave velocity in the canine larynx." In: *Annals of Otology, Rhinology & Laryngology* 103.10 (1994), pp. 758–766 (cit. on p. 17).

[166] Nur Hanani, Z. A. *et al.* "Use and application of gelatin as potential biodegradable packaging materials for food products." In: *International Journal of Biological Macromolecules* 71 (2014), pp. 94–102. DOI: 10.1016/j.ijbiomac.2014.04.027 (cit. on p. 53).

[167] Owaki, S. *et al.* "Relationship between transglottal pressure and fundamental frequency of phonation—study using a rubber model." In: *Journal of Voice* 24.2 (2010), pp. 127–132 (cit. on p. 29).

[168] Oyen, M. L. "Mechanical characterisation of hydrogel materials." In: *International Materials Reviews* 59.1 (2014), pp. 44–59 (cit. on pp. 97, 99).

[169] Panzavolta, S. *et al.* "Electrospun gelatin nanofibers: Optimization of genipin crosslinking to preserve fiber morphology after exposure to water." In: *Acta Biomaterialia* 7.4 (2011), pp. 1702–1709. DOI: 10.1016/j.actbio.2010.11.021 (cit. on p. 53).

[170] Park, S. *et al.* "Silicones for stretchable and durable soft devices: Beyond Sylgard-184." In: *ACS applied materials & interfaces* 10.13 (2018), pp. 11261–11268 (cit. on p. 74).

[171] Peppas, N. A. *et al.* "Hydrogels in pharmaceutical formulations." In: *European journal of pharmaceutics and biopharmaceutics* 50.1 (2000), pp. 27–46 (cit. on p. 74).

[172] Perlman, A. L. *et al.* "Elasticity of canine vocal fold tissue." In: *Journal of Speech, Language, and Hearing Research* 27.2 (1984), pp. 212–219 (cit. on p. 19).

[173] Pershall, K. E. and Boone, D. R. "Supraglottic contribution to voice quality." In: *Journal of Voice* 1.2 (1987), pp. 186–190 (cit. on p. 25).

[174] Pickup, B. A. and Thomson, S. L. "Influence of asymmetric stiffness on the structural and aerodynamic response of synthetic vocal fold models." In: *Journal of biomechanics* 42.14 (2009), pp. 2219–2225 (cit. on p. 30).

[175] Pickup, B. A. and Thomson, S. L. "Flow-induced vibratory response of idealized versus magnetic resonance imaging-based synthetic vocal fold models." In: *The Journal of the Acoustical Society of America* 128.3 (2010), EL124–EL129 (cit. on p. 30).

[176] Piollet, E. *et al.* "Dynamic hysteresis modelling of entangled cross-linked fibres in shear." In: *Journal of Sound and Vibration* 383 (2016), pp. 248–264. DOI: https://doi.org/10.1016/j.jsv.2016.06.023 (cit. on p. 58).

[177] Portier, F. *et al.* "Stabilization of Collagen Fibrils by Gelatin Addition: A Study of Collagen/Gelatin Dense Phases." In: *Langmuir* 33.45 (2017), pp. 12916–12925. DOI: 10.1021/acs.langmuir.7b02142 (cit. on p. 55).

[178] Poursamar, S. A. *et al.* "Gelatin porous scaffolds fabricated using a modified gas foaming technique: Characterisation and cytotoxicity assessment." In: *Materials Science and Engineering C* 48 (2015), pp. 63–70. DOI: 10.1016/j.msec.2014.10.074 (cit. on pp. 53, 54).

[179] Poursamar, S. A. *et al.* "The effects of crosslinkers on physical, mechanical, and cytotoxic properties of gelatin sponge prepared via in-situ gas foaming method as a tissue engineering scaffold." In: *Materials Science and Engineering C* 63 (2016), pp. 1–9. DOI: 10.1016/j.msec.2016.02.034 (cit. on pp. 53, 54).

[180] Püspöki, Z. *et al.* "Transforms and Operators for Directional Bioimage Analysis: A Survey." In: *Focus on Bio-Image Informatics*. Ed. by W. De Vos *et al.* Vol. 219. Advances in Anatomy, Embryology and Cell Biology. Springer International Publishing, 2016. Chap. 3, pp. 69–93 (cit. on p. 90).

[181] Ratanavaraporn, J. *et al.* "Influences of physical and chemical crosslinking techniques on electrospun type A and B gelatin fiber mats." In: *International Journal of Biological Macromolecules* 47.4 (2010), pp. 431–438. DOI: 10.1016/j.ijbiomac.2010.06.008 (cit. on p. 53).

[182] Ravanbakhsh, H. *et al.* "Carbon nanotube composite hydrogels for vocal fold tissue engineering: Biocompatibility, rheology, and porosity." In: *Materials Science and Engineering C* 103 (2019), p. 109861. DOI: 10.1016/j.msec.2019.109861 (cit. on p. 53).

[183] Riede, T. *et al.* "Mammalian laryngseal air sacs add variability to the vocal tract impedance: Physical and computational modeling." In: *The Journal of the Acoustical Society of America* 124.1 (2008), pp. 634–647 (cit. on p. 30).

[184] Romero, R. G. *et al.* "3D-printed synthetic vocal fold models." In: *Journal of Voice* 35.5 (2021), pp. 685–694 (cit. on p. 31).

[185] Rousseau, B. *et al.* "Characterization of vocal fold scarring in a canine model." In: *The Laryngoscope* 113.4 (2003), pp. 620–627 (cit. on p. 34).

[186] Roy, N. *et al.* "Voice disorders in the general population: prevalence, risk factors, and occupational impact." In: *The Laryngoscope* 115.11 (2005), pp. 1988–1995 (cit. on p. 2).

[187] Rubinstein, M. and Colby, R. Polymer physics. *Oxford Univ. Press*, 2003 (cit. on p. 91).

[188] Ruty, N. *et al.* "An in vitro setup to test the relevance and the accuracy of low-order vocal folds models." In: *Journal of the Acoustical Society of America* 121.1 (2007), pp. 479–490 (cit. on pp. 110, 111).

[189] Ruty, N. *et al.* "A mechanical experimental setup to simulate vocal folds vibra-tions. Preliminary results." In: *arXiv preprint arXiv:0710.4286* (2007) (cit. on pp. 28, 29).

[190] Scherer, R. C. *et al.* "Intraglottal pressure profiles for a symmetric and oblique glottis with a divergence angle of 10 degrees." In: *The Journal of the Acoustical Society of America* 109.4 (2001), pp. 1616–1630 (cit. on p. 29).

[191] Schultz, P. "Vocal fold cancer." In: *European Annals of Otorhinolaryngology, Head and Neck Diseases* 128.6 (2011), pp. 301–308. DOI: 10.1016/j.anorl.2011.04.004 (cit. on p. 86).

[192] Schweller, R. M. and West, J. L. "Encoding hydrogel mechanics via network cross-linking structure." In: *ACS biomaterials science & engineering* 1.5 (2015), pp. 335–344 (cit. on p. 74).

[193] Seliktar, D. "Designing cell-compatible hydrogels for biomedical applications." In: *Science* 336.6085 (2012), pp. 1124–1128. DOI: 10.1126/science.1214804 (cit. on p. 53).

[194] Sharma, S. and Bhattacharya, S. "Strain and strain rate dependence of gellan, agar and agar–gellan gels as model systems." In: *Journal of Food Engineering* 141 (2014), pp. 93–98. DOI: https://doi.org/10.1016/j.jfoodeng.2014.05.001 (cit. on p. 62).

[195] Shaw, S. M. *et al.* "Frequency response of synthetic vocal fold models with linear and nonlinear material properties." In: (2012) (cit. on pp. 73, 110).

[196] Silva, F. *et al.* "Contact Pressure Between the Vocal Folds in Reinke's Edema: Experimental Observations on an Excised Human Larynx." In: *Journal of Voice* 35.6 (2021), 931.e15–931.e20. DOI: 0.1016/j.jvoice.2020.02.020 (cit. on p. 102).

[197] Sloan, S. H. *et al.* "Effect of asymmetric vocal fold stiffness on traveling wave veloc-ity in the canine larynx." In: *Otolaryngology—Head and Neck Surgery* 107.4 (1992), pp. 516–526 (cit. on p. 17).

[198] Sohier, J. *et al.* "Novel and simple alternative to create nanofibrillar matrices of interest for tissue engineering." In: *Tissue Eng Part C Methods* 20.4 (2014), pp. 285–96 (cit. on pp. 87, 88, 94).

[199] Sohier, J. *et al.* "The potential of anisotropic matrices as substrate for heart valve engineering." In: *Biomaterials* 35.6 (2014), pp. 1833–44 (cit. on pp. 87, 88).

[200] Stojanović, S. and Belić, B. "Laryngeal manifestations of rheumatoid arthritis." In: *Innovative Rheumatology* (2013), p. 215 (cit. on p. 10).

[201] Subramanian, K. and Vijayakumar, V. "Evaluation of isophorone diisocyanate crosslinked gelatin as a carrier for controlled delivery of drugs." In: *Polymer Bulletin* 70.3 (2013), pp. 733–753. DOI: 10.1007/s00289-012-0821-z (cit. on p. 53).

[202] Sun, S. *et al.* "A review on mechanical properties of pressure sensitive adhesives." In: *International Journal of Adhesion and Adhesives* 41 (2013), pp. 98–106 (cit. on p. 74).

[203] Sundberg, J. "The human voice." In: *Comprehensive human physiology*. Springer, 1996, pp. 1095–1104 (cit. on p. 25).

[204] Sundberg, J. The science of the singing voice. *Northern Illinois University Press*, 1987 (cit. on p. 10).

[205] Švec, J. G. *et al.* "Resonance properties of the vocal folds: In vivo laryngoscopic investigation of the externally excited laryngeal vibrations." In: *The Journal of the Acoustical Society of America* 108.4 (2000), pp. 1397–1407 (cit. on p. 26).

[206] Tanaka, S. and Hirano, M. "Fiberscopic estimation of vocal fold stiffness in vivo using the sucking method." In: *Archives of Otolaryngology–Head & Neck Surgery* 116.6 (1990), pp. 721–724 (cit. on p. 17).

[207] Tateya, T. *et al.* "Collagen subtypes in human vocal folds." In: *Annals of Otology, Rhinology and Laryngology* 115.6 (2006), pp. 469–476. DOI: 10.1177/000348940611500612 (cit. on p. 13).

[208] Temenoff, J. *et al.* "Effect of polyethylene glycol molecular weight on tensile and swelling properties of oligopolyethylene glycol fumarate hydrogels for cartilage tissue engineering." In: *J Biomed Mater Res* 59.3 (2002), pp. 429–37 (cit. on p. 97).

[209] Teratsubo, M. *et al.* "Measurement of stress and strain during tensile testing of gellan gum gels: effect of deformation speed." In: *Carbohydrate Polymers* 47.1 (2002), pp. 1–5. DOI: https://doi.org/10.1016/S0144-8617(00)00338-6 (cit. on p. 62).

[210] Terzolo, A. *et al.* "A micro-mechanical model for the fibrous tissues of vocal folds." In: *Journal of the Mechanical Behavior of Biomedical Materials* 128 (2022), p. 105118. DOI: 10.1016/j.jmbbm.2022.105118 (cit. on pp. 12, 15, 63, 65, 98, 100, 102, 111, 125).

[211] Thibeault, S. L. *et al.* "In vivo engineering of the vocal fold ECM with injectable HA hy-drogels—late effects on tissue repair and biomechanics in a rabbit model." In: *Journal of voice* 25.2 (2011), pp. 249–253 (cit. on p. 35).

[212] Thompson, L. D. "Larynx." In: *Modern Surgical Pathology*. Elsevier, 2009, pp. 208–245 (cit. on p. 25).

[213] Thomson, S. L. *et al.* "Aerodynamic transfer of energy to the vocal folds." In: *The Journal of the Acoustical Society of America* 118.3 (2005), pp. 1689–1700 (cit. on pp. 25, 29).

[214] Titze, I. Principles of voice production. 2nd. Iowa, USA: *National Center for VoiceSpeech*, 2000 (cit. on p. 86).

[215] Titze, I. R. "The physics of small-amplitude oscillation of the vocal folds." In: *The Journal of the Acoustical Society of America* 83.4 (1988), pp. 1536–1552 (cit. on p. 25).

[216] Titze, I. R. "Mechanical stress in phonation." In: *Journal of Voice* 8.2 (1994), pp. 99–105 (cit. on p. 16).

[217] Titze, I. R. and Martin, D. W. *Principles of voice production*. 1998 (cit. on p. 2).

[218] Titze, I. R. and Strong, W. J. "Normal modes in vocal cord tissues." In: *The Journal of the Acoustical Society of America* 57.3 (1975), pp. 736–744 (cit. on p. 26).

[219] Titze, I. R. "The physics of small-amplitude oscillation of the vocal folds." In: *The Journal of the Acoustical Society of America* 83.4 (1988). Publisher: Acoustical Society of America, pp. 1536–1552. DOI: 10.1121/1.395910. (Visited on 09/21/2022) (cit. on p. 110).

[220] Titze, I. R. Principles of Voice Production. *Prentice-Hall*, 1994 (cit. on p. 10).

[221] Titze, I. and Martin, D. "Principles of voice production Prentice Hall." In: *Englewood Cliffs, NJ* (1994) (cit. on p. 12).

[222] Tonsomboom, K. *et al.* "Strong and tough nanofibrous hydrogel composites based on biomimetic principles." In: *Materials Science and Engineering C* 72 (2017), pp. 220–227. DOI: 10.1016/j.msec.2016.11.025 (cit. on pp. 97, 100).

[223] Tran, Q. T. *et al.* "Measurement of Young's modulus in the in vivo human vocal folds." In: *Annals of Otology, Rhinology & Laryngology* 102.8 (1993), pp. 584–591 (cit. on pp. 17, 18).

[224] Triep, M. and Brücker, C. "Three-dimensional nature of the glottal jet." In: *The Journal of the Acoustical Society of America* 127.3 (2010), pp. 1537–1547 (cit. on p. 28).

[225] Unal, B. and Hedden, R. C. "Gelation and swelling behavior of end-linked hydrogels prepared from linear polyethylene glycol and polyamidoamine dendrimers." In: *Polymer* 47.24 (2006), pp. 8173–8182. DOI: 10.1016/j.polymer.2006.09.048 (cit. on p. 97).

[226] Vampola, T. *et al.* "Computer simulation of mucosal waves on vibrating human vocal folds." In: *Biocybernetics and Biomedical Engineering* 36.3 (2016), pp. 451–465. DOI: 10.1016/j.bbe.2016.03.004 (cit. on pp. 21, 22, 86).

[227] Van den Berg, J. "Myoelastic-aerodynamic theory of voice production." In: *Journal of speech and hearing research* 1.3 (1958). DOI: 10.1044/jshr.0103.227 (cit. on p. 110).

[228] Van Rensburg, N. and Van der Merwe, A. "Natural frequencies and modes of a Timoshenko beam." In: *Wave motion* 44.1 (2006), pp. 58–69 (cit. on p. 21).

[229] Verdolini, K. *et al.* "Dependence of phonatory effort on hydration level." In: *Journal of Speech, Language, and Hearing Research* 37.5 (1994), pp. 1001–1007 (cit. on p. 23).

[230] Visser, J. *et al.* "Reinforcement of hydrogels using three-dimensionally printed microfibres." In: *Nature Communications* 6.6933 (2015) (cit. on p. 87).

[231] WanChiew, N. *et al.* "In Vitro Evaluation of Biomaterials for Vocal Fold Injection: A Systematic Review." In: *Polymers* 13.16 (2021). DOI: 10.3390/polym13162619 (cit. on p. 86).

[232] Wang, C. *et al.* "Strain rate dependent nanostructure of hydrogels with reversible hydrophobic associations during uniaxial extension." In: *Soft Matter* 15 (2 2019), pp. 227–236. DOI: 10.1039/C8SM02165A (cit. on p. 62).

[233] Ward, M. A. and Georgiou, T. K. "Thermoresponsive polymers for biomedical applications." In: *Polymers* 3.3 (2011), pp. 1215–1242 (cit. on p. 32).

[234] Weiß, S. *et al.* "Pipette aspiration applied to the characterization of nonhomogeneous, transversely isotropic materials used for vocal fold modeling." In: *Journal of the mechanical behavior of biomedical materials* 17 (2013), pp. 137–151 (cit. on p. 31).

[235] Weiss, S. *et al.* "Measurement and analysis of the material properties and oscillation characteristics of synthetic vocal folds." In: *Acta Acustica united with Acustica* 102.2 (2016), pp. 214–229 (cit. on p. 30).

[236] Woo, P. *et al.* "Diagnosis and treatment of persistent dysphonia after laryngeal surgery: a retrospective analysis of 62 patients." In: *The Laryngoscope* 104.9 (1994), pp. 1084–91. DOI: 10.1288/00005537-199409000-00007 (cit. on p. 86).

[237] Xing, Q. *et al.* "Increasing mechanical strength of gelatin hydrogels by divalent metal ion removal." In: *Scientific Reports* 4.1 (2014), pp. 1–10. DOI: 10.1038/srep04706 (cit. on pp. 53–55).

[238] Xu, C. and Chan, R. "Pore architecture of a bovine acellular vocal fold scaffold." In: *Tissue Eng Part A* 14.11 (2008), pp. 1893–903 (cit. on p. 91).

[239] Yan, X. *et al.* "High strength and self-healable gelatin/polyacrylamide double net-work hydrogels." In: *Journal of Materials Chemistry B* 5.37 (2017), pp. 7683–7691 (cit. on p. 34).

[240] Zhang, K. *et al.* "A two-layer composite model of the vocal fold lamina propria for fundamental frequency regulation." In: *The Journal of the Acoustical Society of America* 122.2 (2007), pp. 1090–1101. DOI: 10.1121/1.2749460 (cit. on p. 86).

[241] Zhang, S. "Fabrication of novel biomaterials through molecular self-assembly." In: *Nature biotechnology* 21.10 (2003), pp. 1171–1178 (cit. on p. 33).

[242] Zhang, X. *et al.* "Static and dynamic material properties of CFRP/epoxy laminates." In: *Construction and Building Materials* 114 (2016), pp. 638–649 (cit. on p. 80).

[243] Zhang, Z. "Mechanics of human voice production and control." In: *The journal of the acoustical society of america* 140.4 (2016), pp. 2614–2635 (cit. on p. 110).

[244] Zhang, Z. "Effect of vocal fold stiffness on voice production in a three-dimensional body-cover phonation model." In: *The Journal of the Acoustical Society of America* 142.4 (2017), p. 21. DOI: 10.1121/1.5008497 (cit. on p. 53).

[245] Zhang, Z. *et al.* "Aerodynamically and acoustically driven modes of vibration in a physical model of the vocal folds." In: *The Journal of the Acoustical Society of America* 120.5 (2006), pp. 2841–2849. DOI: 10.1121/1.2354025 (cit. on p. 86).

[246] Zhang, Z. *et al.* "The influence of subglottal acoustics on laboratory models of phonation." In: *The Journal of the Acoustical Society of America* 120.3 (2006), pp. 1558–1569 (cit. on p. 30).

# Appendices

# Complement to Chapter 5 – Structuration of gelatin-based hydrogels using directional ice-templating and freeze-drying

A second exploratory approach that was taken in order to introduce the anisotropy to the structure of hydrogel is the technique of Ice-templating. Even thought the complicated procedure and feasibility of such technique on crosslinked hydrogels seems to be far from the objectives of the project, however certain results seems to be promising for the further explorations. The idea is briefly is to line up the solid portion of the hydrogel using the ice crystallisation as driving force.

In this regards, Gelatin-based hydrogels (neat and cured) were freezed using Julabo Cryo-thermostat device. As it was predictable, the covalent bonding provoked by the GA crosslinking reaction prior to the freezing; the obtained structure is not fully aligned as desired. But this is not the only reason that prevents the right alignment; but also a high density of the gelatin content can also play a role. Therefore, a pure hydrogel with a decreased concentration of the gelatin was prepared using the same protocol. Then, the achieved results are shown on Figure 10: relatively improved level of alignment in parallel with the solidification direction and more uniform structure in perpendicular cross section.

This was the first observation obtained recently, but the idea at the moment is to evaluate the possibility to perform the crosslinking reaction after the freeze drying and compare the capacity of the structure to maintain the same mechanical performance as the non-lyophilised samples.

A priliminary result of the tensile characterization of the freeze dried sample which was crosslinked by 24 hour immersion in 0.05 % GA solution is presented in figure bellow. It shows promissing capacity of the method to reproduce the Ge-GA hydrogel, even though its failure point is lower. also the transverse loading should be performed to affirm the anisotropic potential of the material.

a) principle

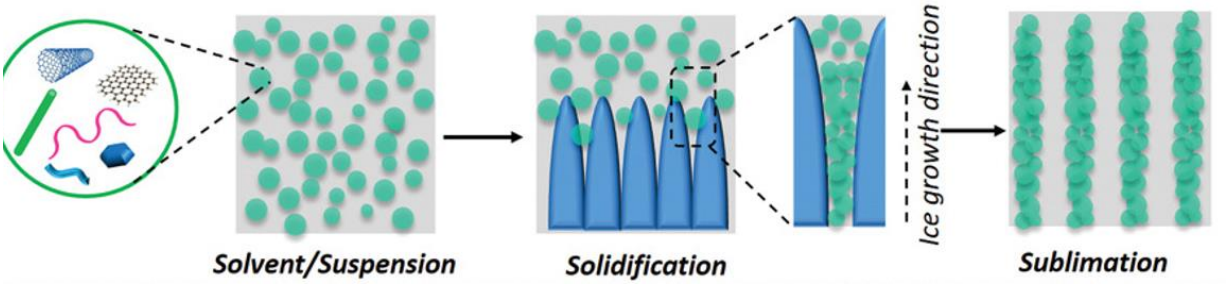


b) Fabrication process

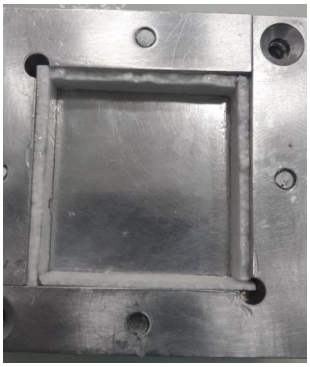

Lateral insulation polystyrene


Refrigerated Circulating Bath: Julabo -30°C

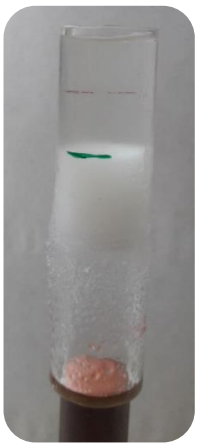

Unidirectional freezing column

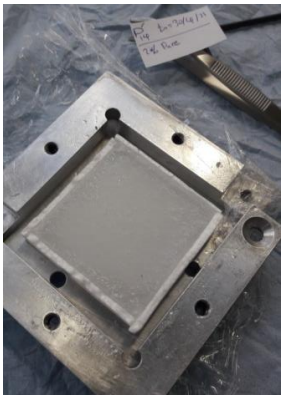

c) Freeze-Drying

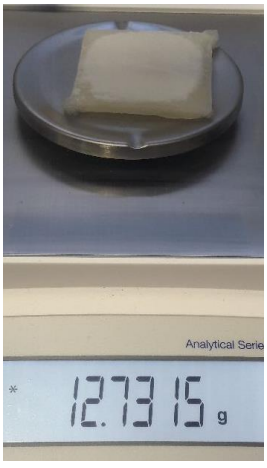




**Supplementary figure 1:** Fabrication process of the freeze-dried gelatin samples

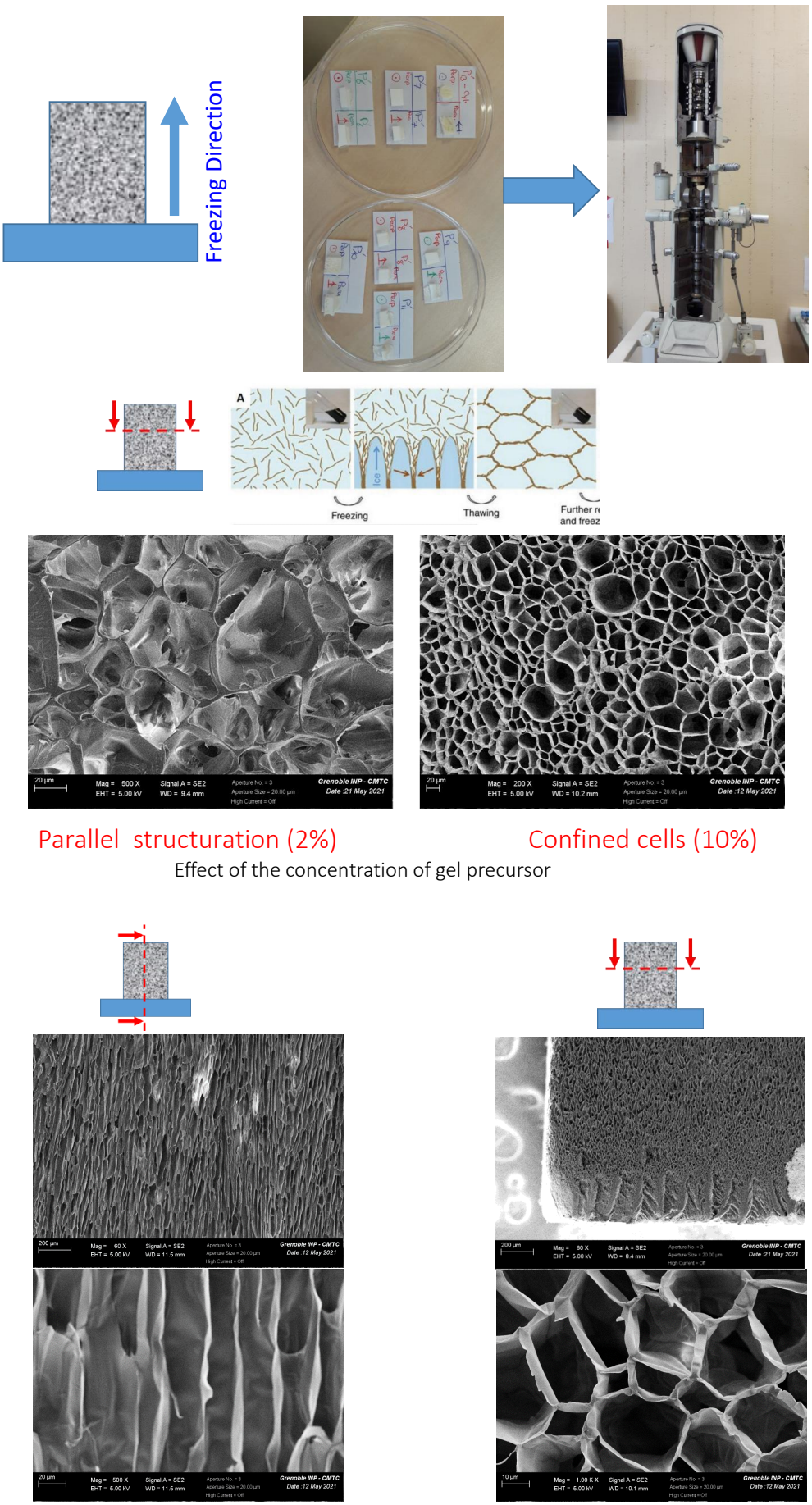


Effect of the concentration of gel precursor

**Supplementary figure 2:** Microstructure of the freezedried sample- Electon microscopy

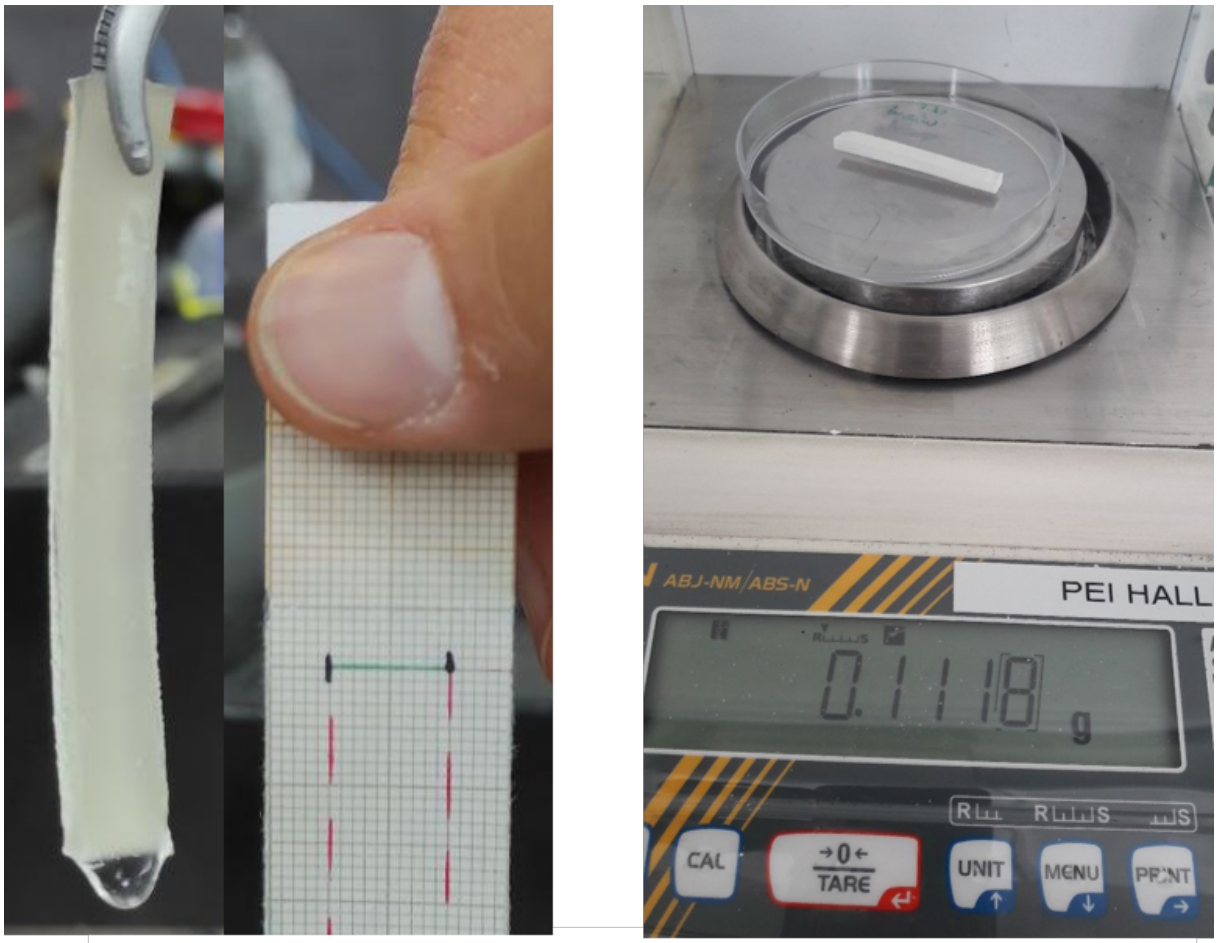


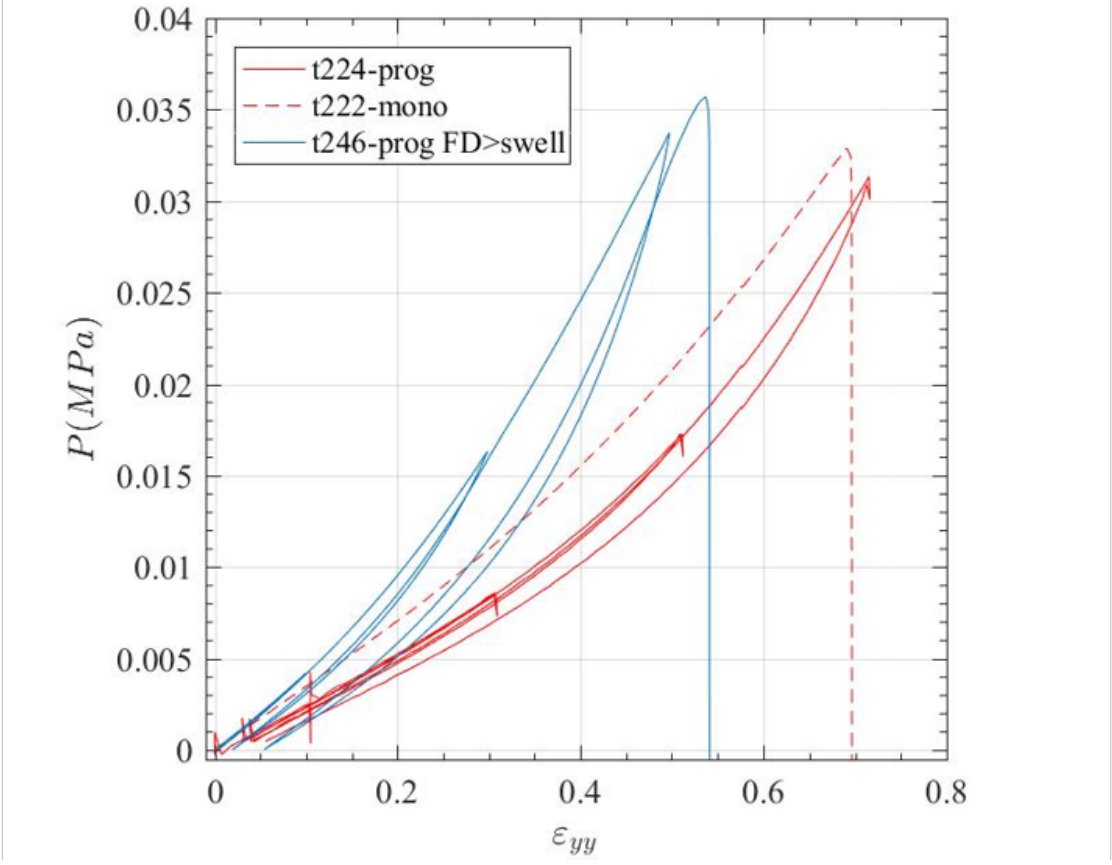


**Supplementary figure 3:** Cyclic tensile response of the ice-templated Gelatin sample ...

# B. Complement to Chapter 6 – Towards the vibratory behaviour of anisotropic vocal-fold replica

# Contents

# 1 Introduction

## 1.1 Vibration properties of composite materials and structures

## 1.2 Back into voice biomechanics : where we stand ?

# 2 Materials and method

## 2.1 Fibre-reinforced 3D replica : processing route

rediger

| Id | Body (EF) | Cover (EF) | $T_{fibre-PCL}$ (mm) | Strain range (Ɛ) of vibr. |
|---|---|---|---|---|
| 32 | 10 | 10 | 0.45 | 0.2 to 0.45 (=12 step) |
| 33 | | | 0.60 | 0,15 to 0,41 (=12 step) |
| 34 | 30 | 30 | 0.45 | 0,36 to 0,47 (=10 step) |
| 35 | | | 0.60 | 0,09 to 0,54 (=17 step) |
| 36 | 30 | 10 | 0.45 | 0,08 to 0,46 (=12 step) |
| 37 | | | 0.60 | 0,11 to 0,37 (=10 step) |

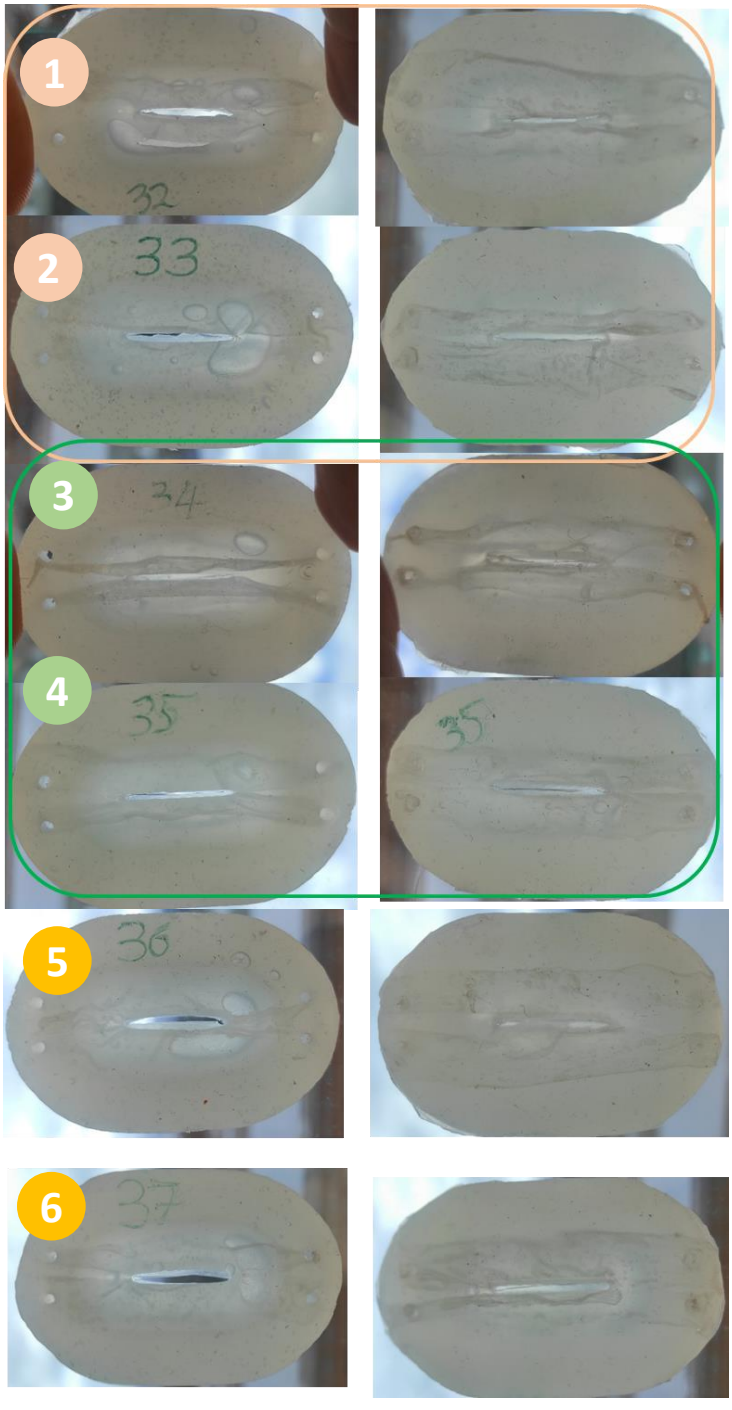


**Supplementary figure 1:** matrix and fiber specificities, fiber integration quality

# 3 Results and discussion

## 3.1 Impact of the microstructure on the aero-acoustical descriptors of the replica

## 3.2 Impact of the mesostructure

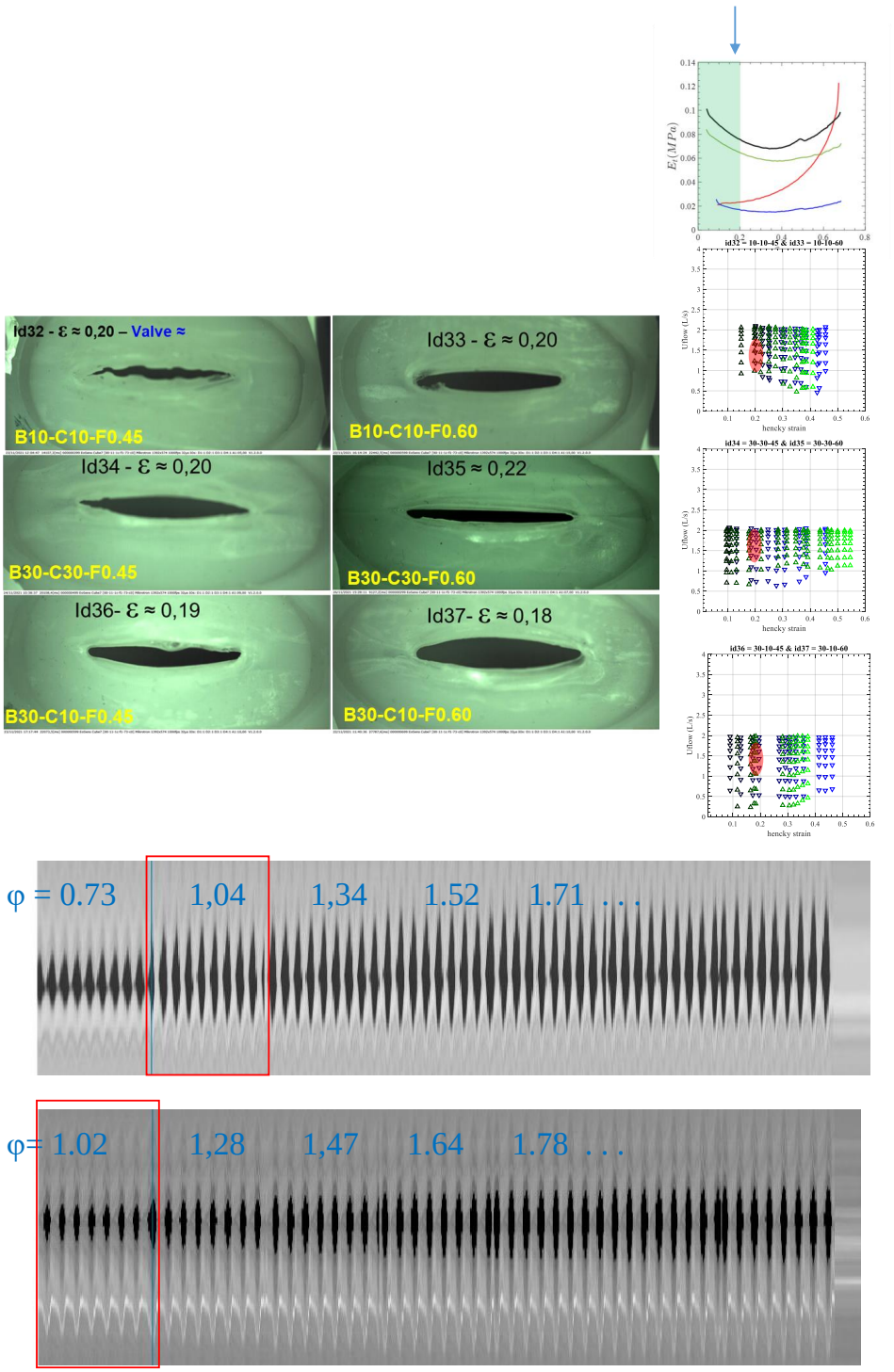


**Supplementary figure 2:** High speed camera shot at $\epsilon = 0.2 and corresponding flow rate and kymo$

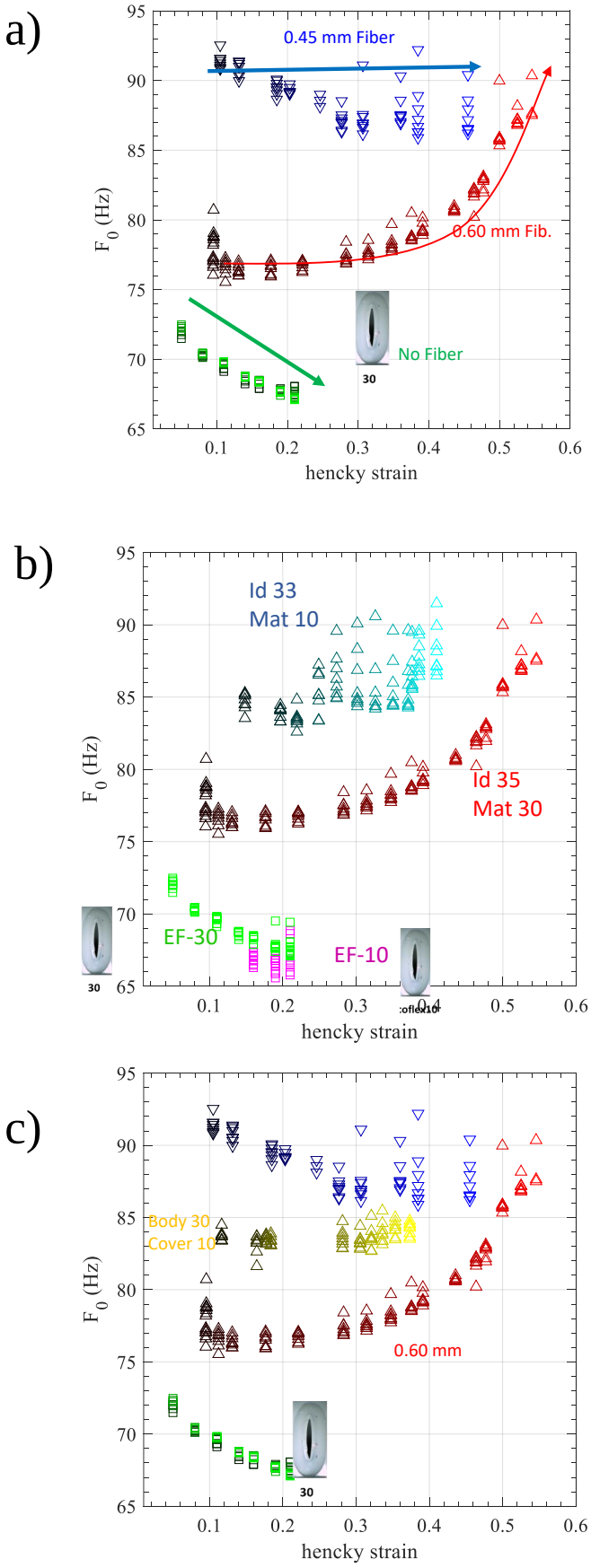


**Supplementary figure 3:** effect of material composition on vibration frequency

# 4 Conclusion